Medical Device Doctoral Training Centre
Department of Bioengineering

DEVELOPMENT OF A BACTERIOPHAGE BASED BIOSENSOR FOR THE RAPID DETECTION OF BACTERIA

MELISSA WEBSTER MEng

A thesis submitted in the fulfilments of the requirements for the degree of Doctor of Engineering

2010

Acknowledgements

Abstract

The sensitive and specific detection of bacteria is important for health and safety reasons. Conventional methods to detect bacteria are sensitive but generally take several days to confirm the detection of a bacterial strain. There is therefore a real necessity to develop a bacterial detection method which will improve on detection times, yet will match the detection limits of conventional methods. Biosensors have emerged as a potential technology to meet this criterion but have yet to attain the required level of sensitivity and specificity.

In this research, the concept of developing a biosensor which uses bacteriophages, in combination with an impedimetric sensor, was investigated for the rapid detection of bacteria. Bacteriophages are viruses which are specific to bacteria and have several potential advantages over commonly used bioreceptor types. They therefore present a potential approach to improving biosensor performance.

A computer based model of the system was developed and extensively studied to investigate the response of impedimetric sensors to bacteria and to optimise sensor design. A comparison of bioreceptor immobilisation methods was carried out with the aim of determining the optimum method for the immobilisation of bacteriophages onto the sensor. An interdigitated microelectrode array impedimetric sensor was investigated in combination with bacteriophages immobilised onto the sensor surface. The results of the biosensor testing showed that bacteria could be rapidly detected (within 10 minutes) at high bacterial concentrations; however, further work is required in order to accurately determine the biosensor's detection limit and to therefore establish the true bioreceptor performance of bacteriophages. The results highlight the complexity of impedimetric bacterial detection, and theories are discussed to try to explain the conflicting experimental results found both in this work and also across related published work.

List of Abbreviations

AC	Alternating current
APTMS	(3-Aminopropyl)trimethoxysilane
ADP	Adenosine diphosphate
AK	Adenylate kinase
ATP	Adenosine triphosphate
BE	Boundary element
BNC	Bayonet Neill-Concelman
BSA	Albumin from bovine serum
CAE	Computer-aided engineering
CFU	Colony forming unit
CPE	Constant phase element
CVD	Chemical vapour deposition
DC	Direct current
DEP	Dielectrophoresis
DMSO	Dimethyl sulfoxide
DNA	Deoxyribonucleic acid
ECM	Equivalent circuit modelling
EIS	Electrochemical impedance spectroscopy
ELISA	Enzyme-linked immunosorbent assay
FDA	Food and Drug Administration
FE	Finite element
FIA	Fluorescent immunoassay
HAI	Healthcare associated infections
IMS	Immunomagnetic separation
LAPS	Light addressable potentiometric sensor
LB	Luria-Bertani
MOI	Multiplicity of infection
MRSA	Methicillin-resistant *Staphylococcus aureus*
NCIMB	National Collection of Industrial, Marine and Food Bacteria

PBS	Phosphate buffered saline
PCR	Polymerase chain reaction
PFU	Plaque forming unit
PMGI	Polymethylglutarimide
PW	Peptone water
RNA	Ribonucleic acid
SAM	Self assembled monolayer
SM	Storage medium
SPR	Surface plasmon resonance
TMB	3,3',5,5'-Tetramethylbenzidine

Statistics

μ_0	Hypothesised mean of the differences
μ_d	Population mean of the differences between paired observations
μ_1	Population mean of sample 1
μ_2	Population mean of sample 2
H_0	Null hypothesis
H_A	Alternative hypothesis
α-level	Level of significance - the value of the maximum acceptable level of risk for rejecting the null hypothesis in a statistical test.

Contents

Chapter 2

THEORY **43**

Chapter 3

BIOSENSOR MODELLING AND DESIGN **68**

Chapter 5

BACTERIOPHAGE IMMOBILISATION **133**

Chapter 7

List of Figures

Chapter 3

xvi

Chapter 6

List of Tables

Chapter 1

INTRODUCTION AND BACKGROUND

This chapter introduces the principles of bacterial detection and provides relevant background information for the project. First, conventional bacterial detection methods are reviewed. The need to develop novel rapid bacterial detection methods is then addressed before discussing some of the emerging rapid bacterial detection methods. Following this, a review is provided on present biosensor technology; although biosensors have wide applications, the focus of this review is specifically on biosensors for the detection of bacteria and in particular those utilising electrochemical transduction methods. Background on the electrical properties of bacteria is provided which will become relevant in later chapters when discussing the impedimetric mode of detection used in this project. Bacteriophages are then introduced and their present applications discussed. Note that a review of immobilisation techniques can be found in the immobilisation chapter (Chapter 5). Chapter 1 concludes with an outline of the project aims.

1.1 <u>Bacterial Detection</u>

Bacteria are found throughout the environment; they exist naturally in soil, water sources, plants and human beings. Bacteria are important microorganisms, responsible for carrying out many vital activities in nature; however, some bacterial species are harmful and can cause infectious diseases in humans. Such species are termed pathogenic bacteria. The detection of pathogenic bacteria is of primary importance for health and safety reasons. Bacterial detection is required for the prevention, diagnosis and treatment of infectious diseases and as a result, a vast amount of research is being conducted in this field. Lazcka et al. (2007) provide a review of bacterial detection methods which covers traditional methods and also recent developments in the area.

1.1.1 Conventional Bacterial Detection

Traditional methods for detecting bacteria are based on culturing techniques. Culturing involves growing bacteria in liquid media or on agar plates which contain the nutrients necessary for growth. The presence of bacteria can then be visually detected after incubation at an optimum temperature for a suitable period of time. Selectivity is achieved by using selective and/or differential media. A selective medium contains inhibitors to suppress the growth of non-target bacteria whilst a differential medium is supplemented with certain substrates which only the target bacteria will interact with and in doing so will lead to a specific colony appearance in terms of either colour, shape or growth pattern. Sometimes a non-selective enrichment culture is adequate if followed by diagnostic testing for identification. Diagnostic tests include biochemical tests, agglutination tests, immunological tests and immunofluorescent assays [Speers et al., 1998]. A range of diagnostic tests are provided by Remel, Oxoid Ltd.

Culturing is the oldest means of detecting bacteria but is still widely used today and remains the gold standard for bacterial detection in hospitals (often in combination with a diagnostic test). This is primarily due to its high sensitivity; in theory, culturing can detect the presence of a single bacterium. The approach is also inexpensive and simple. However, there are some drawbacks to the method, the most significant of which is the time it takes for detection – most bacteria require a minimum of 18 to 24 hours to grow to feasible levels for detection. After initial culturing, further culturing or diagnostic testing is then required for identification, adding to the overall detection time. For example, *Listeria monocytogenes* may take up to 7 days to be cultured and identified using advised protocols (NF EN ISO 11290-1) [Leonard et al., 2003]. Some medically relevant bacteria require considerably longer; for example, it can take up to 6 weeks to distinguish between different strains of *Mycobacterium tuberculosis*.

In addition to their lengthy detection times, culturing techniques can also suffer from adverse effects due to the sampling matrix, a problem common across bacterial detection methods. For example, in food samples, components of the food itself can

be detrimental to bacterial growth and the growth of indigenous microflora in some samples may dominate and therefore interfere with target pathogen detection [Swaminathan and Feng, 1994].

Improvements on culturing detection times are continually being sought and research on culturing methods is still active. For example, new selective media are being developed for improved bacterial detection. Merlino et al. (2000) reported on a new chromogenic plate medium which showed improved sensitivity and specificity compared to other culture media for the detection of *Staphylococcus aureus*. Verkade et al. (2009) evaluated a new selective medium for methicillin-resistant *Staphylococcus aureus* (MRSA) called Oxoid Brilliance^{TM} MRSA and found it to be sensitive to MRSA after only 20 hours incubation of the directly applied sample.

1.1.2 The Need for Rapid Bacterial Detection

Recently, Lazcka et al. (2007) conducted a survey on pathogen detection literature published over the last 20 years. They identified four main areas of interest for pathogen detection: clinical applications; the food industry; water and the environment; and defence.

In the clinical setting, bacterial detection is important for the diagnosis and treatment of disease. If a faster bacterial detection technique was available it is clear to see that improved medical care could be achieved through faster diagnosis and the administration of appropriate medication. This would also reduce or even eliminate the need for pre-emptive or precautionary drug prescription which is important in tackling the issue of antibiotic resistant bacterial strains which are emerging and becoming a serious threat to public health. For example, there has been a significant rise in the number of reported cases of MRSA across Europe [EARSS, 2004] and in 2002 the first case of *S. aureus* resistance to vancomycin, the antibiotic of last resort for MRSA treatment, was reported in the US [Centers for Disease Control and Prevention, 2002]. MRSA has also been identified as a healthcare associated infection (HAI) along with *Clostridium difficile*. Recently there has been increasing concern over HAIs as the number of deaths involving MRSA and *C. difficile* have risen significantly [Office for National Statistics, 2008]. Although levels are

beginning to fall, there were still 6855 reported cases of *C. difficile* between April and June of 2009 for patients aged 2 years and over [Health Protection Agency, 2009]. Screening of patients has been identified as an important means of reducing the number of HAIs [Department of Health, 2006], a task limited by conventional detection methods. The Health Protection Agency recommends that screening for MRSA be carried out using the direct plating method but this procedure takes at least 24 hours. There is therefore a clear need to develop rapid detection techniques for tackling health care problems.

In terms of the food industry, rapid identification of bacteria is important to prevent food poisoning from bacteria and the release of contaminated food. In the UK alone there were 54 716 laboratory confirmed cases of the five key bacterial foodborne pathogens in 2008 (*Salmonella*, *Campylobacter*, *Escherichia coli* O157, *L. monocytogenes* and *Clostridium perfringens*) [Foods Standard Agency, 2009]. In addition to public health concerns there are also substantial financial costs associated with foodborne related illnesses. In 2007, the annual cost of foodborne illnesses was estimated to be £1.5 billion for England and Wales [Foods Standard Agency, 2009]. The detection of pathogenic bacteria in foods is therefore of considerable importance. However, conventional methods for detecting bacteria are not practical for screening foods, especially fresh produce which may perish in the time it would take to detect a pathogenic bacterial contamination. A rapid bacterial detection device could therefore be of benefit to the food industry. Arguably however, adhering to hygiene and sterilisation procedures should be adequate for preventing bacterial contamination in the first instance.

Bacterial detection is also important in water and environmental monitoring. For example, cholera is an acute intestinal infection common in developing countries. It is caused by consuming food or water contaminated with *Vibrio cholerae*. In 2007, the World Health Organisation recorded a total of 177 963 cases of cholera including 4031 deaths from across 53 countries [World Health Organisation, 2008]. A simple and inexpensive rapid bacterial detection system could help prevent the consumption of contaminated water.

A more recent need for rapid bacterial detection techniques has been identified for defence purposes due to the increasing threat of bioterrorism. There are many challenges to detecting biothreat agents [Lim et al., 2005], not least in making a fast identification so that appropriate action can be taken to treat and contain the threat.

The above examples highlight the present shortcomings of conventional bacterial detection methods and illustrate the potential benefits of a rapid technique. However, for a rapid detection system to be successful, it must be highly sensitive and specific. The infecting dose of several pathogenic bacteria, such as some *E. coli* strains, can be as low as ten cells [FDA, 2004] therefore, ideally, detection limits should be capable of reaching this level. Another important characteristic about bacterial growth which makes early detection imperative is their exponential growth rate; typically bacteria reproduce every 30 minutes. Developing a rapid detection method which meets the necessary requirements remains the challenge in the field of bacterial detection today.

1.1.3 Rapid Bacterial Detection Methods

Research in the area of rapid bacterial detection is vast. Several different approaches have been investigated and continue to be developed. In the following section, a general overview is provided on some of these methods. This review does not intend to be all encompassing but aims to highlight some of the most significant developments.

1.1.3.1 Impedance Microbiology

Impedance microbiology is an early example of the attempts made to improve bacterial detection times. Impedance microbiology basically involves monitoring changes in impedance of broth cultures due to the growth and metabolic activity of bacteria. It is based on the principle that as bacteria grow, relatively large uncharged or weakly charged molecules are broken down into smaller more mobile ionic molecules causing an increase in the conductance of the surrounding solution. This in turn results in a decrease in impedance which can be monitored with the appropriate measuring system.

The technique was first identified in 1899 when G. N. Stewart published data on conductivity changes of blood samples which he attributed to bacterial growth [Stewart, 1899]. The technique was significantly developed in the works of Ur and Brown (1975), Cady (1975, 1978) and Eden and Eden (1984) who found that impedance curves obtained during bacterial growth were characteristic for different organisms and media, thus suggesting the technique as a potential bacterial detection method. Importantly, depending on the media and initial bacterial concentration, changes could occur within hours. Therefore the technique was faster than conventional culturing methods.

There are two main approaches in impedance microbiology: direct impedance and indirect impedance measurements. Direct impedance techniques monitor changes in medium conductivity directly by using electrodes placed in the medium. Once the rate of impedance change exceeds the predefined detection criteria, the growth and therefore presence of bacteria is confirmed. One significant drawback to this approach is that the medium must be optimised for electrical signal detection; some media have conductivities which are either too low or too high for signal detection and some bacteria may not induce a sufficient change in the medium conductivity during growth [Bolton, 1990, Dézenclos et al., 1994].

To overcome some of these problems, the indirect impedance microbiology approach was devised. First developed by Owens et al. (1989), this technique detects bacteria by monitoring carbon dioxide levels produced as a by-product of bacterial metabolism. The electrodes, instead of being in direct contact with the medium, are positioned either above or below the bacterial culture and immersed in an electrolyte which absorbs carbon dioxide. The absorbing electrolyte may be a strong alkali such as potassium hydroxide or sodium hydroxide. The absorbed carbon dioxide will combine with hydroxide ions to form carbonate. Since carbonate is of a much lower conductivity than hydroxide ions, there will be an overall reduction in conductivity proportional to absorbed levels of carbon dioxide. This in turn can be related to bacterial detection and initial bacterial levels based on the detection times.

Several automated commercial systems have been developed based on impedance microbiology such as the Bactometer® (BioMérieux Industry, France) and the Rapid Automated Bacterial Impedance Technique (RABIT; Don Whitley, UK). The technique has been successfully used in the food industry where it is an accepted method for the detection of *Salmonella* and has been found to compare well against other detection methods [Quinn et al., 1995]. Despite this, the technique has largely disappeared from use. This is perhaps due to the fact that a pre-enrichment stage is often necessary and so detection times are still in excess of 10 hours. In addition to this, false positive and false negative results are commonly encountered if the medium is not adequate [Silley and Forsythe, 1996].

1.1.3.2 PCR

The polymerase chain reaction (PCR) was first developed in the mid 80s and is now an established method for the detection of bacteria. The basic technique involves isolating, amplifying and quantifying a strand of DNA from the target bacteria. Amplification is achieved through a series of PCR cycles. Each cycle consists of denaturing the extracted DNA by heat. Primers are then added which anneal to the single strands of DNA. The primers are extended to create replicates of the original DNA sample through DNA polymerisation. Repeated PCR cycles results in an exponential increase of the DNA strand. The presence of the target sequence can be subsequently detected by gel electrophoresis.

PCR techniques generally require less time to yield results than culturing methods; they typically take between 5 to 24 hours to generate a result, although a pre-enrichment step may also be necessary [Lazcka et al., 2007]. Some limitations to PCR have been identified and include: high susceptibility to false positive results due to sample contamination; the possibility of false negative results due to the small sample volume and process steps; DNA may be amplified from bacterial concentrations not clinically significant; the sample matrix can sometimes inhibit polymerisation; PCR is limited in how far the bacteria can be characterised i.e. it may not be possible to identify a specific strain; and viable and non viable bacteria can not be distinguished [Albuquerque et al., 2009, Yamamoto, 2002, Yang and

Rothman, 2004]. Also, some PCR protocols can be complex thus requiring some level of expertise for operation.

To overcome some of these limitations, the PCR technique has been further developed and improved variations now exist. Some of these include real-time PCR [Huletsky et al., 2004], multiplex PCR [Schuenck et al., 2006] and quantitative reverse transcription-PCR [Wada et al., 2010].

An example of a commercially available PCR device for bacterial detection is the BD GeneOhm^{TM} MRSA assay which has been approved by the Food and Drug Administration (FDA) for MRSA detection. The assay is based on a real-time PCR assay and detection time is within 2 hours. A recent evaluation of the assay compared to culturing onto BBL^{TM} CHROMagar^{TM} MRSA from BD Diagnostics revealed the sensitivity and specificity of the PCR technique to be close to but less than that for the culturing method [Farley et al., 2007]. Therefore, whilst PCR techniques can be faster, it seems that their performance level has yet to match that of culturing.

1.1.3.3 Immunological Methods

The high specificity of antibodies for their corresponding antigens has been exploited for bacterial detection purposes. Antibodies for the specific detection of bacterial strains have been incorporated into a variety of different assays and devices. Such immunology based methods include the enzyme-linked immunosorbent assay (ELISA), fluorescent immunoassays (FIA), immunomagnetic separation (IMS) and agglutination techniques.

The ELISA is now an established laboratory technique. In its most common form, the 'sandwich ELISA' (illustrated in Figure 1.1), immobilised antibodies capture the target bacteria onto a substrate. A secondary enzyme-labelled antibody is then added which will bind with the captured bacteria. Upon addition of the enzyme substrate, the enzyme will catalyse a reaction which will lead to detectable changes in absorbance, fluorescence or electrical parameter. The ELISA has been successfully investigated for the detection of many bacteria including *E. coli* [Blais et al., 2004] and *Salmonella* [Croci et al., 2004]. Due to its simplicity and relatively inexpensive

features, commercial kits have become widely available. For example, $3M^{TM}$ Tecra^{TM} (Minnesota, USA) provide ELISA kits for the detection of pathogens such as *Salmonella*, *Listeria* and *S. aureus*. However, some studies have found the ELISA to be inferior compared to conventional methods for bacterial detection purposes in terms of their specificity and sensitivity [Eriksson and Aspan, 2007, Jouy et al., 2005, Rompré et al., 2002]. In a review of detection methods for coliforms (a broad group of related bacteria) in drinking water, Rompré et al. (2002) identified cross-reactivity with non-target bacterial strains and interference from sample matrix as the most common causes for poor performance. Detection limits are in the region of 10^3 to 10^5 CFU/ml [Blais et al., 2004, Lazcka et al., 2007] and therefore a pre-enrichment step is usually required before the ELISA which considerably lengthens the total detection time.
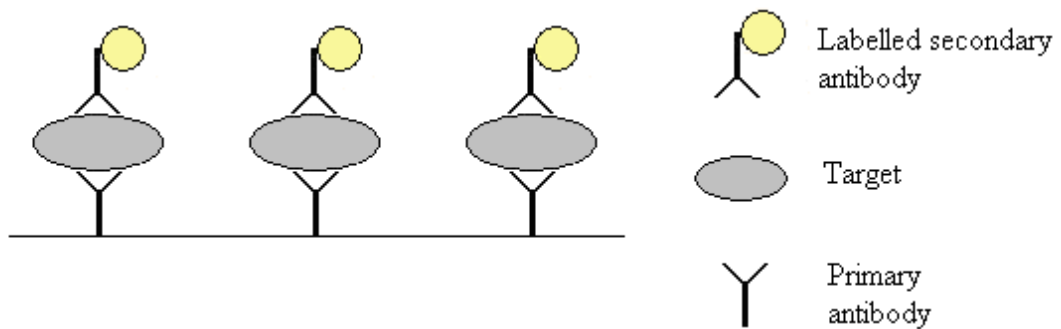
Figure 1.1. Illustration of the sandwich ELISA. Primary antibodies are immobilised onto a substrate which are specific for the target. Secondary antibodies, also specific for the target, are added which are labelled with an enzyme. The enzyme will catalyse a reaction which will elicit a detectable signal.

FIAs are similar in principle to the ELISA but instead of using enzyme-labelled antibodies, fluorescently tagged antibodies are employed to detect target bacteria. FIAs have been investigated for bacterial detection but have been found to experience the same problems of ELISAs with the added complication of autofluorescence [Swaminathan and Feng, 1994].

IMS is an immunological tool which is often used in conjunction with detection techniques. Antibodies are coated onto micro- or nano-sized magnetic beads which are mixed with the sample. By applying an external magnetic field, captured bacteria

can be collected and concentrated into a small volume. IMS is therefore commonly utilised as a pre-concentration step and can be used in combination with almost any detection method. For example, Fu et al. (2005) used IMS with real-time PCR to detect *E. coli* O157:H7. A detection limit of 5×10^2 cells/ml was achieved for cell suspensions and 1.3×10^4 cells/g from ground beef. Similarly, Varshney et al. (2007) used magnetic nanoparticle-antibody conjugates with an impedance sensor to detect *E. coli* O157:H7 and achieved similar detection limits. Dynabeads® (Dynal Biotech, Norway) are an example of commercially available magnetic beads.

Agglutination techniques are a commonly used immunological based diagnostic test. They involve using beads (usually latex beads) coated in antibodies specific for the target bacteria. Upon mixing with the target strain, agglutination occurs through antibody-bacteria interactions and this can be visually detected. Commercially available tests are available, for example Remel (USA) supply tests for pathogenic bacteria such as *S. aureus*, *E. coli* and *C. difficile*. However, suitable detection levels from a clinical or food sample are usually only achieved after at least one overnight culturing step.

1.1.3.4   ATP Bioluminescence

Adenosine triphosphate (ATP) is the chemical compound in which energy is stored and transported for metabolism within all living organisms. The enzyme luciferase uses ATP to convert D-luciferin into oxyluciferin and light in the presence of oxygen and magnesium ions. The light produced is proportional to the level of ATP present which in turn can be related to the presence of living organisms, such as bacteria. A luminometer can be used to measure light levels.

The above theory forms the basis of several commercially available detection systems, such as the ENLITEN® ATP Assay System (Promega, USA) and Profile® 1 Rapid Bacteria Detection Kit (New Horizons Diagnostics Inc., USA). The technique has been widely implemented in the food industry where it can detect 1 CFU/g of foodstuff after a 24 hour period of enrichment [Zourob et al., 2008]. However, again, this enrichment period is necessary to reach adequately low detection limits. Another

drawback to the bioluminescence method is that it lacks specificity. To achieve specificity the technique has to be used in combination with a target specific isolation or assay step. For example, Squirrell et al. (2002) investigated using the bioluminescence reaction with prior IMS and/or specific cell lysis using bacteriophages (bacteriophages will be discussed in detail in Section 1.4). Detection limits of 10^2 CFU/ml were achieved within 5 to 60 minutes.

A modification to this bioluminescence approach involves the detection of adenylate kinase (AK). AK is an essential enzyme present in living organisms which can convert adenosine diphosphate (ADP) into ATP. Therefore, if supplied with ADP, the presence of AK will lead to ATP production which can be detected as previously described. Improved limits of detection have been reported with this approach [Zourob et al., 2008].

1.1.3.5 Biosensors

A biosensor has been defined as a device which incorporates a biological sensing element either closely connected to or integrated with a transducer [Turner et al., 1990]. The sensing element is capable of specifically interacting with the target analyte. Biosensors have become the fastest growing technology in the field of pathogen detection [Lazcka et al., 2007], corresponding with recent advances in micro and nano-technology. They are showing promise for providing a rapid bacterial detection device with several additional advantages over conventional and other developing methods such as miniaturisation, the requirement of small sample volumes and the potential to yield a portable device. At present however, although detection times are beginning to be achieved within an hour, detection limits are often not low enough to reliably match that of conventional techniques. Detection limits of approximately 10^2 CFU/ml are now being reached from pure cultures but this needs to be improved on for biosensors to reach their full potential. Biosensors for rapid bacterial detection will be discussed in more detail in Section 1.2.

1.1.3.6 Summary

In summary, it can be seen that there is a clear need to develop a rapid system for the detection of bacteria. Table 1.1 summarises typical detection times and limits for

some of the general techniques presently available and being developed for the detection of bacteria. Culturing remains the gold standard for detecting bacteria in hospitals. However, it can be seen from Table 1.1 that whilst culturing is the most sensitive, it is also the most time consuming, yet faster detection methods are not reaching adequate sensitivity levels. Often a pre-enrichment step is required for these rapid methods which significantly adds to detection times. However, of these emerging rapid detection techniques, biosensors continue to be developed due to their promising technology, as will be discussed in the following section.

Table 1.1. General summary of conventional bacterial detection methods and developing rapid techniques. Typical detection times and limit ranges are provided based on the literature reviewed in Section 1.1.3 and also in Section 1.2 to follow. Detection times marked with an asterisk (*) indicate that a pre-enrichment step may be required prior to detection in order to reach adequate detection limits (typically < 10 CFU/ml) and this will add considerably to the overall detection times listed. The detection limits listed are those which have been achieved without pre-enrichment.

Technique	Detection time	Detection limit
Culturing	1 day – weeks	< 1 CFU/ml
Impedance microbiology	Minutes – hours*	< 10 CFU/ml
PCR	Hours – 1 day*	< 10 CFU/ml
Immunological methods	Minutes – 1 day*	$10^3 - 10^5$ CFU/ml
ATP bioluminescence	Minutes – 1 day*	$1 - 10^2$ CFU/ml
Biosensors	Minutes – hours*	$10 - 10^4$ CFU/ml

1.2   <u>Biosensors for Bacterial Detection</u>

The two main components of a biosensor are the bioreceptor and the transducer. The basic operating strategy of a biosensor is illustrated schematically in Figure 1.2 and is outlined as follows: the target analyte will interact with the bioreceptor which is specific to that analyte; the interaction is detected by the transducer which converts it into a measureable signal; after appropriate signal processing (if required) an output is obtained which indicates the presence of the target. In the case of bacterial detection, the target analyte will either be the bacterium itself or a component specific to the target bacterium. The target can be detected either directly or in-directly through the use of labels. Typically the bioreceptor is immobilised onto or in close proximity to the transducer.
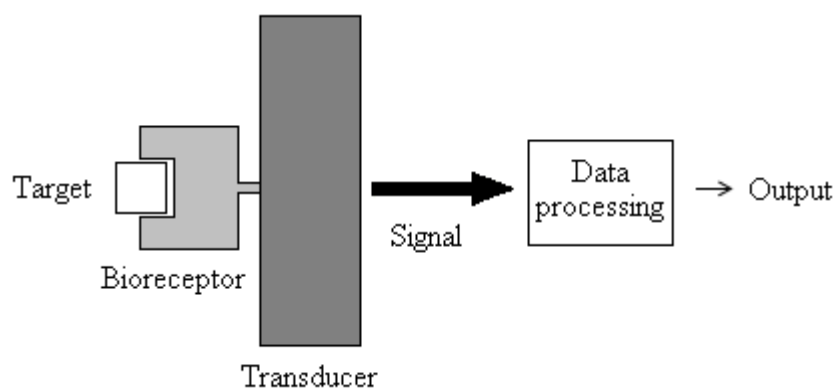
Figure 1.2. Schematic diagram illustrating the basic biosensor operation. The target analyte specifically interacts with the bioreceptor. The transducer converts this interaction into a measurable signal which is processed to yield an output indicating the presence of bacteria.

13

Table 1.2 outlines some of the main requirements for an ideal biosensor in order to realise the present demands for a rapid bacterial detection device. Biosensors could potentially meet these requirements.

Table 1.2. Summary of the ideal requirements of a biosensor for bacterial detection. Adapted from Ivinski et al. (2000) and Leonard et al. (2003).

Detection time	Ideally within an hour.
Sensitivity	Low detection limit – be able to detect a single bacterium in a small sample volume (1 to 100 ml).
Specificity	Discrimination between bacterial strains and species in the presence of non-target organisms.
Accuracy	Low probability of false negative and false positive results.
Reproducibly	Highly reproducible with good resistance towards environmental changes such as pH, temperature, humidity.
Viable cell count	Discrimination between live and dead cells.
Protocol	Simple - few protocol steps, reagentless, no pre-enrichment.
User friendly	Automated format with minimal user skill required.
Size	Small – hand-held and portable device.
Life time	As long as possible – in the order of months.
Cost	The device must be affordable and ideally it should be re-usable.

Examples of common bioreceptor elements and transducer techniques are presented in Figure 1.3. In the following sections, these bioreceptor and transducer components are discussed in terms of their application towards bacterial detection. There is particular focus on electrochemical methods as this was the approach implemented in this study. It is emphasised that this is a vast research area and that the following sections provide an introduction to classic biosensor techniques.
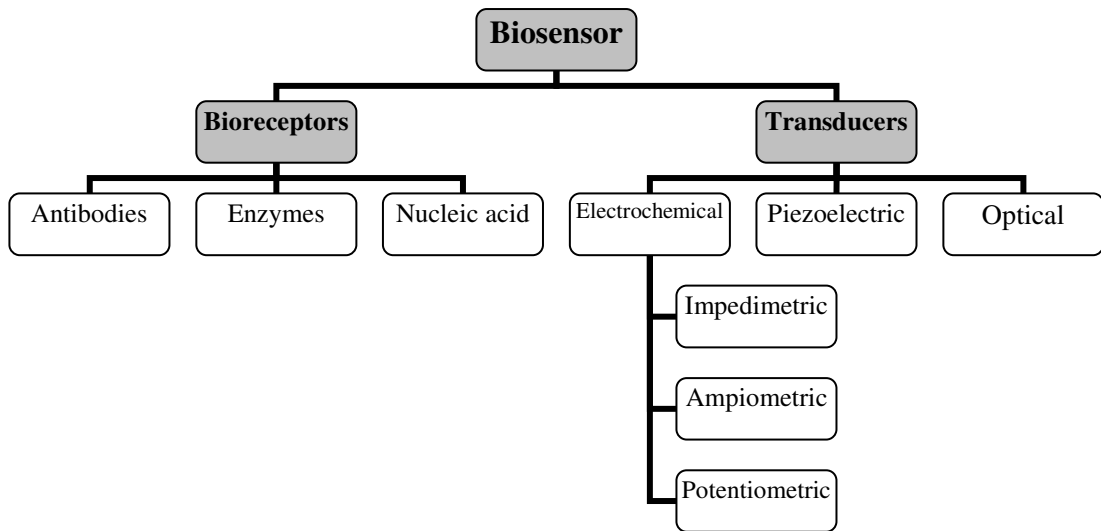
Figure 1.3. Common bioreceptor and transducer elements utilised in biosensors for bacterial detection.

1.2.1 Bioreceptors

The bioreceptor is the sensing component of the biosensor and, in the specific case of biosensors, is made from a biological material. Key requirements of the bioreceptor are that it is sensitive and specific to the target and is capable of a detectable interaction with the target. Sensitivity and specificity are essential so that the bacterial species and/or strain can be detected and so that interactions with other non-specific bacteria and material are minimised. Bioreceptors are typically immobilised onto a substrate such as metal, glass or polymer; this is discussed in detail in Chapter 5. The three most commonly used bioreceptors in biosensor technology are antibodies, enzymes and nucleic acid.

Antibodies

Antibodies are proteins naturally produced by the immune system of vertebrates to bind with and neutralise foreign objects in the body. Biosensors which implement antibodies as the biorecognition element are known as immunosensors and have been widely investigated for bacterial detection techniques. They utilise the formation of stable immunocomplexes between the target antigen and antibody to yield a response from the sensor. Immunosensors can generally be split into two categories: non-labelled and labelled. Typically, for non-labelled immunosensors, changes in

15

physical or electrochemical properties due to the formation of the immunocomplex are directly used to detect the target. Conversely, labelled immunosensors detect the target through a secondary reaction, brought about by introducing a labelled entity (often a secondary labelled antibody). Electrochemical and optical transduction methods have most commonly been implemented with antibodies [Stefan et al., 2000] but piezoelectric methods have also been investigated as will be discussed in Sections 1.2.2 – 1.2.4.

Immunosensing is now a well established tool, as was outlined in Section 1.1.3.3. However, the necessary limits of detection and specificity have yet to be achieved with immunosensors. This is often attributed to inadequate antibody specificity and affinity [Peruski and Peruski, 2003]. For example, polyclonal antibodies, which are relatively simple to produce, are often implemented in immunosensors but tend to recognise and bind with several different sites on the target bacterium which may also be common to other bacteria. They can therefore have reduced specificity. Monoclonal antibodies, which are produced such that they are specific for one antigen site only, are often preferred for their enhanced specificity but are much more difficult and expensive to produce. Recently, artificially derived recombinant antibodies have gained interest due to their potential for improved sensitivity and specificity [Byrne et al., 2009]. Overall, the sensitivity of an immunosensor is largely dependent on the quality of the antibody used and achieving this can be labour intensive and expensive.

Another drawback to using antibodies as a recognition element is that, by focusing antibody production on a specific target, when bacteria become stressed (e.g. by osmotic shock or a change in temperature or pH etc) the antigen may be compromised and antibody recognition may no longer be possible. Reduced responses under stressed conditions have been reported [Hahm and Bhunia, 2006]. Other disadvantages associated with antibodies include the general inability to regenerate and reuse the antibody sensing surface [Buerk, 1993] and the number of reagents and steps involved in the procedure if a labelled detection approach is used.

Nucleic acid

Nucleic acid based biosensors incorporate DNA or RNA probes which hybridise to complementary target sequences. Hybridisation between probe and target nucleic acid has been detected by a number of transduction methods including electrochemical [Wang et al., 1997], optical [Baeumner et al., 2003] and piezoelectric [Mao et al., 2006]. Details of these transduction processes are discussed in the following sections (Sections 1.2.2 – 1.2.4). DNA probes have also been used in combination with enzyme labels which will be discussed further shortly.

Nucleic acid based biosensors have received attention for several reasons. Firstly, the molecular recognition reaction forms strong and stable bonds at regular intervals between the nucleic acid strands through hydrogen bonding. Thus, the association constant between bioreceptor and target is stronger than for antibody based reactions [Ivnitski et al., 1999]. This could help improve on the sensitivity issues encountered with immunosensing and suggests that nucleic acid based biosensors may also be less likely to suffer from cross reactivity problems [Pancrazio et al., 1999]. In addition to this, the immobilised nucleic acid can be denatured through heating in order to reverse the nucleic acid binding and can then be regenerated with controlled buffer concentrations to yield a re-usable bioreceptor surface [Ivnitski et al., 1999].

However, a considerable drawback to nucleic acid based biosensors is the pre-treatment required in order to access the target nucleic acid [Lee and Hsing, 2006]. Extensive sample preparation is often required and can include: target cell isolation, cell lysis, nucleic acid extraction and purification. Sample preparation for nucleic acid based biosensors can therefore be laborious and time consuming. In addition to this, if low numbers of bacteria are present then only low levels of nucleic acid will be available. Therefore, PCR is also often required to amplify the nucleic acid to detectable levels. This considerably adds to detection times and can complicate the detection process, particularly if a portable hand held device is sought.

Another issue affecting the implementation of nucleic acid based biosensors is the fact that such biosensors cannot distinguish between live and dead cells. In attempts

to address this issue, dyes have been introduced before amplification which specifically bind to the DNA of dead cells preventing them from undergoing PCR [Rudi et al., 2002]. However, this is yet another step in the pre-treatment protocol.

Enzymes

Enzymes are typically implemented in biosensor applications through one of two approaches: (1) they are used as the biorecognition element and bring about detection through their ability to bind with the target or (2) their catalytic activity can be harnessed and detection is achieved through monitoring the enzymic reaction. In the case of bacterial detection, enzymes are most commonly implemented following this second mechanism. Enzymes also play a significant role as labels, for example they can be used to label antibodies which are implemented in a similar manner as was described for the ELISA in Section 1.1.3.3 [Chemburu et al., 2005]. The resulting enzyme reaction can be monitored by electrochemical or optical means in order to detect the target, as will be discussed in the following sections on transducer technology (Sections 1.2.2 – 1.2.4).

Generally, enzyme based biosensors are a successful class of biosensors and have been widely studied, particularly for application in the field of blood glucose monitoring [Turner et al., 1990]. Some of the main problems encountered with enzyme based biosensors are ensuring environmental conditions are suitable for enzyme stability and maintaining enzyme life time [Buerk, 1993]. In a practical sense, other bioreceptors such as antibodies and DNA are perhaps more apt for the direct detection of bacteria, and in the case of enzyme labelling, the multiple steps and reagents involved can be considered a drawback.

Summary

In summary, the three main bioreceptor types implemented for bacterial detection (antibodies, nucleic acid and enzymes) have shown promise for yielding a rapid bacterial detection method in the form of a biosensor device. However, as yet, biosensors with such recognition elements have not achieved adequate sensitivity levels, as will now be discussed in the following sections which describe their

implementation with transduction methods. Research therefore continues to progress and investigate conventional and novel bioreceptors options in an attempt to develop a biosensor which is both sensitive and rapid.

1.2.2   Electrochemical Sensors

Electrochemical techniques are one of the most popular transduction methods being investigated for biosensor development [Lazcka et al., 2007]. Generally, electrochemical methods are: sensitive, relatively simple, inexpensive, overcome some of the limitations encountered with optical methods when working with turbid samples, and have the potential to be incorporated into a miniature device [Lazcka et al., 2007, Neufeld et al., 2003, Parkinson and Pejcic, 2005]. Electrochemical methods can be classified into four main techniques based on the parameter being measured: amperometric, potentiometric, impedimetric and conductometric. The basic principles of these transduction methods and their application to bacterial detection will now be discussed.

Amperometric

Amperometric biosensors measure changes in current. They are based on the principle that when a constant potential is applied between two electrodes, the target analyte will either directly or in-directly cause a measurable change in current which can be correlated to the concentration of the analyte. Most amperometric sensors have the bioreceptor immobilised onto the electrode to enhance the electron transfer process. Amperometric biosensors have been said to be the most common electrochemical detection method used in biosensors [Lazcka et al., 2007] and is one of the most appropriate for implementation with immunosensors [Stefan et al., 2000].

An example of an amperometric based biosensor for bacterial detection was described by Mittelmann et al (2002). Polyclonal anti-*E. coli* antibodies were covalently immobilised onto graphite electrodes which captured permeabilised *E. coli* cells. Captured *E. coli* were detected by monitoring the activity of the enzyme *β*-D-galactosidase present within the bacteria; the product of the enzyme reaction is oxidised at the electrode and a current is produced which is linearly proportional to

the level of enzyme present and therefore the number of bacteria present. Bacterial concentrations as low as approximately 1 CFU/ml could be detected but a 6 hour pre-enrichment incubation period was require beforehand. The detection limit without pre-incubation was 10^4 CFU/ml and this was achieved in 60 to 75 minutes.

Labelled amperometric approaches have also been investigated and often involve a mediator, or redox probe, for improved electron transfer. A recent example of such a labelled amperometric system was reported by Lin et al (2008). Antibodies, specific for the target bacteria (*E. coli*), were immobilised onto carbon electrodes and used in the ELISA format described in Section 1.1.3.3. Secondary antibodies labelled with horseradish peroxidise (HRP) were used and electrons generated from the enzyme reaction were monitored. The mediator ferrocenedicarboxylic acid was used to enhance electron transfer to the carbon electrodes. In addition to this, electron transfer between the mediator and electrodes was further enhanced by attaching gold nanoparticles onto the surface of the carbon electrodes. The detection limit of the system was 6×10^2 CFU/ml in PBS buffer and 5×10^3 CFU/ml in milk, achieved in approximately 1 hour. Flow through systems have also been investigated based on a similar immunoassay with improved detection capabilities [Chemburu et al., 2005]. Enzyme labelled DNA has also been used in combination with an amperometric biosensors for the detection of bacteria [Elsholz et al., 2009].

Potentiometric

Biosensors based on potentiometric detection convert the reaction at the bioreceptor into an electric potential signal. A change in potential can be brought about by changes in ionic, pH or redox state. Perhaps one of the most popular and successful potentiometric designs implemented for the detection of bacteria is that of the light addressable potentiometric sensor (LAPS). The LAPS has been developed for the sensitive detection of biochemical systems by combining potentiometric detection with optical methods [Hafeman et al., 1988]. A LAPS consists of an n- or p-type silicon semiconductor coated with an insulating layer which is in contact with the reaction solution. The insulating layer is sensitive to changes occurring in the solution due to the presence of the target, for example changes in pH are often

monitored. Reactions cause a change in potential at the electrolyte-solid interface which changes the electric field within the silicon. When the silicon is activated by a light source (e.g. an LED) a photocurrent is generated which allows the change in potential to be detected. LAPSs have several beneficial features over other potentiometric devices (such as the ion-selective electrode), including potentiometric stability and the ability to measure several different reactions with a single semiconductor device by using different LEDs to address different regions of the device.

LAPS technology has been used in combination with immunoassays and enzyme labelling for bacterial detection. For example, Gehring et al. (1998) reported the detection of 7.1×10^2 cells/ml of heat killed *E. coli* O157:H7 in 45 minutes using the commercial Threshold System device (Molecular Devices Corp.). Uithoven et al. (2000) detected *Bacillus subtilis* to a limit of 3×10^3 CFU/ml in 15 minutes using a LAPS device with a flow-through system. More recently, lower detection limits have been achieved with LAPSs; for example, Ercole et al. (2002) reported the detection of 10 cell/ml in approximately 1.5 hours for *E. coli* detection. The system was later successfully implemented for the detection of *E. coli* cells in vegetable foods [Ercole et al., 2003]. The good level of sensitivity and fast detection time was retained by the group but a 2 hour pre-treatment step was required to eliminate possible interfering effects from the food sample.

Impedimetric

Impedimetric biosensors for bacterial detection generally use bioreceptors to capture target bacteria such that their presence will elicit a detectable change in impedance. Bioreceptors are typically immobilised onto or between electrodes to draw the target into the sensor's electric field. Detection is based on the principle that the presence of the target bacteria will cause changes in electric parameters which can be monitored by measuring impedance. Electrochemical impedance spectroscopy (EIS) has been widely used to carry out impedance measurements. The theory behind impedimetric detection and EIS will be discussed in detail in Chapter 2. Note that impedimetric sensors have also been developed which detect bacteria by monitoring impedance

changes associated with bacterial growth (the principles of which were discussed in Section 1.1.3.1) [Varshney and Li, 2008, Yang et al., 2004b, Yang et al., 2003]. Technically however, such sensors can not be classified as biosensors as they do not incorporate a bioreceptor. They will therefore not be discussed in this section which focuses on impedimetric biosensors in the truest sense of their definition.

Impedimetric biosensors are frequently in the form of an interdigitated microelectrode array and are most commonly used in combination with antibody bioreceptors. This setup is illustrated in Figure 1.4. For example, Radke and Alocilja (2004) have developed an interdigitated microelectrode impedimetric biosensor with immobilised antibodies to detect *E. coli*. Antibodies, specific to the target bacteria, were covalently immobilised in-between gold electrodes and EIS was used to monitor changes in impedance due to binding events between target bacteria and antibodies. The sampling process was achieved within 5 minutes and the detection limit was 10^5 CFU/ml in pure culture. The group later reported lower detection limits of 10^4 CFU/ml and carried out testing in food samples for which a detection limit of 10^7 CFU/ml was obtained [Radke and Alocilja, 2005a, Radke and Alocilja, 2005b]. Similar detection limits (10^6 CFU/ml) were reported by Yang et al. (2004b) for a comparable biosensor with antibodies immobilised onto electrodes who investigated introducing a redox probe to improve detection.
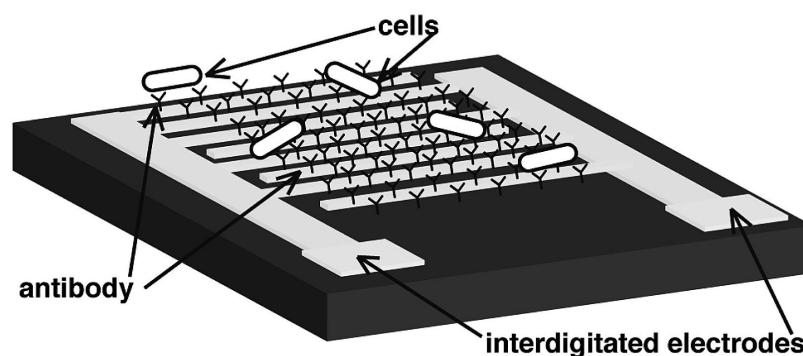
Figure 1.4. Illustration of an interdigitated impedimetric biosensor layout with immobilised antibodies present on the surface of the biosensor. Reproduced from de la Rica et al. (2009) with permission from The American Chemical Society

22

More recently, lower detection limits have been achieved. For example, Nandakumar et al. (2008) were able to detect *Salmonella typhimurium* to a level of 5×10^2 CFU/ml in 6 minutes using a standard three electrode system with immobilised antibodies on the working electrode. A novel statistical signal processing method in combination with EIS was used for an improved analytical evaluation of the results. In the recent work of de la Rica et al. (2009), detection limits of 3×10^2 CFU/ml were obtained in 1 hour using an interdigitated microelectrode array with immobilised anti-*E. coli* antibodies on the sensor surface. The group were able to show distinction between impedance measurements of live and dead cells through careful tuning of the applied AC measuring frequency. The results were attributed to differences in cell volume for live and dead bacteria and the corresponding influence on the electric field.

Impedimetric biosensors have also been investigated in combination with dielectrophoresis (DEP) techniques for the detection of bacteria to try and improve sensitivity levels. DEP is the movement of particles in a non-uniform electric field and can be used to move particles, such as bacteria, towards or away from regions of high electric field strengths. Suehiro et al. (1999) investigated the technique for bacterial detection by using DEP to capture bacteria, in pearl chain formation, onto an interdigitated microelectrode array. The resulting changes in impedance (determined by measuring conductance and capacitance between the electrodes) were used to indicate captured *E. coli* levels in approximately 10 minutes at 10^5 CFU/ml. Later they incorporated antibodies onto the sensor for selective detection of bacteria [Suehiro et al., 2006].

Impedimetric biosensors offer some advantages over amperometric and potentiometric biosensors. For example, no labels are required, thus the number of reagents and steps involved in the detection processes are reduced [Lazcka et al., 2007, Palchetti and Mascini, 2008]. They also provide a simple and cheap sensor format which could easily be incorporated for remote sensing [Lazcka et al., 2007]. However, as illustrated by the examples provided, impedimetric sensing still lacks the necessary sensitivity for bacterial detection. In addition to this, there appears to be a discrepancy amongst the literature describing the effects of bacteria on

impedance. Some groups report an increase in impedance due to the presence of bacteria in the sensor's electric field [Kim et al., 2009, Nandakumar et al., 2008, Radke and Alocilja, 2004, Shabani et al., 2008, Varshney et al., 2007] whilst others report a decrease [Suehiro et al., 1999, Varshney and Li, 2007]. This discrepancy is illustrated plainly by the conflicting results published by the same group in Varshney and Li (2007) and Varshney et al. (2007). Varshney and Li (2007) first reported on an interdigitated microelectrode array coupled with magnetic nano-particle antibody conjugates (MNAC) to detect *E. coli* O157:H7. The MNAC were used to separate and concentrate bacteria from samples. They were then concentrated into the impedance sensor's electric field using a magnet. An overall decrease in impedance due to the presence of bacteria was reported and detection limits were 7.4×10^4 CFU/ml and 8.0×10^5 CFU/ml in pure culture and beef samples respectively. Later, Varshney et al. (2007) published work on what appears to be of almost identical nature but results indicate the opposite trend: impedance increased due to bacteria. The main differences between the works were that the later paper incorporates a flow-through system to apply the sample and used slightly wider electrodes with larger gaps (25 µm versus 15 µm) but this does not adequately explain the opposing results. This discrepancy is not acknowledged or explained by the authors. The inconsistency reflects the conflicting trends in the literature which forms a focal discussion point in this work and will be examined in more detail in Chapter 6.

Conductometric

Conductance biosensors can technically be considered as a subset of impedance biosensors. They are based on the principle that the biorecognition reaction will result in a measurable change in conductance between two electrodes. Muhammad-Tahir and Alocilja (2003) developed a conductometric biosensor which uses a specially designed immunoassay to bring about the detection of bacteria such as *E. coli* and *Salmonella*. When the sandwich immunoassay forms in the presence of bacteria, a conductive polymer (polyaniline), attached to the secondary antibody, creates a conducting wire between electrodes and bacterial detection is achieved through changes in conductivity. The detection limit was reported to be

7.9×10^1 CFU/ml and is achieved in 10 minutes. Generally however, conductometric biosensors are considered to be of low sensitivity compared to other electrochemical transduction methods [Rogers and Mascini, 1998].

1.2.3 Optical Sensors

Optical based biosensors have also been widely investigated for bacterial detection. It has been said recently that optical methods generally offer slightly improved sensitivity and specificity levels compared to equivalent electrochemical methods [Lazcka et al., 2007]. Optical methods can be implemented for either direct or indirect detection approaches and can be split into four main categories based on their principle of operation: adsorption/reflection, chemiluminescence (light emission due to a chemical reaction), fluorescence (light emission when electrons return to a lower energy state having been excited to a higher energy state by an external light source) and phosphorescence (related to fluorescence – energy is absorbed by the material and released in the form of light but more slowly than with fluorescence). Labelled antibodies are commonly used in chemiluminescence and fluorescence based detection [Gehring et al., 2004, Rowe-Taitt et al., 2000]. Of all the optical methods, surface plasmon resonance (SPR; a reflection based technique) and fluorescence techniques are the most common and active in the field of pathogen detection [Lazcka et al., 2007, Parkinson and Pejcic, 2005]. Commercial SPR bacterial detection devices are available, such as the BIAcore systems from GE Healthcare. Phosphorescence techniques are generally less popular compared to fluorescent detection due to the slower processes involved [Parkinson and Pejcic, 2005].

Present limits of detection being reported for optical methods are typically in the range of 10^3 to 10^5 CFU/ml with detection times reaching under 2 hours [Gehring et al., 2004, Oh et al., 2005, Rowe-Taitt et al., 2000]. Reported drawbacks to optical techniques include non-specific interference, unsuitability for real time monitoring in turbid samples, fluorescent conjugates affecting bioreceptor reactivity and relatively expensive components [Meadows, 1996, Parkinson and Pejcic, 2005, Stefan et al., 2000].

1.2.4 Piezoelectric Sensors

Piezoelectric based sensors have also been investigated for bacterial detection but have received less attention than electrochemical and optical based methods [Parkinson and Pejcic, 2005]. They are based on the principle that when an electric field is applied to piezoelectric material, such as quartz crystal, it will vibrate at its resonance frequency. This resonance frequency is mass dependent; increasing the mass of the piezoelectric material will proportionally decrease the resonance frequency. Therefore, if the piezoelectric material is coated with a bioreceptor specific for the target bacteria, then exposure to the target and its subsequent capture onto the crystal will result in an increase in mass and a change in resonance frequency which can be monitored and used to indicate the detection of bacteria.

Limits of detection being achieved with piezoelectric methods are reaching 10^2 CFU/ml in under 2 hours and several different types of bacteria have been detected with the method including *S. typhymurium* [Pathirana et al., 2000, Su and Li, 2005], *E. coli* [Berkenpas et al., 2006, Shen et al., 2007] and *B. anthracis* [Hao et al., 2009]. As a biosensing technique, the piezoelectric method offers advantages such as label-free detection, on-line monitoring, cost effectiveness and ease of use [Leonard et al., 2003]. Disadvantages to the technique include: relatively long incubation times with bacteria, the need for several washing and drying steps, problems with surface crystal regeneration for multiple use, interference from the sample matrix and limitations on sensitivity and specificity [Ivnitski et al., 1999].

1.2.5 Summary and Future Trends

The review of biosensor technology for bacterial detection illustrates the considerable and varied amount of research being conducted in this area. However, it can also be seen that, presently, biosensors are yet to reach the necessary levels of detection in order to be comparable to conventional culturing methods. In addition to this, although detection times involving biosensors are now beginning to reach the level of hours and minutes, often a pre-enrichment period is required which increases overall detection times to almost a day.

In summary, whilst there have been notable advances in biosensor technology and they present a promising means of rapidly detecting bacteria, improvements are necessary. In terms of the bioreceptor component, an inexpensive, stable and highly specific and sensitive bioreceptor still needs to be developed. At the same time, for transducer technology, optical methods have been said to provide better sensitivity but electrochemical methods are more cost effective and simple [Lazcka et al., 2007] and so a device still needs to be developed which fully incorporates these necessary and desired aspects.

In order to meet these aims, recent trends in biosensor technology have included investigating alternate bioreceptors such as peptide nucleic acid (synthetic nucleic acid with improved hybridisation characteristics and stability), aptamers (a library of DNA or RNA strands from which high affinity nucleic acid molecules can be selected and amplified using target sequences and iterative incubation cycles) and phage display libraries (which will be discussed in more detail in Section 1.4.4) [Deisingh and Thompson, 2004, Palchetti and Mascini, 2008]. There has also been considerable progress in micro- and nano-scale systems towards developing lab-on-chip devices [Lin et al., 2008, Radke and Alocilja, 2004, Yang et al., 2004a, Zou et al., 2007]. Potential advantages of reducing the scale of biosensor devices include reduced sample sizes, low power consumption and the possibility of mass production [Lazcka et al., 2007, Zou et al., 2007]. Additionally, micro-fluidic systems can be incorporated and have been investigated to help improve analysis times [Boehm et al., 2007, Han et al., 2008, Varshney et al., 2007].

1.3 Electrical Properties of Bacteria

In the following section, the electrical properties of bacteria will be discussed in terms of their main cell constituents. Background knowledge on these aspects will help in understanding the performance of electrochemical biosensors, for which the detection principle is based on the interaction of bacteria with an electric field. Such background information will be of particular importance for impedimetric based bacterial detection, as was investigated in this research.

The basic cell constituents of a bacterium are the cell wall, cell membrane and cytoplasm as illustrated in Figure 1.5. Other structural features which some bacteria possess include: a capsule (a surrounding layer of loose polysaccharide or protein), flagella (protein 'tail' used to provide motility) and pili (hair-like structures surrounding the bacterium which are used to promote adherence to other bacteria or their host).
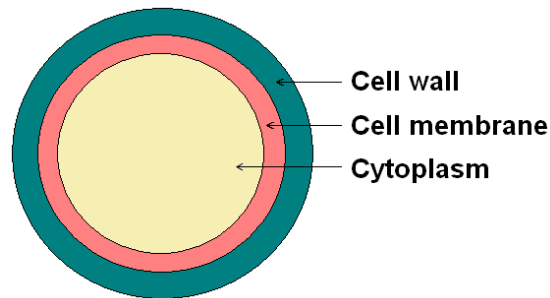
Figure 1.5. Illustration of the basic constituents of a bacterium.

1.3.1 Cell Wall

The primary function of the cell wall is to provide cell rigidity and protection. Its structure is complex and depends on the type of bacteria. Generally however, the cell wall can be classified according to two groups: Gram-positive and Gram-negative bacteria. Classification is derived from the bacterium's response to the Gram stain procedure in which Gram-positive bacteria are able to retain a crystal violet stain due to the high level of peptidoglycan in the cell wall and so appear dark blue/violet under a light microscope. In contrast, Gram-negative bacteria have less peptidoglycan and can not retain the crystal violet stain and instead take up the counterstain (safranin is often used as a counterstain in which case Gram-negative bacteria will appear pink). The differences between the two types of cell wall are illustrated in Figure 1.6.

28
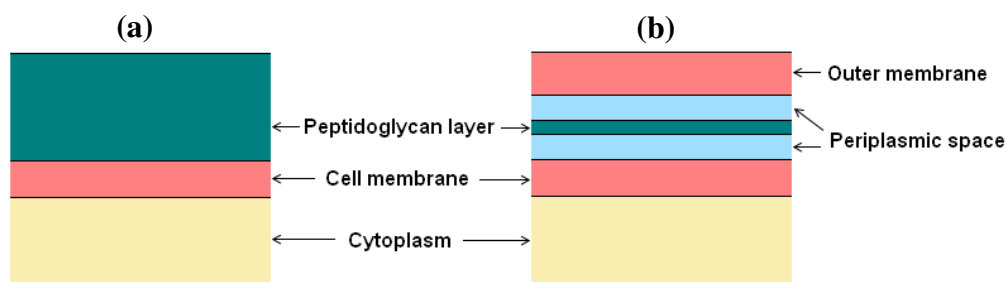
Figure 1.6. Bacterial cell wall structure for (a) Gram-positive bacteria and (b) Gram-negative bacteria.

Carstensen and his group have conducted considerable research on the electrical properties of the cell wall which has otherwise been largely neglected compared to the other main cell structures. It has been demonstrated that the cell wall behaves as an ion exchanger and as a result its electrical properties are dependent on that of the external suspending fluid [Carstensen et al., 1965]. The isolated cell wall is relatively conductive; it has a mobile ion concentration similar to that of the cytoplasm [Carstensen, 1967] and conductivity has been found to be in the region of 0.4 S/m [Carstensen and Marquis, 1986]. Due to the high resistance of the cell membrane (to be discussed in Section 1.3.2), the conductance and dielectric permittivity of bacteria at low frequencies has been attributed to the electrical properties of the cell wall [Einolf and Carstensen, 1969]. The relative dielectric permittivity of the cell wall has been quoted as 60 [Markx and Davey, 1999].

1.3.2   Cell Membrane

The cell membrane is composed of a lipid bilayer; each layer is made up of phospholipids with their hydrophobic tails pointing inwards and their hydrophilic heads facing towards either the cytoplasm or the external environment. The bacterial cell membrane is responsible for several functions including energy production, electron transfer, the uptake of metabolites and it also contains ion pumps to maintain the membrane potential. The transport of ionic species across the cell membrane is highly regulated and generally ions can not permeate the lipid bilayer unless through embedded transport proteins.

The early experimental work of Fricke et al. (1956) on *E. coli* indicated that bacteria were surrounded by a poorly conducting membrane. Thus, in contrast to the cell wall, the cell membrane is generally regarded as being non-conductive. In the presence of an electric field, charge will therefore accumulate on either side of the cell membrane (Figure 1.7) and so the membrane can be said to have capacitive properties. The capacitance of the cell membrane has been estimated to be near $1\,\mu F/cm^2$ and the thickness of the cell membrane to be between 4 and 10 nm [Schwan, 1957].
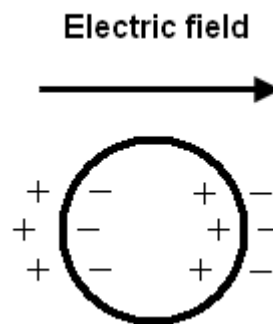
Figure 1.7. Illustration of charge accumulation on the cell membrane of a bacterium in an electric field.

Values reported for the relative dielectric permittivity and conductivity of the cell membrane vary. Markx and Davey (1999) reviewed that the relative dielectric permittivity for cell membranes have typically been found to range from 2 to 10 and cell membrane conductivity is in the region of 10^{-8} to 10^{-4} S/m.

1.3.3 Cytoplasm

The cell membrane encloses the cytoplasm. Unlike plant and animal cells, bacteria do not contain any membrane bound organelles and thus the bacterial cytoplasm can effectively be considered as a conductive water based salt solution containing ions, nutrients, proteins, the bacterial chromosome and other essential components. The reported electrical properties of the bacterial cell cytoplasm vary widely. As reviewed by Davey and Kell (1995), literature values for the conductivity of the bacterial cytoplasm range from 0.2 S/m to over 5.5 S/m and relative dielectric permittivity values range from 50 to over 400.

1.4   **Bacteriophages**

Bacteriophages (commonly referred to as phages) are viruses which specifically infect bacteria. Phages are estimated to be the most abundant biological entities on the planet [McGrath and Sinderen, 2007]. They exists anywhere that bacteria inhabit, including sea water, soil, mammal intestines, essentially anywhere where there is moisture. They were co-discovered independently by Frederick Twort in 1915 and Felix d'Herelle in 1917. Kutter and Sulakvelidze (2004) provide a good overview of phage biology and related experimental methodologies.

1.4.1   Structure

Phages exist in a variety of shapes and sizes. They can be filamentous, icosahedral or have a distinct tail and head region as illustrated in Figure 1.8 [Kutter and Sulakvelidze, 2004]. In size, they typically range from tens of nanometers to a few hundred nanometers. The main structural component of a phage is the protein capsule called a capsid which contains and protects the viral genome. The type of viral genome also depends on the phage and can be either single or double stranded DNA or RNA and in a circular or linear form [Skurnik and Strauch, 2006]. Phages contain only the genetic information required for their replication; no other components or organelles are present. The phage tail, present for some phages, is a hollow structure, the size of which again varies for different phages. For some of the more complex phages, the tail is covered by a contractile sheath. A base plate with tail fibres may also be present on the end of the tail.
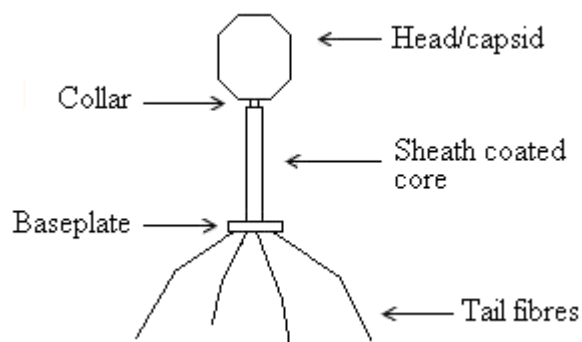
Figure 1.8. Illustration of a bacteriophage with distinct head and tail sections.

1.4.2 The Infection Process

As discussed in the previous section (Section 1.4.1) phages are essentially genetic elements in which the genome is protected by an outer protein shell. They do not contain any components for generating energy or producing proteins and so require a host in order to replicate. Phage replication is achieved through infection processes which will now be described.

The host for each phage is usually a group of bacteria; often this group comprises a subset of one bacterial species but some phages can have a particularly wide host range and are able to infect bacteria of different but related species. When a phage encounters a suitable host, the infection process can begin and one of two pathways will be followed: (1) the lytic pathway in which phages replicate within the bacterial host and eventually cause cell lysis (death) or (2) the lysogenic pathway where phages integrate into the host DNA or exists as a particle of circular genetic material in the host's cytoplasm [Kutter and Sulakvelidze, 2004]. These pathways are illustrated in Figure 1.9.
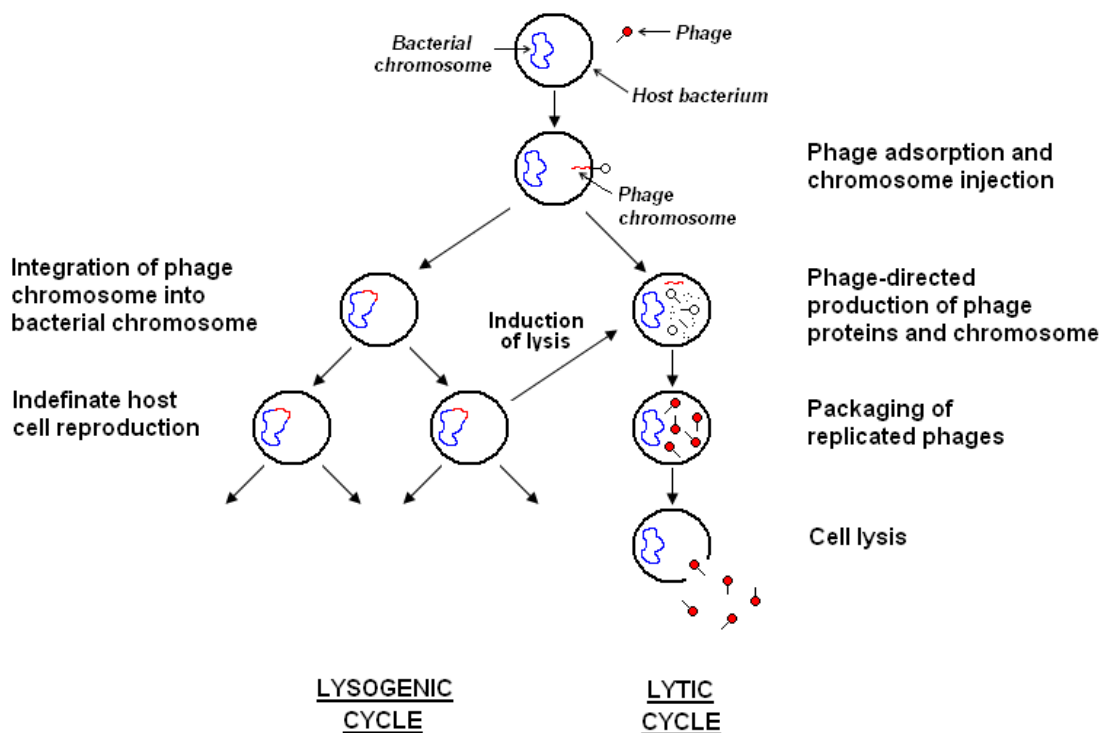
Figure 1.9. General illustration of the lysogenic and lytic pathways of phage replication.

Phages which follow the lytic cycle are termed virulent phages. The replication process begins with phage adsorption onto the surface of the host bacterium. This involves phage structures, such as the tail fibres of tailed phages, binding to specific molecules on the surface of the host. It is generally understood that phage adsorption involves two stages: first, a reversible attachment of fibres for initial host recognition and positioning and secondly, an irreversible binding. The receptors involved in phage adsorption vary depending on the phage and host and some phages require co-factors such as Ca^{2+} and Mg^{2+} or any divalent cation [Kutter and Sulakvelidze, 2004]. Once the phage has irreversibly attached to the host, the cell wall and membrane are penetrated and the phage chromosome enters into the cell. For tailed phages with a contractile sheath, contraction aids in delivering the genome into the bacterium. Next, the host cell is effectively re-programmed by the phage to synthesise phage proteins and chromosomes; a series of genes are transcribed in order to complete the process of host takeover. The phage chromosome is then packaged into the assembled protein capsids. The final step is lysis of the host cell. This releases the new phages into the surrounding environment. The timing of the lysis step is critical and is tightly controlled. For tailed phages, lysis is achieved by using a combination of a lysin (an enzyme which can breakdown the peptidoglycan of the cell wall) and a holin (a protein which assembles pores in the cell membrane, allowing the lysin to reach the cell wall). For non-tailed phages, a protein is produced which controls the peptidoglycan-processing enzyme in various ways in order to achieve cell lysis. Examples of virulent phages include the T-phages (a group of seven phages, T1 to T7, which infect *E. coli*) and bacteriophage K (which has a wide host range for *S. aureus* strains [O'Flaherty et al., 2005]).

In the case of the lysogenic cycle, after phage adsorption and penetration of the phage chromosome, the phage chromosome either integrates into the host chromosome or exists in plasmid form (a circular segment of DNA, separate from the hosts chromosomal DNA). Phage replication and cell lysis does not take place immediately; instead, the host continues to reproduce, replicating the phage chromosome as it does so such that it is present in each cell. Properties of the host bacterium are often altered by the presence of the phage chromosome. At some stage,

the lytic cycle may be induced by an agent, such as UV light. Otherwise the phage chromosome will continue to exist in this condition indefinitely. Phages which are capable of following either a lytic or lysogenic cycle are commonly referred to as temperate phages. The route taken by a temperate phage typically depends on the host physiology and environmental conditions. Examples of temperate phages include bacteriophage lambda, which is a coliphage i.e. it can infect *E. coli*, and bacteriophage Mu which has a broad host range that includes *E. coli*, *Salmonella*, *Citrobacter* and *Erwinia* [Kutter and Sulakvelidze, 2004]

The latent period is an important characteristic of a phage. It is the time from infection until the first new phages are released from the host cell. Another important parameter specific to each phage is the burst size i.e. the typical number of phages released after the infection processes. Burst size is defined as the ratio between the number of phages before and after lysis. Both the latent period and burst size are characteristic of the phage type but also depend on the host, medium and temperature [Kutter and Sulakvelidze, 2004].

1.4.3   Detection of Bacteriophage

The detection and enumeration of phages is limited by their nano-scale size as they can not be observed with conventional light microscopy like bacteria. Although phages can be viewed by electron microscopy [Kutter and Sulakvelidze, 2004], the most commonly used method to detect phages is the plaque assay. The plaque assay protocol is outlined in detail in Chapter 4, Section 4.2.2.3. It is based on the principle that when a phage encounters a host bacterium it will infect and lyse it and the released progeny phage will repeat this infection cycle with neighbouring bacteria. When this process occurs on a lawn of bacteria grown on an agar plate, a clearing will develop where the phages are lysing bacteria. The plaque size is limited by the fact that bacterial lysis will occur only for as long as the bacteria are growing. This usually results in a clearly defined circular clearing in the bacterial lawn if the ratio of phages to bacteria is suitable. Plaque assay results are illustrated later in Chapter 5, Table 5.1. To enumerate phage suspensions, samples are plaque assayed and the resulting plaques are counted and concentrations are calculated in terms of plaque forming units per millilitre (PFU/ml). The plaque assay is a simple and cost

effective means of detecting and enumerating phages. Note that it is only suitable for lytic phages.

1.4.4 Applications

Phages have been used in a wide variety of applications since their discovery. Some of their main applications are listed and described in Table 1.3. Phages have also been implemented in bacterial detection systems which will be discussed in detail in Section 1.4.4.1 to follow.

Table 1.3. Description of some of the main applications of phages.

Application	Description
Phage therapy	The application of the lytic nature of phages to treat bacterial infections. The treatment of human, animal and plant infections has been investigated.
Phage display	Peptide or protein genes are integrated into the phage genome so that they are then expressed on the surface of the phage. A phage display library can be generated consisting of phages representing in the region of 10^9 different proteins or peptides [Smith, 1985]. Such libraries can be used to identify appropriate receptors for target molecules. Applications include finding target receptors for affinity reactions, drug discovery and identifying new receptors, all of which aid in finding treatments for diseases.
Phage typing	Utilising the specificity of phages for their hosts to characterise unidentified bacterial strains.

In addition to the applications mentioned in Table 1.3, phages also have active and potential uses in the following areas: incorporation into anti-bacterial products for use in clinical settings and the food industry [Petty et al., 2007]; immobilisation onto medical sutures [Holland, 2010]; protection of plant and vegetable crops [Goodridge and Abedon, 2003]; defence against biological threat agents [Petrenko and Vodyanoy, 2003]; targeted gene delivery and vaccine delivery vehicles [Clark and March, 2006, Matsuzaki et al., 2005]. They have even been used to create ultra-small batteries [Nam et al., 2006]. In summary, it can be seen that phages have wide applications, reflecting their versatility and robustness.

1.4.4.1 Bacterial Detection

Phages have also been utilised for bacterial detection purposes through various different means which have exploited different stages of the phage infection cycle such as adsorption, the introduction of reporter genes and cell lysis. For example, perhaps the simplest means in which phages are employed to detect bacteria is by the phage amplification assay. The detection principle is briefly described as follows: phages are mixed with the target bacteria; after a suitable period of time to allow for specific phage infection, all remaining free phages are destroyed by a suitable virucide (successfully infecting phages are protected within their hosts); helper bacterial cells which can also be infected by the phages are added to the sample which is spread onto an agar plate; the original target cells then lyse and progeny phages go on to infect and lyse helper cells; this will eventually lead to the formation of plaques in the bacterial lawn where each plaque represents a target cell. An example of this approach to bacterial detection was reported by McNerney et al. (1998) who used a phage amplification assay to detect *Mycobacterium smegmatis* and *M. tuberculosis*. Low detection limits were achieved (10^2 CFU/ml) but detection times were in the region of 48 hours. The assay has been used to detect several other bacteria such as *S. typhimurium*, *S. aureus* and *E. coli* [Schmelcher and Loessner, 2008] and commercial products are also available such as the FASTPlaqueTB^{TM} (Biotec Laboratories Ltd., UK) which reduces the detection time of *M. tuberculosis* to two days instead of several weeks with conventional culturing methods.

Alternatively, instead of assaying for progeny phages after the lytic cycle, intracellular components released after phage induced bacterial lysis can also be assayed to provide a means of detecting bacteria. For example, Squirrell et al. (2002) reported on an assay in which phages were used to lyse specific bacteria and the released cell-derived AK was used to convert the supplied ADP into ATP which could then act as a substrate in the firefly bioluminescence reaction as first described in Section 1.1.3.4. This method has been used to detect *E. coli* O157 and was reported to be capable of detecting in the region of 10^2 CFU/ml in less than 1 hour.

The principle of such assays has also been investigated for implementation with biosensor technology. Neufeld et al. (2003) used amperometric measurements to monitor the release of a specific enzyme (β-D-galactosidase) from phage lysed *E. coli*. The product of the enzyme reaction is oxidised at a carbon electrode and the resulting current can be measured. A detection limit of 10 CFU/ml was reported and achieved in 6 to 8 hours. Later, the sensor was also demonstrated to successfully detect models for *B. anthracis* and *M. tuberculosis* [Yemini et al., 2007]. Potentiometric measurements have also been used: ion leakage upon phage infection was monitored by Dobozi-King et al. (2005) using nano-scaled wells and microlitre samples with a technology they termed SEPTIC (SEnsing of Phage-Triggered Ion Cascade). The detection limit for *E. coli* was 10^3 CFU/ml and was achieved in less than 10 minutes.

The immobilisation of phages onto solid surfaces and their subsequent interaction with target bacteria has also been investigated for biosensor applications [Bennett et al., 1997, Handa et al., 2008, Sun et al., 2001]. Immobilised phages have been integrated with biosensor transduction techniques such as SPR [Balasubramanian et al., 2007] and magnetoelastic sensors (similar detection principle to piezoelectric based sensors but a magnetic field, instead of an electric field, is used to oscillate the sensor) [Lakshmanan et al., 2007]. Phage immobilisation will be discussed in more detail in Chapter 5.

Until very recently, there had not been any reports found on the implementation of phages with impedimetric transduction techniques for bacterial detection. However, during the course of this project, work was published by Shabani et al. (2008) in which phages, covalently immobilised onto screen-printed carbon electrode microarrays, were used to specifically detect *E. coli* by monitoring changes in impedance. Impedance was found to increase with the initial binding of bacteria. Then, after 20 minutes, impedance began to decrease which was attributed to the onset of bacterial lysis. A detection limit of 10^4 CFU/ml was reported.

Display phages (also referred to as landscape phages, see Table 1.3) have also been investigated as bioreceptors in biosensors. They are selected so that their displayed protein binds with the target bacteria [Olsen et al., 2006, Sorokulova et al., 2005] or intracellular components of the target bacteria (such as bacteria specific enzymes) [Nanduri et al., 2007b]. Display phages have been used in combination with QCMs [Nanduri et al., 2007b, Olsen et al., 2006] and SPR [Nanduri et al., 2007a] transduction methods.

Other ways in which phages have been used to detect bacteria include: using fluorescently labelled phages [Goodridge et al., 1999, Mosier-Boss et al., 2003, Tanji et al., 2004]; the impedimetric detection of impeded bacterial metabolism and growth due to phage infection [Schmelcher and Loessner, 2008]; and through the use of reporter phages where a reporter gene carried by the phage is only expressed once introduced into the bacterium (approaches include incorporation of luciferases for light emitting reactions, ice nucleation proteins and *E. coli*-galactosidase which can be assayed for) [Goodridge and Griffiths, 2002]. An example of licensed technology which makes use of a reporter phage is the Phast Swab developed at The University of Wyoming. It is capable of detecting *E. coli* O157:H7 in approximately 10 hours.

1.4.5   Bacteriophages as Bioreceptors

Phages have the key characteristics necessary for bioreceptor functions i.e. they can recognise and attach to bacteria and do so in a specific manner. In addition to possessing this required quality for successful bioreceptor performance, phages offer several other features which could lead to improved bioreceptor performance compared to traditional bioreceptors [Handa et al., 2008, Lakshmanan et al., 2007, Shabani et al., 2008]. These include:

- High adsorption rate constants between phages and bacteria. This suggests that most collisions will result in adsorption [German et al., 2006].
- Low costs involved in production and storage of phages.
- An abundant supply of phages from natural resources.
- Phages co-evolve with bacteria meaning that phages can be found even for mutated resistant bacterial strains.

- Phages are most likely to be implemented in label free detection and so there is no need for the addition of any reactants.
- A 'cocktail' of phages could be incorporated to achieve any desired host/target range.
- Production of a high concentration phage suspension is simple to achieve and hundreds of millilitres can be produced from one phage harvest (see Chapter 4, Section 4.2.3, for protocol).
- Good stability in adverse environmental conditions such as temperature, humidity and pH (this will be discussed in more detail in Chapter 5).
- Good life time – phages will remain active for months when stored in solution. The life time of immobilised phages has yet to be fully established but is in the order of months [Verrecchia, 2007].
- Phages are likely to be stable and resistant to samples prepared from food and biological mediums (phages naturally evolve in such systems).

These potential benefits are considerable and could lead to significant advances in biosensor development. Additionally, phages have previously been shown to be amenable to immobilisation procedures, as will be discussed further in Chapter 5, and a patent is held by the University of Strathclyde for the immobilisation of viruses, such as phages [Scott and Mattey, 2003].

However, it is also important to consider possible limitations of using phages as bioreceptor elements. For example, the physiological state of the cell can affect surface molecules (as first discussed for antibody-antigen interactions in Section 1.2.1) and therefore receptor sites for phage adsorption [Kutter and Sulakvelidze, 2004]. Further to this, depending on the condition of the cells, phages may not be capable of discriminating between dead and live bacterial cells.

1.5 <u>Staphylococcus aureus</u>

The bacterial species *Staphylococcus aureus* was used throughout the project (details of the particular strain used can be found in Section 4.1.1). *S. aureus* is a spherical bacterium, approximately 0.5 to 1 µm in diameter, and typically appears in grape-

like clusters [Bremer et al., 2004]. Conditions under which *S. aureus* can grow are outlined in Table 1.4.

Table 1.4. Optimum environmental conditions for the growth of *Staphylococcus aureus* and also for toxin production. The range of environmental conditions over which *S.aureus* will grow and produce toxins is also listed. Data adapted from New Zealand Food Safety Authority (2001).

Parameter	Conditions for growth		Conditions for toxin production	
	Optimum	Range	Optimum	Range
Temperature	37°C	6 - 48°C	35 - 40°C	10 - 45°C
pH	7.0 – 7.5	4.2 – 9.3	5.3 – 7.0	4.8 – 9.0
Atmosphere	Oxygen present	Can grow anaerobically	Oxygen present	Less produced anaerobically
Water activity	0.99	0.85 – 0.99	≥ 0.90	0.86 – 0.99

In general, bacterial growth can be split into four phases: the lag phase, exponential phase, stationary phase and death phase. By enumerating bacteria over time (such as through standard bacterial plating procedures, as outlined in Section 4.2.2.2 to follow), a bacterial growth curve can be produced in which the logarithm of cell numbers is plotted against time. The form of a typical bacterial growth curve is illustrated in Figure 1.10 and indicates the four main phases of bacterial grow. In the lag phase, bacteria are adapting to their surroundings and very little growth occurs. During the exponential phase (also known as the log phase), bacteria grow by dividing into two daughter cells in a process called binary fission and the bacterial population doubles rapidly. This exponential growth is represented as a straight line on the bacterial growth curve. The slope of this straight line provides the growth rate which is dependent on the growth conditions (such as temperature and the nutrients available). Unless nutrients are continuously replenished, the growth rate slows and bacteria enter the stationary phase as a result of nutrient depletion and the build up of toxic products; the rate of growth is offset by bacterial death. Eventually the bacteria enter a death phase due to the lack of nutrients and unfavourable environmental conditions. The time taken for a bacterium to complete one binary fission, i.e. for a single bacterium to divide into two bacterial cells, is known as the generation time. Under optimal conditions (see Table 1.4), the generation time for *S. aureus* is approximately 30 minutes [Pommerville, 2006]. After overnight culturing (18 hours)

at optimal conditions, it is widely accepted that *S. aureus* are in the stationary phase of the growth curve.
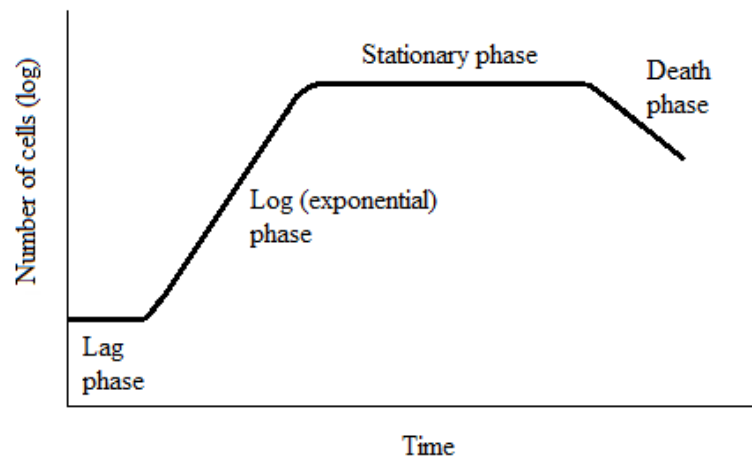
Figure 1.10. Typical growth curve for bacteria.

An important clinical characteristic of *S.aureus* is that it can produce and excrete enterotoxins. These protein toxins have a particularly marked effect on the gastrointestinal tract and cause food poisoning when consumed at high enough levels. Less than 1 µg of toxin can produce symptoms related to food poisoning (such as nausea, vomiting and diarrhoea) which is reached when *S. aureus* populations exceed 10^5 cells/g [Bremer et al., 2004]. Conditions under which toxins can be produced are summarised in Table 1.4. *S. aureus* is commonly associated with the human body and is carried by many healthy individuals. Therefore food handlers are often the main source of food contamination. In addition to this, whilst *S. aureus* can be killed at cooking temperatures, enterotoxins are difficult to destroy by heating. The rapid detection of significant *S. aureus* levels could therefore play an important role in reducing the incidence of Staphylococcal food poisoning. *S. aureus* was used as a model for the biosensor developed in this research.

1.6 Project Aims

This chapter has illustrated that conventional bacterial detection methods, although sensitive and specific, take too long to yield results (detection times are in the order of days and weeks). This is a major drawback as the fast detection of pathogenic

bacteria can be critical for health and safety reasons. There is therefore a clear need to develop a rapid bacterial detection technique. However, despite extensive and continued research in this area, emerging rapid detection methods are presently falling short of the necessary levels of sensitivity and specificity and so conventional methods remain the favoured choice.

The aim of this project is to investigate the use of phages as bioreceptors, specifically in an impedimetric based biosensor, for the sensitive and rapid detection of bacteria. *S. aureus* was chosen as the model bacterium. Several potential benefits have been identified for the use of phages over traditional bioreceptors and it is proposed that by investigating the bioreceptor performance of phages with the established impedimetric detection technique, an improved rapid detection method may be achieved. At the outset of this work, this was believed to be a novel concept. However, during the course of this research, as mentioned in Section 1.4.4, Shabani et al. (2008) published work of similar intention. However, although the principle of the work was similar, there were still notable differences between the biosensor researched in this project and that of Shabani et al. (2008), such as the electrode layout, electrode material and the approach taken to immobilise phages. In addition to this, it was proposed to combine experimental testing of the sensor investigated in this study with extensive analytical work and to conduct a survey of immobilisation procedures in order to optimise phage immobilisation.

Specific aims of the study are listed below:

- To develop a computer based model of the proposed biosensor and to utilise the model to investigate optimum sensor parameters for bacterial detection.
- To assess and compare common immobilisation methods in order to establish the most appropriate for the immobilisation of phages in bioreceptor applications.
- To investigate and analyse the developed biosensor's performance for the detection of *S. aureus* (the model bacterium chosen in this study).
- To evaluate the potential of phage based impedimetric biosensors for the rapid detection of bacteria, and in particular *S. aureus*.

Chapter 2

THEORY

In the previous chapter the various biosensor transduction methods employed for the detection of bacteria were discussed, one of which was impedimetric based transduction. Through examples in the literature it was shown that impedance measurements can be employed to detect bacteria. As outlined in the project aims (Chapter 1, Section 1.6), it was intended to use the existing principles of impedimetric based biosensors to investigate the potential of immobilised phages as bioreceptors for the detection of bacteria. Whilst it was not a specific intention to further develop impedimetric techniques in this work, it is still important to have an understanding of this mode of analysis when interpreting results. Therefore, in the following chapter some background theory is provided on the electrical aspects of impedimetric biosensors when used with liquid samples.

Basic electrical theory is first included to introduce the concept of electrical impedance. Through electrolytic theory, specific aspects of the biosensor system are then considered in more detail, such as the processes occurring in the bulk electrolyte and at the electrode/electrolyte interface when a voltage is applied to the system. A succinct summary of the relevant dielectric theory is provided with specific focus on the dielectric properties of biological material (herein, biological material defines a material that is living, has lived or is component of such a material). Electrochemical impedance spectroscopy is a technique employed to measure the impedance of a system and was implemented in this research, therefore a summary of the method is provided. A technique often used to analyse impedance is that of equivalent circuit modelling. This technique is described and its application to modelling electrode/electrolyte systems it discussed specifically. Finally, the basic principle of impedimetric bacterial detection and the biosensor design adopted in this research are outlined.

2.1 Fundamentals of Electrical Impedance

2.1.1 Direct and Alternating Currents

Current can be of two forms: direct current (DC) or alternating current (AC). DC current is the movement of electric charge in only one direction. In AC current, the flow of charge alternates direction back and forth at a frequency ω (rad/s). AC current can be expressed as a sinusoidal function:

$$i(t) = I_{max} \sin(\omega t + \varphi)$$ *Equation 2.1*

where i(t) is the current (amperes, A) at a time t (seconds, s), I_{max} is the peak value of the current and φ is the phase angle (radians) between the current and the voltage (the associated voltage, v(t), will also be of a sine wave form). The waveforms of an AC current and voltage signal are illustrated in Figure 2.1.
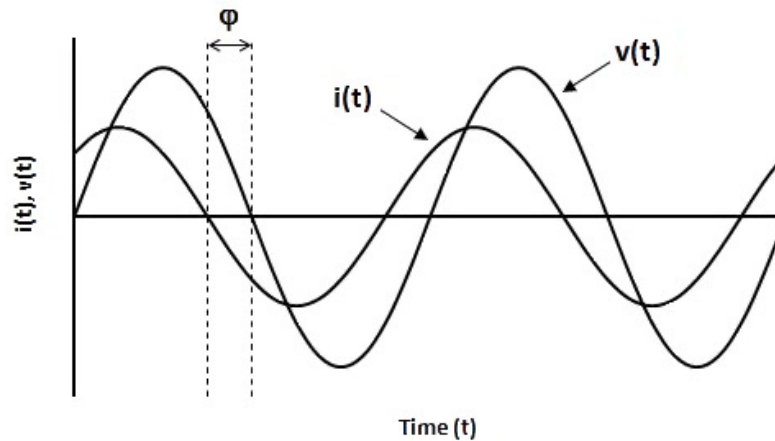
Figure 2.1. AC sinusoidal waveforms for an applied potential, v(t), and the resulting current, i(t), where φ is the phase angle between the signals.

2.1.2 Resistance

Electrical resistance, R, (ohms, Ω) is the opposition to a flow of DC current. It is defined as the ratio of voltage to current according to Ohm's law:

$$R = \frac{V}{I}$$ *Equation 2.2*

where V is the applied voltage (volts, V) and I is current. If an AC voltage is applied to a resistor, the resulting current is in phase with the voltage signal i.e. for Equation 2.1 $\varphi = 0$. The reciprocal of resistance is conductance, G (siemens, S):

$$G = \frac{1}{R}$$ *Equation 2.3*

2.1.3 Capacitance

Physically, a capacitor consists of two electrical conductors separated by a dielectric material. A dielectric material can be defined as a substance without free charges and thus is a non-conducting material. An electric field can penetrate a dielectric and when a voltage is applied across the capacitor, charge (Q; coulombs, C) is stored according to Equation 2.4 where C is capacitance (farads, F).

$$C = \frac{Q}{V}$$

Equation 2.4

A capacitor will block the flow of DC current once the capacitor is charged but will allow AC current to flow due to the frequency regulated continual charging and discharging of the capacitor. When an AC voltage is applied to a capacitor, the current signal leads the voltage signal by 90° ($\varphi = \pi/2$) and thus the waveforms are said to be out of phase.

The capacitance of a parallel plate capacitor can be related to its geometry through the following equation:

$$C = \frac{\varepsilon A}{D}$$

Equation 2.5

where ε is the dielectric permittivity of the material (farads per meter, F/m), A is the area of the electrode plate (m^2) and D is the distance between electrode plates (m). There is no such standard equation for the capacitance of coplanar interdigitated electrodes, as were utilised in this work, however various analytical expressions have been developed and will be discussed further in Chapters 3 and 6.

Permittivity is commonly described in terms of the dimensionless parameter known as relative dielectric permittivity (ε_r) or the dielectric constant:

$$\varepsilon = \varepsilon_r \varepsilon_0$$

Equation 2.6

where ε_0 is the permittivity of a vacuum (8.854×10^{-12} F/m). Permittivity indicates how a material will respond to an applied electric field and the resulting effect on the electric field, as will be discussed further in Section 2.3.

2.1.4   Impedance

Electrical impedance, Z, (Ω) is a similar concept to resistance: it is a measure of an electrical system's opposition to current, but AC rather than DC current. Thus the impedance due to capacitance and inductance must be taken into consideration in addition to resistance. Ohms law (Equation 2.2) can also be used to describe impedance, as shown in Equation 2.7, where voltage and current are both sinusoidal signals as defined in Section 2.1.1.

$$Z = \frac{v(t)}{i(t)} = \frac{V_{max}\,\sin(\omega t + \varphi)}{I_{max}\,\sin(\omega t + \varphi)} \qquad \qquad \textit{Equation 2.7}$$

Due to the involvement of sinusoidal functions, impedance is often represented by a complex number. In Cartesian form, impedance can be conveniently split into a real (Z') and imaginary part (Z'') as follows:

$$Z = Z' + jZ'' \qquad \qquad \textit{Equation 2.8}$$

where j denotes an imaginary unit ($j = \sqrt{-1}$).

The real and imaginary terms of impedance can be used to obtain the absolute value of impedance, |Z|, and the phase angle, φ, through the following relationships:

$$\left| Z \right| = \sqrt{(Z')^2 + (Z'')^2} \qquad \qquad \textit{Equation 2.9}$$

$$\varphi = \tan^{-1}\frac{Z'}{Z'} \qquad \qquad \textit{Equation 2.10}$$

The relationships of Equations 2.9 and 2.10 are illustrated in the complex plane plot of –Z'' versus Z' in Figure 2.2.
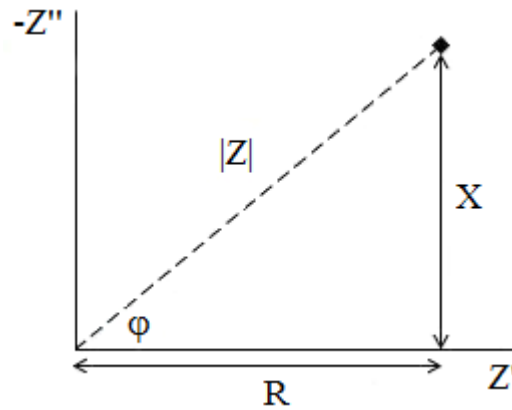
Figure 2.2. Complex plane plot illustrating vector representation of impedance (Z = Z' + jZ''). Axes are defined as real (Z') and imaginary (Z''). The real component is resistance (R) and the imaginary component is reactance (X). The absolute value of impedance (|Z|) and the phase angle (φ) are related to real and imaginary components through Equations 2.9 and 2.10.

From Figure 2.2 it can also be seen that the absolute value of impedance and the phase angle can be used to determine Z' and Z'' as follows:

$$Z' = |Z| \cos \varphi \qquad \qquad \textit{Equation 2.11}$$

$$Z'' = |Z| \sin \varphi \qquad \qquad \textit{Equation 2.12}$$

The inverse of impedance is admittance and the collective term used to describe impedance, admittance and their associated variables (such as resistance and conductivity etc) is immittance.

When considering electrical circuit elements, the impedance of an ideal resistor (Z_R) is purely real:

$$Z_R = R \qquad \qquad \textit{Equation 2.13}$$

For a capacitor, impedance is purely reactive and is dependent upon frequency. Capacitive impedance (Z_C) is represented as follows:

$$Z_C = \frac{1}{j\omega C} = -jX_C \qquad \qquad \textit{Equation 2.14}$$

where X_C is capacitive reactance and is equal to $1/\omega C$.

47

The inductor is another common circuit element and also has a purely reactive impedance. However, inductance is generally considered negligible for both biological material and the sensor system under investigation in this work [Turner et al., 1990] and so will not be considered in the following impedance theory.

Figure 2.3 shows a resistor and capacitor connected in series.

Figure 2.3. Circuit diagram of resistor (R) and capacitor (C) connected in series.

The total impedance for circuit elements connected in series is simply the sum of the circuit element impedances. Therefore, for the series RC circuit of Figure 2.3, total impedance is as follows:

$$Z = R - jX_C$$

Equation 2.15

When impedance is plotted on a graph of imaginary versus real impedance over a range of frequencies, the plot is known as a Nyquist plot. Nyquist plots are frequently used to display impedance data. Figure 2.4 illustrates a Nyquist plot for a series RC circuit.
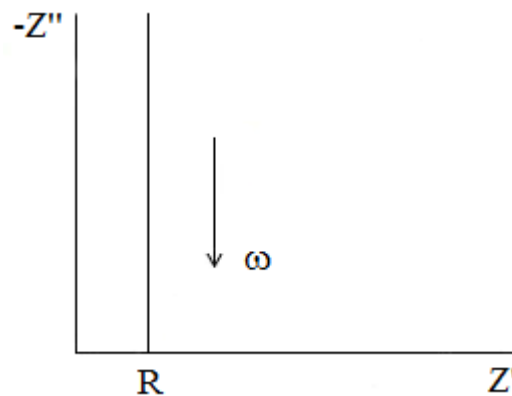
Figure 2.4. Nyquist plot for a resistor and capacitor connected in series as depicted in Figure 2.3. Axes are defined as real (Z') and imaginary (Z''). The arrow indicates the direction of increasing frequency (ω).

Figure 2.5 shows a resistor and capacitor in parallel. The total impedance for a parallel circuit is calculated by summing the reciprocal value of individual circuit

element impedances (as would be the case when dealing with resistors in parallel). This is represented in Equation 2.16.
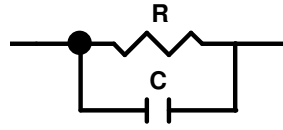
Figure 2.5. Circuit diagram of resistor (R) and capacitor (C) connected in parallel.

$$\frac{1}{Z} = \frac{1}{R} + \frac{1}{-jX_C}$$

Equation 2.16

After some mathematical manipulation of Equation 2.16 (see Appendix A), the impedance of the RC parallel circuit can be expressed in real and imaginary parts as follows:

$$Z = \frac{RX_C^2}{R^2 + X_C^2} - j\frac{R^2 X_C}{R^2 + X_C^2}$$

Equation 2.17

The Nyquist plot for the parallel RC circuit of Figure 2.5 is depicted in Figure 2.6. The Nyquist plot takes the form of a semi-circle, the centre of which coincides with the real axis. It can be seen that there are two limiting conditions: (1) under DC conditions ($\omega = 0$), impedance is equal to resistance (R) as the capacitor will block a DC current (see Section 2.1.3) and (2) as the frequency tends towards infinity, impedance approaches zero.
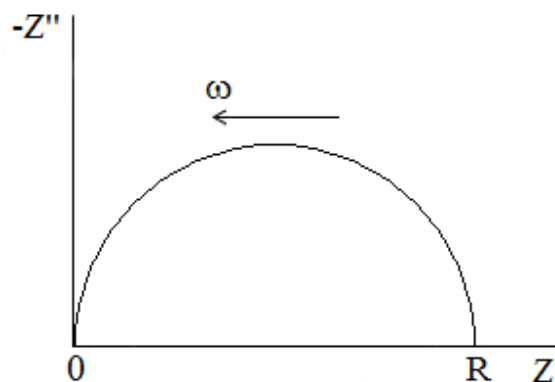
Figure 2.6. Nyquist plot for a resistor and capacitor connected in parallel as depicted in Figure 2.5. Axes are defined as real (Z') and imaginary (Z''). The arrow indicates the direction of increasing frequency (ω).

49

2.2 Electrolytic Theory

2.2.1 Bulk Conductance

The conductive solution between two electrodes is commonly termed the electrolyte. Typically, an electrolyte consists of a compound (the solute) which dissolves in a solvent, such as water. The compound dissociates into ionic species in the solvent and it is by these ionic species that charge is carried through the electrolyte. The electrolyte is therefore an ionic conductor as opposed to an electronic conductor in which charge is transported by electrons, such as in a metal electrode. Water itself is an electrolyte of low conductivity due to the following self-ionising process:

$$H_2O + H_2O \leftrightarrow H_3O^+ + OH^-$$ **Equation 2.18**
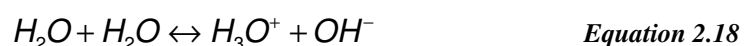
The bulk electrolyte obeys the following version of Ohm's law which is applicable for volume conductors:

$$J = \sigma E$$ **Equation 2.19**

where J is the current density (A/m^2), σ is conductivity (S/m) and E is the electric field strength (V/m). The bulk electrolyte can therefore be represented by a resistor in equivalent electrical terms (the application of this will be discussed further in Section 2.5). When a potential is applied across the electrolyte, the positive ions will move towards the negative electrode and vice versa. This movement of charged species under the influence of an electric field is termed migration. Redox reactions occurring at the electrodes arising from ionic species in the electrolyte, such as dissolved salts in water, also contribute to the bulk conductance (to be discussed in Section 2.2.2.2).

2.2.2 Electrode Processes

In addition to the bulk electrolytic conductance, complex processes also occur at the electrode/electrolyte interface. It was anticipated that this work would focus on identifying changes in the bulk solution but it could not be ruled out that effects from electrode processes would also be detected. Therefore, it is important to have a general understanding of the processes which may occur at the electrodes in order to help identify and explain any electrode polarisation impedance effects observed. Succinct outlines of electrode processes will now follow.

2.2.2.1 Faradaic and Non-Faradaic Processes

Two types of processes occur at electrodes: faradaic and non-faradaic processes. Faradaic processes involve the transfer of charge across the electrode/electrolyte interface through redox reactions. The current associated with these reactions is called a faradaic current and can be related to Faraday's law of electrolysis which states that the quantity of substance produced through chemical reactions occurring at an electrode is proportional to the quantity of electricity transferred (i.e. the total electric charge passed at the electrode). Faradaic reactions will be discussed in more detail in the following section (Section 2.2.2.2)

A non-faradaic process is a more complex concept. They occur when the electric potential, electrode area or electrolyte composition changes. In non-faradaic processes, charge does not cross the electrode/electrolyte interface but they still result in a short lived current flow in the external circuitry. The adsorption and desorption of species at the electrode surface is a non-faradaic process.

In electrochemistry, faradaic reactions are often the main interest of experiments. However, non-faradaic reactions can contribute significantly to the overall current flow and can not be ignored.

2.2.2.2 Electrolytic Reactions

When two electrodes are placed in an electrolyte solution, a potential will exist across the electrodes which is dependent on the electrode material and the electrolyte composition. This potential, developed without an external power supply, is called the equilibrium potential. If an external potential is applied which is greater than the equilibrium potential then the energy provided will be great enough to cause electrolytic reactions to occur during which electrical energy is converted into chemical energy. At the positive electrode (the anode), negatively charged ions (anions) will be attracted and will lose electrons at the electrode in a process known as oxidation. Conversely, positively charged ions (cations) will be attracted to the negative electrode (the cathode) where they will gain electrons through the reduction

reaction. Reduction and oxidation reactions are the two components of a redox reaction.

Redox reactions are faradaic processes which, as mentioned previously, are governed by Faraday's law of electrolysis. These processes are therefore affected by several factors including the mass transfer (migration, diffusion, and convection) of species to and from the electrode, the electron transfer rate at the electrode surface and other reactions such as adsorption and desorption of species at the electrode surface. These slow processes can limit current flow and are thus called rate-determining steps.

If the applied potential is not high enough to provide sufficient energy to impose electron transfer at the electrodes then redox reactions involving the ions of the electrolyte will not occur. In this case, two other processes become important: (1) the reduction of dissolved neutral oxygen and (2) the decomposition of water at the electrodes [Grimnes and Martinsen, 2000]. Again, the current can be limited by the mass transfer of oxygen and water molecules to the electrodes and since these particles are neutral, it is mass transfer by diffusion which is of importance (rather than migration, described in Section 2.2.1). Diffusion is the movement of species under the influence of a chemical gradient such as a concentration gradient. At the electrodes, reactions can occur in which these non-charged species become ionised (the process of converting an atom or molecule into an ion through the addition or removal of an electron or another ion) and a small current will flow.

Electrochemical reactions are key to the functioning of some biosensors but for impedimetric biosensors, redox reactions are not necessarily the main focus. Their contribution depends on the voltage supplied and the composition of the electrode and electrolyte.

2.2.2.3 The Electrical Double Layer

At the electrode/electrolyte interface, an electrical double layer exists due to the interaction of free, charged species in solution near the electrode surface in response to an opposite charge on the metal electrode surface. This double layer of ions can be represented by a capacitor. Thus, when a potential is applied, an external transient

current will flow but no charge will cross the electrode/electrolyte interface. This is therefore classified as a non-faradaic process. The double layer will be present as long as the metal electrode is wetted. However, the structure and therefore the capacitance of the double layer are dependent on several factors such as the electrode material, electrode surface conditions, the electrolyte composition and the applied potential. The double layer is illustrated in Figure 2.7.
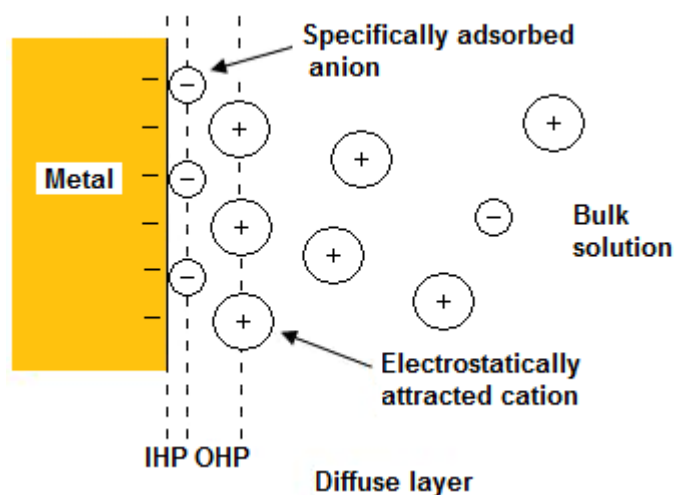
Figure 2.7. Schematic illustration of the electrical double layer. Negative ions (anions) may be specifically adsorbed onto the metal surface whilst positive ions (cations) are electrostatically attracted to the metal. The Inner Helmholtz Plane (IHP) consists of molecules and ions specifically adsorbed onto the metal surface. The Outer Helmholtz Plane (OHP) consists of ions at their closest position to the oppositely charged metal surface. Beyond the OHP is the diffuse layer which extends into the bulk solution. The diffuse layer contains ions which exchange with other ions electrostatically attracted to the metal surface. The concentration of ions in the diffuse layer decays with distance from the metal surface.

There is a diffuse layer of electrostatically attracted charged species on the solution side of the double layer in addition to which may be a layer of specifically adsorbed molecules and ions on the metal surface. These adsorbed species are not involved in any electron transfer reactions but can alter the surface charge at the electrode and thus result in a non-faradaic current. The currents associated with the electric charging of the double layer and the adsorption and desorption of species at the electrode can be significant, especially if the electrolyte contains a low concentration

of ionic species available for redox reactions (thus producing only small faradaic currents).

If no electron transfer occurs at the electrode/electrolyte interface, irrespective of the potential applied, then the electrode is said to be an ideal polarisable electrode. In reality, no electrode will behave as a true ideal polarisable electrode but for some electrode-electrolyte systems there is no electron transfer over a fairly wide electrode potential range and thus such systems approach the ideal polarisable electrode case. The impedance of an ideally polarisable electrode can be modelled by a resistor and capacitor in series. This produces a straight line, perpendicular to the real axis on a Nyquist plot, as illustrated in Figure 2.4. In contrast to the ideal polarisable electrode is the ideal non-polarisable electrode. The electrode potential of an ideal non-polarisable electrode will not change from its equilibrium potential upon passage of a current due to fast electron transfer. Whilst actual electrodes are neither ideally polarisable nor ideally non-polarisable, they tend to be closer in performance to one case or the other. The electrode polarisation impedance is dependent upon several factors including the electrode material and its surface treatment, electrode area, the electrolyte and temperature [Ferris, 1974]. Table 2.1 lists some examples of polarisable electrode materials as well as some electrodes which approach ideally non-polarisable conditions.

Table 2.1. Examples of electrodes which are polarisable and examples of electrodes which are capable of approaching ideal non-polarisability [Ferris, 1974, Potter, 1961].

Polarisable	Non-polarisable
Nickel	Silver-silver chloride
Copper	Platinum
Mercury	
Gold	

2.3 Dielectric Theory

In Section 2.2, electrolytic systems were considered. Another approach to analysing biological systems is to consider them as a dielectric system. As first mentioned in

Section 2.1.3, a dielectric can be defined as a material without free charges and is thus an electrical insulator. An applied electric field will penetrate a dielectric and cause polarisation of the material. Whilst an electrolytic system is characterised by immittance parameters obtained from applying a sinusoidal excitation, a dielectric system is characterised by permittivity or capacitance and a step waveform is applied. In non-ideal dielectrics, currents can be generated by both conductivity and polarisation effects.

Biological materials can be considered as a non-ideal dielectric as they have both electrolytic and dielectric properties i.e. they can dissipate and also store energy. They can therefore be regarded as either a conductor or a dielectric and the passive electrical properties of the material can be characterised by both conductivity and capacitance respectively. If being considered as a conductor, complex conductivity ($\sigma^* = \sigma' + j\sigma''$) is used to describe biological materials which takes into consideration some capacitive properties. Conversely, if being treated as a dielectric, complex permittivity ($\varepsilon^* = \varepsilon' + j\varepsilon''$) is used to describe a biological material as a dielectric with losses. Losses are due to the conductivity associated with charge carriers when an electric field is applied. Permittivity data is often used in the study of biological systems, including cell suspensions.

Much of the dielectric characteristics of a material can be related to the response of dipoles within the material. An electric dipole is present when opposite charge is separated by a small distance; this can be a permanent characteristic of a molecule (such as with polar water molecules and many proteins) or induced by the application of an electric field. When an external electric field is applied to a material, dipoles are either formed or the permanent dipoles present will re-orientated to align with the electric field and the material is said to be polarised. Dipoles are characterised by their dipole moment. Polarisation (P) and permittivity are related through Equation 2.20 where E is the electric field strength. Equation 2.20 illustrates that high polarisation equates to high permittivity.

$$P = (\varepsilon - \varepsilon_0)E \qquad\qquad \textit{Equation 2.20}$$

2.3.1   Relaxation and Dispersion

Polarisation does not occur instantaneously. At high frequencies, this means that if there is not enough time for charges to re-orientate according to the applied electric field, then polarisation and permittivity will decrease. This introduces an important characteristic of dielectric measurements known as relaxation. When a system is excited with a step function signal and then allowed to relax, the resulting phenomena are related to relaxation processes. These processes occur in the time domain and are described in terms of relaxation time.

Relaxation can also be examined in the frequency domain where the relaxation concept is considered in terms of dispersion. On a plot of permittivity versus frequency, a single dispersion is characterised by a transition of permittivity to a lower value and is associated with one relaxation time. The transition has a characteristic frequency and corresponds to the fact that complete relaxation is no longer possible at the higher frequencies.

Relaxation times and dispersions are dependent on the polarisation mechanism. Biological material has been found to exhibit three major dispersions, each of which represent a type of relaxation occurring over a specific frequency range and are related to different polarisation mechanisms [Schwan, 1957]. These dispersions are termed α, β and γ dispersions and are represented on a plot of real permittivity (ε') versus frequency as illustrated in Figure 2.8. Typically, the permittivity of biological materials decreases with increasing frequency due to the reducing ability of charges to follow the changing electric field. Note that there is a corresponding increase in conductivity for regions of decreasing permittivity.
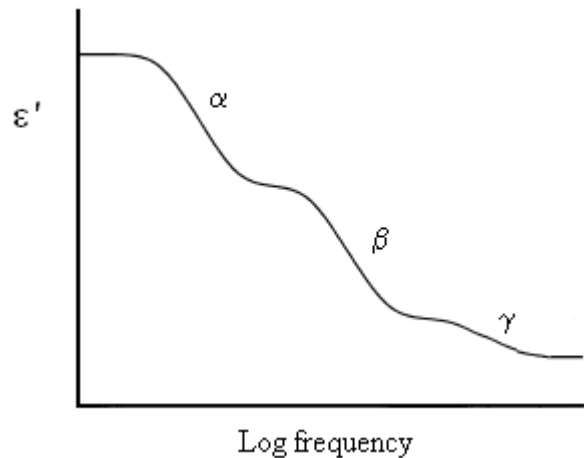
Figure 2.8. Real permittivity (ε') as a function of frequency. The three main dielectric dispersions for biological tissues are illustrated (α, β and γ).

The higher permittivity of biological material at low frequencies is explained by the fact that there is sufficient time for charge to accumulate and discharge at the cell membrane, resulting in large capacitive effects. Current will therefore pass through the extra-cellular medium and not through the cells. The measured conductivity at these low frequencies will also reflect this. Since α, β and γ dispersions may well be relevant over the frequency range analysed in this work, these dispersions will now be discussed briefly.

The α dispersion occurs at low frequencies (approximately mHz to a few kHz) and is mainly attributed to counterion polarisation due to ionic diffusion in the electrical double layer formed at the cell membrane/electrolyte interface (the accumulation of charge at the cell membrane and associated capacitance was first discussed in Chapter 1, Section 1.3.2). Under an applied electric field, counterions are considered to move laterally along the cell surface.

The β dispersion dominates in the radio frequency range (typically between tens of kHz to hundreds of MHz) and is due to the structure of the cell membrane and the associated capacitive charging. Essentially, as frequency increases, the time available for charge to accumulate at the cell membrane interface is reduced, the cell capacitive reactance decreases and a corresponding reduction in permittivity is

exhibited. Current starts to penetrate the intracellular medium and there is therefore an associated increase in conductivity. Due to the heterogeneous nature of biological materials, the relaxation process known as the Maxwell-Wagner effect will occur. Maxwell-Wagner interface relaxation will occur in any medium in which the current must pass through an interface between two different dielectrics and is related to the interface single layer surface charge (not to be confused with the double layer charge at wet interfaces for which counterion effects occur in addition to the Maxwell-Wagner effects).

At high frequencies (microwave frequencies i.e. from hundreds of MHz to hundreds of GHz), γ dispersion occurs. This dispersion is mainly due to dipolar water molecules which will re-orientate on the application of an applied electric field and thus a dipolar relaxation occurs. This is relevant since the majority of biological materials are made up of water. Water molecules have a relaxation frequency of approximately 25 GHz. Dipolar relaxation can also occur for proteins and other polar macromolecules. At these high frequencies the cell membrane capacitance is effectively short-circuited and current can therefore pass through the membrane resulting in an increase in conductivity. It should be noted that within each dispersion (α, β and γ), multiple relaxation processes may be occurring.

Based on this theory, the low and high frequency current paths can be summarised as illustrated in Figure 2.9. At DC and low frequencies, current is unable to penetrate the non-conductive cell membrane and so predominately travels through the extracellular medium. At higher frequencies, charged species no longer have sufficient time to accumulate and the cell membrane does not become fully charged. Under these circumstances the cell membrane is effectively short-circuited and current can penetrate the cell. The intracellular properties therefore become more important and influence measurements.
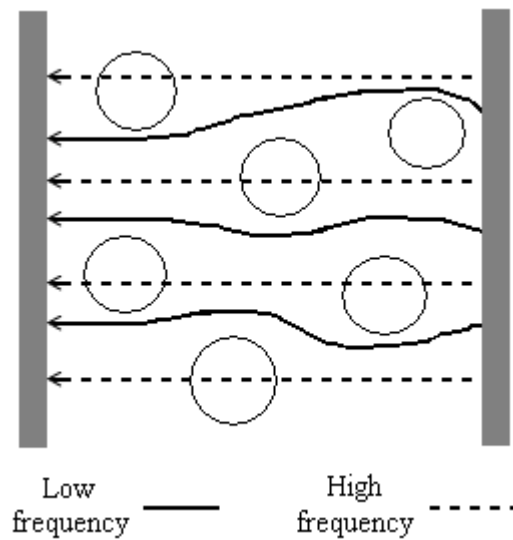
Figure 2.9. Low and high frequency current paths in a cell suspension between two electrodes.

It should be noted that whilst the term biological material is useful when describing general dielectric properties, the majority of studies from which the above theory has been derived have focused on human cells. Human cells are classified as eukaryotic cells, i.e. they have a nucleus. Bacterial cells are prokaryotic cells and do not have a nucleus and generally do not contain any other intracellular organelles. Another significant difference between human and bacterial cells is the cell wall which is present for bacterial cells, as mentioned in Chapter 1 (Section 1.3.1), but absent for human cells. These factors will influence the dielectric data but the electrical properties of bacterial cell suspensions still exhibit characteristics of the general dielectric behaviour of biological material over the frequency range commonly used to analyse biological bacterial (100 Hz to 10 MHz) [Schwan, 1957].

2.4 Electrochemical Impedance Spectroscopy

Electrochemical impedance spectroscopy (EIS), or just impedance spectroscopy, is a technique used for measuring the impedance of a system. The data obtained can be used to provide information on the substance between the electrodes and/or the electrochemical reactions occurring at the electrodes. EIS involves applying a small AC voltage signal to the system over a range of frequencies (typically within 10^{-4} to 10^7 Hz) and then measuring the resulting current response (both magnitude and phase). From these measurements, impedance values can be calculated and presented

in terms of magnitude and phase angle variations with frequency (Bode plots) or plots of imaginary versus real impedance components (Nyquist plots). These terms are interrelated as described in Section 2.1.4. The data can then be used to interpret and analyse the system. The main advantage of EIS over other techniques (for example cyclic voltammetry) is the requirement of only a very small voltage excitation signal, thus the properties being measured are relatively unaffected by the measuring process. An instrument called an impedance analyser can be used to perform EIS.

Conventional applications of EIS include the investigation of corrosion processes, electrodeposition and coating evaluations. More recently, EIS has found application in the field of bioimpedance. For example, EIS has been used to characterise tissues [Wegener et al., 1996], investigate biological molecule interactions [Katz and Willner, 2003] and in biosensor development [Radke and Alocilja, 2004, Yang et al., 2004a]. A common approach to analysing EIS data is with equivalent circuit modelling which will be described in the following section.

2.5 <u>Equivalent Circuit Modelling</u>

The impedance obtained from EIS is an overall impedance; it is a result of contributions from all the processes occurring in a system, that is all faradaic and non-faradaic processes. A useful means of breaking down the data to reflect these different processes is through equivalent circuit modelling (ECM). In this section the theory behind ECM will be demonstrated through example; mathematical proofs are not provided.

ECM is based on the principle that the experimental impedance data can be replicated with electrical circuit elements. Elements are chosen to best explain the actual physical and chemical processes occurring. The experimental data is computer fitted to a proposed equivalent circuit from which parameter values are extracted. In the case of biosensor design, ECM can be used to determine the elements which are most sensitive to changes due to the presence of the target analyte.

The Randles equivalent circuit is commonly used for modelling EIS data obtained from an electrochemical cell (a two electrode system separated by an electrolyte). This situation is comparable to that of a basic interdigitated electrode array immersed in a conductive solution, as is the case in this project. The Randles equivalent circuit is displayed in Figure 2.10.
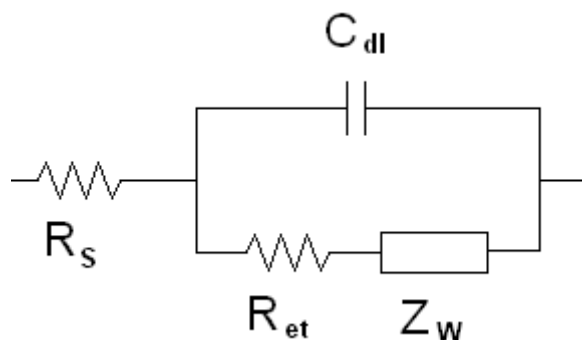
Figure 2.10. The Randles equivalent circuit. This circuit is commonly used in ECM to represent electrochemical systems. R_S is the bulk solution resistance, C_{dl} is the double layer capacitance at the electrode/electrolyte interface, R_{et} represents the electron transfer resistance at the electrode/electrolyte interface and Z_W is Warburg's impedance used to account for the diffusion-limited processes.

The Randles equivalent circuit includes a resistor corresponding to the bulk solution resistance (R_S) which obeys Ohm's law, as first mentioned in Section 2.2.1. This is in series with a parallel combination. The parallel combination consists of a capacitor to represent the double layer effects at the electrode/electrolyte interface (C_{dl}) in parallel with the series combination of a resistor, corresponding to the electron transfer resistance at the electrode/electrolyte interface (R_{et}), and Warburg's impedance element (Z_W). Warburg's impedance is incorporated to represent the limiting process of reaction component diffusion through the solution as discussed in Section 2.2.2.2. Together, R_{et} and Z_W represent the faradaic impedance of the system and in combination with C_{dl}, the electrode processes are characterised, which is in series with the bulk effects (R_S).

Rather than analysing an equivalent circuit by deriving its equation, it is simpler to present the equivalent circuit impedance in the form of either a Bode plot or a Nyquist plot. This also allows comparison to EIS data. Typical Bode plots and a

Nyquist plot for the Randles equivalent circuit are displayed in Figure 2.11 and Figure 2.12 respectively.
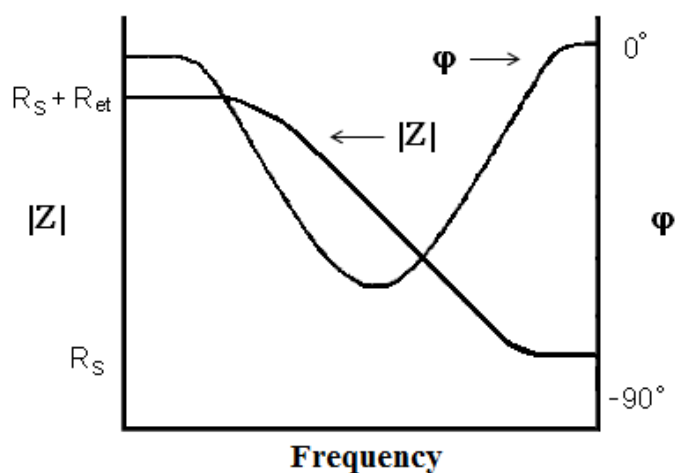
Figure 2.11. Bode plots of absolute impedance (|Z|) and phase angle (φ) for the Randles circuit model. Plateau regions indicate $R_S + R_{et}$ and R_S where R_S is the bulk solution resistance and R_{et} is the electrode transfer resistance.
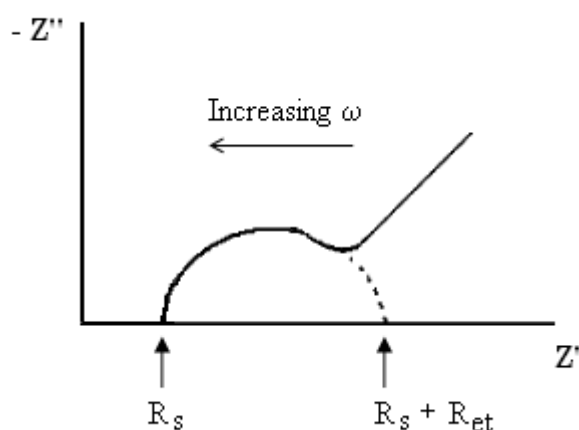
Figure 2.12. Nyquist plot for the Randles circuit model. Intercepts of the semicircle portion on the real impedance axis (Z') indicate values for the bulk solution resistance (R_S) and the electron transfer resistance at the electrode/electrolyte interface (R_{et}). The linear portion of the plot indicates the influence of Warburg impedance.

Parameters relating to the circuit are displayed on the plots. Examining the Randles circuit (Figure 2.10), it can be seen that at very high frequencies the capacitor will be short-circuited and impedance of the system is controlled by the bulk solution resistance. At very low frequencies, the capacitor will behave as an open-circuit and

this arm of the parallel component will effectively be eliminated. In this case, if no Warburg impedance is present then the circuit impedance becomes the sum of the two resistors: $R_S + R_{ct}$. Over the intermediate frequency range, the double layer capacitor will have an effect and impedance will decrease as frequency increases (as demonstrated through Equation 2.14).

If Warburg impedance is to be incorporated into the model (due to dominating diffusion effects) then the circuit's impedance behaviour is not quite as simple. It can be shown (but is not presented here) that Warburg impedance will result in a current 45° out of phase with the applied voltage. On a Nyquist plot this will produce a straight line at 45° to the real axis for which impedance increases with increasing frequency. The effect of Warburg impedance on the circuit impedance is illustrated in Figure 2.12 which shows the plot to have both semicircle and straight line portions. The semicircle portion at higher frequencies corresponds to processes in which electron-transfer at the electrode is the rate limiting process. At lower frequencies, when the straight line portion is observed, processes are limited by diffusion. The overall influence of the Warburg impedance will depend on system parameters such as solution conductivity and on the electrode reactions. For example, for very fast electron transfer processes only the linear portion may be present due to the dominating Warburg impedance effects.

The Randles circuit model is able to represent some of the processes occurring in an electrode/electrolyte system. However, it is just one example of a possible equivalent circuit representation and in theory the experimental data can be modelled by more than one circuit design. It should also be pointed out that whilst it is desirable to describe a system in terms of standard, physically realisable circuit components (i.e. resistors and capacitors) this is not always possible, as illustrated by the inclusion of Warburg impedance in the Randles circuit.

The constant phase element (CPE) is another example of a conceptual circuit element which can sometimes better model the data. A CPE models the behaviour of an imperfect capacitor. The impedance of a CPE is as follows:

$$Z_{CPE} = \frac{1}{A(j\omega)^n}$$

where A is a constant parameter related to properties of the electrode surface and electroactive species and n is also a constant with a value between -1 and 1. As the name implies, the phase angle of the CPE impedance is independent of frequency. The value of this phase angle is equal to: $-90° \times n$. EIS data can sometimes be better modelled when the double layer capacitor is replaced by a CPE to reflect a non-homogenous double layer nature. For example, it was mentioned in Section 2.2.2.3 that the impedance of an ideally polarisable electrode can be modelled by a resistor and capacitor in series which produces a straight line, perpendicular to the real axis on a Nyquist plot. However, in reality, perpendicular lines are not observed and lines are often at lower angle with respect to the real axis as illustrated in Figure 2.13. The CPE is used to describe this behaviour and Figure 2.13 illustrates that the value of n in Equation 2.21 dictates the angle. Pure capacitance is represented when $n = 1$, Warburg impedance is demonstrated for $n = 0.5$ and pure resistance when $n = 0$.
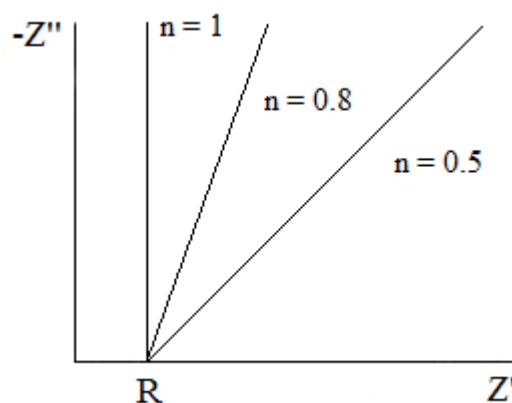
Figure 2.13. Nyquist plot for an ideally polarisable electrode in the presence of a CPE.

In the presence of faradaic reactions, the CPE can account for a depressed semicircle on a Nyquist plot i.e. when the centre of the semicircle portion is below the real axis. The introduction of a CPE can be particularly useful for systems involving interactions of biomolecules and biological substances at the electrode interface and electrode surface adsorption, as it can account for inhomogeneities in the double

layer and associated distribution of relaxation times [Bardea et al., 2000, Creager and Wooster, 1998, Moulton et al., 2004, Omanovic and Roscoe, 1999].

Under certain circumstances it may be possible to simplify the Randles circuit. For example, in biosensor applications a redox probe is often added to the system. In such cases the presence of Z_W and R_{ct} are of particular importance. However, when not dealing with a redox probe and when a suspension of low ionic concentration is used, Z_W and R_{ct} are infinitely high and so they can effectively be removed from the model. The equivalent circuit simplifies to a resistor and capacitor in parallel (R_S and C_{dl}) to respectively account for bulk and non-faradaic impedance only.

ECM has been widely implemented in the analysis of biosensors and many different circuit designs have been generated. Varshney and Li (2009) provide a review of the equivalent circuit models used to represent interdigitated microelectrode arrays for the impedimetric detection of bacterial cells and at least seven different designs were identified. ECM has also been used to represent bacteria; the cell membrane and cytoplasm can be modelled by a capacitor and resistor respectively.

2.6   <u>Overview of Biosensor Design</u>

As outlined in the project aims (Chapter 1, Section 1.6), this research focused on investigating the performance of immobilised phages as bioreceptors in a rapid bacterial detection device. Phages were introduced in Chapter 1, Section 1.4 and their potential for bioreceptor performance was outlined in Section 1.4.5.

It was decided to use an impedimetric based detection technique for the investigation. Reasons for this included the relatively simple device structure, access to appropriate measuring equipment, no redox probes are required and, as outlined in Chapter 1, Section 1.2.2, this technology had already been proven to be capable of detecting bacteria. This last factor was important for ensuring that bioreceptor functionality could be made the focus of the investigation and would also allow comparisons to be made with other bioreceptors through published literature. In addition to this, at the project outset, phages had not been implemented with

impedimetric transduction for bacterial detection and so the combination was considered novel at the time. However, as mentioned previously, a paper was published during the course of this work by Shabani et al. (2008) which reported on an impedimetric biosensor with immobilised phages.

The basic principle of the proposed biosensor is illustrated in the schematic diagram of Figure 2.14.
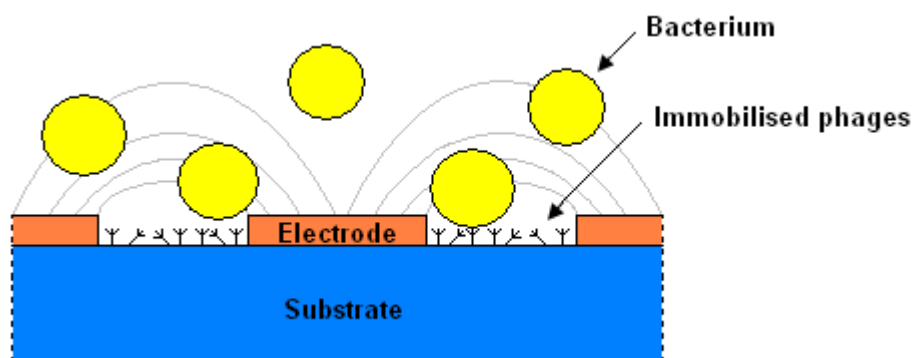
Figure 2.14. Schematic representation of the proposed biosensor. Phages are immobilised onto the substrate in-between electrodes. Phages are chosen so that they will specifically bind with the target bacterium. In doing so, bacteria are brought into the sensor's electric field (illustrated by the grey semi-circular lines). Impedance measured from the sensor should then be altered according to the theory outlined in this chapter.

A layer of phages is immobilised onto the sensor's substrate surface, in-between the electrodes. The phages are chosen so that they are specific for the target bacterium. On interaction with a bacterium, phages bind with bacteria, capturing them in the sensor's electric field. As outlined in this theory chapter, biological material, including bacteria, have dielectric properties which can be detected and thus the impedance measured from the sensor should be altered accordingly. The approach intends to measure changes in the bulk electrolyte between the electrodes (another approach would have been to focus phage immobilisation onto the gold electrodes and monitor changes occurring at the electrode/electrolyte interface for which the theory outline in Section 2.2.2 would have been of most relevance). It should be noted that the single bacterial cell model illustrated in Figure 2.14 considers a simplified model of *S. aureus* in order to create a foundation platform for the work.

In reality, *S. aureus* are likely to form clusters, as first mentioned in Section 1.5. The effect of this is considered in the computer based modelling work presented in the following chapter (Section 3.1.2.2) in which the biosensor's design is investigated. Details of the sensor's physical parameters such as materials and dimensions will also be discussed in the following chapter.

Chapter 3

BIOSENSOR MODELLING AND DESIGN

Computer-aided engineering (CAE) integrates the design and manufacturing of an object such that the complete process is controlled using modern computer technology. Engineering problems can be designed, simulated and analysed with CAE software which is now a well established tool in both industry and academia. One of the main benefits of CAE is that it allows the optimisation of a component or device to be carried out through theoretical modelling. This eliminates the need to repeatedly manufacture and test components and can thus significantly reduce the time and costs involved in the design process.

The previous chapter outlined the theory behind the impedimetric biosensor to be developed in this research. Here, CAE modelling software was used prior to manufacturing to aid in sensor development. The ultimate aim of the CAE work was to further the understanding of bacterial detection by electrical means and to use the modelling results to determine an optimum sensor design for improved sensitivity.

In brief, this chapter will first outline the computer based model of the sensor which was developed and will then detail the sensor's response to bacteria based on this model. The results of the sensor optimisation are then presented in which sensor topology and measuring conditions were investigated. Finally, an overview of the sensor design which was decided upon, based on the optimisation work, will follow, detailing the finalised dimensions and sensor materials along with the chosen fabrication method. The experimental testing of the resulting sensors will be discussed in Chapter 6.

3.1 Biosensor Modelling

There has been little work published on the modelling of biosensors for the detection of bacteria. A brief study was reported by Srinivasan et al. (2006) in which a

computer based three-dimensional finite element (FE) model was created of an impedimetric biosensor for the detection of *E. Coli*. Two electrodes were included in the model, along with simple ellipsoids to represent bacteria. Changes in impedance were computed as various parameters were altered such as the position and orientation of bacteria and the bacterial concentration. Although the model incorporated the effects of both permittivity and conductivity, the bacterium model was simplified by not including the cell wall and membrane of *E. coli* cells (only the cell cytoplasm was considered). Electrodes were also simplified by approximating zero thickness and physical characteristics of the sensor were not investigated in the study.

Radke and Alocilja (2004) also used a FE analysis method to simulate the electric field of a biosensor for the detection of *E. coli*. The modelling work was supplementary to experimental results and although they stated that the electrode geometry was altered in their FE analysis to determine optimum parameters for bacterial detection, details of the methodology and results of the optimisation work were not reported. Similarly, de la Rica et al. (2009) used FE modelling to analyse the electric field distribution between electrodes for the detection of bacteria. Analytical values were found to compare well to experimental results but the modelling work was not used to further investigate the biosensor design.

ECMs of biosensors have been reported in which electrical components are used to represent the biosensor's behaviour [Radke and Alocilja, 2004, Varshney et al., 2007, Yang et al., 2004a]. However, these models have primarily been used as a means to describe and explain experimental data which have been fitted to a proposed ECM.

There has been significant work published on the modelling of suspensions of microorganisms, including bacteria. Early examples of theoretical models include the work of Fricke (1953) and Asami et al. (1980). Initially, a simple shell model was adopted in which the conductive cell cytoplasm was enclosed by an insulating cell membrane. More complex multi-shell models have since emerged to incorporate

other cellular components such as the cell wall and periplasm [Bai et al., 2006, Castellarnau et al., 2006, Raicu et al., 1996]. Early models were used to determine values for cell membrane thickness [Fricke, 1925]. More recently, models have been used in studies of biological cells under dielectrophoresis [Huang et al., 1992] and for investigating electroporation and inactivation of cells by pulsed electric fields [Pavlin and Miklavcic, 2003, Timoshkin et al., 2006a]. As with biosensors, biological cells have also been modelled using ECMs in which their response to electric fields was investigated [Campbell et al., 2006, Schoenbach et al., 1997].

Despite continued progress in the modelling of cell suspensions, there has been little work reported on combining bacterial models with a biosensor model to investigate and optimise sensor sensitivity. Typically the dimensions of biosensors utilised in experimental work are not discussed or justified other than to acknowledge the intention to have the sensor's electrodes on the same scale as the target bacteria i.e. micro-scale dimensions. Given that the biosensor's electrical parameters are dependent on these dimensions, a more detailed investigation into the optimisation of the sensor could prove to be important in overcoming the present shortcomings of biosensor sensitivity for bacterial detection as highlighted in Chapter 1.

It was therefore decided to carry out a computer based modelling investigation of the biosensor, using CAE software, to determine how fundamental aspects of the biosensor's design, such as electrode width and spacing, might be optimised to improved bacterial detection. A description of the model and results of the optimisation will now follow. The effect of altering the dielectric permittivity of the external medium and substrate material on sensor sensitivity were also investigated.

3.1.1 The Electrostatic Model

CAE is conducted using specialised software. In this study, the FE software package ELECTRO, version 6.2 (Integrated Engineering Software, Canada), was used to create and analyse the biosensor model. ELECTRO is a two-dimensional electrostatic field simulator. Although the actual sensor will be tested under an AC voltage over a wide frequency range, it was decided to begin the modelling work with a simplified two-dimensional DC analysis.

CAE tasks are often distinguished into three main steps: pre-processing, solution and post-processing. In the pre-processing step, the geometric model is created and user defined boundary parameters are set, including material properties and applied voltages. Parameters of the model, such as electric field strength and surface charge density, can then be solved for using the software's solution method which is typically based on a FE or boundary element (BE) analysis. Finally, in the post-processing step, data is collected from the model and results are analysed. The model and analysis of the biosensor will now be described following this three part structure.

In the pre-processing step, the model geometry was initially guided by impedimetric biosensors reported in the literature, such as those mentioned in Chapter 1, and which will be discussed further in Section 3.2.2. An interdigitated microelectrode array was modelled and a schematic top view section of this design is shown in Figure 3.1. In the modelling work, an ideal situation was assumed in which m bacteria are aligned in n rows in the gap, G, between electrodes. The two-dimensional sensor model was based on the cross-section indicated in Figure 3.1 by the dashed line along the single bacterial row ($n = 1$) with four bacteria ($m = 4$).
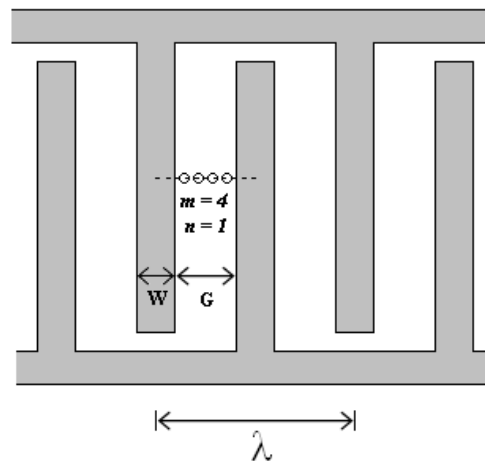
Figure 3.1. Schematic top view of a section of an interdigitated electrode array with four bacteria ($m = 4$) in a single row ($n = 1$) across the electrode gap, G. The electrode width, W, is also indicated, as is the spatial wavelength, λ, which is the distance between two adjacent fingers of the same electrode. The dotted line indicates the cross-section on which the two-dimensional model is based (shown in Figure 3.2).

The resulting topology of the model is shown in Figure 3.2. This is a half wavelength model where one wavelength (λ) is the distance between two adjacent fingers of the same electrode. Modelling only half a wavelength simplified the model to a manageable size yet it still represents the real situation. The model included a polymer layer between electrodes onto which the bioreceptors could be immobilised. For the modelling work, it was assumed that the majority of the bioreceptors would be present between the electrodes as this was the focus of the immobilisation work that is presented in Chapter 5.
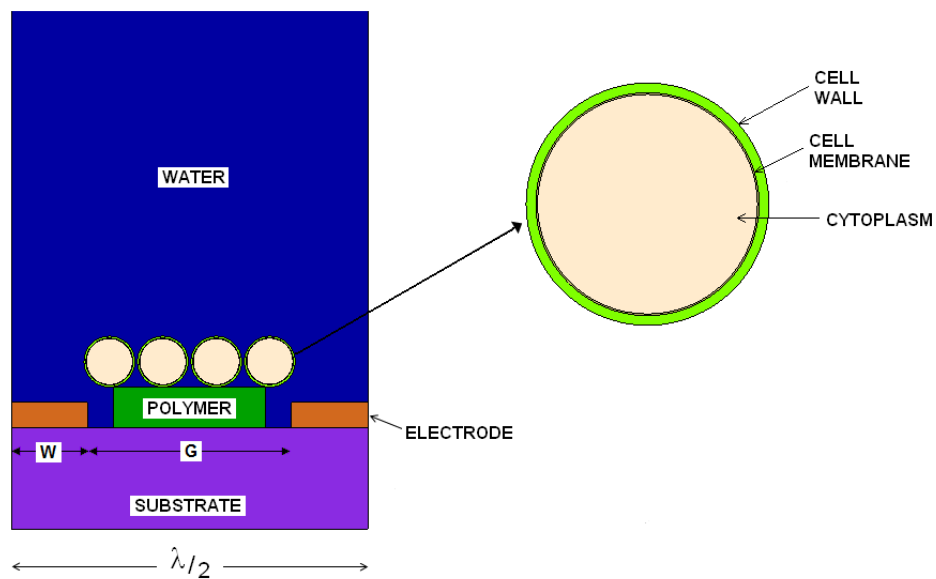
Figure 3.2. The half wavelength (λ/2) model of the sensor with four bacteria located in the gap, G, between electrodes on the sensor's polymer substrate (PMGI in the case of the actual sensor). The model is presented in scale. An enlargement of the bacterium model is also shown which illustrates the cell wall, membrane and cytoplasm.

Initially, sensor geometries were set with an electrode width (W) of 3 µm and gap of 4 µm. These dimensions were chosen as they had previously been found to yield a sensor sensitive to the detection of bacteria based on the experimental work by Radke and Alocilja (2004) and thus seemed a logical starting point. These dimensions were also within the capabilities of standard photolithography fabrication techniques which could be used to create the sensors.

The dimensions of other sensor parameters are listed in Table 3.1. The thickness of the electrode and polymer layer were based on estimates provided by Dr David Hutson [personal communication, 2008] who has considerable experience in photolithography and electrode fabrication techniques and who later made the sensors. The estimated values (0.5 µm and 0.8 µm for electrode and polymer thickness respectively) were close to actual values determined after the sensor had been fabricated (approximately 0.2 µm and 0.7 µm for electrode and polymer thickness respectively, as measured by a Dektak surface profiler by Dr David Hutson). The difference in polymer and electrode height is intrinsic to the fabrication procedure.

Table 3.1. Fixed values of the model's dimensions and relative dielectric permittivity values.

Dimensions	
Electrode thickness	0.5 µm
Polymer thickness	0.8 µm
Substrate thickness	2 µm
Total model height	30 µm
Cell radius	0.5 µm [Holt et al., 2000]
Cell wall thickness	40 nm [Beveridge and Graham, 1991]
Cell membrane thickness	7 nm [Markx and Davey, 1999]
Relative Dielectric Permittivity	
Cell wall (ε_W)	60 [Markx and Davey, 1999]
Cell membrane (ε_M)	6 [Markx and Davey, 1999]
Cell cytoplasm (ε_C)	80 [Markx and Davey, 1999]
Substrate (ε_{SB})	11.9
Polymer (ε_P)	4
Suspension (ε_S)	80

The bacterium model, also shown in Figure 3.2, was a two-shell model which accurately incorporated both the cell wall and cell membrane of *S. aureus* on which the model was based. Dimensions were assigned from literature values which are displayed in Table 3.1. There was a minimum gap of 0.05 µm between bacteria to avoid sharp contact angles which might result in computational instabilities in the ELECTRO solver. As first mentioned in the previous chapter (Section 2.6), it was elected to initially consider *S. aureus* as single cells. This is a simplified model of *S.*

aureus as the bacteria are likely to exist in clusters. However, this simplified model was adopted in order to create a foundation platform for the work.

Electrical characteristics and boundary conditions were also set in the pre-processing step. Table 3.1 displays the relative dielectric permittivity values applied. The analysis was based on dielectric permittivity only, i.e. electrical conductivity of the intra- and extra-cellular liquid and cell wall was not taken into consideration at this stage. Bacterium parameters were based on permittivity values available in the literature. The substrate material was initially based on silicon with bacteria suspended in a water based medium. The relative dielectric permittivity of PMGI is unknown but most polymers typically have a dielectric constant between 2 and 5 and so a value of 4 was used for the model. A 50 mV DC potential (V) was applied across the electrodes to correspond with the experimental value as stated in the protocol, outlined in Chapter 4, Section 4.5.3; however, since the model was a static representation, this value was actually not of significance.

After the pre-processing stage, a hybrid method solver within the framework of ELECTRO was used to solve for electrical parameters. The hybrid solver is a combined FE and BE solver which is claimed to be faster and more precise than FE and BE methods alone [Integrated Engineering Software, 2009]. The self-adaptive mode of the solver was utilised in which subareas and boundary elements are automatically assigned and the element distribution is refined until the solution is within the required accuracy. Accuracy is based on user defined values for the accuracy factor and the self-adaptive accuracy. The default setting for the accuracy factor has a value of one and it has been found that this will give a good solution for 99% of models [Integrated Engineering Software, 2001]. Increasing the accuracy factor dramatically increases the solution time required. The self-adaptive accuracy value, however, has a less dramatic effect on solution time and dictates the number of elements introduced into the model. Therefore, to maintain consistency, the accuracy factor was set to one for all solutions and the self-adaptive accuracy value was reduced as far as possible for each solution before the accuracy factor automatically increased. Reducing the self-adaptive accuracy value as far as possible

meant that the maximum number of elements was formed for each model solution for an accuracy factor of one.

In the post-processing stage, the electric field strength between the sensor's electrodes and the surface charge density on the electrodes, Q_0, (C/m^2) were obtained. The surface charge density allows calculation of a capacitance per unit area, C_0, (F/m^2) using the following relation, based on Equation 2.4:

$$C_0 = \frac{Q_0}{V}$$

Equation 3.1

Herein, the capacitance per unit area, C_0, is referred to as normalised capacitance. Variations in normalised capacitance were used to evaluate the performance of the sensor. It is expected that the maximum change in normalised capacitance due to bacteria will translate to the maximum sensitivity of the sensor.

3.1.2   Results

3.1.2.1   Model Validation

ELECTRO has previously been used for optimising electrode systems designed on a micro-scale and for which large variations in dimensions occur [Lakdawala et al., 2008]. Timoshkin et al. (2006b) also used ELECTRO to analyse electric fields and forces in biological systems. They found that the electric field strength in the membrane of a spherical biological cell, obtained using the hybrid solver, was in very good agreement with analytical values obtained by solving the Laplace equation. It was surmised from this previous work that the ELECTRO solver would be suitable for modelling the biosensor with bacteria.

To further confirm the validity of the results obtained from the simulation, the capacitance of the sensor without bacteria, computed in ELECTRO, was compared to that obtained from an analytical expression developed for planar interdigitated electrodes by Olthuis et al. (1995). For simplicity, results were compared for the case of no polymer present in-between the electrodes. Olthuis et al. (1995) initially derived analytical equations for two planar electrode fingers and so they were suitable for comparison with the ELECTRO model (also consisting of two planar

electrodes). The expression for the capacitance between two planar interdigitated electrodes, per unit length (C_l), presented by Olthuis et al. (1995) is as follows:

$$C_l = \frac{\varepsilon_0 \varepsilon_r}{2} \frac{K(1-k^2)^{1/2}}{K(k)}$$

Equation 3.2

where ε_0 is the permittivity of free space, ε_r is the relative dielectric permittivity of the medium between electrodes and $K(k)$ is the complete elliptic integral of the first kind:

$$K(k) = \int_{t=0}^{1} \frac{dt}{[(1-t^2)(1-k^2 t^2)]^{1/2}}$$

Equation 3.3

For two planar electrode fingers, k is approximated to:

$$k = \frac{G}{G+W}$$

Equation 3.4

The resulting total capacitance, C, can be obtained from the following formula, where N is the total number of electrode fingers ($N = 2$ for the case of two planar electrodes) and L is the length of the electrode finger:

$$C = (N-1)LC_l$$

Equation 3.5

The expression presented by Olthuis et al. (1995) considers the half space above the electrodes only. Therefore, capacitance values obtained from the analytical expression were multiplied by a factor of two to account for this and the value for ε_r was the average of the medium and substrate relative dielectric permittivities.

The result from the ELECTRO model compared well to the analytical value. For a sensor with 3 µm wide electrodes and a 4 µm gap on a silicon substrate and with a water based external medium, the total sensor capacitance computed from the ELECTRO model was C = 2.08 pF compared to C = 1.92 pF obtained from the analytical expression. This result gave confidence in the model.

A quick assessment of the solver was made by comparing results from all three solution methods available within ELECTRO (BE, FE and hybrid). The results are

presented in Table 3.2. For the case of no bacteria ($m = 0$), the normalised capacitance calculated by all three solvers was the same. For the case of one bacterium ($m = 1$), the BE and hybrid solver yielded similar results. However, the FE solver was unable to generate a mesh when a bacterium was present. It is likely that this is due to the scale of the model and the resulting severe curvature of the bacterium (when only half a bacterium was inserted, the model could be solved). The lack of success with the FE solver and the similarities between the hybrid and BE solutions suggests that the hybrid solver was the optimal choice.

Table 3.2. Normalised capacitance computed from different solution methods within ELECTRO for no bacteria present ($m = 0$) and one bacterium present on the sensor surface ($m = 1$).

| Solver method | Normalised capacitance ($\mu F/m^2$) | |
	$m = 0$	$m = 1$
BE	159.54	158.43
FE	159.84	-
Hybrid	159.54	158.43

3.1.2.2 Effect of Bacteria

To determine the effect of bacteria on sensor capacitance, the ELECTRO model was solved for increasing numbers of bacteria present on the polymer layer in-between electrodes. For the initial model ($W = 3\,\mu m$ and $G = 4\,\mu m$), a maximum of four bacteria ($m = 4$) could be positioned on top of the sensor (as illustrated in Figure 3.1 and Figure 3.2). Normalised capacitance was determined for increasing numbers of bacteria and results are displayed in Figure 3.3.
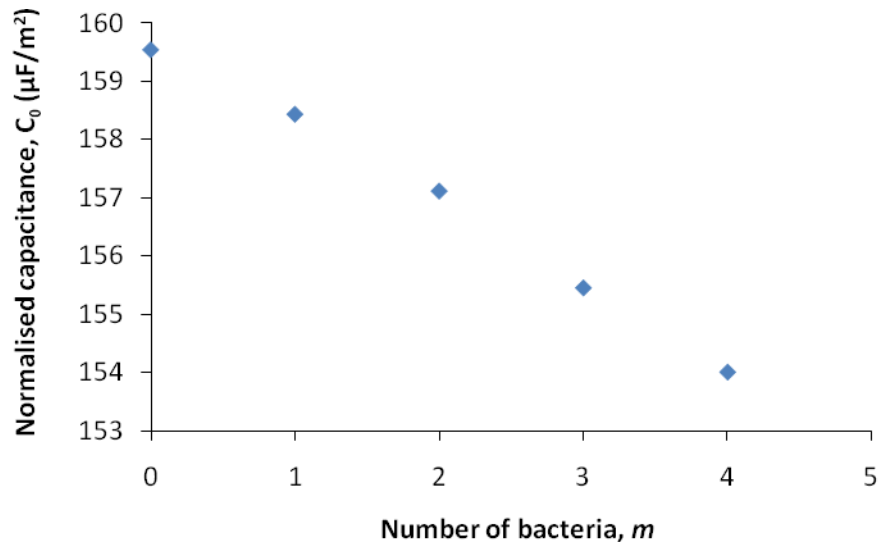
Figure 3.3. Normalised capacitance, C_0, of the sensor (W = 3 µm and G = 4 µm) as a function of the increasing numbers of bacteria in a row, *m*, on the sensor's surface.

It was found that as the number of bacteria present on the sensor's surface increased, normalised capacitance consistently decreased. Reasons for this will be considered in the discussion (Section 3.1.3). Figure 3.4 presents the results in terms of a percentage change in normalised capacitance, ΔC_0, with respect to the case of no bacteria present ($m = 0$). For the maximum number of bacteria ($m = 4$) there was a corresponding 3.47% reduction in normalised capacitance.
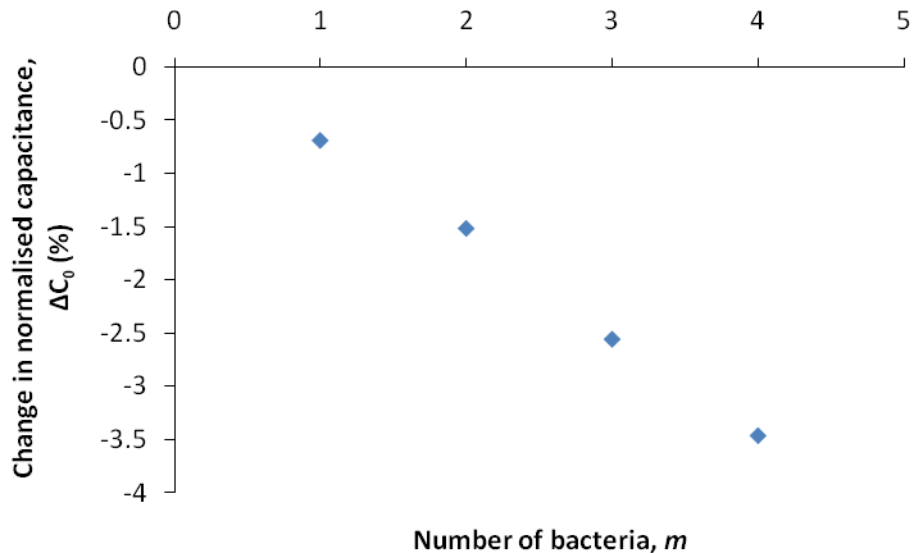
Figure 3.4. Percentage change in normalised capacitance, ΔC_0, due to increasing numbers of bacteria on the sensor's surface, *m*, with respect to the case of no bacteria present ($m = 0$).

It was also decided to look into the effect of increasing layers of bacteria (*l*) on top of the sensor as some bacteria exist in particular formations when in solution depending on their species. For example, *Streptococcus* species tend to form chains and *Staphylococcus* species exist in clusters. It was intended that introducing increasing layers of bacteria would provide an indication of this aggregating effect. Figure 3.5 shows the model (W = 3 µm and G = 4 µm) with four layers of bacteria (*l* = 4). Note that bacteria were now also positioned on top of the electrodes so that *m* = 6. Such a situation might arise due to the attachment of bacteria to other bacteria captured onto the polymer surface. In addition to this, bacteria could also be captured by phages which have physically adsorb onto the gold surface of the electrodes [Nanduri et al., 2007b, Olsen et al., 2006].
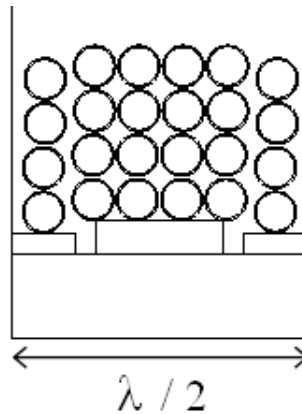
Figure 3.5. The ELECTRO model (W = 3 µm and G = 4 µm) with four layers of bacteria (*l* = 4) on the sensor surface to simulate bacterial aggregation effects.

The result for increasing numbers of bacterial layers is shown in Figure 3.6. The results demonstrate that for up to four layers of bacteria, normalised capacitance significantly decreased with increasing layers but beyond this point, additional layers lead to only a very small reduction in capacitance. This is further illustrated by the percentage change in normalised capacitance with respect to the case of *l* = 0, reported in Table 3.3. The maximum change in normalised capacitance is approximately 11% and this first occurs with four layers of bacteria present on the sensor's surface. The results will be discussed in Section 3.1.3.
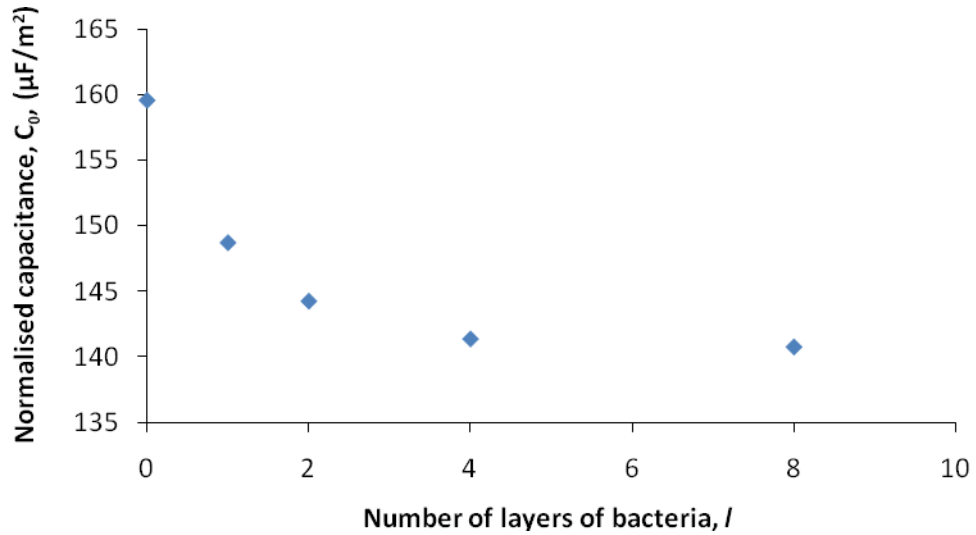
Figure 3.6. The effect of increasing layers of bacteria, *l*, on top of the sensor on normalised capacitance, C_0, computed from the ELECTRO model.

Table 3.3. Normalised capacitance, C_0, and percentage change in C_0, ΔC_0, due to increasing layers of bacteria, *l*, on the surface of the sensor as computed from the ELECTRO model of the sensor.

Layers of bacteria, *l*	C_0 ($\mu F/m^2$)	ΔC_0 (%)
0	159.54	-
1	148.68	-6.8
2	144.22	-9.6
4	141.34	-11.41
8	140.73	-11.79

As well as examining the changes in capacitance due to bacteria, electric field strength was also used to analyse the effect of bacteria. Electric field strength was obtained across the width of the model at a fixed height of 3.3 μm from the base of the model (y = 3.3 μm). This line is depicted in Figure 3.7; it passes 0.5 μm above the polymer surface and through the centre of any bacteria sitting on the polymer. Figure 3.8 shows electric field strength along this line for the case of no bacteria on the sensor and for one bacterium on the sensor.
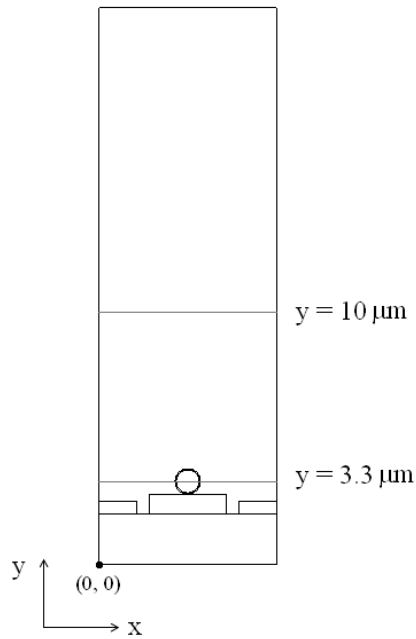
Figure 3.7. Image of the ELECTRO model depicting lines along which electric field measurements were taken for model analysis.
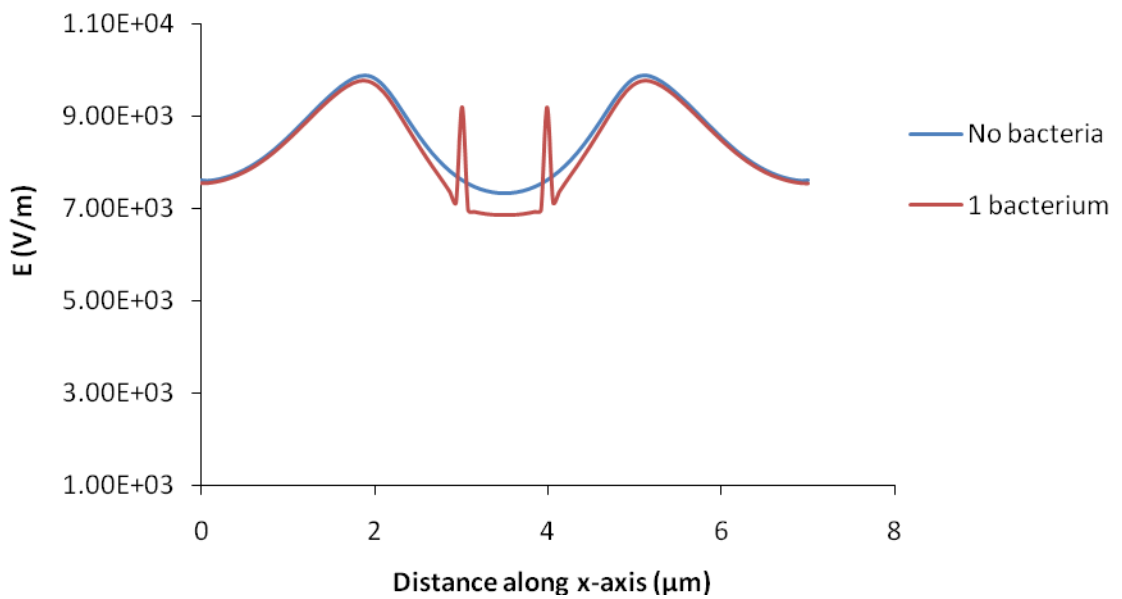
Figure 3.8. Electric field strength, E, along the horizontal (x-direction) line y = 3.3 μm (depicted in Figure 3.7) for the case of no bacteria on the sensor and for one bacterium on the sensor.

Correlating the x-distance to model features, it was observed from Figure 3.8 that the electric field strength was greatest in regions near the corner of the electrodes and

also in regions corresponding to the bacterium's cell membrane. This will be discussed further in Section 3.1.3. Generally, in areas outside of the bacterium, the electric field strength was very similar for the case with and without the bacterium.

3.1.2.3 Optimisation of Electrode Topology

Electrode topology was optimised by investigating electrical parameters for varying electrode gap and width sizes. The effect of changing electrode gap on sensor capacitance is demonstrated in the results presented in Table 3.4. Electrode width remained constant (W = 3 µm).

Table 3.4. Effect of increasing electrode gap size on normalised capacitance, C_0, for the case of no bacteria present on the sensor ($m = 0$) and maximum number of bacteria on the sensor (m = maximum). The maximum number of bacteria for each gap size is indicated in parenthesis. The percentage change in normalised capacitance, ΔC_0, due to the maximum number of bacteria is also presented. Electrode width was constant at 3 µm.

| Gap (µm) | Normalised capacitance, C_0, for: | | ΔC_0 (%) |
	$m = 0$	m = maximum (no.)	
2	205.70	192.75 (2)	-4.55
4	159.54	153.74 (4)	-3.47
6	137.57	133.60 (6)	-2.89
10	115.88	112.36 (10)	-3.03

It can be seen from Table 3.4 that for the case of no bacteria ($m = 0$), sensor capacitance consistently decreased with increasing electrode gap. The percentage change in normalised capacitance due to the maximum number of bacteria possible between electrodes (m = maximum) is also presented in Table 3.4 for the different electrode gap sizes. Note that as the gap size increases, so does the maximum number of bacteria possible between the electrodes (no.). It was observed that sensors of smaller electrode gap (2 µm and 4 µm) exhibited larger changes in capacitance due to the corresponding maximum number of bacteria and were thus more sensitive than sensors of larger electrode gap size for these conditions.

Changes in the electric field strength were also examined for changing electrode gap sizes for the case of no bacteria present. Figure 3.9 shows the electric field strength along y = 3.3 µm (previously depicted in Figure 3.7) for the different gap sizes. It

can be seen that as the gap size increases, the electric field strength along this line decreases. Figure 3.10 shows the electric field strength for increasing sensor gaps along $y = 10\,\mu m$ (also depicted in Figure 3.7). At this greater height, the opposite trend was observed: electric field strength increases with increasing gap size.
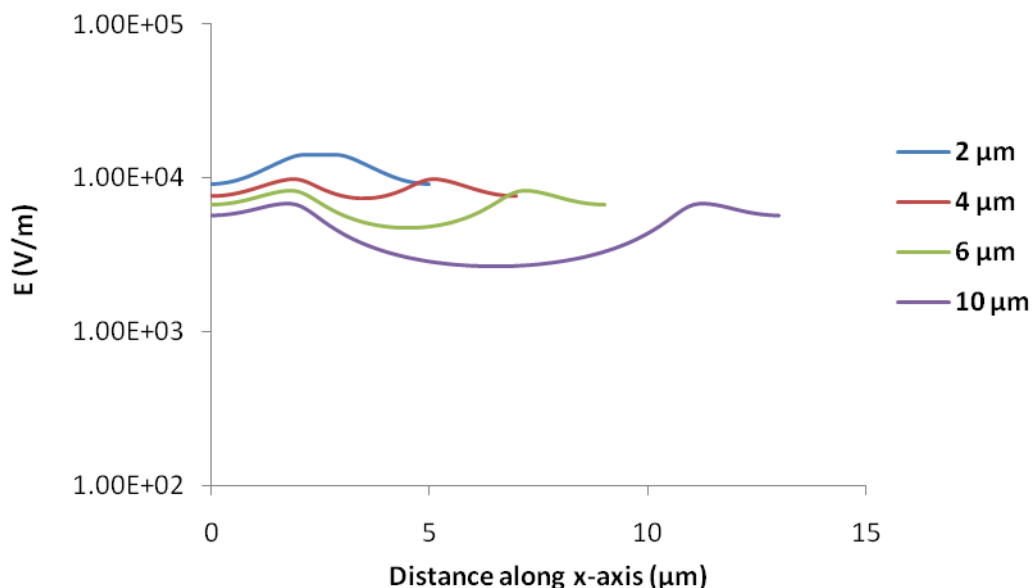
Figure 3.9. Electric field strength, E, along the line y = 3.3 µm for sensors of increasing electrode gap and constant electrode width (W = 3 µm). Bacteria were not present.
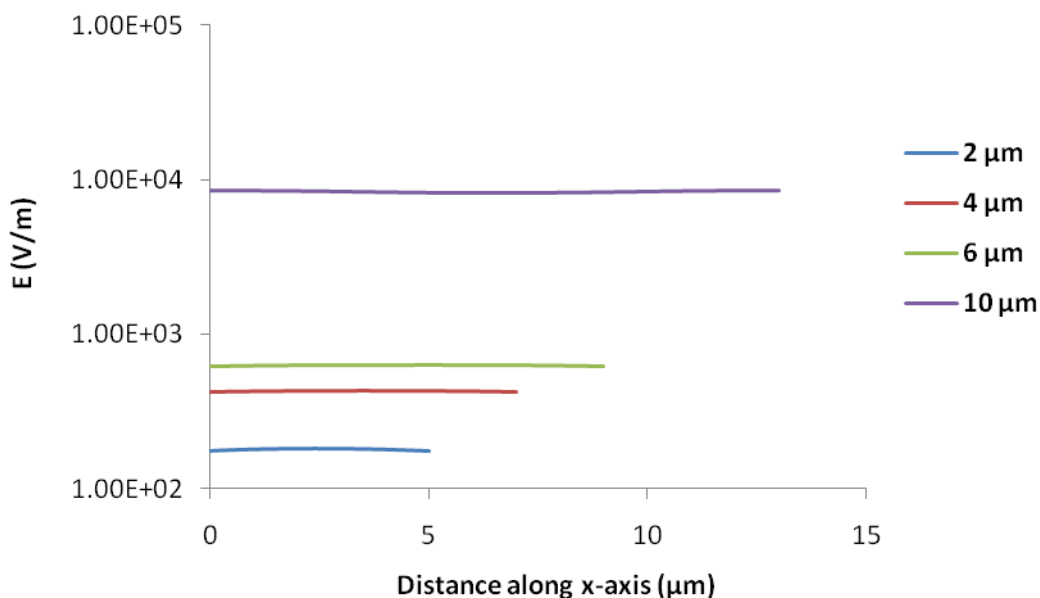
Figure 3.10. Electric field strength, E, along the line y = 10 µm for sensors of increasing electrode gap and constant electrode width (W = 3 µm). Bacteria were not present.

This result is further illustrated in Figure 3.11 which shows the electric field in the form of streamlines for $G = 2\,\mu m$ and $G = 10\,\mu m$. ELECTRO generated these streamlines by simulating the path of small electrically charged particles released from the surface of the positively charged electrode. Figure 3.11 shows that for the sensor of larger gap, electric field lines penetrate further into the external medium.
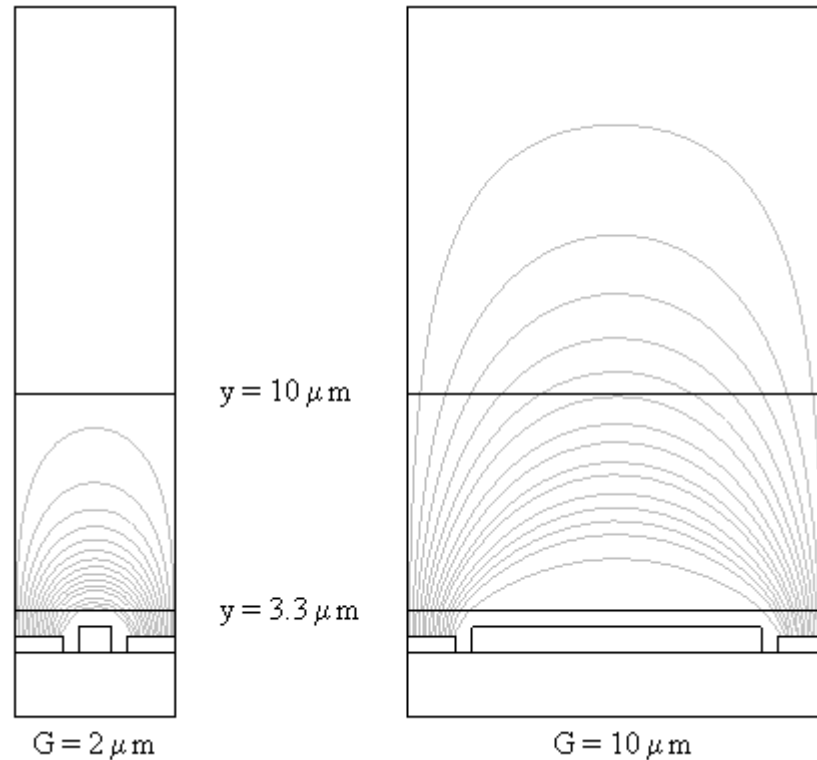
Figure 3.11. Electric field streamlines generated for sensors of 2 μm and 10 μm electrode gaps. ELECTRO generated streamlines by simulating the path of a small negatively charged particle released from the surface of the positively charged electrode. The lines y = 3.3 μm and y = 10 μm are indicated.

The effect of increasing the sensor's electrode width was also investigated. Electrode gap size was kept constant at $4\,\mu m$ which meant a maximum of four bacteria could be inserted between electrodes on the sensor's surface. As with increasing electrode gap, normalised capacitance consistently decreased for increasing electrode width (this observation is discussed further in Section 3.1.3). The maximum change in normalised capacitance due to bacteria was calculated for each electrode width and results are displayed in Figure 3.12. It was found that reducing the electrode width

improved the sensitivity of the sensor i.e. the absolute value of the percentage change in normalised capacitance increased with decreasing electrode width.
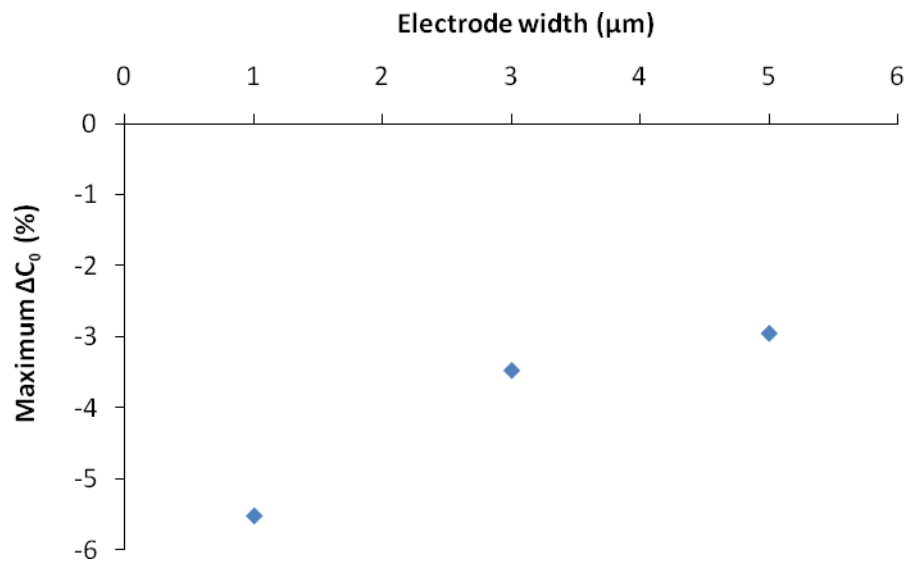
Figure 3.12. Maximum percentage change in normalised capacitance, ΔC_0, due to the maximum number of bacteria between electrodes ($m = 4$) compared to $m = 0$ for increasing electrode width. Gap size was constant at 4 µm.

The electric field strength along the line y = 3.3 µm for increasing electrode width size is shown in Figure 3.13. It can be seen that whilst there is very little change in the value of the maximum electric field strength for increasing width along this line, the minimum value of electric field strength in the inter-electrode space increases with increasing width. It was also found that, along the line y = 10 µm, a trend similar to that seen with increasing electrode gap was observed (Figure 3.10) i.e. electric field strength values along y = 10 µm were relatively constant for each electrode width size and as electrode width increased so did electric field strength.
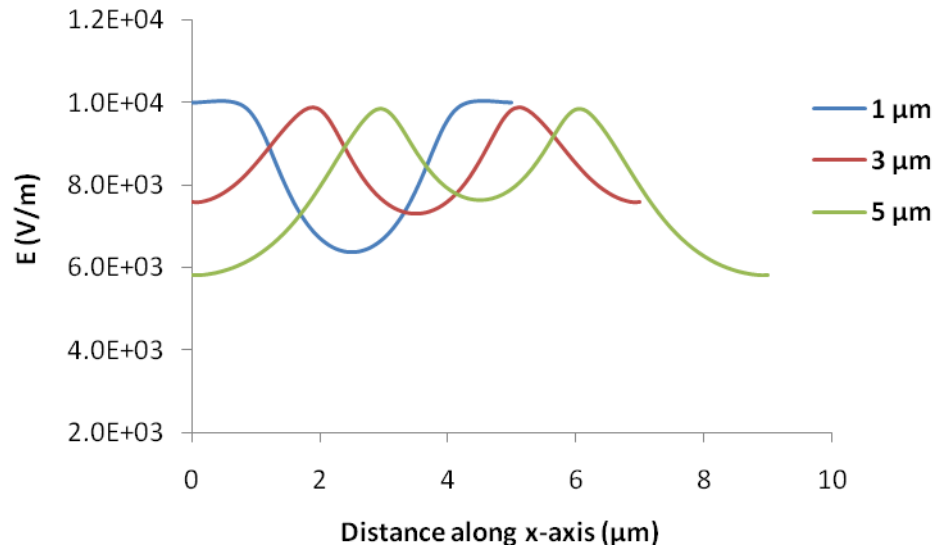
Figure 3.13. Electric field strength along the line y = 3.3 µm for sensors of increasing electrode width and constant electrode gap (G = 4 µm). Bacteria were not present.

The varying response of sensors with different topologies gave reason to investigate the possibility that a particular sensor may be more sensitive to detecting bacteria of a specific size. Bacteria of different diameters (d) were therefore analysed with the original sensor topology (W = 3 µm and G = 4 µm). Normalised capacitance values were obtained for the case of maximum bacterial capture i.e. the maximum number of bacteria in a single row was inserted between electrodes for each bacterial diameter. Maximum normalised capacitance values and the corresponding maximum number of bacteria inserted into the model for each bacterial diameter are shown in Figure 3.14. The results show that, compared to the case of no bacteria ($m = 0$), normalised capacitance initially decreases with increasing bacterial diameter, reaching a minimum for a diameter of approximately 1 µm. Normalised capacitance then begins to increase for further increases in bacterial diameter, returning towards the value for $m = 0$.
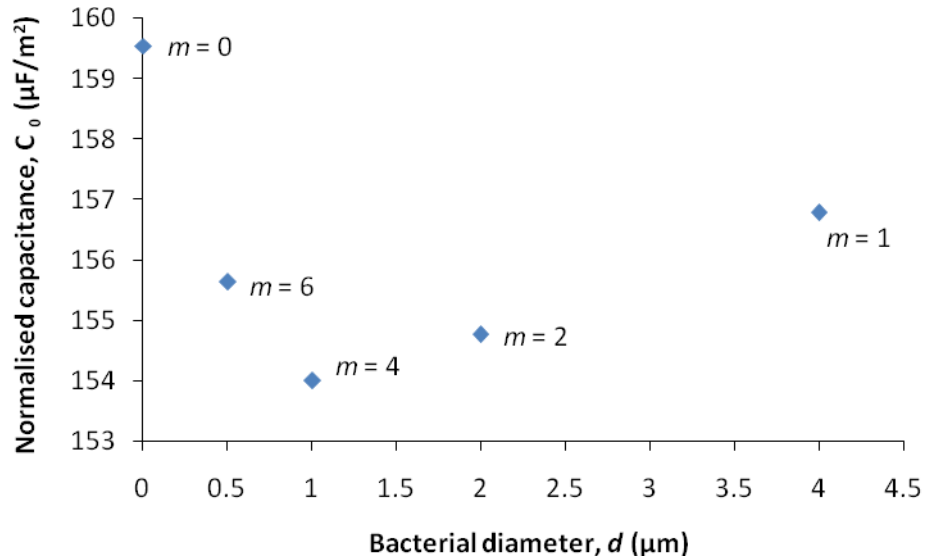
Figure 3.14. Maximum normalised capacitance, C_0, as a function of bacterial diameter, d. For each case, the maximum number of bacteria were inserted between electrodes in the model for which W = 3 µm and G = 4 µm. The number of bacteria between electrodes (m) is also displayed; for each bacterial diameter, the maximum number of bacteria were inserted.

The maximum percentage changes in normalised capacitance for different bacterial diameters are reported in Table 3.5. Again, percentage changes were determined with respect to the case of no bacteria present ($m = 0$). Also included in Table 3.5 are results for a sensor with electrodes 5 µm wide and 10 µm apart. For the sensor of smaller electrode dimensions, larger changes in normalised capacitance were observed with smaller bacteria whilst for the sensor of larger electrode dimensions, larger changes occurred with bacteria of larger diameter.

Table 3.5. Percentage change in normalised capacitance, ΔC_0, due to bacteria of varying diameter. The maximum percentage change was calculated for each bacterial diameter i.e. normalised capacitance values were computed for the case when the number of bacteria between the electrodes (m) was a maximum. Two sensor topologies were investigated: electrode width (W) = 3 µm and electrode gap (G) = 4 µm; W = 5 µm and G = 10 µm.

Bacteria diameter (µm)	W = 3 µm, G = 4 µm		W = 5 µm, G = 10 µm	
	m	ΔC_0 (%)	m	ΔC_0 (%)
1	4	-3.47	9	-1.76
2	2	-2.99	5	-2.44
4	1	-1.72	3	-2.52

3.1.2.4 Effect of External Medium

To investigate the effect of external medium permittivity on the sensor's sensitivity towards detecting bacteria, values for the external medium permittivity were reduced from $\varepsilon_S = 80$ for a water based medium to $\varepsilon_S = 5$ and $\varepsilon_S = 1$ to represent an oil based medium and air respectively. Normalised capacitance values for increasing numbers of bacteria in these external mediums are displayed in Table 3.6. The percentage change in normalised capacitance is also included for increasing numbers of bacteria present between the electrodes.

Table 3.6. The effect of external medium on the sensitivity of the sensor. Normalised capacitance, C_0, and the percentage change in normalised capacitance with respect to the case of no bacteria present, ΔC_0, were calculated for increasing numbers of bacteria on the sensor's surface in external medium permittivities of 1, 5 and 80.

| Number of bacteria | External medium dielectric permittivity | | | | | |
| | $\varepsilon_S = 1$ | | $\varepsilon_S = 5$ | | $\varepsilon_S = 80$ | |
	C_0 (F/m^2)	ΔC_0 (%)	C_0 (F/m^2)	ΔC_0 (%)	C_0 (F/m^2)	ΔC_0 (%)
0	2.713×10^{-6}	-	1.133×10^{-5}	-	1.595×10^{-4}	-
2	2.890×10^{-6}	6.54	1.253×10^{-5}	10.58	1.571×10^{-4}	-1.52
4	3.903×10^{-6}	43.88	1.680×10^{-5}	48.23	1.540×10^{-4}	-3.47

The results firstly show that there was a consistent decrease in normalised capacitance with decreasing medium permittivity. The change in normalised capacitance due to bacteria demonstrates the opposite tendency however: the absolute value of ΔC_0 increases with decreasing medium permittivity. In addition to this, as illustrated in Figure 3.15, reducing the permittivity of the external environment resulted in an increase in normalised capacitance with increasing numbers of bacteria whereas previously, in a medium of high relative dielectric permittivity, normalised capacitance decreased with increasing levels of bacteria. This can be related to the relative changes in permittivity caused by introducing bacteria into a medium of lower or higher overall permittivity and will be discussed further in Section 3.1.3.
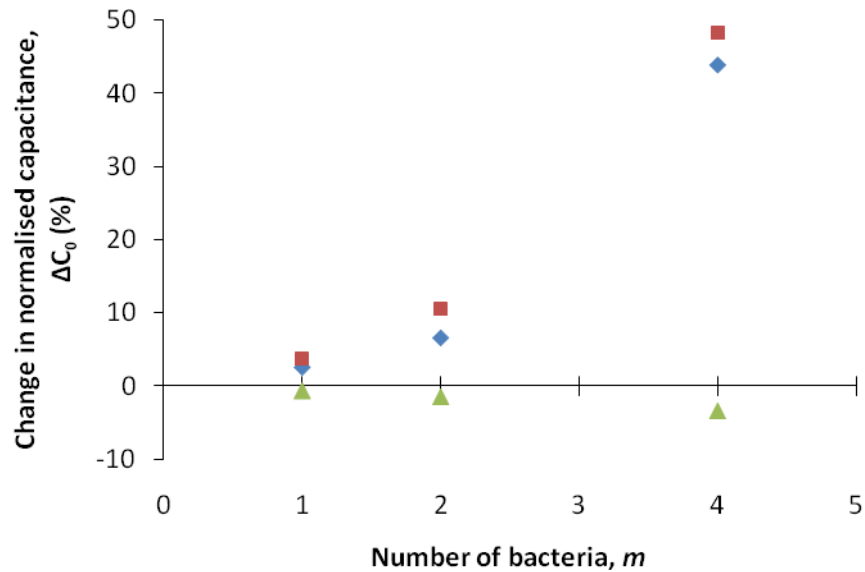
Figure 3.15. The percentage change in normalised capacitance, ΔC_0, due to increasing numbers of bacteria in suspensions of relative permittivity: 1 (♦), 5 (■), 80 (▲).

3.1.2.5 Effect of Substrate Material

Thus far, all modelling work has been carried out with a silicon based substrate ($\varepsilon_{SB} = 11.9$). To assess whether using a substrate of lower relative dielectric permittivity would significantly alter the results collected, data from the original model were compared to some results collected from a model with a reduced substrate permittivity. Lower substrate permittivities will be encountered if a glass wafer is used for sensor fabrication or if there is a relatively thick silicon dioxide layer covering the surface of the silicon wafer. A value of $\varepsilon_{SB} = 4$ was applied to the model as this is in the region of permittivity values quoted for glass and silicon dioxide based materials.

The electric field strength along the line $y = 3.5\,\mu m$ obtained with substrate permittivities of $\varepsilon_{SB} = 11.9$ and $\varepsilon_{SB} = 4$ are displayed in Figure 3.16. No bacteria were present.
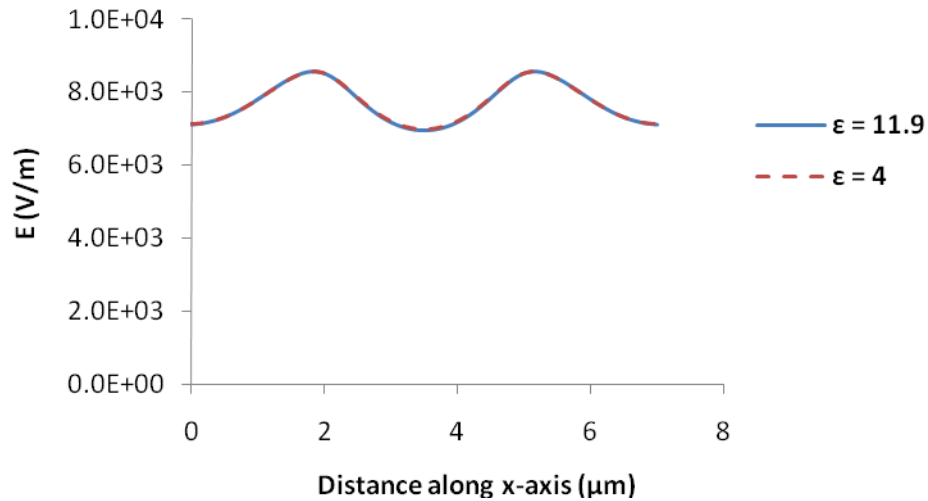
Figure 3.16. Electric field strength along a line 1 μm above the surface of the sensor's electrodes (y = 3.5 μm) for a sensor with substrate permittivities of $\varepsilon_{SB} = 11.9$ and $\varepsilon_{SB} = 4$. The external medium was water ($\varepsilon_S = 80$) and electrode geometries were: W = 3 μm and G = 4 μm.

It can be seen from Figure 3.16 that there was no significant difference between the electric field results obtained from the two different substrates. This was also found to be the case at y = 10 μm and for when bacteria were present on the surface of the sensor.

3.1.3 Discussion

The initial validation work indicated that ELECTRO, and specifically the hybrid solver within ELECTRO, was suitable for the modelling of the biosensor and bacteria: previous work of similar dimensions had been successfully carried out, including the determination of electric field strength in bacteria [Lakdawala et al., 2008, Timoshkin et al., 2006b], and capacitance values obtained from the ELECTRO model of the sensor compared well to analytical results. Obviously considerable simplifications had been applied, such as using a two-dimensional half-wavelength model and carrying out an analysis based on permittivity only. However, it is still expected that the greater the change in capacitance computed in the modelling work, the more sensitive the sensor will be. Thus, it is reasonable to expect the present investigation to supply useful information on the behaviour of the sensor and on aspects which might lead to improved sensitivity.

The analysis of the effect of bacteria showed that introducing increasing numbers of bacteria onto the sensor's surface, in a water based medium, decreased the sensor's normalised capacitance. This firstly indicates that the sensor is sensitive to the presence of bacteria between the electrodes. If it is assumed that the decrease in capacitance would result in a corresponding increase in sensor impedance then this trend is consistent with the simulation work of Srinivasan et al. (2006) who reported increasing impedance with increasing cell concentration with their model. Similar trends in impedance have been reported in experimental results such as by Radke and Alocilja (2004) who used a sensor of the same electrode dimensions as was modelled here. Increasing sensor impedance with increasing concentrations of bacteria has also been reported for other sensors of similar microelectrode dimensions [de la Rica et al., 2009, Kim et al., 2009, Shabani et al., 2008].

A decrease in normalised capacitance with increasing bacterial number seems sensible: capacitance is proportional to dielectric permittivity and so by displacing water ($\varepsilon_S = 80$) with a medium of overall lower permittivity in the inter-electrode space (bacteria have a membrane of low dielectric permittivity, $\varepsilon_S = 6$, and cell wall and cytoplasm permittivities of $\varepsilon_S = 60$ and $\varepsilon_S = 80$ respectively) then there should be a corresponding reduction in capacitance. The electric field results of Figure 3.8 demonstrated the permittivity changes across the bacterium by indicating increased electric field strength in regions over the bacterium's cell membrane i.e. where permittivity was low (high dielectric permittivity results in lower electric field strength). Incidentally, it was also observed in Figure 3.8, and similar plots, that the electric field strength was often highest in regions close to the electrode corners. This is not an unexpected result as high electric field strengths are generated at sharp changes in electrode geometry such as at electrode edges [Hammond, 1997].

When layers of bacteria were introduced on top of the sensor to represent the aggregation effects of bacteria such as *S. aureus*, larger changes in capacitance were observed, as might have been expected from the results of adding single bacteria. However, the results of Table 3.3 showed that saturation occurred with four rows of

bacteria, beyond which there was no further significant decrease in capacitance. Saturation is likely to be due to the layers of bacteria beginning to fall outside the sensor's region of high electric field strength. As illustrated in Figure 3.17, the sensor's electric field strength is greatest close to the sensor's surface near the electrodes and reduces with increasing distance away from the electrodes. It can be seen from Figure 3.17 that the majority of the electric field (approximately 78%) is below a height of 4 µm from the polymer surface; this height is equivalent to four layers of bacteria. The sensor is sensitive to permittivity changes occurring in this region, close to the sensor surface, whilst changes further away have less of an effect, thus explaining the saturation observed. This finding is also consistent with the modelling work of Srinivasan et al. (2006) in which it was reported that as the vertical position of a single layer of bacterial cells was moved further away from the electrode surface, the change in impedance consistently decreased, attributed to the corresponding drop in electric field strength. Overall, the results indicate that the sensor is sensitive to detecting clusters of bacteria (such as would be the case for *S. aureus*) as well as single cells. In addition to this, the results suggest that saturation of the sensor signal may be achieved more readily when the target bacteria is capable of forming chains and/or clusters.
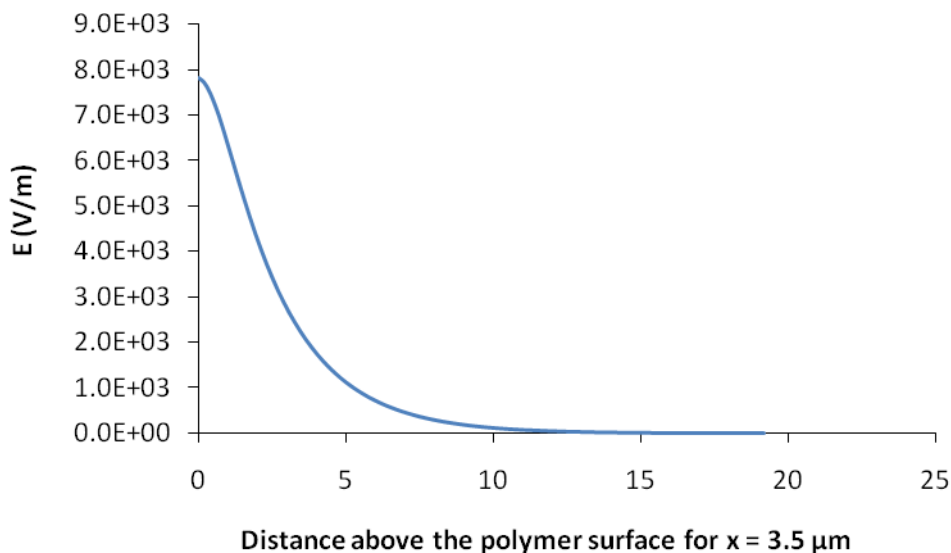
Figure 3.17. Electric field strength above the polymer surface along the vertical line x = 3.5 µm (the centre of the half wavelength model).

In the optimisation work, it was found that normalised capacitance decreased with both increasing electrode gap and width i.e. normalised capacitance decreased with increasing spatial wavelength (λ). This result is consistent with experimental work reported by Mamishev et al. (1999). Note that whilst it would be expected to observe an increase in absolute capacitance (C) for increasing electrode width due to the increased electrode surface area (as is consistent with Equation 2.5 for parallel plate capacitors and as will be demonstrated in Chapter 6, Section 6.2.2, when analytical sensor capacitance results are compared to measured values), a decrease in normalised capacitance with increasing width can be justified if the increase in electrode area (electrode width × length) is larger than the decrease in normalised capacitance, as illustrated through the following relationship where L is electrode length:

$$C_0 = \frac{C}{WL}$$

<div align="right">*Equation 3.6*</div>

More significantly however, sensor topology was revealed to play an important role in defining the sensor's sensitivity. It was found that sensors of small electrode dimensions, both in terms of electrode width and gap, exhibited larger changes in normalised capacitance when bacteria of 1 μm diameter were inserted between electrodes and were thus more sensitive to the bacteria. Radke and Alocilja (2004) stated similar findings from their simulation work in which *E. coli* of 2.57 μm length and 0.49 μm diameter were investigated but results were not presented. More substantially, experimental findings indicating this trend for improved sensitivity have been reported by Kim et al. (2009): interdigitated microelectrode array sensors with electrode gap sizes of 2 μm and 5 μm had lower detection limits for *Salmonella enteritidis* (rod shaped and approximately 2 – 5 µm long and 0.7 – 1.5 µm diameter [Holt et al., 2000]) than a sensor of larger gap size (10 μm).

This result can be attributed to the effect on the sensor's spatial wavelength and the corresponding changes in electric field penetration depth. Figure 3.10 effectively showed that along a line 7.5 μm above the surface of the electrodes (y = 10 μm), electric field strength decreased with decreasing electrode gap. This was also the case

for decreasing electrode width. Thus, it can be said that as the sensor's spatial wavelength decreases the electric field penetration depth decreases. This was confirmed by the streamline plots of Figure 3.11 which demonstrated a more concentrated electric field near the sensor's surface for the sensor of $G = 2\,\mu m$ whereas the electric field streamlines extended further above the sensor's surface for $G = 10\,\mu m$. This finding, of decreasing electric field penetration depth with decreasing spatial wavelength, is consistent with the FE simulations of planar electrodes by Mamishev et al. (1999) and other literature [Li et al., 2006]. It seems logical to conclude that the improved sensitivity obtained with sensors of smaller spatial wavelengths is a result of bacteria interfering with a greater proportion of a more concentrated electric field and a reduced influence from the surrounding medium.

In addition to this, results also showed that sensors could be tailored towards the size of the bacteria for improved sensitivity by altering the electrode dimensions. The non-linear trend of Figure 3.14 indicates that there is an optimum sensitivity for this particular sensor ($W = 3\,\mu m$ and $G = 4\mu m$) and that it occurs with bacteria of approximately $1\,\mu m$ diameter. Reduced sensitivity (i.e. smaller changes in normalised capacitance) was observed with bacteria of smaller and larger diameters. Interestingly, these were also the optimum dimensions reported by Radke and Alocilja (2004) for the detection of bacteria $2.57\,\mu m$ long and $0.49\,\mu m$ in diameter. Although Radke and Alocilja did not report details of their simulation and so an accurate comparison can not be made, the proximity of the results at least support the work reported here.

Again, these optimisation results could be explained by considering the dielectric permittivity of the medium occupying the sensor's region of high electric field strength. For example, for small bacteria ($d = 0.5\,\mu m$) and large bacteria ($d = 4\,\mu m$) it is conceivable that the cross-sectional proportion of low permittivity cell components falling into the region of high electric field strength is not as great as that for bacteria of $d = 1\,\mu m$ for this particular sensor. Another contributing factor could be the high electric field strengths observed at the corner of the electrodes

(Figures 3.8 and 3.9): Van Gerwen et al. (1998) reported that if the spacing between the electrodes is too small, the signal will be less influenced by events occurring between the electrodes due to the extremely high electric field strengths at the electrode corners. Overall, the results suggest that optimising sensor topology for target detection could be important for improving the sensitivity of biosensors.

The modelling work also revealed that the external medium had a significant effect on capacitance measurements and the sensitivity of the sensor. The consistent decrease in capacitance with decreasing medium permittivity was in line with theory (capacitance is proportional to dielectric permittivity). More significantly however, larger changes in capacitance were observed with lower external medium permittivities: for a maximum of 4 bacteria, capacitance changed by 48.23% when an oil based medium ($\varepsilon_S = 5$) was simulated compared to a 3.47% change in capacitance with a water based medium ($\varepsilon_S = 80$). In addition to this, with the lower permittivities, capacitance now increased with the addition of bacteria whereas with the higher permittivity of the water based suspension, capacitance decreased. These results are logical when the relative change in permittivity is considered: when the low permittivity media (oil $\varepsilon_S = 5$ or air $\varepsilon_S = 1$) is replaced with the now overall higher permittivity of bacteria (membrane $\varepsilon_M = 6$; wall $\varepsilon_W = 60$; cytoplasm $\varepsilon_C = 80$) in the inter-electrode space, there will be an increase in permittivity and therefore a corresponding increase in capacitance.

The outcome of the investigation into external medium permittivity suggests that by applying a low permittivity medium for measurements or allowing the sensor to dry after sample application, the sensitivity of the sensor may be improved. Indeed, the majority of published experimental results for bacterial detection with biosensors have been carried out in water based media and so this could present a potential route for improved sensitivity. However, ensuring consistent measuring conditions, especially under drying, could prove to be difficult.

Finally, a brief investigation was carried out to check that the general trend of the results obtained with a silicon sensor substrate ($\varepsilon_{SB} = 11.9$) could also be applied if a

glass substrate were to be used instead ($\varepsilon_{SB} = 4$). This became important for reasons which will be discussed in Chapter 6, Section 6.2. It was found that the electric field strength along a horizontal line, $1\,\mu m$ above the surface of the electrodes ($y = 3.5\,\mu m$), was the same for both substrate permittivities. This was also the case for $y = 10\,\mu m$ and also $y = 3.3\,\mu m$ when bacteria were present on the sensor surface. Based on a permittivity analysis only, this outcome suggests that the relative dielectric permittivity of the substrate material does not have a significant effect on the sensitivity of the sensor when substrate permittivity is low (at least for the range $\varepsilon_{SB} = 4$ - 11.9) and with a water based external medium. This was shown to be the case experimentally by Berezhetskyy (2007).

3.2   <u>Biosensor Design Overview</u>

The computer-aided modelling of a biosensor reported in the previous section provided useful information for the design of the actual biosensor which could now be considered. In the following sections, the fabrication method chosen is discussed and decisions on the initial biosensor design and materials are outlined.

3.2.1   Fabrication Method

Recent advances in micro- and nanotechnology have aided the development of microfabrication techniques which are now capable of creating microelectrodes of only a few microns in size. Arguably, photolithography is one of the most commonly used methods for fabricating microelectrodes and has been widely employed for biosensor fabrication [Gomez-Sjoberg et al., 2005, Kim et al., 2009, Lu et al., 2008, Radke and Alocilja, 2004, Suehiro et al., 1999]. Screen printing methods have also been successfully utilised to fabricate microelectrode arrays. For example, Shabani et al. (2008) created an impedimetric biosensor for the detection of bacteria by screen printing microelectrodes onto polyester sheets using graphite ink.

In this work it was decided to employ a photolithography method to fabricate the sensors. There were two main reasons for this: (1) micro-scale resolution can easily and accurately be achieved with the technique and (2) photolithography facilities were available within the Physics Department at the University of Strathclyde. This latter point was important as Dr Colin Pegrum of the Department of Physics at the

University of Strathclyde, and Dr David Hutson, presently at the University of the West of Scotland, were willing to collaborate on the work, allowing direct participation in sensor fabrication and continued expert advice. Details of the photolithography method can be found in Chapter 4 (Section 4.4.2).

Another appealing feature of the photolithography method was that sensors of varying electrode dimensions could easily be incorporated into the photomask (the template for wafer design, discussed further in Chapter 4, Section 4.4.1). Thus, a single wafer could generate several different electrode arrays. This flexibility would allow design aspects to be investigated experimentally, as is discussed in the following section.

3.2.2   Dimensions

It was decided to adopt an interdigitated array electrode format (as illustrated in Figure 3.1) as this would provide a relatively large active area for bioreceptor immobilisation and bacteria capture compared to the case of just two microelectrodes. It is also an uncomplicated design for this early stage of the sensor development and could easily be fabricated using photolithography.

In terms of dimensions, as mentioned previously, published experimental results have shown that biosensors, sensitive to the presence of bacteria, can be created if electrodes are of similar size to the target bacteria i.e. electrode width and spacing of a few microns [Kim et al., 2009, Radke and Alocilja, 2004, Shabani et al., 2008]. Microelectrodes offer several advantages over larger electrodes such as: small surface areas resulting in low currents and therefore low power requirements and the reduction of any possible thermal effects; high signal-to-noise ratios; rapid attainment of steady state conditions; improved sensitivity; the requirement of only small sample volumes; and they will also yield a miniature device [Zou et al., 2007, Stulik et al., 2000, Montenegro et al., 1990]. The requirement of only a small applied voltage is particularly important for avoiding unwanted electrochemical reactions at the electrode's surface whilst in solution as this could interfere with measurements [Montelius et al., 1995].

The optimisation work presented in this chapter demonstrated that for the detection of *S. aureus*, optimum sensitivity appeared to be achieved with electrodes 3 µm wide with a 4 µm gap. It was therefore decided to fabricate sensors of these dimensions. If electrode fingers were made 4 mm long then each sensor would be approximately 16×8 mm in size making them easy to handle for testing purposes and 24 sensors could be incorporated onto a 3 inch diameter wafer (as is commonly used in photolithography fabrication). It was therefore decided to also include sensors of other electrode widths and gaps into the photomask design. This would allow for investigations into electrode dimensions and other bacteria in the future without having to re-design and fabricate a new photomask which would be expensive. In the end, sensors with electrode gaps of 2, 4, 6 and 10 µm and widths of 3, 5 and 10 µm were incorporated into the photomask layout. The number of sensors allocated to each design is indicated in Table 3.7.

Table 3.7. Sensor details. G is electrode gap size, W is electrode width, N_P is the number of electrode pairs. The total area of the gold electrode array and the number of sensors allocated to each sensor design per wafer is also included.

W (µm)	G (µm)	N_P	Total area (mm^2)	No. sensors per wafer
3	2	1000	26.3	2
	4	715	19.4	6
	6	555	15.6	2
	10	385	11.5	2
5	2	715	30.9	2
	4	555	24.5	2
	6	455	20.5	2
	10	355	16.5	2
10	4	360	31.1	2

A schematic illustration of the sensor is shown in Figure 3.18 and an image of the actual wafer post-fabrication can be found in Chapter 6 (Figure 6.7). Details of the number of electrode pairs and total active area (electrode area plus contact pad area) for each sensor are also included in Table 3.7. The number of electrodes was dictated by the area available per sensor and also the geometry of the electrodes and was such that the sensor area available was maximised. The total active area was the electrode

area plus the contact pad area (incorporated for connection to the impedance measuring device and indicated in Figure 3.18). Radke and Alocilja (2004), who also developed an interdigitated microelectrode array impedimetric biosensor for bacterial detection, used a sensor which had an active area of 9.6 mm^2.
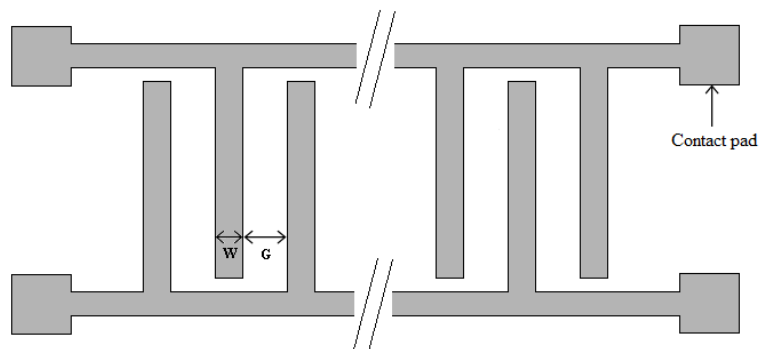
Figure 3.18. Schematic illustration of the interdigitated microelectrode array sensor (not drawn to scale). The parallel lines indicate repeated array pattern. Electrode width (W) and gap (G) are illustrated. Note that although four contact pads were incorporated into the design, only two (one for each electrode) were in contact with the test rig probes at any time.

It was also decided to include sensors of a double interdigitated electrode array format in the photomask design (as well as the single interdigitated electrode array format illustrated in Figure 3.18). The double array format is illustrated schematically in Figure 3.19.
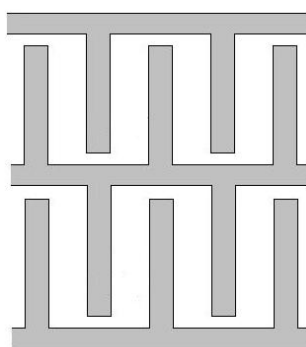
Figure 3.19. A schematic top view section of the double electrode array sensor format also incorporated into the photomask design.

Initial intensions were that this double array sensor could be set up such that one array would act as a control with a 'blank' sample (consisting of the suspending solution only) whilst the second array would take measurements from the test sample

99

(suspending solution with bacteria). By incorporating the sensor into a Wheatstone bridge arrangement it was intended to investigate this layout to further improve sensitivity. Allocating even only two places for this sensor format into the photomask design at this stage would obviate the need to create a second photomask later and would therefore also eliminate the associated financial costs involved in this. Unfortunately, due to time limitations this double array sensor could not be investigated during the project time frame. Instead, it is an option for future work, as will be discussed in Chapter 7, Section 7.2.

3.2.3   Materials

Metal and carbon electrodes are commonly implemented in biosensor applications. The photolithography facility available at the University of Strathclyde was set up to deposit chromium and then gold onto wafer substrates (the initial chromium layer aids in the adhesion of gold). It has been confirmed that bacteria can be successfully detected with impedimetric biosensors consisting of gold electrodes [Kim et al., 2009, Nandakumar et al., 2008, Radke and Alocilja, 2004, Varshney and Li, 2008]. Since previous literature also indicated that immobilised phages remained viable on a gold surface [Gervais et al., 2007, Nanduri et al., 2007b] it was decided that gold electrodes would be adequate for initial investigations. Importantly, as mentioned in Section 3.2.2, only very low voltages are required with microelectrodes (10s of millivolts) reducing any electrochemical effects that might occur at the surface of the gold electrodes [Montelius et al., 1995].

Also, opportunities existed to modify the gold electrodes later if desired. It has been demonstrated that sensor sensitivity can be improved with platinum electrodes for a variety of biosensor types, such as conductometric and amperometric biosensors [Berezhetskyy, 2007, O'Neill et al., 2004]. This could be investigated by platinising the gold electrodes i.e. coating the gold electrodes with a layer of platinum [Israel et al., 1984, Mohr et al., 1996, Zheng et al., 2006]. This could prove to be important as it was illustrated in Table 2.1 of Section 2.2.2.3 that gold electrodes are polarisable whereas platinum electrodes are relatively non-polarisable.

Initially it was decided to use a silicon wafer with a 0.3 µm thick silicon dioxide layer for the sensor's substrate. Silicon with an insulating layer of silicon dioxide is commonly implemented with photolithography fabrication methods and in biosensor construction, as illustrated in the work of Radke and Alocilja (2004), Lu et al. (2008) and Gomez-Sjoberg et al. (2005). The use of glass substrates has also been reported [Kim et al., 2009, Suehiro et al., 1999, Varshney and Li, 2008, Yang et al., 2004b] and later glass was also investigated for reasons which will be discussed in Chapter 6, Section 6.2. The ELECTRO modelling work showed that there was no difference in sensitivity between sensors of glass and silicon substrates based on the permittivity analysis (Section 3.1.2.5). Therefore it was concluded that the same outcomes from the modelling work with the silicon substrate could be applied for sensors on a glass substrate.

3.3 <u>Summary</u>

Despite the clear potential of CAE to assist in the development of biosensor design, there have been few reports of its implementation in this field. The novel CAE work carried out in this research clearly illustrated that the micro-scale sensor was sensitive to the presence of bacteria when a dielectric permittivity only electrostatic analysis was conducted: increasing the number of bacteria present on the sensor's surface and in its region of high electric field strength resulted in increasing changes in capacitance. Optimisation work indicated that electrode topology could be tailored to improve the sensor's sensitivity based on the specific dimensions of the target bacteria. In addition to this, performing sensor measurement with a low dielectric permittivity external medium may lead to improved sensitivity. Finally, it was shown that the difference between results obtained with silicon and glass substrates are not expected to be significant based on a permittivity analysis.

The results of the modelling work were used as a guide for the actual sensor design. Results indicated that electrodes 3 µm wide with 4 µm gaps would be the most sensitive for the detection of *S. aureus* but it was also decided to fabricate sensors of varying electrode dimensions for possible experimental investigations. Sensors would initially be made onto a silicon wafer with a 0.3 µm silicon dioxide layer and

with gold electrodes. It was decided to employ a photolithography technique to fabricate the sensors. Experimental results of the fabricated sensors are reported in Chapter 6.

Chapter 4

MATERIALS AND METHODS

This chapter outlines the materials and methods used throughout the research and will serve as a reference for all experimental work discussed in the following chapters. Details of materials, including microorganisms and phages, are first provided. Methods are then split into four main sections: general microbiological methods, immobilisation protocols, sensor fabrication and sensor testing.

4.1 <u>Materials</u>

4.1.1 Bacterial Strains

The bacterial strain *Staphylococcus aureus* 8588 (*S. aureus* 8588) was used in all bacteriological experiments. The culture was obtained from the National Collection of Industrial, Marine and Food Bacteria (NCIMB; UK).

4.1.2 Bacteriophage

Bacteriophage 9563 was used throughout the research and was obtained from NCIMB. Bacteriophage 9563 is known to infect and lyse *S. aureus* 8588 and this was further demonstrated in Chapter 5 to follow.

The complete host range of bacteriophage 9563 is not known, however, through DNA sequencing it was found that bacteriophage 9563 has significant DNA homology to bacteriophage K [Bell, 2008]. This suggests that bacteriophage 9563 and bacteriophage K have similar structures, host ranges and life cycles. It is known that bacteriophage K is a tailed phage and infects several *Staphylococci* species including both antibiotic resistant and sensitive *S. aureus* strains [O'Flaherty et al., 2005]. However, at this proof of concept stage of the research, only a single phage and host strain (*S. aureus* 8588) were used.

4.1.3 Media and Solutions

Table 4.1 lists the materials used in the preparation of solutions for: microbiological work, immobilisation processes and the enzyme-linked immunosorbent assay (ELISA) for anti-phage antibodies. Protocols for preparing solutions are then described.

Table 4.1. Materials used in the preparation of solutions for microbiological, immobilisation and ELISA work and their corresponding suppler.

Material	Supplier
Tryptone	
Yeast extract	Oxoid, UK
Bacteriological agar	
Sodium chloride	
Tris[hydroxymethyl]aminomethane	
Magnesium sulphate (anhydrous)	
Albumin from bovine serum (BSA)	
Biotin labelled bovine albumin	
Calcium chloride	Sigma-Aldrich, UK
Potassium chloride	
Tween® 20	
3,3',5,5'-Tetramethylbenzidine (TMB)	
Dimethyl sulfoxide (DMSO)	
Hydrogen peroxide (30% w/w)	
Sodium hydroxide	
Calcium carbonate	Thermo Fisher Scientific, UK
Sulfo-NHS-Biotin	
NeutrAvidin	
Gelatin	
Sodium carbonate	
Sodium bicarbonate	British Drug Houses (BDH) Ltd, UK
Sodium acetate	
Solid citric acid	
Mannitol	

Luria-Bertani Media

S. aureus 8588 was cultured with Luria-Bertani (LB) media. For liquid cultures, bacteria were grown in LB broth:

1 M sodium hydroxide*	4 ml
Tryptone	10 g
Sodium chloride	10 g
Yeast extract	5 g
Distilled water	1 litre

*For 1 M sodium hydroxide (NaOH) 40 g NaOH was added to 1 litre distilled water.

For plate culturing, LB agar was used. To make LB agar, 15 g of agar was included in the 1 litre LB broth mixture described above. For 'soft' top agar (used in plaque assays, described in Section 4.2.2.3), 6.6 g of agar was included.

Media and agar were autoclaved at 121°C for 15 minutes. After autoclaving, the agar was allowed to cool to 48°C in a water bath. Top agar was maintained at this temperature during use to keep it in a molten state and plate agar was poured into 90 mm Petri dishes and allowed to set.

Storage Medium

Phage were harvested and stored in storage medium (SM). SM was autoclaved at 121°C for 15 minutes.

1 M Tris. Cl (pH 7.5):	50 ml
Tris[hydroxymethyl]aminomethane	*31.52 g*
1 M Sodium hydroxide	*22 ml*
Distilled water	*178 ml*
Sodium chloride	5.8 g
Magnesium sulphate (anhydrous)	0.98 g
Gelatin	0.1 g
Distilled water	1 litre

Peptone Water (0.1% w/v)

Peptone water (PW, 0.1%) was used as one of the bacterial suspending solutions when testing the sensors. The solution was autoclaved at 121°C for 15 minutes.

Peptone	1 g
Sodium chloride	0.5 g
Distilled water	1 litre

Mannitol Solution (0.1 M)

Mannitol solution (0.1 M) was also used to re-suspend bacteria for sensor testing. The solution was autoclaved at 121°C for 15 minutes.

Mannitol	1.822 g
Distilled water	100 ml

Saline

The following saline was used to re-suspend bacteria. The saline was autoclaved at 121°C for 15 minutes.

Sodium chloride	2.25 g
Calcium chloride	0.12 g
Calcium carbonate	0.05 g
Potassium chloride	0.105 g
Distilled water	1 litre

Phosphate Buffered Saline

Phosphate Buffered Saline (PBS) was made up using tablets purchased from Oxoid, UK. One tablet was dissolved per 100 ml distilled water. PBS solutions were autoclaved at 115°C for 10 minutes.

PBS-Tween

PBS was mixed with a mild detergent (Tween® 20) for washing. For 1 litre of PBS-Tween, 0.5 ml Tween® 20 was added to 1 litre sterile PBS.

Coating Buffer

Coating buffer was used in ELISA work to help coat the bottom of well plates with the desired molecules.

Sodium carbonate	0.32 g
Sodium bicarbonate	0.58 g
Distilled water	100 ml

Acetate-Citrate Buffer

Acetate-citrate buffer was used in making up the ELISA substrate.

Sodium acetate	8.29 g
Distilled water	1 litre

The solution pH was adjusted to pH 5.5 using solid citric acid.

ELISA Substrate

This substrate was used to react with peroxidase conjugated antibodies. First, TMB was dissolved in DMSO. Then, 250 µl of this mixture was added to the acetate-citrate buffer along with the hydrogen peroxide. Volumes were as follows:

TMB	3 mg
DMSO	1 ml
Acetate-citrate buffer	25 ml
Hydrogen peroxide	4 µl

Sulphuric Acid

Sulphuric acid (4 M) was used to stop the ELISA substrate reaction. A 1 litre solution was made up using 222 ml of sulphuric acid and distilled water.

4.1.4 Chemicals

Table 4.2 lists chemicals used and from where they were purchased.

Table 4.2. Chemicals used in experimental work and their corresponding supplier.

Chemical	Supplier
Acetone	
Ethanol (absolute, 200 proof, $\geq$ 99.5%)	
Methanol (99.93%)	Sigma-Aldrich, UK
Toluene (anhydrous, 99.8%)	
Glutaraldehyde (25% in H_2O)	
(3-Aminopropyl)trimethoxysilane (APTMS)	
Sulphuric acid	BDH Ltd, UK
Hydrochloric acid	Thermo Fisher Scientific, UK

4.1.5 Sensor Materials

Table 4.3 details the materials used in the fabrication of the sensors and their suppliers.

Table 4.3. Materials used in sensor fabrication and their corresponding source.

Material	Supplier
Acetone	Rockwood Electronic Materials Ltd., UK
S1818 photoresist	ROHM HAAS (UK) Ltd., UK
Polymethylglutarimide	Microchem Corp, Chestech Ltd, UK
Microposit remover 1165	Shipley, UK
Gold Chromium	Kurt J. Lesker Company, UK

Silicon wafers with a 0.3 μm thick layer of silicon dioxide were purchased from Virginia Semiconductor, Inc. (Virginia, USA) and Schott Borofloat 33 (borosilicate glass) wafers were purchased from IDB Technologies Ltd, UK. Wafers were 3 inches in diameter and 525 μm thick.

4.1.6 Antibodies

Anti-protein A antibody produced in rabbit, peroxidase conjugated-goat anti-rabbit IgG and anti-rabbit IgG-Mega 485 antibody were purchased from Sigma-Aldrich, UK.

4.2 <u>General Microbiological Methods</u>

4.2.1 Bacterial Culturing

The bacterial strain (*S. aureus* 8588) was received in freeze dried form from NCIMB and was reconstituted with 1 ml LB broth. The strain was then stored for future use using a cryo bead preservation system (Fisher Scientific, UK). Firstly, the reconstituted culture was streaked onto an LB agar plate. (Streaking involves dipping a sterile inoculation loop into a bacterial broth then spreading the collected broth across an agar plate in streaks in order to achieve growth of single colonies.) After overnight incubation at a temperature appropriate for bacterial growth (37°C), an inoculation loop was used to pick a bacterial colony from the plate and to add it to a pre-prepared cryo vial (contains cryo beads in cryo fluid). The vial was shaken to disperse the bacteria before the cryo fluid was removed using a pipette. The vial was then stored at −18°C. The cryo beads could be used to inoculate broths for experimental use. One bead was added to 10 ml LB broth and incubated for 18 hours at 37°C, 180 rpm.

In addition to inoculating broths with a cryo bead, broths were also cultured by inoculating directly from broths and agar plates streaked with the bacteria (these can be stored at 4°C for up to about one month). An inoculation loop was either dipped into a stored broth or used to collect bacteria from the surface of an agar plate and then used to transfer the bacteria into fresh LB prior to overnight incubation at an appropriate temperature (37°C for *S. aureus* 8588). As discussed in Section 1.5, it

was assumed that, after overnight incubation, *S. aureus* will be in the stationary phase of the growth curve and that when inoculating fresh broth with overnight cultures bacteria would resume growth from the start of the lag phase.

4.2.2 Bacterial and Bacteriophage Enumeration

The concentration of bacterial and phage suspensions were determined by plating samples of the suspensions and then incubating them overnight at 37°C (full protocols will be described in Sections 4.2.2.2 and 4.2.2.3). The resulting colony forming units (CFU) and plaque forming units (PFU) were counted to enumerate bacterial and phage suspensions respectively. In most cases it was first necessary to dilute suspensions to suitable levels in order to ensure the appearance of single countable units.

4.2.2.1 Serial Dilutions

In a serial dilution the dilution factor (DF) is kept constant between dilutions and is calculated as follows:

$$DF = \frac{Final\ Volume}{Aliquot\ Volume}$$

Equation 4.1

where the aliquot is the sample being diluted and the final volume is the sum of the diluting fluid (diluent) and aliquot volumes. For a ten-fold serial dilution the dilution factor is 10.

To prepare a ten-fold serial dilution, 0.1 ml of the neat sample solution was added to 0.9 ml PBS (the diluent) giving a 10^{-1} dilution of the neat solution. This was then thoroughly mixed and 0.1 ml of this solution was added to another 0.9 ml PBS giving a further ten-fold dilution and a 10^{-2} dilution of the original neat solution. This process was repeated until the desired dilution was reached. When necessary, aliquot and diluent volumes were adjusted to give the appropriate dilution factor.

4.2.2.2 Plating

Bacterial cultures and suspensions were enumerated by plating samples (typically dilutions of the neat solution) and counting the resulting CFUs. A CFU is a single,

observable colony which has arisen from one, or possibly more than one, viable bacterial cell.

After carrying out a serial dilution on the bacterial sample, dilutions expected to yield single CFUs were plated (for example, 10^{-7} and 10^{-8} dilutions for a typical broth culture of 10^9 CFU/ml). This involved pipetting 100 µl of the sample onto an LB agar plate and spreading the sample evenly around the plate using a sterile plastic L-shaped spreader. This was repeated in triplicate for each dilution. Plates were incubated overnight at 37°C. The resulting CFUs were counted for each plate and bacterial concentrations were calculated by multiplying CFU counts with the appropriate dilution factor and averaging to give a concentration in CFU/ml.

4.2.2.3 Plaque Assay

Plaque assays were used to determine phage concentrations. A plaque is a discrete circular clearing in a bacterial lawn caused by a lytic phage which has prevented the growth of bacteria (see Chapter 1, Section 1.4.3, for more details).

A standard double agar layer procedure was used. If necessary, a serial dilution was carried out on the sample first. A sample of the phage suspension (100 µl) was then mixed with 100 µl overnight bacterial broth and 4 ml LB top agar. The mixture was poured onto an LB agar plate and the soft agar layer was allowed to set. This was carried out in triplicate for each sample and plates were incubated overnight at 37°C. The number of plaques on each plate was then counted. The number of plaques was multiplied by the appropriate dilution factor to give the concentration of the neat solution in plaque forming units per millilitre (PFU/ml).

4.2.3 Bacteriophage Harvest

Phages were harvested by promoting repeated phage infection and replication with bacteria and then collecting the progeny phages in SM. To do this, excess phages were added to overnight bacterial broth, for example 2 ml phages mixed with 1 ml bacteria. The mixture was incubated at 37°C and 180 rpm for 10 to 15 minutes. Samples of the mixture (150 µl) were then combined with 5 ml LB top agar and poured onto LB agar plates. Plates were incubated overnight at 37°C. SM (4 ml) was

then added to each plate. After 4 hours, the fluid was collected from the plates. Finally, the collected phage suspension was syringe filtered through a 0.22 µm pore membrane filter unit (Millipore, Ireland) to remove any bacteria and agar debris. Phage suspensions can be kept at 4°C for several months with little reduction in activity.

4.2.4 Bacteriophage Purification

It was often beneficial to re-suspend phages in a fresh solution to remove any remaining protein debris, especially for use in immobilisation procedures. Aliquots of the phage suspension (1 ml) were centrifuged at $18\,625 \times g$ for 30 minutes using a mircocentrifuge (Hettich Mikro 200, Switzerland). The supernatant was removed and the remaining pellet (not normally visible due to the size of the phages) was re-suspended in the desired fluid using a WhirliMixer (Nickel Electro Ltd, UK). This process was repeated a further two times.

4.3 Bacteriophage Immobilisation

4.3.1 Substrate Test Sample Preparation

In reference to phage immobilisation, the term 'substrate' is used to define the surface onto which phages are immobilised. Two materials were investigated for use as substrates: glass and polymethylglutarimide (PMGI). Immobilisation methods were tested on samples of these substrates before experimenting with actual sensors.

Glass samples were prepared by cutting 1 mm thick glass microscope slides (Chance Propper Ltd, UK) into 16×9 mm sections using a diamond scribe (RS Components Ltd, UK). Glass coverslips, 22×22 mm and 0.13 to 0.17 mm thick (Thermo Fisher Scientific, UK) were also used as substrates. Samples were cleaned with 70% ethanol. They were then ready for use in an immobilisation procedure.

To prepare PMGI substrate samples, the glass (either 1 mm thick glass microscope slides cut into 25×25 mm sections or glass cover slips) went through the same cleaning and PMGI application process as would be carried out on the actual sensor

substrates. The details of these steps can be found in Section 4.4.2.2. Samples prepared from glass microscope slides were halved before testing using the scribe.

It is likely that phages will also become attached to the gold electrodes when immobilisation procedures are applied to the sensors. It is know that phages can at least physically adsorb into gold [Olsen et al., 2006]. However, gold substrates were not tested for immobilised phages as the initial focus was on immobilising phages between the gold electrodes onto either glass or PMGI.

4.3.2 Immobilisation Methods

Four different immobilisation methods were investigated for the immobilisation of phages: physical adsorption, corona activation, silanisation with glutaraldehyde coupling and immobilisation via biotin-avidin linking.

4.3.2.1 Physical Adsorption

Phages were allowed to physically adsorb onto a surface by incubating purified phage suspension with the substrate for a period of time. Typically, the substrate was placed in a 35 mm diameter Petri dish with 3 ml of re-suspended phage (unless otherwise stated, phages were re-suspended in PBS) and incubated either overnight at 4°C or for 2 hours at room temperature (incubation times are discussed in Chapter 5, Section 5.2.3.1). Substrates were then washed three times (see Section 4.3.3 for details on the washing procedure).

4.3.2.2 Corona Activation

Two corona treatment systems were used during the study: a high power system and a low power system. In the following sections the equipment and method used for each corona system are described. Details on corona, corona generation and the basis for defining these corona systems are presented in Chapter 5, Section 5.1.3.

4.3.2.2.1 High Power System

In the 'high power system' a Sherman Treaters GX10 corona treatment machine (Figure 4.1) was used for the corona treatment of PMGI substrates. The machine has multiple needle electrodes which create the corona discharge at an operating

frequency of 20 kHz. Output power was controlled by a dial which could be adjusted on a scale from 0 to 100. Unfortunately the manufacturer does not specify a relationship between the power output scale and actual power so it was not possible to determine the power used. However, it is stated in the manual that the maximum voltage output is 600 V (RMS) and maximum current output is 7.5 Amps (RMS), giving a maximum possible power output of 4.5 kW. The manual also states a 'treatment power' of 1 kW which may be an average power over time.

Figure 4.1. Sherman Treaters GX10 corona treatment machine used in the high power corona treatment of substrates.

During treatment, substrates were fixed onto the machine's moveable ground plate and passed though the corona discharge. The distance between the sample and electrodes was altered such that the gap was minimal. Adjustable machine parameters include the number of passes through the corona (two or four), plate speed (5 to 25 mmin^{-1}) and power output (normalised on a scale of 0 to 100). Substrates were passed though the corona under the machine parameters detailed in Table 4.4.

Table 4.4. High power corona treatment machine parameters.

Parameter	Value
Number of passes	2
Plate speed	5 mmin^{-1}
Power output	75

These machine parameters were based on previous optimisation work carried out by Holland (2010). Immediately after corona activation, substrates were transferred into a 35 mm diameter Petri dish with 3 ml purified phage suspension for 10 minutes [Holland, 2010]. Substrates were then washed until no free phages were detected in the wash fluid (see Section 4.3.3 for further details on washing).

4.3.2.2.2 Low Power System

The 'low power system' was a custom built corona treatment system designed by Dr Igor Timoshkin (University of Strathclyde, UK) for the corona activation of nylon beads (also for phage immobilisation). The system comprised of an impulse generator (TLG-05, Samtech Ltd, UK) connected to a custom built test rig shown in Figure 4.2.
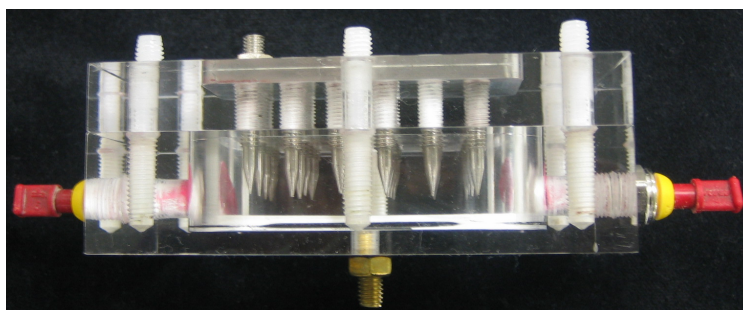
Figure 4.2. Low power corona treatment test cell. Substrates to be treated are placed on the surface directly below the electrodes.

Substrates were placed directly below the electrodes in the test cell which was screwed closed so that the substrate was enclosed in a chamber. The impulse generator applied a peak output voltage of 3 kV at 5 pulses per second (pps). This treatment was carried out for 15 minutes after which substrates were retrieved from the test cell and placed in a phage suspension for 10 minutes followed by washing (see Section 4.3.3 for washing details).

4.3.2.3 Silanisation and Glutaraldehyde Coupling

Phages were immobilised onto glass substrates based on the silanisation protocol described by Bhatia et al. (1989). First, glass substrates needed to be thoroughly cleaned. Substrates were acid cleaned by immersion into a 1:1 mixture of hydrochloric acid and methanol for 30 minutes followed by rinsing with distilled water. Next, substrates were immersed in sulphuric acid for 30 minutes, again followed by rinsing in distilled water. Finally, substrates were boiled in distilled water for 30 minutes before being left to air dry.

The next step was silanisation. A 2% (v/v) solution of APTMS in toluene was prepared. Substrates were immersed in the solution for 1 hour at room temperature [Sapsford and Ligler, 2004]. Substrates were rinsed in toluene followed by distilled water and were then allowed to air dry.

Next, substrates were immersed in a 10% (v/v) glutaraldehyde solution (diluted with distilled water) for 2 hours [Shriver-Lake et al., 2002, Singh et al., 1999]. They were then thoroughly rinsed with distilled water and left to air dry.

Finally, substrates were incubated with a purified phage suspension for 2 hours at room temperature. Substrates were then washed until no free phages were detected in the wash fluid (see Section 4.3.3 for washing details).

4.3.2.3.1 Chemical Vapour Deposition Method

A chemical vapour deposition (CVD) method was also investigated for forming the silane layer on glass as an alternative to the solution based approach described in Section 4.3.2.3. The protocol used was adapted from Song et al. (2006) as follows.

Samples were cleaned as outlined in Section 4.3.2.3. APTMS (0.5 ml) was added to 2.8 ml toluene in a 5 ml vessel which in turn was placed into a 250 ml vessel. Samples were also placed in the 250 ml vessel which was sealed and put in an oven at 100°C for 1 hour. After allowing the vessel to cool, samples were removed and underwent the post silanisation washing treatment as outlined in Section 4.3.2.3.

Substrates were then incubated with glutaraldehyde and then phages as also described in Section 4.3.2.3.

4.3.2.4 Biotin-Avidin Immobilisation

In this section the protocol used to immobilise phages by the biotin-avidin system is described. Further details on the system and the determination of method parameters are outlined in Chapter 5, Section 5.1.4.

4.3.2.4.1 Biotinylation of Bacteriophages

A pre-packaged vial of 1 mg Sulfo-NHS-biotin (sulfosuccinimidyl-6-[biotin-amido]hexanoate) stored at -18°C was allowed to equilibrate to room temperature before being dissolved with 100 µl PBS. Phages were conjugated with biotin (a process known as biotinylation) by mixing 1 ml of re-suspended phages in PBS with the appropriate volume of Sulfo-NHS-biotin (the optimum concentration of biotin was determined and results are reported in Chapter 5, Section 5.1.4.2). It was important that phages were purified and suspended in an amine-free buffer, such as PBS, to remove any traces of amine groups which may also react with biotin. The reaction was incubated at room temperature for 30 minutes.

To remove the excess biotin, a Zerba™ Desalt Spin Column (Thermo Fisher Scientific, UK) was used. The desalting column was prepared following the manufacturer's instructions. This essentially involved centrifuging the column at $1000 \times g$ for 2 minutes to remove the storage buffer and repeating this a further three times with 2.5 ml PBS to equilibrate the column. Having placed the desalting column into a fresh 15 ml collecting tube, the phage sample was then applied to the column and centrifugation repeated. The collected flow through was the purified phage sample which was stored at 4°C until use. The stability of the biotinylated phages was unknown so biotinylated phages were always prepared and used on the same day where possible.

4.3.2.4.2 Immobilisation of Biotinylated Bacteriophage via Biotin and Avidin

The procedure developed for the immobilisation of biotinylated phages onto a substrate was adapted from protocols described in Kim et al. (2009) and Koo et al.

(2009). All solution incubations were carried out at room temperature. First, substrates were incubated with 1 mg/ml biotin labelled bovine albumin suspended in PBS (B-BSA) for 2 hours. Substrates were then washed three times with PBS. Next, 0.1 mg/ml NeutrAvidin was applied to the substrates for 20 minutes followed by three washes. The substrates were then incubated with biotinylated phages for 3 hours. Finally, substrates were washed ten times to remove excess phages (the number of washes required was determined through experimental work which is reported in Chapter 5, Section 5.1.4.2).

4.3.3 Substrate Washing

Washing substrates after incubation with phage suspensions was necessary to remove any free phages, that is phages that are only loosely bound to the substrate's surface or attached to other immobilised phages and are therefore easily removed. Typically, washing involved running 20 ml PBS down the substrate's activated surface using a pipette and then transferring the substrate into a fresh universal of PBS followed by a period of soaking with gentle agitation (usually for 20 to 30 seconds). This complete process was defined as one wash. The physical force of applying a stream of fluid down the substrate and then agitating it in solution were relied upon to remove loosely bound phages.

To test for the presence of free phages coming off a substrate's surface, 1 ml of wash fluid was run down the substrate's surface and collected. A 100 µl sample of the collected wash fluid was then plaque assayed to check for any free phages (see Section 4.2.2.3 for the plaque assay protocol). This was carried out in triplicate.

Substrates with physically adsorbed phages were washed three times. Phages immobilised through biotin-avidin binding were washed ten times (the determination of this values is discussed in more detail in Chapter 5, Section 5.1.4.2). Samples with covalently immobilised phages were washed until no free phages were detected from two consecutive washes.

4.3.4 Detection of Immobilised Bacteriophages

Detection of immobilised phages was important for determining whether each immobilisation method was successful and also to make a comparison of the efficacy of the various immobilisation methods. There is no common standard method for detecting immobilised phages. Here, two methods were used to detect for the presence of immobilised phages: a broth culture method which gave a positive/negative result for the presence of active phages; and a quantitative fluorescent detection method.

4.3.4.1 Broth Culture Detection Method

The broth culture method of detecting immobilised phages is a microbiological based technique which relies on the immobilised phages infecting, replicating within and then lysing bacteria. The free progeny phages can be detected in a broth culture at the end of an incubation period by a plaque assay. A positive result from the plaque assay (i.e. visible signs of plaques) confirms the presence of successfully immobilised active phages on the substrate.

Substrates were put in 10 ml LB media and then inoculated with 10 µl bacterial broth culture. For each immobilisation method three substrates were prepared and the same overnight broth culture was used to inoculate each sample. Samples were then incubated for 20 hours at 37°C, 180 rpm. Aloquots (1 ml) of each overnight broth were then centrifuged for 5 minutes at $13\,684 \times g$ and the supernatant fluid was filtered through a 0.22 µm syringe filter. This process separated any phages from bacteria and other culture debris.

Next, the supernatant fluid was plaque assayed (see Section 4.2.2.3). Since the levels of phage present in the broth cultures were unknown, a range of supernatant dilutions were plated. Typically the neat supernatant was plaque assayed as well as 10^{-2}, 10^{-4} and 10^{-6} dilutions. Results were reported in terms of the plaque assay outcome at each dilution (this is defined in detail in Chapter 5, Section 5.2.1).

4.3.4.2 Fluorescent Detection

A customised indirect fluorescent immunoassay (FIA) was devised in order to quantitatively evaluate immobilisation methods. In the following sections, protocols relevant for the FIA are described and in Chapter 5 (Section 5.3.1) a detailed discussion on the method can be found.

4.3.4.2.1 Generating Anti-Bacteriophage 9563 Antibodies

An anti-bacteriophage 9563 antibody, i.e. an antibody active against bacteriophage 9563, was kindly donated by Dr Janice Spencer (formerly of Blaze Venture Technologies, UK, and currently employed at Glasgow University, UK). Briefly, the antibody was generated by injecting a rabbit with phages and an adjuvant (an agent used to stimulate the immune system and thus raise antibodies against its conjugate, in this case bacteriophage 9563). After a second booster injection and a suitable period of time (the process of generating antibodies takes several weeks), the blood serum was collected. Anti-bacteriophage 9563 antibodies should be present in the blood serum (blood from which blood cells and clotting factors have been removed) which was stored in 1 ml aliquots at -18°C.

4.3.4.2.2 ELISA for the Detection of Active Anti-Bacteriophage 9563 Antibodies in Rabbit Serum

In order to confirm that the blood serum contained active anti-bacteriophage 9563 antibodies, a simple ELISA was performed.

The first step of the ELISA was to add 100 µl of bacteriophage 9563 to each well in two rows of a 96 well plate with 100 µl of coating buffer. This was left overnight at 4°C. The wells were washed three times with PBS-Tween and excess liquid was removed from the wells by beating the well plate against tissue paper. Then, 200 µl of BSA in PBS (10 mg/ml) was added to each well for 30 minutes at 37°C to block non-specific binding sites, after which the washing and drying steps were repeated. Next, 100 µl of the rabbit blood serum was added to the wells at two different dilutions: to one row a 1 in 1000 dilution was added and to the other a 1 in 10 000 dilution. The well plate was left for 2 hours at room temperature. The washing and

drying steps were repeated after the incubation period. Peroxidase conjugated anti-rabbit IgG (100 μl) was then added to each well and incubated at room temperature for 1 hour before repeating the washing and drying steps. Finally, 150μl of substrate was added to each well and incubated at room temperature in the dark for 30 to 40 minutes, until the reaction mixture turned blue. To stop the reaction, 50 μl of 4 M sulphuric acid was added to the substrate causing it to turn yellow in colour.

Absorbance was read at 450 nm using a plate reader (Labsysytems iEMS Reader MF, Finland). Results were compared to control rows of 1:1000 and 1:10 000 dilutions of pre-bleed serum (taken before the rabbit was injected with phages). Additional control rows were also prepared in which only PBS was initially incubated with the coating buffer in the first step of the protocol.

4.3.4.2.3 FIA for Immobilised Bacteriophages

The FIA developed within this research for the detection of immobilised bacteriophage 9563 is discussed in detail in Chapter 5, Section 5.3.1. Here, the protocol used is outlined.

The FIA was first tested with phages which had been fixed onto poly-l-lysine coated glass coverslips. Poly-l-lysine was diluted 1:10 with sterile distilled water. Coverslips which had been cleaned with 70% ethanol were immersed in the poly-l-lysine solution for 5 minutes. Coverslips were dried at 60°C for 1 hour. The phage suspension (200 μl) was applied to the centre of the coverslip and left overnight followed by washing with PBS three times.

For the testing of immobilisation methods, substrates were prepared for the FIA by immobilising phages onto glass coverslips following the immobilisation procedures described in Section 4.3.2. Again, 200 μl phage suspension (200 μl) was applied to the centre of each coverslip which were washed according to the relevant immobilisation procedure.

Once the coverslips were prepared, they were incubated with BSA in PBS (20 mg/ml) for 2 hours at 37°C to block non-specific binding sites. Samples were then washed twice with PBS-Tween and once with PBS as described in Section 4.3.3. Samples were then incubated with the anti-bacteriophage 9563 antibody (the primary antibody). A 1 in 1000 dilution of the rabbit serum, containing the anti-bacteriophage 9563 antibody, was used as this dilution had previously been successful in the ELISA (Section 4.3.4.2.2). Samples were incubated with the primary antibody solution for 2 hours at room temperature. Coverslips were then washed as described previously. The last step was incubation with the fluorescently labelled anti-rabbit IgG-Mega 485 antibody. A 1 in 1000 dilution of this secondary antibody was used according to the manufacturer's recommendation and samples were incubated for 1 hour at room temperature before a final wash. The coverslips were then allowed to dry.

Slides were prepared by inverting the coverslip and placing it onto a clean standard microscope slide and sealing the edged of the coverslip with clear nail varnish. Three slides were prepared for each immobilisation method. Three control slides were also prepared for which the coverslips underwent exactly the same procedure described in this section but were not exposed to phages. Instead, when samples were incubated with phages, control coverslips were incubated with the same volume of the suspending medium (PBS) only.

4.3.4.2.4 Image Capture and Analysis

The microscopy work was performed using a Nikon Eclipse TE2000-E inverted fluorescent microscope. This microscope allows both optical phase contrast microscopy and fluorescent microscopy to be performed with either UV, blue or green excitation light.

To examine slides prepared using the FIA, two microscope shutters were used: one with a brightfield filter for optical microscopy and a second that was assigned a fluorescent filter appropriate for the fluorescently labelled antibody. In this case, the fluorescent conjugate of the secondary antibody used in the FIA has an excitation wavelength of 485 nm (blue light) and an emission wavelength of 552 nm (green

light) therefore the FITC-HQ fluorescent filter was used which has an excitation bandwidth of 460 – 500 nm and an emission bandwidth of 510 – 560 nm. A 100 × oil emersion objective lens was used for viewing the slides.

In addition to the direct observation of slides though the eyepiece, the microscope was also connected to a Hamamatsu digital camera which allowed images of the slides to be captured, enhanced and analysed on a PC. The camera was controlled via the scientific image processing software package IPLab, version 4.04 (BD Biosciences, USA), installed on a PC and through which image capture parameters could be set.

A 1 × 1 bin camera setting was used for maximum resolution. The 100 × objective had previously been calibrated for the 1 × 1 binning setting for which it was found that each pixel is 0.0903 µm in width and height. The exposure times of the brightfield and FITC-HQ fluorescent shutter were 5 ms and 500 ms respectively. For each slide, five images (1344 × 1024 pixels) were acquired at different locations on the centre of the coverslip (where the coverslip had been exposed to phages).

Images were then processed and enhanced for analysis. First, images from treated slides were normalised against control slide images to account for any non-specific background fluorescence. This was achieved by adjusting the control images using a normalisation tool within IPLab so that all fluorescence was eliminated on the image. The normalisation parameters at this point were then applied to the treated slide images. Images were pseudocoloured with the appropriate fluorescent colour (in this case, green) and enhanced if necessary through adjustments to brightness and contrast levels. The enhanced colour images were converted to 24-bit Colour 24 types and saved as TIFF files.

Enhanced images were used to count the fluorescent spots representing immobilised phages. This could be done automatically within IPLab using the segmentation tool. First, the segmentation tool was used to identify the fluorescent spots as regions of interest with a coloured overlay. By adjusting the threshold for segmentation, the

user is given control over defining the regions of interest. The coloured overlay segments (regions of interest) were then counted automatically using the 'Measure/Quantify Segment' command. An average count was obtained for each slide from the five images captured and typically three slides were prepared for each immobilisation method tested.

When it was not possible to apply the automatic approach for analysing the fluorescent images, a manual method was adopted. In this approach, instead of counting the number of fluorescent spots in the image area, manual counts were taken from three smaller areas which were one sixth of the size of the image (224×170.67 pixels). Values from the three sample areas were averaged and then scaled up to represent the whole image area and so would be comparable with results from the automatic method. The differences between the automatic and manual approaches to analysing images are discussed in detail in Chapter 5, Section 5.3.1.

4.3.5 Method to Investigate the Ability of Immobilised Bacteriophages to Capture Bacteria

An experiment was devised in order to confirm and analyse the ability of immobilised phages to capture bacteria onto a substrate surface. Phages were immobilised onto four glass coverslips using the silanisation and glutaraldehyde coupling method as outlined in Section 4.3.2.3. In addition to this, four control coverslips were prepared which underwent the same immobilisation procedure but were not incubated with phages (instead they were incubated with PBS, the suspending medium). All substrates, including the controls, were blocked with BSA in PBS (10 mg/ml) for 30 minutes followed by three washed with PBS as per Section 4.3.3.

Once the immobilisation procedure was complete, a bacterial suspension was prepared by centrifuging an overnight broth culture of *S. aureus* 8588 at 13 684 × *g* for 5 minutes and then re-suspending the bacteria in saline solution. This process was repeated a further two times to remove any cell debris. The concentration of the bacterial re-suspension was estimated by following the plating procedure described in Section 4.2.2.2.

Next, 0.7 ml of the bacterial re-suspension was applied to each cover slip (samples and controls). At 2, 5, 10 and 20 minute incubation times, one sample and one control cover slip were rinsed with 10 ml PBS and placed into absolute methanol for 10 minutes to fix the bacteria. Coverslips were then removed from the methanol and allowed to dry before they were inverted and placed onto a microscope slide and sealed with nail varnish.

The slides were viewed using phase contrast microscopy. A Nikon Eclipse TE2000-E inverted microscope was used under the brightfield settings described in Section 4.3.4.2.4. The number of bacteria and bacterial clusters were manually counted for five images taken from each slide from which an average was calculated.

Substrates were also prepared with immobilised anti-protein A antibodies in order to compare phage performance to that of antibodies. Anti-protein A antibodies can bind to protein A on the surface of *S. aureus* 8588. Substrate treatment was exactly the same as for phage samples but after the silane and glutaraldehyde treatment, substrates were immerssed in a solution of 185 μg/ml anti-protein A antibody. This antibody concentration was based on that used by Radke & Alocilja (2004).

4.4 <u>Biosensor Fabrication</u>

The sensors were fabricated by Dr David Hutson (Department of Physics, University of the West of Scotland). Dr Colin Pegrum (Department of Physics, University of Strathclyde) acted as a consultant on the sensor design and fabrication.

4.4.1 Photomask

The photomask acts as a master template from which the sensors are created. It is typically a quartz or glass plate covered in a chrome layer depicting the pattern to be transferred onto the wafer substrate. During the photolithography process, light passes through the transparent areas of the photomask which ultimately leads to the creation of the desired pattern onto the wafer. In this case the pattern will be that of the sensors.

A specialised software package, WaveMaker® LAYOUT (Barnard Microsystems Limited, UK), was used to create a drawing of the desired photomask layout. Based on this drawing, the photomask was then manufactured by Compugraphics (Glenrothes, UK). Details of the sensor designs incorporated into the photomask were outlined in Chapter 3, Section 3.2, and are discussed further in Chapter 6, Section 6.2.

4.4.2 Photolithography

Details of the photolithography method used to create the sensors will now be provided. Here, the term 'substrate' refers to the material onto which the sensor's electrode array was created. The wafers used are detailed in Section 4.1.5.

4.4.2.1 Photolithography Equipment

The sensors were fabricated in a class 10 000 cleanroom. A class 10 000 cleanroom is one which is designed to maintain less than 10 000 particles (0.5 µm or larger in diameter) per cubic foot of air space. Humidity and temperature were regulated at 56% and 18 – 19°C. A cleanroom suit, safety glass and latex gloves were worn whilst working in the cleanroom.

A supply of nitrogen gas and deionised water was available in the cleanroom. A photoresist spinner (Model 3000, Electronic Micro Systems, UK) was used for coating substrates with the polymer and photoresist and a hot plate (Model 1000-1, Electronic Micro Systems, UK) was used for heating substrates. For UV exposure of the photoresist and polymer, a mask aligner (Karl Suss, Germany) and a flood exposure system (Cole-Palmer, UK) were used. The substrate was milled and sputtered with chromium and gold in a custom designed spluttering vacuum chamber.

4.4.2.2 Photolithography Method

In any photolithography process it is essential that the substrate is first thoroughly cleaned so that it is free from small particles which might compromise the adhesion of materials. To achieve this, the wafers were ultrasonicated in acetone for 2 minutes

followed quickly by rinsing in deionised water. Wafers were then placed in a bath of deionised water with nitrogen bubbling for 2 minutes followed by drying with nitrogen gas. Finally, the wafers were heated to 190°C on the hot plate for 5 minutes to evaporate any remaining water.

The photolithography process is summarised in Figure 4.3 (presented at the end of this section). The first step was to coat the wafer with PMGI and S1818 photoresist. This involved vacuum fixing the wafer onto the spinner and applying a small volume of PMGI onto the centre of wafer. The spinning speed was then slowly ramped to 4000 rpm which was maintained for 40 seconds. This gave the wafer a polymer layer coating approximately 0.7 µm thick. The wafer was hot plate baked for 5 minutes at 190°C to remove all of the polymer solvent, followed by a period of cooling at room temperature. The wafer was then coated with S1818 photoresist using a similar process with the wafer spun at 4000 rpm for 30 seconds and baked at 115°C for 5 minutes.

Next, the photoresist and then polymer layer were exposed to UV light in a series of steps necessary to develop the photomask design onto the wafer prior to sputtering. First, the photomask was inserted into the mask aligner and aligned with the wafer. The photoresist surface was exposed to 436 nm UV radiation for 25 seconds. The wafer was returned to the hot plate for 2 minutes and allowed to cool before being placed in developer fluid (Microposit Remover 1165) for 1 minute. After, the wafer was rinsed with deionised water, placed in a nitrogen bubbling bath, and dried with nitrogen.

The PMGI layer was then exposed to deep UV (DUV, 254 nm) for 5 minutes using the flood exposure system. Following this, the wafer was put in developer fluid (Microposit Remover 1165) for 1 minute and rinsed with deionised water and dried by nitrogen.

The next stage took place in the custom designed sputtering chamber. Once the wafer was in position, its surface was cleaned by ion milling for 30 seconds before DC

sputtering of chromium in argon at 250 W and a pressure of 6 mT for 30 seconds. Next, gold was deposited for 6 minutes at 200 W and 9 mT. The final step was lift off: the wafer was placed in acetone for approximately 30 seconds or enough time for the photoresist (covered in a layer of gold) to come away from the wafer surface.
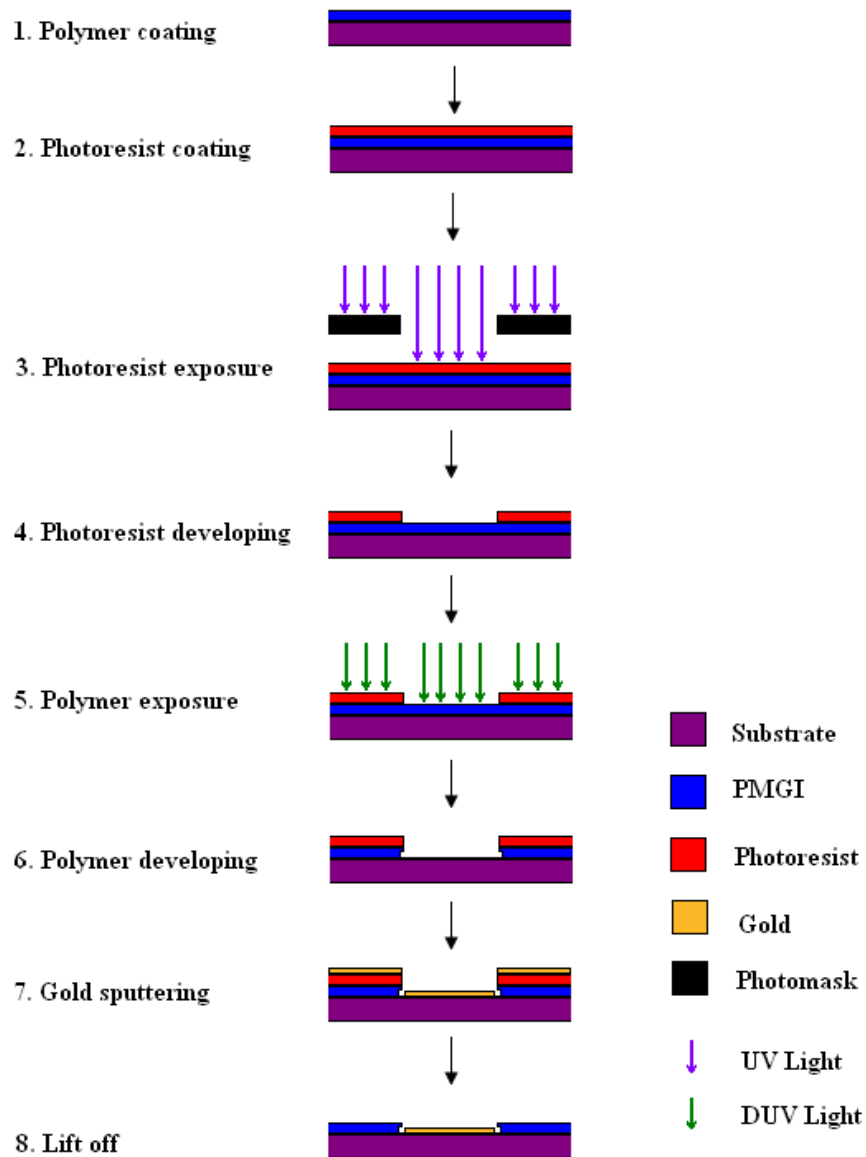
Figure 4.3. Schematic summary of the photolithography process for sensor fabrication.

4.4.3   Wafer Cutting

Individual sensors were cut from the wafer using a diamond saw. There were 24 sensors per wafer, each 16×8 mm. Before cutting, the wafer was covered in

photoresist to protect the sensors from possible debris and damage during cutting. The photoresist layer was removed after cutting by placing each sensor in acetone for 2 minutes followed by rinsing in deionised water and drying with nitrogen gas.

4.5   <u>Biosensor Testing</u>

4.5.1   Equipment and Set-up

An HP 4194A Impedance/Gain-Phase Analyser (Hewlett Packard, Tokyo, Japan) was used to measure the impedance of the sensor. The impedance analyser was controlled using the software package PRAP, Version 2.2 (TASI Technical Software Inc., Canada), installed on a PC connected to the impedance analyser. Measurement parameters were set and data acquisition was carried out within PRAP. The data collected was exported from PRAP to a Microsoft Excel file.

A test rig for the sensors was designed and fabricated and is shown in Figure 4.4. The principal functions of the test rig were: (a) to connect the impedance analyser to the sensor in a practical manner which did not risk damaging the sensor and (b) to provide a rigid support for the sensor during testing. To achieve this, a lever arm design was decided upon. The lever arm is attached to a rigid base and is spring loaded so that it can be gently raised and lowered to make contact with a sensor via two spring loaded gold plated probes (Coda Systems Ltd, UK) incorporated into the arm. Each probe head (1.27 mm in diameter) made contact with a sensor contact pad (1.5×1.5 mm) as demonstrated in Figure 4.6 to follow. A printed circuit board (PCB) is fixed on top of the arm which connects each probe to two coaxial cables (four coaxial cables in total). Each cable was 2.79 mm in diameter, 40 cm long and fitted with a BNC (Bayonet Neill-Concelman) connector for attachment to the four terminals of the impedance analyser. The coaxial cable and BNC connectors had a characteristic impedance of $50 \, \Omega$ to match that of the impedance analyser (this minimised signal loss).
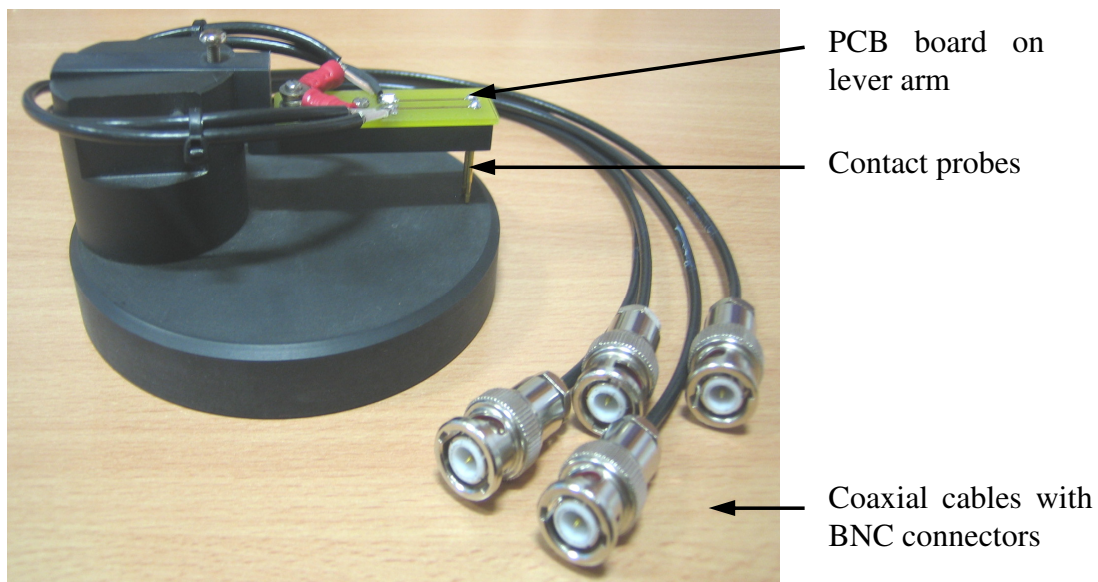
Figure 4.4. Sensor test rig.

Figure 4.5 shows the equipment set-up for recording impedance measurements: the test rig is connected to the impedance analyser which is connected to a PC with the installed PRAP software.
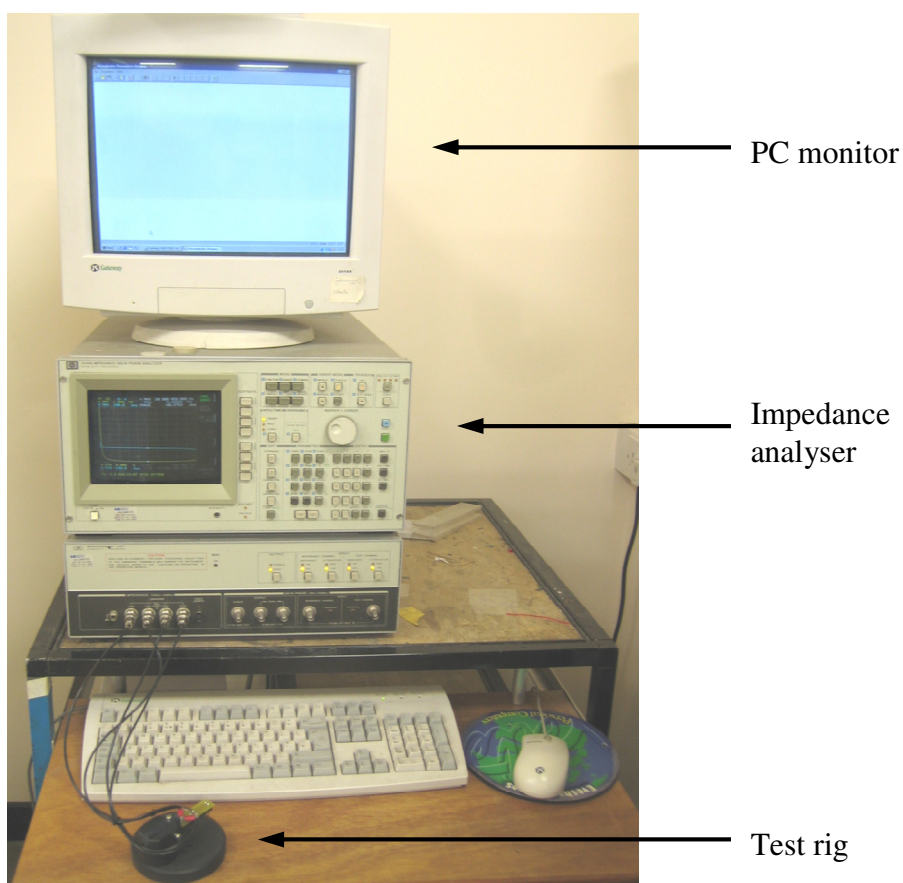
Figure 4.5. Equipment set-up for sensor impedance measurements.

4.5.2 Sample Preparation

Bacterial samples were prepared in three different suspending solutions for sensor testing: 0.1% peptone water, 0.1% PBS and 0.1 M mannitol. In each case, an overnight broth culture of *S. aureus* 8588 was centrifuged at $13\,684 \times g$ for 5 minutes and re-suspended in the desired solution. The re-suspending process was repeated a further two times to remove as much culture debris as possible. Bacterial solutions were prepared immediately prior to sensor testing and used 10 minutes after preparation. Bacterial solutions were kept at room temperature. Control solutions were the suspending solutions only, without bacteria. The concentrations of test samples were determined following the standard plating method as described in Section 4.2.2.2.

4.5.3 Testing Method

After immobilisation treatment, sensors were positioned in the test rig such that the test rig probes were in contact with the sensor's electrodes via the contact pads as illustrated in Figure 4.6. Two approaches were used to test the sensors. In Testing Method 1, a 0.1 ml sample of the control solution was applied onto the sensor's surface such that the solution completely covered the sensor's electrode array area but did not reach the test rig probes or contact pad areas. Figure 4.6 shows an image of the sensor mounted in the test rig with a 0.1 ml sample on the sensor surface. Impedance measurements were then recorded: a 50 mV AC potential was applied across the sensor's electrodes and impedance was measured at 100 Hz, 1 kHz, 10 kHz, 100 kHz, 1 MHz and 10 MHz. The control solution was then removed and the bacterial solution was applied (0.1 ml). Impedance measurements were then taken and repeated every 5 minutes over a period of time (usually 1 hour). Solutions were applied and removed using a pipette.
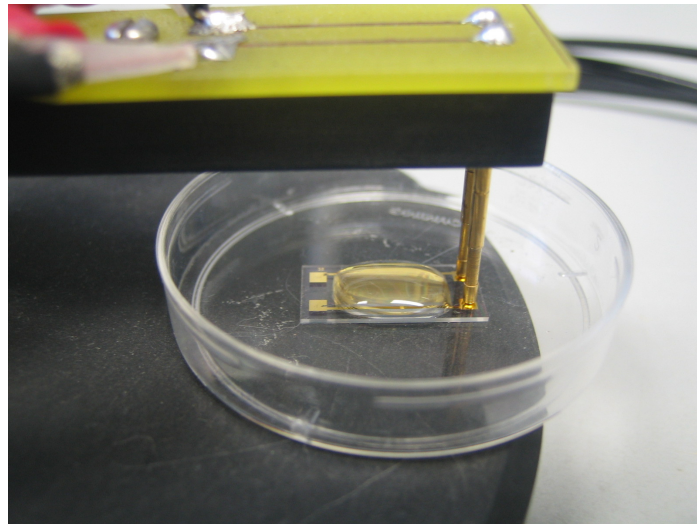
Figure 4.6. A sensor positioned in the test rig with a 0.1 ml sample covering the sensor's electrode array area.

Later, a second testing approach was adopted (Testing Method 2) in which the sensors were placed into the bacterial solution for 10 minutes after the control measurement (which was carried out as described previously). The sensor was then removed, rinsed with 10 ml of control solution and re-positioned in the test rig. The control solution (0.1 ml) was then re-applied to the sensor and impedance measurements recorded. Sensor performance was assessed by comparing impedance of the sensor before and after exposure to a bacterial solution.

Chapter 5

BACTERIOPHAGE IMMOBILISATION

This chapter details the results of the investigation into phage immobilisation. Phages have previously been immobilised by a number of methods including physical adsorption [Bennett et al., 1997, Carnazza et al., 2007, Nanduri et al., 2007b, Olsen et al., 2006, Wan et al., 2007], the biotin-avidin system [Gervais et al., 2007, Sun et al., 2001] and covalent bonding through corona activation [Holland, 2010] and chemical coupling agents [Handa et al., 2008, Shabani et al., 2008]. However, to the author's knowledge, a detailed comparative study of different immobilisation methods for the specific immobilisation of phages has not been reported. Yet optimising bioreceptor immobilisation is critical to biosensor performance. It was therefore decided to investigate several different immobilisation methods for the immobilisation of bacteriophage 9563 onto both glass and PMGI with a view to selecting the most appropriate method for application with the sensor developed in this study and previously described in Chapter 3.

Within this chapter, first background information is provided on the common immobilisation procedures investigated in this study with particular focus on phage immobilisation. The immobilisation methods investigated were: physical adsorption; covalent immobilisation by corona activation; covalent immobilisation via silanisation and glutaraldehyde coupling; and the biotin-avidin system. Details on the methods are provided in this chapter where considerable method development was necessary. Results are then presented and discussed for the immobilisation methods investigated. Two approaches were used to assess the immobilisation techniques. First, a simple microbiological method was used to obtain positive/negative results for the presence of active immobilised phages. Secondly, a fluorescent immunoassay method was developed to provide quantitative data. Protocols for the immobilisation procedures and analysis approaches are provided in Chapter 4.

5.1 Immobilisation Methods

5.1.1 General Aspects of Bioreceptor Immobilisation

Biosensors require that the bioreceptor is immobilised onto or in the vicinity of the transducer where interactions between the bioreceptor and its target will lead to detection. Immobilisation therefore plays a critical role in determining the performance of a biosensor and requires careful consideration if the biosensor is to be successful.

Ideally the immobilisation procedure should yield a high density of immobilised bioreceptors onto the substrate to maximise the chance of target capture but should not in any way affect the activity of the bioreceptor i.e. its ability to bind with the target molecule. Other critical aspects which need to be considered include: the strength of the bond between the substrate and bioreceptor, the stability of the immobilised bioreceptor, the substrate material and the effect of the procedure (such as the chemicals used) on the substrate/sensor. The cost, procedure time and complexity of the method are also important factors.

The immobilisation of proteins is a vast research area which is continually developing with advances in technology. As well as for biosensor development, other applications of immobilised proteins include the immobilisation of enzymes for industrial applications, such as in the sterilisation and purification of food and drink products, and the immobilisation of proteins onto medical devices for improved compatibility. Currently however, the immobilisation process is presenting several challenges to biosensor development, such as ensuring adequate levels of immobilised bioreceptor and controlling their orientation. Arguably, improvements to bioreceptor immobilisation could be key in overcoming the shortfalls of some of the present biosensor technology, as previously discussed in Chapter 1.

The use of a wide variety of immobilisation methods is reported in biosensor literature. A review on general aspects of immobilisation can be found in Bickerstaff (1997) along with details on a number of immobilisation methods. In this work, four

broadly diverse immobilisation methods have been implemented and some background on these methods is provided in the following sections with particular focus paid to the immobilisation of phages for the detection of bacteria. Other immobilisation techniques do exist, such as entrapment and encapsulation, but these methods are less practical for the intended application in this research and so were not investigated.

5.1.2   Physical Adsorption

Physical adsorption is a long established method of protein immobilisation. It is the process by which bioreceptors become attached to a substrate via weak molecular forces such as Van der Waals forces and hydrogen, ionic and hydrophobic bonding. The bond is created through the inherent physical nature of the bioreceptor and substrate, such as their surface charge. For this reason, physical adsorption offers several advantages: it is cheap, simple, immobilisation conditions are mild and there is therefore usually very little or no detrimental effect on bioreceptor activity. It has also been found that phages remain active for longer when physically adsorbed onto a surface compared to when free in solution [Mattey, 2005b].

However, because only very weak bonds are created through physical adsorption, bioreceptors tend to 'leak' from the substrate's surface. Certain environmental conditions such as pH and temperature must be controlled to prevent increased desorption [Kierstan and Coughlan, 1991]. Bioreceptor leakage could result in reduced biosensor sensitivity, and shelf life will also be limited. In addition to this, the orientation of immobilised bioreceptors is not controlled with physical adsorption.

Despite these drawbacks, physical adsorption as a method to immobilise bioreceptors for the detection of bacteria has and continues to be used. With specific respect to phage immobilisation, physical adsorption was recently used to successfully immobilise phages onto the gold surface of QCM electrodes [Lakshmanan et al., 2007, Nanduri et al., 2007b, Olsen et al., 2006, Wan et al., 2007]. Bennett et al. (1997) investigated the use of phages, physically adsorbed onto polymers, to specifically separate and concentrate bacteria from culture media containing other

non-target bacteria. However, although Bennett et al. (1997) demonstrated the potential of such technology, the capture efficiency was considered inadequate i.e. bacteria detection was only achieved with very high bacterial concentrations. It was speculated that unfavourable orientation of the immobilised phages could be responsible for this.

Carnazza et al. (2008) successfully immobilised filamentous display phages (phages genetically engineered to present specific foreign proteins on their surface, as first mentioned in Chapter 1, Section 1.4.4) onto quartz through physical adsorption with only a two hour phage incubation period but generally there are few reports of the adsorption of phages onto glass substrates for biosensor applications. However, research has been conducted into the ability of viruses, including phages, to adsorb onto silica based substrates for other applications, such as filtration, for which success has been reported [Penrod et al., 1996, Yuan et al., 2008, Zerda et al., 1985].

5.1.3 Covalent Immobilisation

The covalent immobilisation of bioreceptors has been widely implemented across biosensor research. A covalent bond is one in which electrons between atoms are shared, forming a very strong and stable bond. For bioreceptor immobilisation, the potential exists to covalently bind protein functional groups present on the surface of bioreceptors with substrate functional groups. For example, carboxyl groups, present on the outer protein surface of phages, could react with amine groups made available on a suitable substrate to form a stable covalent bond.

Covalent bonding is often favoured as an immobilisation technique for biosensors as it is much stronger than those associated with physical adsorption. The strong bonds greatly reduce the chance of bioreceptor leakage and improve stability [Carr and Bowers, 1980]. This will increase the life time of the immobilised layer, especially under adverse conditions [Scouten et al., 1995]. Therefore covalent immobilisation could yield a commercially viable biosensor. Also, because there are a number of different reactions possible to bring about covalent bonding it is likely that a successful chemistry can be found even if little is known about the surface of the materials involved.

However, there are some drawbacks to covalent immobilisation. Methods can often be complicated and time consuming with several steps and reagents involved. Reagents may be expensive leading to increased costs compared to physical adsorption. Arguably the most important consideration is the effect on bioreceptor activity. The harsh nature of the reagents involved and any conformational changes due to the strong bonds may adversely affect the bioreceptor function. A decrease in the activity of covalently immobilised antibodies, for example, has been reported [Stefan et al., 2000].

In this research, two approaches were investigated to achieve covalent immobilisation of phages: corona activation of the substrate surface and chemical coupling. Details of these methods will now follow.

5.1.3.1 Corona Activation

5.1.3.1.1 Background

Plasma is an overall electrically neutral matter, typically in the form of an ionised gas, containing charged and neutral particles such as electrons, ions, atoms and molecules. Plasma can occur naturally or it can be induced artificially by the appropriate application of an electric field. There are various forms of induced plasma, one of which is corona discharge.

Corona discharge is an electrical discharge which can be induced between two electrodes where one is set up such that its geometry and charge creates a high potential gradient and a strong subsequent electric field. Often one electrode takes the form of a series of sharp points and the second electrode is flat. If the electric field created around this electrode is strong enough, ionisation of the surrounding medium will occur. In this study, corona was activated in air at atmospheric pressure. The resulting effect is a corona discharge which can appear as a blue glow.

Surface modification using corona discharge involves the direct application of the corona onto a polymer. The interaction of plasmas with a polymer is a complex

process and so it is difficult to obtain a detailed understanding of the process. In general terms, it is believed that active species within the plasma react with surface species to create functional groups [Chan et al., 1996]. For example, when creating corona discharge in air, ozone is formed (an unstable and harmful oxidising agent) and this could interact with the polymer. Since oxygen and nitrogen molecules are present in air, the possibility exists for oxygen and nitrogen functional groups to be formed on the polymer surface which could then form covalent bonds with bioreceptor molecules.

Immobilisation using corona discharge provides several potential advantages over other immobilisation techniques such as:

- fast and simple surface activation (often plasmas only need to be applied for a matter of seconds for surface changes to occur [Chan et al., 1996]),
- no requirement for a coupling agent and therefore no harsh chemicals,
- uniform surface modification can be achieved and can be confined to a thin layer (typically tens of nanometers [Chan et al., 1996]),
- the possibility exists to scale up the procedure for industrial and commercial production.

The technique is, however, limited to certain substrates; primarily the treatment has only been applied to polymers, although all polymers are thought to be suitable [Chan et al., 1996]. Also the lack of understanding of the chemistry involved can lead to difficulties in determining procedure parameters, such as power, exposure time and temperature, and also in controlling the levels of a particular functional group being formed.

Despite the potential of plasma modification, the method has not been widely adopted to immobilise bioreceptors in the field of biosensors. However the success of plasma modification to immobilise proteins on a more general level has been reported. For example, ammonia gaseous plasma was utilised in the immobilisation of glucose oxidase and peroxidase onto polypropylene beads [Sipehia et al., 1988]. In another example, corona discharge was successfully used to immobilise phages for

medical purposes; phages were immobilised onto nylon sutures and their presence was shown to improve wound healing [Holland, 2010].

5.1.3.1.2 Corona Systems

In the investigation of corona discharge for immobilisation of phages onto PMGI, two corona discharge systems were used: a Sherman Treaters GX10 corona treatment machine and a custom built corona system. Precise values for the electric power dissipated by the corona of each system were not available, either from the manufacturer (in the case of the Sherman Treaters machine) or by measurement. However, a qualitative assessment of their comparative powers was possible as one system was clearly more powerful than the other based on visual evidence of the coronas created. Figure 5.1 shows that the corona generated by the Sherman Treaters GX10 machine appeared as a purple glow, indicative of the corona's high power. However no such glow was visible from the custom built system, illustrating its lower power. Therefore, the systems were defined as such: a high power system and a low power system. More details of the equipment and immobilisation procedure can be found in Chapter 4, Section 4.3.2.2.
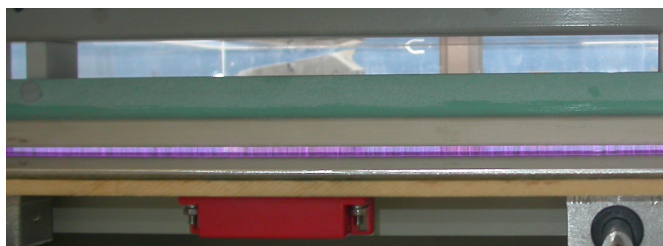
Figure 5.1. Image of the corona (purple glow) generated by the Sherman Treaters GX10 corona treatment machine (high power system).

5.1.3.2 Silanisation and Glutaraldehyde Coupling

5.1.3.2.1 Background

One of the most common approaches to covalently bind a bioreceptor onto a substrate is via a coupling agent. A coupling agent is a chemical which can react with both the substrate and the bioreceptor (or in some cases with a second coupling agent). Glutaraldehyde is a common coupling agent and has frequently been used to immobilise antibodies [Lee et al., 2006, Wong et al., 2002]. Carbodiimides are

another example of frequently used coupling agents. Shabani et al. (2008) used a carbodiimide to immobilise phages onto carbon electrodes through binding with amide bonds on the phage protein coat and electrochemically generated carboxyl groups on the electrode.

Carbodiimides have also been used in conjunction with organosilanes, another common coupling reagent, to successfully immobilise phages onto glass with a view for use with surface plasmon resonance and acoustic biosensor applications [Handa et al., 2008]. The use of organosilanes to prepare glass substrates for protein immobilisation is well documented [Lee et al., 2006, Plueddemann, 1991, Yakovleva et al., 2002, Shriver-Lake et al., 2002]. In a process called silanisation, silane molecules assemble on a glass surface by reacting with hydroxyl groups. The reactive group of the silane (for example a thiol-, amine-, phenyl- or alkyl-group) is then available for covalent binding with the bioreceptor or a second coupling agent.

A detailed experimental investigation of phage immobilisation onto nylon by chemical coupling with carbodiimide has been conducted [Mattey, 2005a]. Bacteriophage 9563 was used with *S. aureus* 8588. The results of the investigation provide useful information on the performance of covalently immobilised phages under a variety of environmental conditions (although it should be kept in mind that the outcome of different covalent immobilisation techniques may be slightly different due to the varying chemicals and functional groups involved). The main findings of the work can be summarised as follows:

1. The covalently immobilised phages were still active two weeks after immobilisation (i.e. they could still lyse their target bacteria).

2. Immobilised phages were unaffected after two weeks incubation over a range of different temperatures (0 to 45°C) whereas the activity of free phages (phages in solution) was significantly reduced. For example, after two weeks at temperatures above 5°C, free phage activity had dropped to 40% or less of its original level whilst immobilised phage activity remained the same.

3. Immobilised phages remained viable when dried, even after two weeks, whilst free phages were unable to withstand any decrease in relative humidity.

4. The optimum pH range for both immobilised and free phages was the same (pH 6 to pH 8) but there was a significant drop in free phage activity after seven days in this pH range (only 30% of phage activity was retained) whereas immobilised phages were largely unaffected.

Although phage sensitivity to chemical and physical agents can vary depending on the phage type and should be determined experimentally for each case, generally phages show good and improved stability compared to traditional bioreceptors such as enzymes which tend to be more sensitive to environmental pH and temperature and immobilisation processes [Buerk, 1993].

As with immobilised enzymes, the improved stability of immobilised phages compared to free phages could be attributed to a number of possibilities including the creation of a favourable microenvironment and/or through chemical modification, such as the addition of extra hydrogen bonds [Cao, 2006, Carr and Bowers, 1980].

5.1.3.2.2 Method Development

In this study, an aminosilane layer coupled with glutaraldehyde was investigated as a means to covalently immobilise phages via a wet chemistry technique. The aminosilane, (3-aminopropyl)trimethoxysilane (APTMS) was chosen. APTMS can form a silane layer on glass [Handa et al., 2008, Lee et al., 2006] and successfully reacts with glutaraldehyde [Bonini et al., 2007, Manesse et al., 2008, Simpkins et al., 2007, Shriver-Lake et al., 2002]. The immobilisation method was adapted from that reported by Lee et al. (2006) who utilised APTMS and glutaraldehyde to immobilise antibodies onto glass.

The basic chemistry involved in the immobilisation process applied to phages is outlined in Figure 5.2. APTMS is a bi-functional silane and can react with exposed hydroxyl groups on the surface of glass to form stable siloxane bonds (Figure 5.2(a)). The amine functional group of the silane is then presented on the surface, available for reacting with glutaraldehyde (Figure 5.2(b)). The carboxyl groups of

glutaraldehyde can then covalently conjugate with amine groups of phage surface proteins.
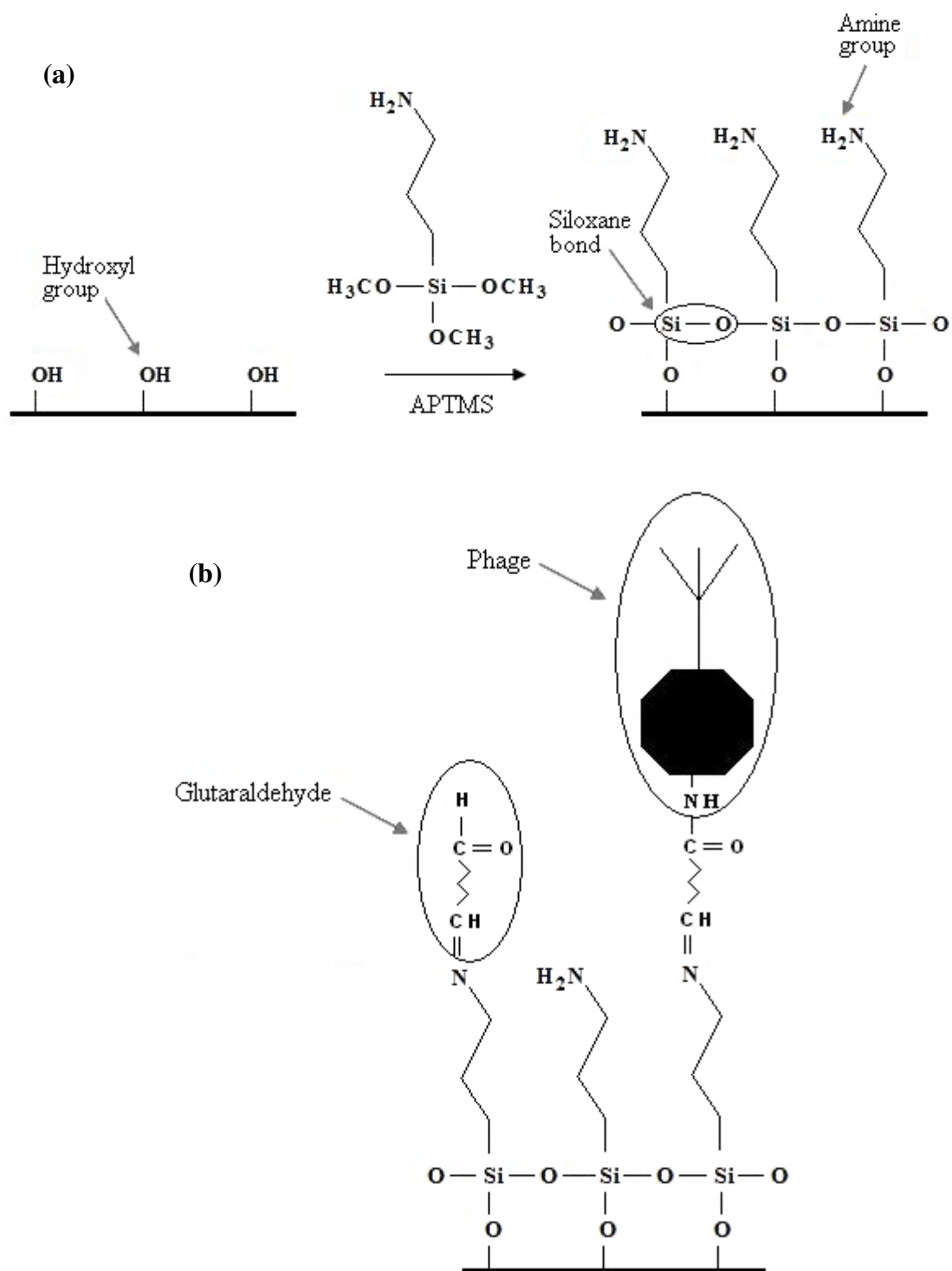
Figure 5.2. (a) Silanisation process onto glass with APTMS and (b) the subsequent binding of glutaraldehyde and then phage onto the silane layer.

Hydroxyl groups on the glass surface can be introduced in the cleaning step. The literature clearly indicates the importance of the initial cleaning process to the successful outcome of the silanisation procedure [Cras et al., 1999]. Cleaning is necessary for two main reasons: (1) to remove any organic matter on the surface of the substrate which might hinder the formation of the silane layer and (2) to expose hydroxyl groups on the substrate's surface. In this work it was decided to follow the cleaning method outlined by Bhatia et al. (1989). Cras et al. (1999) showed this method to be highly effective compared to other cleaning methods but avoids the use of Piranha solution (another common cleaning agent) which would require special safety precautions due to its explosive nature. The cleaning method is outlined in Chapter 4, Section 4.3.2.3. Briefly, a 1:1 volume mixture of methanol and hydrochloric acid is used to remove organic particles and sulphuric acid is used to hydroxylate the glass surface. The cleaning process is examined in more detail in Section 5.2.3.3.

It should be pointed out that glutaraldehyde is known to have some toxic effects towards viruses and bacteria [Gorman et al., 1980]. The de-activation mechanism could be attributed to protein damage [Maillard et al., 1996]. Despite this, there was still reason to believe that the immobilisation method would be compatible with phages as glutaraldehyde has successfully immobilised other protein based bioreceptors such as antibodies [Lee et al., 2006] and enzymes [Torrey, 1983] whilst retaining acceptable activity levels. Therefore, substrates were thoroughly washed to remove excess glutaraldehyde solution before phage exposure and, as with all covalent immobilisation methods, the activity of the bioreceptor post-immobilisation was carefully analysed.

5.1.4   Biotin-Avidin System

5.1.4.1   Background

Utilising the strong affinity between biotin and avidin molecules is another proven immobilisation technique. Avidin is a glycoprotein which can bind with biotin, a naturally occurring vitamin. Each avidin molecule can bind with four biotin

molecules. The dissociation constant between avidin and biotin has been calculated to be 10^{-15} M making it an extremely strong non-covalent bond [Green, 1963].

To immobilise bioreceptors using biotin-avidin affinity, first the bioreceptor molecule must be biotinylated i.e. labelled with biotin. Biotinylation can be achieved simply by mixing the bioreceptor with biotin, as reported in Kim et al. (2009) and Koo et al. (2009). This approach has previously been used to biotinylate phages [Sun et al., 2001]. Advances in genetic engineering have also enabled phages to be genetically engineered to express small proteins on the capsid's surface which can then be biotinylated without the phages being exposed to chemical procedures [Edgar et al., 2006]. Gervais et al. (2007) investigated this approach to immobilise phages onto a biosensor device and improved phage immobilisation was reported compared to physical adsorption.

Once phages have been biotinylated they can be immobilised through binding with a layer of avidin prepared on the substrate's surface. The avidin layer can be generated through various means such as by binding avidin to a layer of adsorbed biotinylated BSA molecules (B-BSA) [Koo et al., 2009, Kim et al., 2009] or a self assembled monolayer (SAM) of sulfo-NHS-SS-biotin molecules on gold [Gervais et al., 2007].

5.1.4.2 Method Development

In the biotin-avidin immobilisation procedure developed here, phages were biotinylated by mixing them with biotin in solution. Sulfo-NHS-biotin was used: the N-Hydroxysuccinimide (NHS) ester reacts with primary amine groups (NH_2) when in buffers of pH 7 – 9 to form stable amide bonds [Pierce Biotechnology Inc., 2006]. Proteins, including phages, are likely to have several amine groups available on their surface and so sulfo-NHS-biotin is suitable for phage biotinylation.

The first step was to determine the optimum biotin concentration for biotinylation. This was crucial as too much biotin will have a detrimental effect on phage activity (by binding to the infecting tail of bacteriophage 9563 and thus preventing its interaction with, and subsequent lysis of, bacteria) yet it is desirable to incorporate as much biotin onto the phages as possible to maximise the chances of immobilisation.

To determine this optimum biotin concentration for a suspension of bacteriophage 9563 of about 10^{10} PFU/ml, phage suspensions were plaque assayed before and after being mixed with increasing $\log_{10}$ concentrations of biotin following the biotinylation procedure outlined in Chapter 4, Section 4.3.2.4.1. The results are displayed in Figure 5.3.
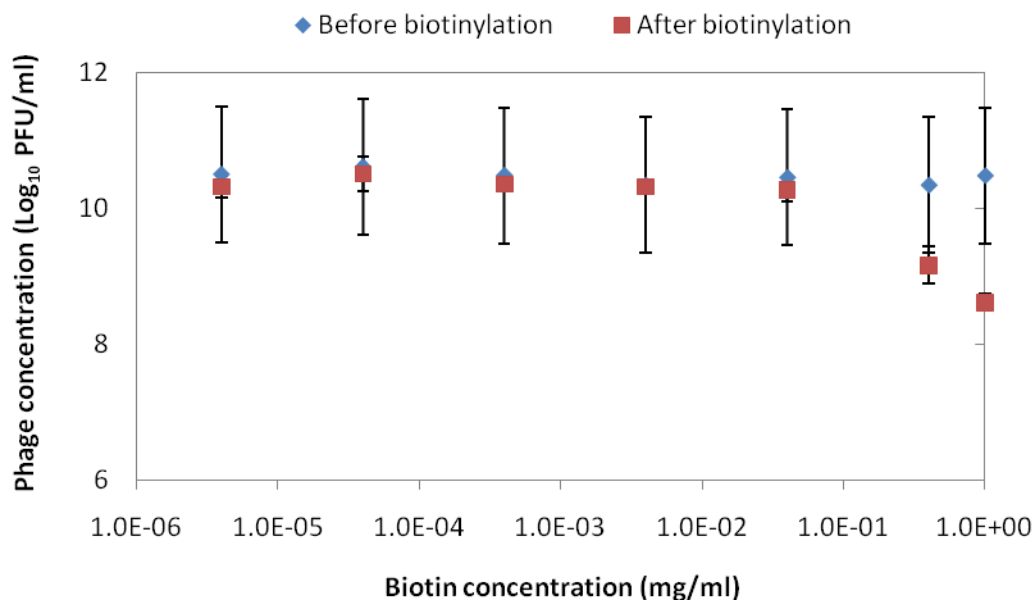
Figure 5.3. The effect of biotin concentration on the activity of bacteriophage 9563. Data points show the mean and standard deviation of plaque assays carried out in triplicate at two different dilutions (n = 6) before and after biotinylation.

The results show that for phage suspensions in the order of 10^{10} PFU/ml, biotin concentrations equal to and greater than 4×10^{-2} mg/ml caused a notable reduction in phage activity. At biotin concentrations of 4×10^{-3} mg/ml and less, generally there was only a very small reduction in phage activity and in fact the PFU count before and after biotinylation for 4×10^{-3} mg/ml and 4×10^{-5} mg/ml were not statistically different as indicated by a paired t-test (H_0: $\mu_d = \mu_0 = 0$, H_A: $\mu_d \neq \mu_0$, $\alpha = 0.05$). Therefore, as anticipated, there was an upper limit for the biotin concentration (approximately 4×10^{-2} mg/ml) at which phages began to be adversely affected by biotin but below which phage activity is retained. This is likely to be due to the majority of biotin molecules binding with the larger and more protein dense phage head at the lower concentrations, leaving the infecting phage tail largely unaffected.

Based on these results it was decided to use a biotin concentration of 4×10^{-3} mg/ml. This value is considerably lower than the limiting biotin concentration found by Sun et al. (2001). However, in their procedure, biotin was mixed with a significantly lower phage concentration (10^7 PFU/ml) and so it is likely that a greater excess of biotin would be required to achieve a similar level of biotinylation [Pierce Biotechnology Inc., 2006]. In addition to this, different phages were also used (bacteriophage SJ2) which may interact differently with biotin.

To check that the pre-determined biotin concentration of 4×10^{-3} mg/ml was a reasonable value, a simple calculation was performed to estimate the number of biotin molecules available per phage during biotinylation. The following standard formula for estimating the number of entities, N, (such as the number of molecules) in a known mass, M, was used were MW is the molecular weight of the substance and L is Avogadro's constant (6.02214×10^{23} mol^{-1}):

$$N = \frac{M}{MW} \times L \qquad\qquad \textit{Equation 5.1}$$

The molecular weight of biotin is known to be 443.43. Therefore, in 1 ml of the phage suspension used (2.2×10^{10} PFU/ml) there were approximately 5.43×10^{15} biotin molecules, giving a ratio of approximately 2.5×10^5 biotin molecules available per phage. Based on this calculation, the biotin concentration seems a realistic value with which to achieve biotinylation.

A 5 ml Zerba™ desalting column was used to remove the un-reacted biotin from the solution as recommended by Thermo Fisher Scientific for use with their Sulfo-NHS-biotin product when mixed with sample sizes of 500 – 2000 µl. It is worth mentioning briefly that a control was carried out in which a phage suspension (not treated with biotin) was passed through a de-salting column. Plaque assays before and after this revealed that full recovery of phages could be achieved.

At the time of testing the 1 mg/ml biotin concentration, a HABA assay was available which could be used to estimate the level of biotin labelling. The procedure and results of the HABA assay can be found in Appendix A. In summary, the results indicated a biotin/phage ratio of 1.17×10^3 was achieved with 1 mg/ml biotin which is consistent with the number of biotin molecules available estimated from Equation 5.1 previously.

The HABA/avidin solution only remains stable for two weeks after which it can not be reliably used and it was after this two week period that both the 4×10^{-3} mg/ml and 4×10^{-6} mg/ml concentrations were tested so HABA assay results are not available for these biotin concentrations. However the results obtained with 1 mg/ml biotin at least indicate that biotinylation had been successful and there was a high ratio of biotin incorporation per phage, which is likely to account for the phage de-activation observed. It seems reasonable that lower biotin concentrations should result in reduced levels of biotin incorporation but improved retention of phage activity. The results presented in Appendix B also indicated that the de-salting column successfully removed the excess biotin.

After phage biotinylation, immobilisation was then relatively straight forward. Details of the procedure are provided in Chapter 4, Section 4.3.2.4.2. Figure 5.4 shows a schematic representation of a phage immobilised by the biotin-avidin method. B-BSA was used to anchor avidin molecules onto the substrate. This approach was chosen due to its mild effects at the substrate's surface which would be beneficial for application to the sensor. The use of B-BSA for this purpose had previously been reported by Kim et al. (2009) and Koo et al. (2009). It should be noted that whilst Figure 5.4 illustrated attachment via the phage head, other portions of the phage may be biotinylated, i.e. the phage tail, and so phage orientation may not always be in this optimal position. However, since the phage head is more protein dense than the tail, it was assumed that the majority of biotinylation was with the head section. This assumption is strengthened by the retention of phage activity after biotinylation, demonstrated in Figure 5.3.
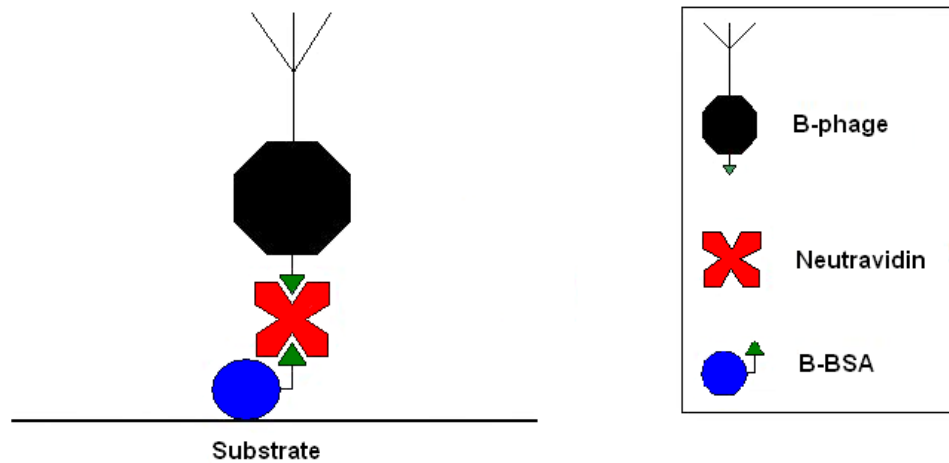
Figure 5.4. Schematic illustration of phage immobilisation by the biotin-avidin system. First, B-BSA is physically adsorbed onto the substrate. NeutraAvidin then binds with B-BSA and is available for binding with biotinylated phages.

A derivative of avidin, NeutrAvidin, was used instead of avidin itself. Recently, such derivatives (also including streptavidin) have become available and are often favoured over avidin. This is because streptavidin and NeutrAvidin are less susceptible to non-specific adsorption onto substrates due to their relatively neutral isoelectric point, pI, (whereas avidin's pI is 10) yet they have similar binding affinities for biotin.

One aspect which needed consideration was the substrate washing step after incubation with biotinylated phages. Although the biotin-avidin bond is relatively strong, it is not covalent and thus some leakage during washing may be expected. In addition to this, the whole biotin-avidin system is anchored to the substrate via B-BSA which itself is only physically adsorbed onto the substrate. As a result, wash fluid from such substrates may always contain some level of phages and therefore, unlike substrates with covalently immobilised phages, they can not be washed until wash plaque assays are free of phages. Instead, an experiment was carried out to establish a practical level of washing which would remove as much excess phage suspension as possible. Wash fluid was collected at intervals over twenty washes. Note that after 16 washes, substrates were incubated in PBS overnight and washing resumed the following day. The wash fluid was then plaque assayed, the results are presented in Figure 5.5.
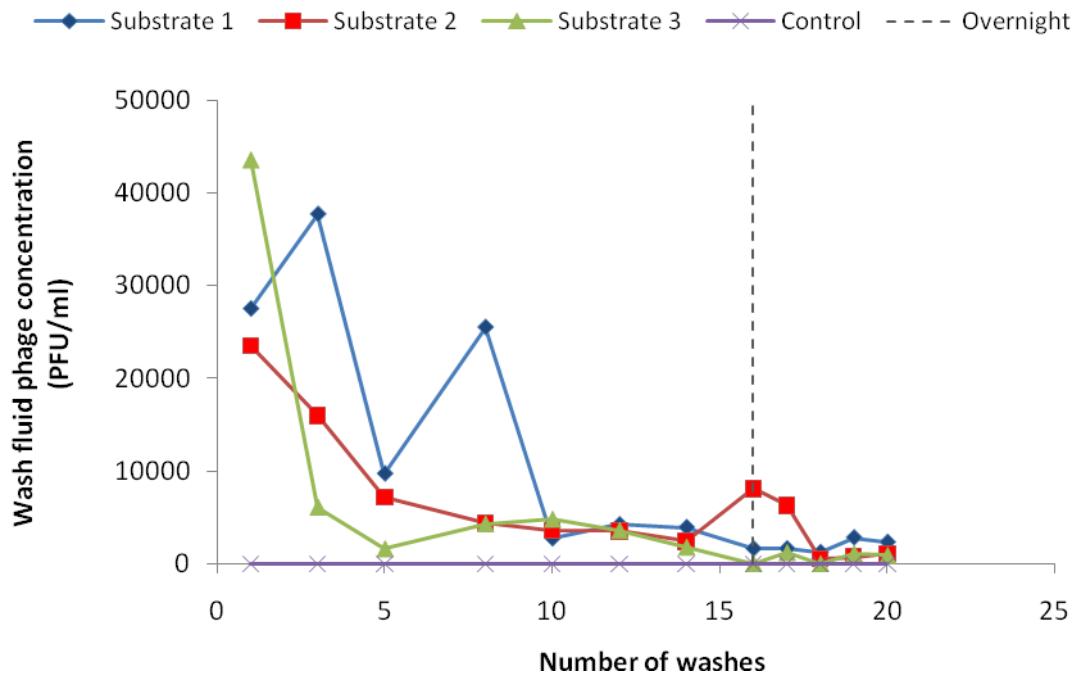
Figure 5.5. Washing of biotin-avidin treated substrates after incubation with biotinylated phages. Wash fluid from three different substrates was collected and plaque assayed to detect for free phages coming away from the substrate's surface (n = 3). Results are displayed in terms of phage concentration (PFU/ml) in the wash fluid for increasing numbers of washes. The control substrate was not incubated with phages.

It can be seen from Figure 5.5 that after ten washes the number of phages detected in the wash fluid is relatively constant for further washes. It was concluded that in ten washes the majority of the loosely bound free phages had been removed and that most of the phages present in the wash fluid are likely to be immobilised phages which are leaking from the substrate's surface. It was therefore decided to wash substrates ten times after the biotin-avidin immobilisation procedure. The abnormal variation observed for substrate 1 in early washes could not be accounted for. It is acknowledged that a control experiment consisting of a substrate incubated with phages but not biotin and avidin may have revealed useful information. For example, the point at which non-specifically bound phages were removed from the glass substrate may have been determined for comparison with the biotin-avidin treated substrates.

5.1.5 Techniques for Assessing Bacteriophage Immobilisation Methods

The detection of phages can be challenging as they are not visible with a standard light microscope due their nano-scale size. A variety of methods have been reported for confirming the presence of immobilised phages. For example, Handa et al. (2008) used atomic force microscopy (AFM) images to directly detect immobilised phages. They also used an ELISA to detect bacteria captured by the immobilised phages thus indirectly confirming the presence of phages. Shabani et al. (2008) used time-of-flight secondary ion mass spectroscopy to detect phage immobilisation by examining changes in surface chemical components. They also used fluorescence microscopy and scanning electron microscopy (SEM) images to verify bacteria binding to surfaces modified with immobilised phages. Gervais et al. (2007) were able to obtain SEM images of phages using an ultra-high resolution SEM. Phages have also been detected using fluorescent microscopy, for example Serwer et al. (2007) stained phages with a nucleic acid dye and then used a high resolution fluorescent microscope to detect them.

In this work, the phage detection method needed to be accessible and cost effective as multiple measurements would be carried out during the course of the immobilisation method investigation. It was also preferable to have a method which would provide quantitative data or at least easily allow comparisons of the different immobilisation methods. Several methods were considered for detecting immobilised phages including a protein assay (such the bicinchoninic acid assay) and SEM images and also the indirect approach of detecting the bacteria captured by phages through either an ELISA or fluorescence microscopy.

Ultimately, it was decided to use a broth culture test for each immobilisation method to first establish whether active phages had been successfully immobilised. After this initial evaluation, successful immobilisation methods would then be further assessed using a fluorescent immunoassay (FIA) to quantitatively compare the different immobilisation methods. More details of these methods and the results will now follow.

5.2   Initial Assessment of Immobilisation Methods

It is obviously of critical importance that the immobilisation procedure implemented can reliably immobilise active phages. Although variations of some of the immobilisation methods investigated here have previously been used to immobilise phages it was important to check that they would be compatible with bacteriophage 9563 and the particular substrates used in this investigation. Therefore, the broth culture testing method was used to initially assess each immobilisation method to this effect. In the following sections, the broth culture method is discussed and results are presented and analysed.

5.2.1   Broth Culture Testing Method

Incubating substrates in a broth culture (growth media inoculated with bacteria) is a simple and effective way of determining whether active phages have been immobilised onto a substrate. If immobilised lytic phages are present and active they will infect the growing bacteria and the subsequent progeny phages will be released and so the cycle will continue whilst bacteria are present and growing (as described in Chapter 1, Section 1.4.2). Detecting the progeny phages in the media after a suitable period of incubation will confirm the presence of immobilised phages from which they must have originated.

Details of the broth culture testing method can be found in Chapter 4, Section 4.3.4.1. The broth culture test was only used to give a positive or negative indication to the presence of immobilised phages; the dynamic interaction of phages with bacteria means that a backwards calculation from estimations of the number of progeny phages generated would not be accurate. However, the method did serve as a good initial indicator of the potential success of each immobilisation procedure and was utilised for this purpose.

For each individual immobilisation method, samples were inoculated using the same broth culture thus ensuring (as far as reasonably possible) that each sample started with the same bacterial concentration and would be in the same phase of the growth curve after incubation. Since the samples were incubated overnight it was assumed

that this would put them in the stationary phase of the growth curve (see Chapter 1, Section 1.5).

Broth culture testing results are presented in terms of the plaque assay results obtained from dilutions of the broth culture supernatant. Plaque assay classification is summarised in Table 5.1. If the plaque assay was clear, i.e. bacterial growth had been completely prevented by a high concentration of phages, then the result was denoted by '++'. Confluent plaques in the plaque assay were indicated by '+', and where individual plaques could be counted, the average number of plaques on a plaque assay plate was reported.

Table 5.1. Classification of broth culture plaque assay results.

Plaque Assay Description	Example
Clear (++) The agar plate is clear of bacteria i.e. bacteria have not been able to grow due to a high multiplicity of infection, MOI, (ratio of phage to bacteria). Some single bacterial colonies may be present due to phage resistant strains.	
Confluent plaques (+) The MOI is not high enough to completely prevent bacterial growth but single plaques can not be distinguished. Instead, plaques merge into each other.	
Single plaques (PFU) Single plaques are present and can be counted individually.	
Control: Bacterial lawn This image shows a bacterial lawn. Bacteria have been allowed to grow in the absence of any phages.	
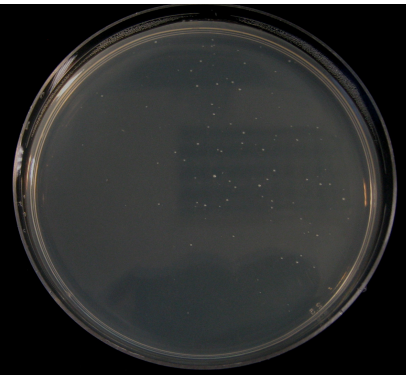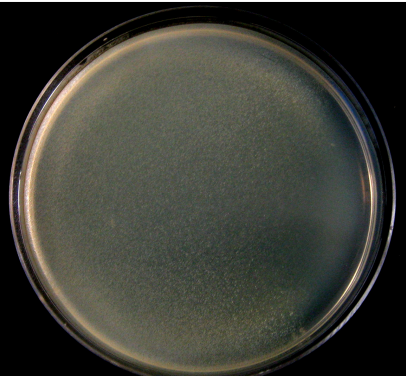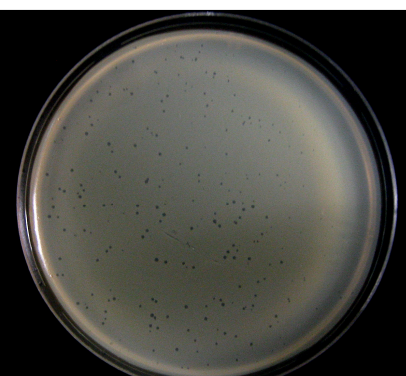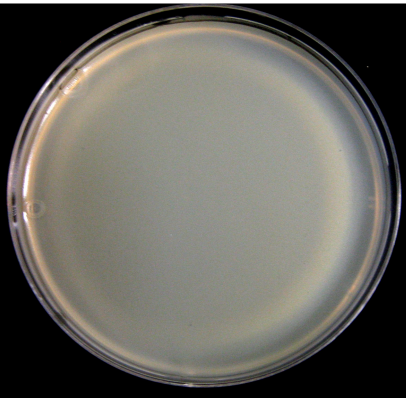
Careful consideration of the level of washing carried out after each immobilisation method was required before broth culture testing, as this could influence the outcome of the broth culture test. For immobilisation methods seeking to achieve covalent attachment of phages, it was important that substrates were washed until free phages (phages not covalently immobilised) were removed. Thus, it could be concluded that any phages detected in the broth culture after incubation with the substrates could be attributed to the successful covalent immobilisation of active phages only. However, the same washing approach was not appropriate for physically adsorbed phages or phages immobilised via biotin and avidin due to the weaker nature of the bond. Instead, substrates with physically adsorbed phages were washed three times and biotin-avidin treated substrates were washed ten times as discussed in Section 5.1.4.2. Details of the washing procedure can be found in Chapter 4, Section 4.3.3.

5.2.2 Experimental Parameters

Details of the phage suspensions used in the preparation of substrates tested by the broth culture method are presented in Table 5.2. Variations in phage concentrations were due to the different phage harvests used (typically, a phage harvest would yield between 10^8 to 10^{10} PFU/ml) and in each instance it was decided to use the highest phage concentration available at the time of testing to maximise immobilisation levels.

Glass and PMGI substrates were both investigated (see Table Table 5.2). Samples were prepared as described in Chapter 4, Section 4.3.1. The wafers used in sensor fabrication were actually either silicon dioxide or borosilicate glass but the initial immobilisation testing and optimisation was carried out on glass microscope slides. Although the composition and surface properties of glass will not be completely identical to the wafers, it is still largely similar as the common main component of the materials is silicon dioxide and also both glass and silicon dioxide are negatively charged in a solution of neutral pH [Behrens and Grier, 2001]. However, glass is considerably cheaper and more readily available than the wafers.

Table 5.2. Phage suspension properties used for preparing substrates in broth culture testing. Phage concentrations were estimated from three agar plate replicates at two different dilutions.

Substrate	Immobilisation method	Phage concentration (PFU/ml)	Suspending medium	pH
PMGI	Physical adsorption	1.0×10^8	Phage harvest	7.72
	Corona			
	High power	1.0×10^8	Phage harvest	7.72
	Low power	1.0×10^9	Distilled water	7.07
Glass	Physical adsorption	4.2×10^8	PBS	7.10
	Silanisation	5.5×10^8	PBS	7.10
	Biotin-avidin			
	1 mg/ml biotin	3.4×10^{10}	PBS	7.10
	4×10^{-6} mg/ml biotin	3.2×10^{10}	PBS	7.10

It should be explained that in the first immobilisation tests carried out (physical adsorption and high power corona activation onto PMGI) the neat phage harvest suspension was used i.e. the phages were in SM and had not been re-suspended. However, it was considered that small proteins and any remaining cell debris in the phage harvest may also be adsorbing to the substrate and therefore competing with phage immobilisation. By re-suspending phages in a fresh solution, such particles could be removed. Since re-suspension is associated with only a small drop in phage concentration, all further immobilisation work was carried out with solutions of re-suspended phages.

A 'negative' control was carried out for each experiment for which substrates went through the same immobilisation procedure but were not incubated with phages. This allowed confirmation that any positive results from the broth culture testing was due to immobilised phages and not a phage contamination. A control in which the substrate was only incubated with phages and did not go through the prior immobilisation steps was not considered a practical means of confirming the efficacy of each immobilisation method. This is because some physical adsorption of phages is likely to occur on untreated control substrates over the incubation periods used,

particularly in the silane and glutaraldehyde and biotin-avidin methods for which substrates are incubated with phages for at least 2 hours, and thus a positive result in broth culture testing will arise regardless. Therefore such controls were unlikely to add to the investigation.

5.2.3 Results and Discussion

5.2.3.1 Physical Adsorption

The broth culture results for the physical adsorption of phages are shown in Table 5.3. Results confirmed active phages were present on PMGI and glass substrates after both a two hour and overnight incubation with phages. This result is especially significant given that after washing substrates three times, no free phages were detected in all but one of the wash plaque assays (a plaque assay of the wash fluid from one of the PMGI substrates had one plaque present). This result suggests that the majority of free phages had been removed from the substrates' surfaces and that the broth culture results could be attributed to physically adsorbed phages which were attached strong enough to withstand the forces exerted during washing.

Table 5.3. Average broth culture results for PMGI and glass substrates incubated with phages for two hours and overnight for physical adsorption (n = 3). Agar plates completely clear of bacteria are indicated by '++', agar plates with confluent plaques by '+' and where plaques could be counted average numbers are reported (see Table 5.1).

Sample	Plaque assay results from broth culture supernatant dilutions:			
	0	10^{-2}	10^{-4}	10^{-6}
PMGI				
2 hours	++	++	+	287
Glass				
2 hours	++	++	+	17
Overnight	++	+	269	1
Negative control	0	0	0	0

The two incubation periods were primarily chosen based on previously published results for the physical adsorption of bioreceptors, including phages. For example, Nanduri et al. (2007) reported the successful physical adsorption of phages onto gold

within one hour whilst Carnazza et al. (2007) detailed phage adsorption onto quartz within two hours. However, it was indicated by Olsen et al. (2006) that although the majority of phage adsorption onto gold occurred within the first few hours of exposure, adsorption continued to occur over a 24 hour period and so improved levels may be achieved with extended incubation times. Although the broth culture results can not confirm that increased phage immobilisation occurred with overnight incubation, they are at least in agreement with the literature results by demonstrating that phage adsorption can occur within two hours.

Although the exact forces involved in the physical adsorption of bacteriophage 9563 onto glass and PMGI were not determined in this study, it has been shown that forces arising from the surface charges of the materials involved in virus immobilisation play a significant role in determining adsorption. Therefore electrostatic forces are likely to be one of the main forces involved [Yuan et al., 2008, Zerda et al., 1985]. Hydrophobic forces (ones which tend to be non-polar, repelling polar water molecules) on the surface of phages and the substrate are also believed to encourage adsorption [van Voorthuizen et al., 2001].

5.2.3.2 Corona Activation

In the investigation of corona activation immobilisation, the broth culture results, displayed in Table 5.4, indicated that the high power corona was not effective for immobilising phages onto PMGI. On average, only one plaque was detected in the plaque assays on the neat broth culture. This infers an extremely small progeny phage level in the broth cultures (10 PFU/ml) after a twenty hour incubation period. In fact, it should perhaps be considered that the plaques may have arisen from a contamination, especially since the plaque count was obtained solely from one plate. In any case, it can be concluded that under the corona settings outlined in Chapter 4, Section 4.3.2.2.1, this approach to phage immobilisation had not been successful.

Table 5.4. Average broth culture results for corona activation immobilisation testing (n = 3). Agar plates completely clear of bacteria are indicated by '++', agar plates with confluent plaques by '+' and where plaques could be counted average numbers are reported (see Table 5.1).

Sample	Plaque assay results from broth culture supernatant dilutions:			
	0	10^{-2}	10^{-4}	10^{-6}
PMGI				
High power corona	1	0	0	0
Low power corona	0	0	0	0
Negative control				
High power corona	0	0	0	0
Positive control				
High power corona	++	++	+	270

The result was surprising as it had been expected that corona activation would be compatible with all polymers. A positive control was carried out on a nylon membrane (Amersham Hybond[TM]-N+, GE Healthcare, UK) for which the system had previously shown positive results [Holland, 2010]. The result of the positive control (reported in Table 5.4) verified that corona activation was possible under these settings and with the phage suspension utilised. The positive control result also made it unlikely that phages were being immobilised onto PMGI but were being inactivated by some means.

It was initially considered that the lack of success could perhaps be attributed to the relatively aggressive nature of the corona, as indicated by the visible corona in Figure 5.1. The corona was so aggressive that it could create small holes in the nylon sheet. It was therefore speculated that the corona may actually be removing or damaging the PMGI layer instead of modifying it with reactive surface groups (the PMGI layer was only approximately 0.7 µm thick as first mentioned in Chapter 3, Section 3.1.1). This theory was investigated by examining the PMGI post corona treatment under a standard light microscope (40× objective lens). The tip of a pair of sharp tweezers was used to scrape at the substrate's surface to see if PMGI could be lifted and thus indicate if it remained after corona treatment. This micro-scale examination revealed that the polymer was still present after treatment and so the

inability of the method to immobilise phages could not be attributed to the complete removal of PMGI from the substrate.

Considering the plasma modification processes further, it is known that for oxygen containing plasmas a balance exists between two concurrent processes: plasma etching (i.e. the chemical and physical removal of particles from the substrate surface) and the formation of oxygen functional groups [Chan et al., 1996]. The parameters controlling this balance are likely to vary for different polymers. Based on this understanding, it is not unfeasible that for the high power corona system, the optimised settings for nylon (outlined in Chapter 4, Section 4.3.2.2.1) can not necessarily be successfully employed with PMGI.

An alternative polymer, SU8 (Microchem Corp, Chestech Ltd, UK), was briefly investigated with the high power corona treatment. SU8 can be used as a photoresist in the sensor fabrication process instead of PMGI. However, immobilised phages were also not detected on SU8 samples. Therefore, attention was returned to PMGI and an investigation of the corona parameters instead.

In a first attempt to investigate alternative corona parameters for the treatment of PMGI, the extremes of the power settings on the Sherman Treaters GX10 machine were investigated. Substrates were treated with the machine's power settings set to '35' and '95' to produce corona's of lower and higher powers respectively (the original setting was '75', see Chapter 4, Section 4.3.2.2.1, for more details). However, again the plaque assay results from broth culture testing did not indicate the presence of any immobilised phages.

It was then decided to try a second corona activation system which was available. This system was termed the 'low power corona' system relative to the Sherman Treaters machine as the corona was not visible. The system was designed by Dr Igor Timoshkin (University of Strathclyde, UK) for the corona activation of nylon beads for phage immobilisation. Details of the system and the procedure used can be found in Chapter 4, Section 4.3.2.2.2. The results of the weaker power corona treatment are

also displayed in Table 5.4 and again show that corona activation had not been achieved.

In the case of the low power system, several practical aspects could be responsible for the negative result. For example, there is a gap of approximately 4 mm between the electrodes and the substrate and so the corona's active species may not be reaching the substrate. Also, as described in Chapter 4, Section 4.3.2.2.2, the substrate is put into a chamber for treatment which is then screwed shut. Consequently, there is a delay in retrieving substrates and placing them into the phage suspension immediately after corona exposure. The stability of plasma treated surfaces has been shown to change with time [Chen and Lindner, 2007] and so this delay may be detrimental for the binding of phages with reactive surface groups. Possible options to try and improve the low power corona system could include: sharper electrodes to increase the corona intensity so that it can reach the substrate, modification of the chamber to raise the substrate platform towards the electrodes, the introduction of a system to 'blow' the active species downwards towards the substrate and/or introduce a mechanism to retrieve the substrate from the chamber faster.

However, it was becoming apparent that in order to achieve corona activation of PMGI, considerable investigation and development of the corona parameters would be required. The general lack of understanding of the mechanisms involved in corona modification would likely require that a trial and error approach be adopted for development. Therefore such an investigation would be time consuming and ultimately positive results may not be obtained within the project time frame. It was also considered that the photosensitive nature of the polymer may be playing a role in the unexpected outcome, especially if UV light was being generated from the corona. It was therefore decided not to pursue the corona activation method for phage immobilisation and to focus on alternative methods at this stage of the investigation.

5.2.3.3 Silanisation and Glutaraldehyde Coupling

The broth culture results obtained from substrates treated with APTMS and glutaraldehyde are reported in Table 5.5. The results confirm that phages could be covalently immobilised by this method: high levels of progeny phages were detected in the neat broth culture with consistent reductions down each serial dilution whilst the negative control (a substrate not treated with phages) indicated no phages present. The results also confirmed that the low levels of glutaraldehyde used did not have a toxic effect on the phages.

Table 5.5. Broth culture results for silane and glutaraldehyde coupling immobilisation testing. Results for each sample (all of the same glass substrate) are reported. Agar plates completely clear of bacteria are indicated by '++', agar plates with confluent plaques by '+' and where plaques could be counted average numbers are reported (see Table 5.1).

Sample	Plaque assay results from broth culture supernatant dilutions:			
	0	10^{-2}	10^{-4}	10^{-6}
Sample 1	++	+	355	1
Sample 2	+	136	2	0
Sample 3	++	++	+	154
Negative control	0	0	0	0

However, as shown in Table 5.5, there was considerable variation across the results for the three samples despite having gone through the same procedure at the same time. For example, at 10^{-2} dilutions of each broth culture, plaque assay results varied from a clear plate (++) down to individual plaques. Although broth culture testing can not be reliably used to quantify levels of immobilised phages, this degree of variation was not observed for any other immobilisation treatment and implies that there were differences amongst the treated samples. This is a concern as, if the treatment is to be applied to the sensor, poor repeatability of the bioreceptor surface will lead to inconsistent sensor measurements.

A possible explanation for the variability could lie with silane layer formation. As with most solution based approaches to forming a self-assembled chemical layer, it

can not be guaranteed that a homogeneous monolayer will be created and some holes and aggregation may occur. It is feasible that such defects in the silane layer could result in inconsistent phage immobilisation.

A second potential problem of the silanisation method could be the effect of the chemicals involved on the sensor's components and structure. Although none of the chemicals used were expected to react with sensor materials, some incubation periods were quite long (for example 30 minutes in a 1:1 volume mixture of hydrochloric acid and methanol) which might promote some adverse effects. It had already been discovered that not all sensors could survive the removal of the protective photoresist layer after wafer dicing (this will be discussed in more detail in Chapter 6, Section 6.2). This is indicative of perhaps quite a fragile sensor structure which may be susceptible to damage through chemical treatments.

To try and establish whether the sensor could withstand the multiple chemical treatments, the continuity of a sensor was monitored over the course of the silanisation and glutaraldehyde coupling procedure. Continuity was assessed by measuring the resistance across the sensor's electrodes using a digital multimeter (Fluke, UK) and by recording sensor impedance over the frequency range 100 Hz to 10 MHz (method outlined in Chapter 4, Section 4.5). For sensitive and reliable measurements to be made with the sensor it was necessary that it remained an open circuit after the immobilisation procedure i.e. that it was not short circuited by contact between damaged electrodes as this would then dominate signal measurements.

Resistance measurements are displayed in Table 5.6 and corresponding impedance measurements are shown in Figure 5.6. The results indicate that after cleaning, the sensor could be returned to its original working condition but that the brief application of 15 V across the electrodes (denoted by 'VA') was required to do so. This was necessary to 'blast' away connections formed between electrodes due to delamination of the gold and is discussed in more detail in Chapter 6, Section 6.2. After silanisation, the open circuit status of the sensor was not regained even after a

voltage application. However, the resistance measurement was very high and fluctuating around 17 MΩ and impedance measurements were only slightly lower than original values which could suggest the results were due to some moisture retained on the surface after drying. The most significant effect, however, was observed after glutaraldehyde coupling; a low resistance measurement was recorded after the voltage application (85 Ω) and the impedance spectrum was now constant over most of the frequency range. This result implies that the sensor had irreversibly short circuited. This outcome and the fact that a voltage application was required after each step imply that this immobilisation method is unlikely to be adequate for immobilising phages onto the sensor.

Table 5.6. Sensor resistance after stages of the silane and glutaraldehyde coupling procedure. VA denotes voltage application; a voltage was applied across the sensor's electrodes in an attempt to recover open circuit sensors (see Chapter 6, Section 6.2, for more details).

Immobilisation stage	Sensor resistance	
	Without VA	After VA
Before treatment	Open circuit	-
After cleaning	280 Ω	Open circuit
After silanisation	270 Ω	~17 MΩ
After glutaraldehyde coupling	20 Ω	85 Ω
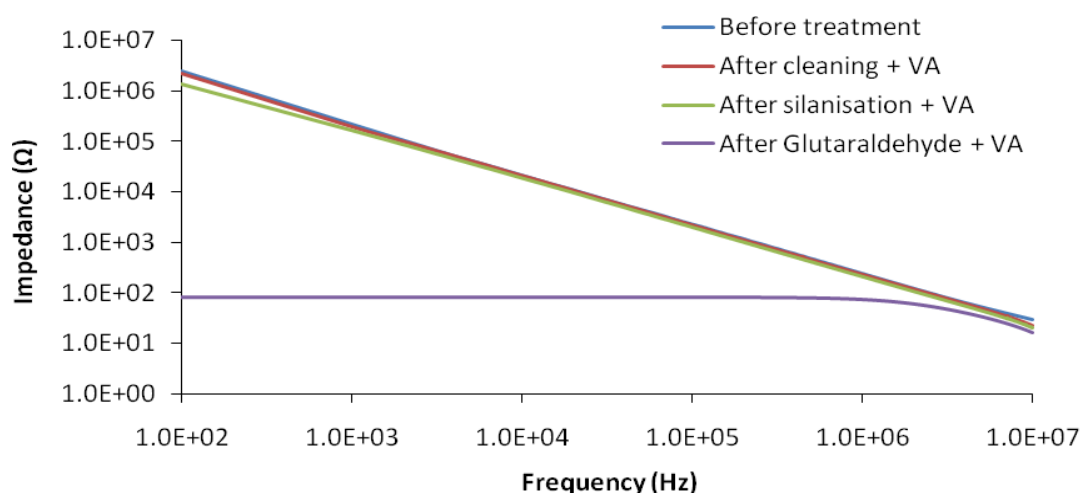
Figure 5.6. Impedance spectrum of the sensor after stages of the silane and glutaraldehyde coupling procedure. Impedance measurements were recorded after a voltage was applied (VA) to try and recover open circuit sensors.

Two approaches were investigated to try and overcome this problem, both of which aimed to reduce the sensor's exposure to chemicals. Firstly, the possibility of cutting down the cleaning procedure was examined and secondly a chemical vapour deposition (CVD) method was attempted. The possibility of eliminating cleaning steps was not entirely unreasonable given that the sensors will already be very clean post-fabrication and in addition to this, reduced levels of cleaning had been reported in the literature with some success [Cras et al., 1999]. The reduced cleaning methods investigated are described in Table 5.7 and results are presented in Table 5.8. The results obtained using the original cleaning method (Method 1) are also included for comparison.

Table 5.7. Cleaning methods applied to substrates prior to silanisation and glutaraldehyde coupling for the investigation into a reduced cleaning procedure.

Method	Cleaning protocol
1	30 minutes in 1:1 MeOH:HCl + 30 minutes in sulphuric acid + 30 minutes boiling in sterile distilled water
2	30 minutes in 1:1 MeOH:HCl only
3	30 minutes in sulphuric acid only
4	No cleaning (other than initial ultrasonication in acetone)

Table 5.8. Broth culture results for the silanisation and glutaraldehyde immobilisation method on glass in combination with different substrate cleaning methods as described in Table 5.7. Agar plates completely clear of bacteria are indicated by '++', agar plates with confluent plaques by '+' and where plaques could be counted average numbers are reported (see Table 5.1).

| Cleaning method | Plaque assay results for dilutions of broth culture supernatant: | | | |
	0	10^{-2}	10^{-4}	10^{-6}
	++	+	355	1
Method 1	+	136	2	0
	++	++	+	154
	169	0	0	0
Method 2	1132	31	0	0
	268	2	0	0
	++	++	+	177
Method 3	++	+	451	3
	+	317	5	0
	914	10	0	0
Method 4	1304	9	2	0
	++	++	+	327

Although positive broth culture results were obtained with all four cleaning methods, some distinct patterns emerged from the results. The results obtained with just sulphuric acid cleaning (Method 3) were very similar to those obtained with the full cleaning procedure, implying that similar levels of phages had been immobilised. However, cleaning with only the methanol and hydrochloric acid mixture (Method 2) yielded comparatively lower numbers of plaques across the broth culture plaque assays and this was also generally the case for substrates without any cleaning (Method 4).

If it is assumed that the considerably different broth culture results obtained with the different cleaning methods is indicative of varying levels of immobilised phages then overall, the results of the cleaning investigation suggest that the methanol and hydrochloric acid mixture step was not necessary but sulphuric acid cleaning was. This conclusion seems reasonable as the substrates have already been cleaned and should be free of organic particles before treatment and so further cleaning with the

methanol and hydrochloric acid mixture is not necessary but the sulphuric acid exposure is still required to introduce hydroxyl groups onto the substrate's surface for binding with the silane.

In a second approach to investigate improving the silane and glutaraldehyde method for phage immobilisation, CVD was considered. CVD is an emerging alternative method to solution based procedures for creating monolayers. CVD involves vaporising a solution of the molecules to be deposited in an enclosed environment thus enabling a monolayer of the molecules to self-assemble on the substrate. In this instance, CVD will not only eliminate the need to submerge the sensor into a mixture of APTMS and toluene but CVD has been reported to produce a more homogenous silane monolayer [Dong et al., 2006, Sugimura et al., 2002], so may improve the reproducibility of the immobilised phage layer. CVD often requires specialised equipment to apply a vacuum and high temperature conditions. However, Sugimura et al. (2002) developed a very simple CVD method which has been implemented with APTMS [Song et al., 2006]. Details of the method can be found in Chapter 4, Section 4.3.2.3.1, and broth culture results for substrates having undergone CVD are displayed in Table 5.9.

Table 5.9. Broth culture results for the silanisation and glutaraldehyde immobilisation method on glass in which the silane layer was prepared by CVD. In Trial 1, CVD was carried out as outlined in Chapter 4, Section 4.3.2.3.1. In Trial 2, substrates were not washed after CVD. Agar plates completely clear of bacteria are indicated by '++', agar plates with confluent plaques by '+' and where plaques could be counted average numbers are reported (see Table 5.1).

Sample	Plaque assay results from neat broth culture supernatant
Trial 1	
Sample 1	+
Sample 2	2
Sample 3	0
Trial 2	
Sample 1	++
Sample 2	++
Sample 3	+

The results show that the CVD method (Trial 1) seemingly achieved very low levels of immobilised phages. In a second attempt (Trial 2), the substrates were not rinsed after CVD but were immersed directly into the glutaraldehyde solution and improved results were achieved. This outcome suggests that the silane layer remaining after washing was not adequate for phage immobilisation and that the parameters of the CVD method, such as the substrate's incubation time with vaporised APTMS, vessel size and APTMS solution concentration, needed to be optimised. However, due to time constraints the necessary optimisation work could not be carried out.

5.2.3.4 Biotin-Avidin System

The broth culture results for biotin-avidin treated substrates are displayed in Table 5.10. Substrates were prepared with phages which had been biotinylated at the two extremes of the biotin concentration range investigated (4×10^{-6} mg/ml and 1 mg/ml), as previously reported in Section 5.1.4.2. Results show that active phages were successfully immobilised at both biotin concentrations indicating that phage immobilisation can be achieved over this biotin concentration range. The successful immobilisation of biotinylated phages via biotin-avidin attachment is consistent with published literature [Gervais et al., 2007, Sun et al., 2001].

Table 5.10. Average broth culture results from glass substrates treated with the biotin-avidin immobilisation method (n = 6). Substrates were incubated with phages biotinylated with either 1 mg/ml or 4×10^{-6} mg/ml biotin. Agar plates completely clear of bacteria are indicated by '++', agar plates with confluent plaques by '+' and where plaques could be counted average numbers are reported (see Table 5.1).

Sample	Plaque assay results from broth culture supernatant dilutions:			
	0	**10^{-2}**	**10^{-4}**	**10^{-6}**
1 mg/ml biotin	++	++	+	204
4×10^{-6} mg/ml biotin	++	++	+	225
Negative control	0	0	0	0

Unexpectedly, the broth culture results obtained at the two different concentrations were very similar despite the phage de-activation known to occur with biotin concentrations of 1 mg/ml (Section 5.1.4.2). This is perhaps symptomatic of the

broth culture method's inability to accurately distinguish between different levels of immobilised phages unless the difference is substantial (as might be the case when different levels of cleaning were investigated prior to the silane and glutaraldehyde immobilisation method reported in Section 5.2.3.3).

5.2.4 Summary

The broth culture method successfully discriminated between immobilisation methods which could and could not immobilise active phages onto a chosen substrate. As mentioned in the discussions of the individual method developments throughout Section 5.1 and again in Section 5.2.1, as far as possible the appropriate precautions were taken to ensure that the broth culture results could be attributed to phages immobilised by the applied immobilisation procedure. The negative control substrate for each immobilisation method went through the same treatment as the actual samples but was not incubated with a phage suspension. As was expected, plaque assays did not detect any phages in the negative control broth cultures confirming that the results obtained from treated substrates were a result of immobilised phages and not a phage contamination.

The results of the broth culture testing are summarised in Table 5.11. Of the four immobilisation methods tested, only the corona activation technique did not successfully immobilise active phages. It is believed that under the present settings of the corona systems (both high and low power) it is not possible to activate the PMGI surface with reactive groups and that further investigation and optimisation of the system's parameters is required in order to achieve this.

Table 5.11. Summary of results from the broth culture test for immobilised active phages where by phages were immobilised by different immobilisation methods onto glass and PMGI substrates.

Immobilisation method	Substrate	Detection of active immobilised phages
Physical adsorption	Glass and PMGI	Yes
Corona activation	PMGI	No
Silanisation	Glass	Yes
Biotin-avidin system	Glass	Yes

Of the immobilisation methods which were yielding positive results from the broth culture test, physical adsorption and the biotin-avidin system were most promising for the immobilisation of phages onto the sensor. These methods were more consistent than the silanisation method based on the broth culture results. In addition to this they also involved less, if any, chemical exposure compared to the silanisation approach. This is an important factor when considering the application of an immobilisation method to the sensor as it was shown that the silane and glutaraldehyde immobilisation method had detrimental physical effects on the sensor. However, potential improvements to the silane and glutaraldehyde method were identified (reduced cleaning and CVD of the silane layer) and to the author's knowledge this was the first demonstration of the specific immobilisation of phages onto a glass substrate using an aminosilane in combination with glutaraldehyde.

To determine more precisely what method would yield the highest levels of immobilised phages and should be used to immobilise phages onto the sensor, it was decided to quantitatively compare physical adsorption, silanisation and biotin-avidin methods for the immobilisation of phages using a specifically developed FIA, as will now be discussed in the following section.

5.3 Quantitative Analysis of Immobilisation Methods

A quantitative comparison would be useful when comparing different immobilisation methods and in understanding the subsequent biosensor performance. Therefore a FIA method was developed with the aim of providing information on the immobilised phage densities (phages/μm^2) achieved with immobilisation techniques investigated within this study.

5.3.1 The FIA Method

5.3.1.1 FIA Method Development

The FIA reported here was adapted for the specific detection of bacteriophage 9563 and was developed during the course of this study. The method was designed to provide a visual indication of immobilised phage levels by utilising relatively

inexpensive and easily obtainable materials so that it was amenable to frequent use. Most importantly, the method was designed as a means to provide reliable quantitative comparisons of the immobilisation methods.

The FIA is based on the commonly used indirect ELISA format, but instead of using an enzyme linked secondary antibody, a fluorescently labelled secondary antibody is used. The assay is illustrated in Figure 5.7.
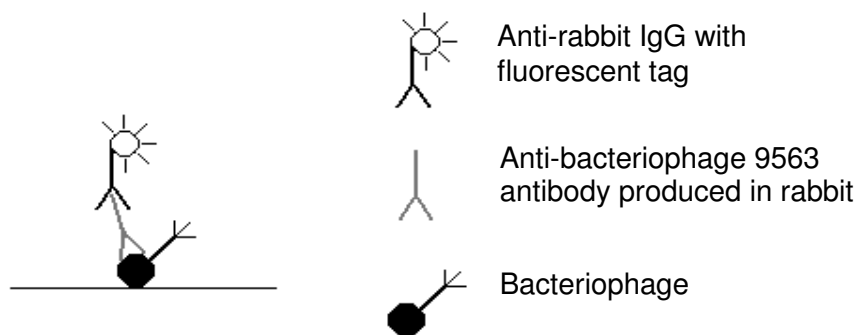
Figure 5.7. Schematic illustration of the fluorescent immunoassay used in the fluorescent detection of immobilised bacteriophage 9563.

Anti-bacteriophage 9563 antibodies had been raised in a rabbit and were kindly donated by Dr Janice Spencer (see Chapter 4, Section 4.3.4.2.1, for further details). The collected rabbit serum had not previously been tested for anti-bacteriophage 9563 antibodies and so an ELISA was performed to confirm this (described in Chapter 4, Section 4.3.4.2.2). The results are presented in Table 5.12. Since it was unknown at what dilution the anti-bacteriophage 9563 (if present) would be most effective at binding with phages, rows A and B of the well plate were of two different serum dilutions (1:1000 and 1:10 000). Rows C to G were control rows used to confirm the presence of anti-bacteriophage 9563 antibodies. Note that 'pre-bleed' serum had been taken before the rabbit was injected with bacteriophage 9563.

Table 5.12. Results of the ELISA for anti-bacteriophage 9653 antibodies in rabbit sera. 2Y is the peroxidase conjugate-goat anti-rabbit IgG (secondary antibody).

Well plate row	Treatment	Mean absorbance
A	Bacteriophage + serum (1:1000) + 2Y	0.774
B	Bacteriophage + serum (1:10 000) + 2Y	0.573
C	Bacteriophage + pre-bleed serum (1:1000) + 2Y	0.201
D	Bacteriophage + pre-bleed serum (1:10 000) + 2Y	0.132
E	Bacteriophage + 2Y	0.064
F	No bacteriophage + serum (1:1000) + 2Y	0.085
G	No bacteriophage + serum (1:10000) + 2Y	0.068
H	No bacteriophage + 2Y	0.143

Critically, the ELISA showed the absorbance of rows A and B to be significantly different from their corresponding pre-bleed serum control results (by a paired t-test; H_0: $\mu_d = \mu_0 = 0$, H_A: $\mu_d \neq \mu_0$, $\alpha = 0.05$) and the other control rows of E to H (based on two-sample t-tests; H_0: $\mu_1 - \mu_2 = 0$, H_A: $\mu_1 - \mu_2 \neq 0$, $\alpha = 0.05$). The results therefore confirm that active anti-bacteriophage 9563 antibodies are present in the serum. In addition to this, a significantly higher absorbance was obtained with the 1:1000 serum dilution compared to the 1:10 000 serum dilution (based on a two-sample t-test; H_0: $\mu_1 - \mu_2 = 0$, H_A: $\mu_1 > \mu_2$, $\alpha = 0.05$) whilst the control results of row F indicated very few non-specific reactions occurring. Therefore, in future testing, a 1:1000 dilution of the serum was used.

The protocol for the FIA was effectively based on the anti-phage ELISA but scaled up for utilisation with the glass coverslips rather than a 96 well plate and a fluorescently tagged secondary antibody was used rather than an enzyme labelled antibody. Full details of the FIA protocol can be found in Chapter 4, Section 4.3.4.2.3. Before applying the FIA to the investigated immobilisation methods, a trial was first conducted using a common tissue adhesive, poly-l-lysine. Poly-l-lysine was coated onto coverslips in order to promote the binding of phages and ensure their presence for the initial test. Incidentally, it was borne in mind that the use of poly-l-lysine could be considered as an immobilisation approach for

employment with the sensor. Details of the microscopy work which followed the FIA can be found in Chapter 4, Section 4.3.4.2.4.

An example of the images obtained from the trial is shown in Figure 5.8. As anticipated, green fluorescent spots were visible on the treated substrate due to the secondary antibody in the FIA emitting green light under appropriate excitation (Figure 5.8(a)) compared to the control which had none (Figure 5.8(b)). The fluorescent spots were easily distinguishable for counting. The results demonstrated that the FIA could be used to detect immobilised phages. Phage suspension concentration was approximated to be 4.2×10^8 PFU/ml as listed in Table 5.13 to follow.
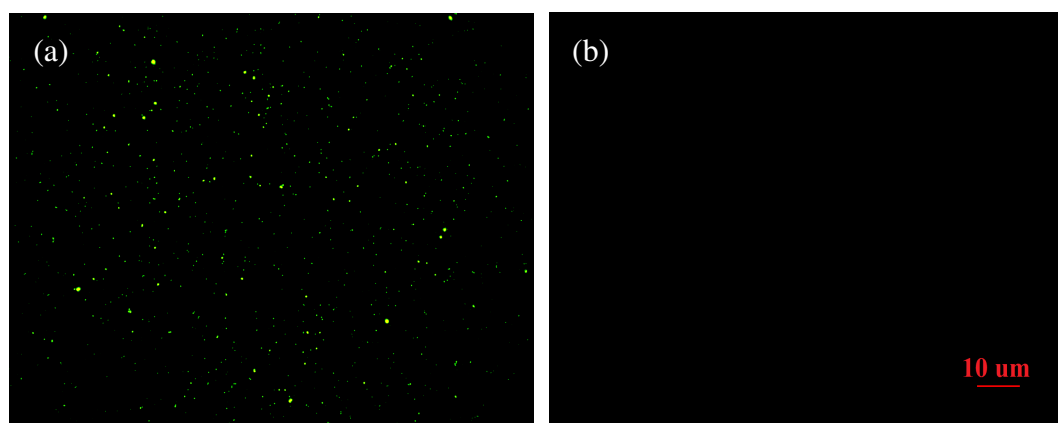
Figure 5.8. Normalised fluorescent image acquired from (a) phage treated substrate coated with poly-l-lysine and (b) a control substrate coated with poly-l-lysine but not treated with phages.

It is worth pointing out that all fluorescent images were normalised against control images apart from when images were analysed using the manual method (details on this to follow). The normalisation parameters were chosen such that they could eliminate any fluorescence on images taken from the controls which were not exposed to phages but otherwise went through the same coating and FIA procedure. This ensured that any fluorescence observed in images obtained from phage treated substrates could be attributed exclusively to the presence of phages and not any background fluorescence from non-specifically adsorbed antibodies.

172

5.3.1.2 FIA Method Discussion

It is important to discuss the validity and suitability of the FIA method for enumerating immobilised phages as although the assay format itself is a commonly used technique, its application to quantifying immobilised phages is novel as far as the author is aware. Further to this, the anti-bacteriophage 9563 antibodies had not previously been used.

Several steps were taken to ensure that the results obtained from the FIA would be indicative of immobilised phages:

- A blocking step was included after phage immobilisation to minimise non-specific binding of the antibodies as this could lead to false positive results. BSA was used which is a commonly applied blocking agent. A higher concentration of BSA was applied over a longer period of time than in the ELISA to further ensure adequate blocking.

- Substrates were washed after each incubation step to remove excess blocker or antibodies. A PBS solution mixed with the mild detergent (Tween) was used as is typically employed in ELISAs and FIAs. Of the three washes, the last wash was with PBS only as, upon drying, a crystallised residue sometimes appeared on substrates washed with PBS-Tween which was thought to be traces of the detergent.

- The activity and an appropriate working concentration of the anti-phage antibody were reliably determined with an ELISA (Section 5.3.1.1).

These measures appeared to be adequate for ensuring the removal of non-specific adsorption as there was generally very little evidence of fluorescence on the control substrates and parameters which rendered control images completely black did not eliminate fluorescent spots when applied to images from treated substrates.

However, some inaccuracies may be introduced elsewhere and these should be acknowledged. For example, although non-specific antibody adsorption is minimised, conversely, both the primary and secondary antibody may not necessarily bind with every phage and some phages may desorb from the substrate during

washing, resulting in an underestimation. Autofluorescence of foreign particles may occur (such as with dust or bacterial cell debris) which will result in the inclusion of false positive counts. Also, clusters of phages will be counted as one fluorescent spot (although one cluster probably represents only one 'active' phage due to the fact that bacteria are considerably larger than phages). Finally, the orientation of immobilised phages can not be taken into account and so not all phages detected by the FIA will be capable of binding to a bacterium.

Inaccuracies may also be introduced with the analysis approach. The automatic and manual analysis methods are described in detail in Chapter 4, Section 4.3.4.2.4. Basically, where possible, a counting tool available within the image capture and analysis software (IPLab) was used to automatically compute the number of fluorescent spots in an image. However, defining the regions of interest to be counted is user controlled and so some inaccuracies may be introduced here. Likewise, when the manual method was necessary (discussed further in Sections 5.3.2 and 5.3.3), counting errors may occur. Therefore both analysis methods entail an unavoidable degree of human judgement which will inevitably introduce some errors. However, for a comparative analysis, as is the case here, at least the error should be common across the results. To ensure that the two different methods were yielding similar results and thus comparisons were valid, the trial samples with poly-l-lysine were analysed with both the automatic and manual analysis methods and results were compared. The counts were within an acceptable 10% of each other, with the automatic count being slightly lower.

In the images acquired (for example Figure 5.8) it was observed that some of the fluorescent spots were larger than others. The smallest fluorescent spots were only two pixels wide. When the image resolution is considered this does not appear to be unreasonably small for a phage particle. It is known that each pixel is 0.0903 µm in width and height and bacteriophage 9563 has a volumetric diameter of approximately 236 nm [Boonmee, 2009b]. Therefore, a spot two pixels wide could feasibly represent a single phage. Larger spots could be attributed to phage aggregation which has previously been reported to occur [Olsen et al., 2006, Serwer et al., 2007].

Another possible explanation for the size discrepancy in fluorescent spots could lie with the phage-antibody interaction. The epitopes on the phage surface, i.e. the portions to which antibodies bind via their corresponding paratope, were not identified for the anti-bacteriophage 9563 antibody. However, for a comparatively large antigen molecule such as phage, it is possible that there will be several epitope sites available for antibody binding and, furthermore, depending on how the antibody was generated there may be several different types of epitopes [Price and Newman, 1997]. Therefore it is highly probable that several anti-phage antibodies are capable of attaching to one phage and that the more antibodies present the brighter and larger the fluorescent spot. Incidentally, it was decided to try the FIA approach to detecting phages and not to directly stain phage nucleic acid, as had previously been reported by Serwer et al. (2007), as there were concerns over whether the resolution of the fluorescent microscope available would be adequate. These observations tend to indicate that detecting phage by direct staining may not have been successful. Also, it was more desirable to treat the phages after immobilisation rather than before in case the staining procedure in anyway affected the immobilisation of phages. In addition to this, the components necessary for the FIA were readily available and did not have any of the safety issues associated with a nucleic acid stain.

Overall, it was concluded that the FIA was successfully indicating immobilised phages and could be used to compare different immobilisation methods.

5.3.2 Results

Figure 5.9 shows typical examples of the fluorescent images acquired from glass substrates treated with the different phage immobilisation procedures. The images have been normalised against control images as described in Chapter 4, Section 4.3.4.2.4, with the exception of images from silane and glutaraldehyde treated slides (Figure 5.9 (e) and (f)) for reasons which will be discussed later. Normalised control images had no fluorescence as was illustrated previously in Figure 5.8. For phage treated substrates, green punctated images were observed as expected. Note that the solution based method of generating the silane layer was used

and not CVD. Estimated phage concentrations used with each immobilisation method are listed in Table 5.13.
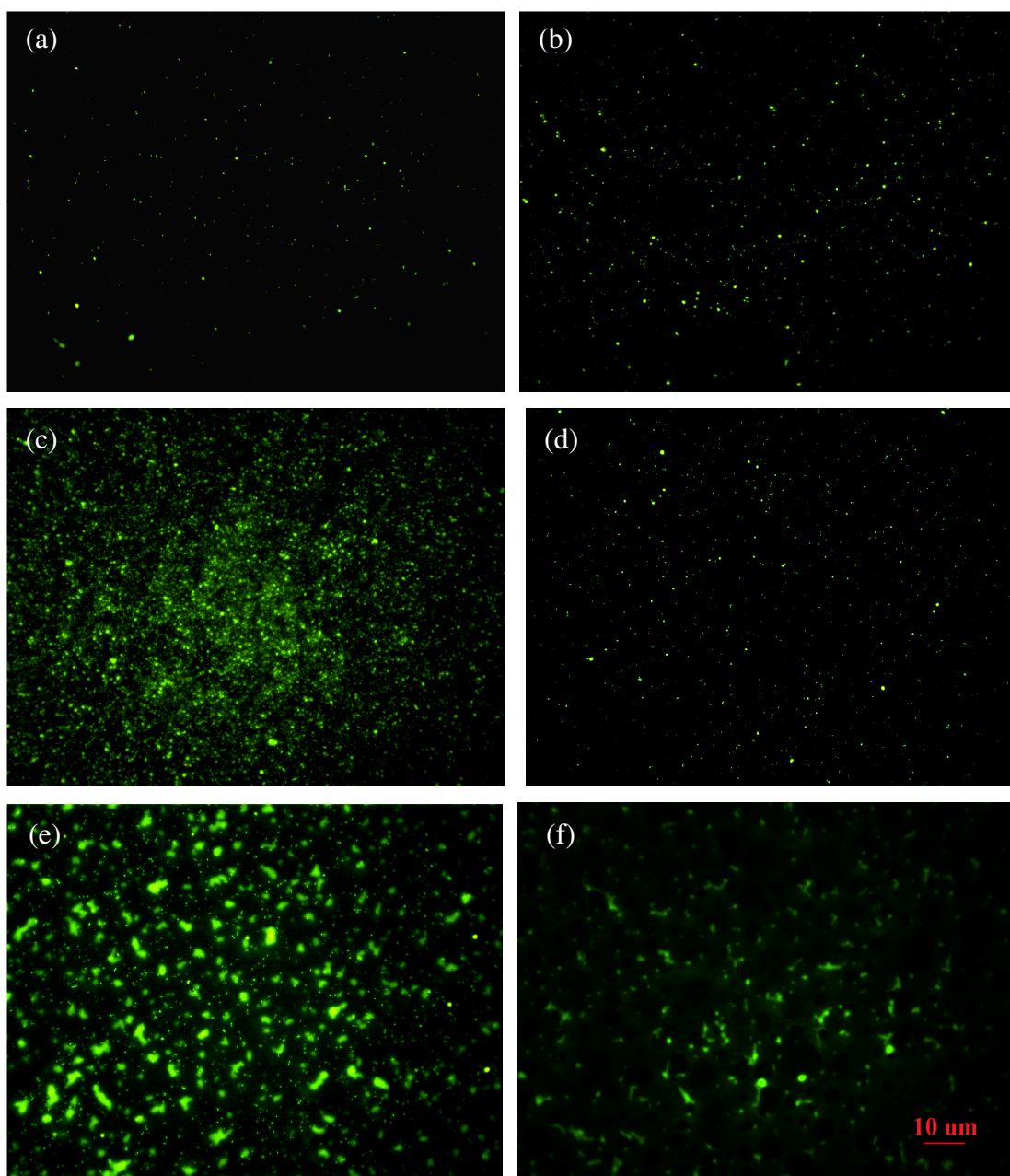
Figure 5.9. Examples of fluorescent images obtained from substrates treated with the following immobilisation procedures: (a) two hour physical adsorption, (b) overnight physical adsorption, (c) biotin-avidin system, (d) poly-l-lysine adhesive layer, (e) silane and glutaraldehyde and (f) the control for silane and glutaraldehyde (no phage). Images were aquired in grey scale and then a single pseudo colour was applied (green).

Table 5.13. Concentration of phage suspension used with each immobilisation procedure.

Immobilisation method	Estimated phage concentration applied to substrates (PFU/ml)
Two hours physical adsorption	2.4×10^8
Overnight physical adsorption	2.4×10^8
Biotin-avidin system	2.3×10^{10}
Poly-l-lysine	4.2×10^8
Silanisation and glutaraldehyde coupling	7.3×10^8

An initial visual inspection of the images suggests that the biotin-avidin system immobilised the most phages based on the number of fluorescent spots appearing in images. It should be pointed out that, as shown in Table 5.13, a significantly higher phage concentration was utilised in the biotin-avidin procedure compared to other methods (10^{10} PFU/ml compared to 10^8 PFU/ml) due to different phage harvests available at the time. It might be expected that the improved immobilisation was due to this. However, Figure 5.10 displays some data collected during the initial FIA trial with poly-l-lysine which illustrates that immobilisation levels achieved with phage concentrations in the order of 10^8 PFU/ml and 10^{10} PFU/ml were not significantly different (two-sample t-test, H$_0$: $\mu_1 - \mu_2 = 0$, H$_A$: $\mu_1 - \mu_2 \neq 0$, $\alpha = 0.05$). In fact, higher immobilised phage values were actually obtained with the lower phage concentration. This result suggests that the seemingly improved levels of immobilisation observed in Figure 5.9(c) can not necessarily be attributed to the higher phage concentration used.
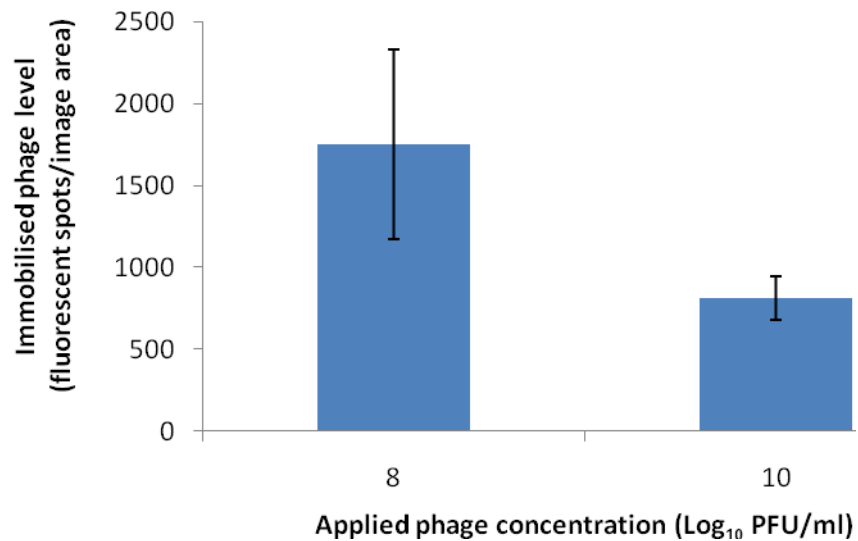
Figure 5.10. Level of phage immobilisation onto poly-l-lysine coated substrates achieved with different incubating phage concentrations. The mean fluorescent spot counts per image area (121.36 μm × 92.47 μm) are reported ± the standard deviation (n = 3).

It is also suggested from Figure 5.9 that overnight incubation (Figure 5.9(b)) allowed more phages to physically adsorb onto the glass substrate than the two hour incubation period (Figure 5.9(a)) and that overnight physical adsorption directly onto the substrate yielded similar results to overnight incubation onto poly-l-lysine coated substrates. These observations were confirmed by the average fluorescent spot counts obtained from the different immobilisation methods which are presented in Figure 5.11.
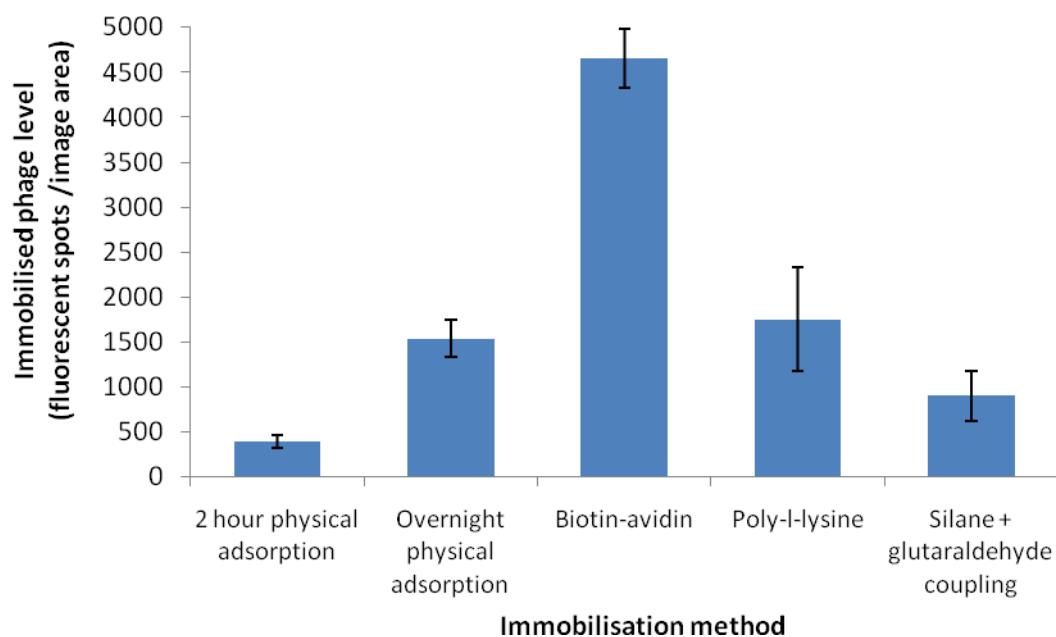
Figure 5.11. Level of phage immobilised onto glass by each method, indicated by the mean fluorescent spot count per image area (121.36 µm × 92.47 µm) ± the standard deviation (n = 3). Note that all results were obtained using the automatic counting method apart from the silane and glutaraldehyde results for which the manual counting method was used (both methods are described in Chapter 4, Section 4.3.4.2.4).

Before examining the results of Figure 5.11 it is important to point out that the average fluorescent spot count obtained from the silane and glutaraldehyde treated substrates had to be obtained by the manual counting method rather than the automatic method as was used for all other immobilisation methods. This was because, as illustrated in Figure 5.9(e) and (f), there was considerable interfering fluorescence in images obtained from substrates treated with silane and glutaraldehyde. This fluorescence, which sometimes appeared more intense in patches, was actually yellow/orange but because images were acquired in grey scale and then only a single pseudo colour could be applied, the true colour images can not be re-created. When the normalisation parameters required to completely eliminate the fluorescence in the silane and glutaraldehyde control images were applied to images of phage treated substrates, almost all fluorescence was eliminated from the phage treated images as well, including the green fluorescence. Thus, a manual counting method was required. The average fluorescent spots count was determined for both phage treated and control silane and glutaraldehyde images. On average

179

there were 990 ± 275 and 88 ± 30 green fluorescent spots per image for phage treated and control slides respectively. These values were significantly different from each other (by two-sample t-test, H_0: $\mu_1 - \mu_2 = 0$, H_A: $\mu_1 - \mu_2 \neq 0$, $\alpha = 0.05$). For comparison with automatic count results displayed in Figure 5.11, the average result obtained from control images was subtracted from the average result obtained from treated images.

Values of the fluorescent spot counts displayed in Figure 5.11 confirmed that the biotin-avidin procedure yielded the highest level of detectable phages, an average of 4656 ± 326 fluorescent spots were counted per image area. A statistical analysis of the results revealed that the results from the biotin-avidin system were significantly different from all other methods (ANOVA, $\alpha = 0.05$, followed by Tukey's comparison). There was no significant difference between the results of the overnight physical adsorption, poly-l-lysine and silane and glutaraldehyde coupling treatments suggesting that the level of phages immobilised with these methods are comparable. However, there was a significant difference between the two hour and overnight incubation results for physical adsorption. As might have been expected, the fluorescent spot count from the images for substrates incubated overnight with phages was higher than that for the two hour incubation: an average of 1539 ± 208 spots per image area compared to 398 ± 72.

It is useful to consider the FIA results in terms of estimated immobilisation densities i.e. the number of phages immobilised in a unit area. Since the area of each image is known to be $121.36 \, \mu m \times 92.47 \, \mu m$ for the microscope settings used, the data presented in Figure 5.11 can be represented as estimated phage densities, assuming that each fluorescent spot denotes one phage. Values are displayed in Table 5.14.

Table 5.14. Estimated immobilised phage densities achieved by different immobilisation methods.

Immobilisation Method	Estimated phage density (phages/μm^2)
Two hours physical adsorption	0.04
Overnight physical adsorption	0.14
Biotin-avidin system	0.41
Poly-l-lysine	0.16
Silane and glutaraldehyde coupling	0.08

The biotin-avidin immobilisation procedure was also used with PMGI coated substrates. FIA results are presented in Figure 5.12 along with the results for glass substrates. Results were very similar with an average of 4656 ± 326 spots per image area counted on glass substrates compared to 4558 ± 584 spots per image area on PMGI substrates. There was no significant difference between the fluorescence levels obtained with the different substrates (by two-sample t-test, H$_0$: μ_1 - $\mu_2 = 0$, H$_A$: μ_1 - $\mu_2 \neq 0$, $\alpha = 0.05$).
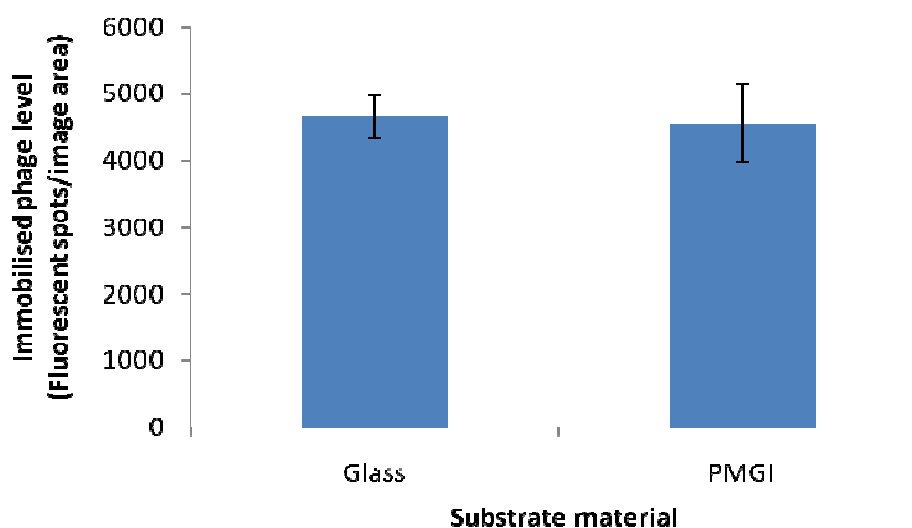
Figure 5.12. Comparison of immobilised phage levels on glass and PMGI substrates immobilised by the biotin-avidin system.

Table 5.15 lists the coefficient of variation (CV) for the FIA data presented in Figure 5.11 for each immobilisation method. This statistical parameter can be used to assess the variation in the data under normalised conditions. The results show that the poly-l-lysine method and silane and glutaraldehyde coupling have the highest CV value. This suggests that results from these methods exhibited the greatest variation which in turn suggests that phage immobilisation was the least consistent over the substrates for these methods. Results with biotin-avidin had the lowest CV value suggesting that phage immobilisation was the most consistent over substrates with this method.

Table 5.15. Coefficient of variation values for the data collected from the FIA on the different immobilisation methods.

Immobilisation Method	Coefficient of variation
Two hours physical adsorption	0.18
Overnight physical adsorption	0.14
Biotin-avidin system	0.07
Poly-l-lysine	0.33
Silanisation and glutaraldehyde coupling	
Phage treated	0.28
Control (not phage treated)	0.34

5.3.3 Discussion

The validity of utilising the specially developed FIA to detect immobilised phages was discussed in detail in Section 5.3.1. It was concluded that the approach could be used with confidence to compare different immobilisation methods and to give an indication of the level of phages immobilised.

Further confirmation that the FIA was yielding viable results was obtained by comparing the estimated number of phages immobilised (obtained from the FIA results) to that which was available in the suspension applied. For every experiment it was found that the estimated number of phages immobilised did not exceed the number of phages present and thus the results are feasible.

Based on the results of the FIAs, the biotin-avidin system appears to be the most promising immobilisation method both in terms of the number of phages immobilised and also in producing the most uniform phage layer (as indicated by having the lowest CV value reported in Table 5.15). Although a higher phage concentration was used in the biotin-avidin procedure, a comparison of different incubating phage concentrations with poly-l-lysine coated substrates implies that this is unlikely to entirely account for the improved immobilisation levels (see Figure 5.10).

Conversely, it was found that immobilisation levels did depend on incubation time; a significantly higher number of phages were indicated on substrates incubated with phage suspensions overnight as compared to just two hours. The results for two hour physical adsorption were the lowest out of all the immobilisation methods investigated. When the influence of incubation time is considered, the potential of the biotin-avidin system is even more evident as treated substrates were incubated with the phage suspension for only three hours yet the results indicated significantly higher levels of phages on these substrates compared to overnight physical adsorption.

The improved immobilisation results obtained with the biotin-avidin method is likely to be due to the strong affinity between biotin and avidin in combination with adequate deposition of the B-BSA layer onto the substrate, as had previously been reported by Kim et al. (2009) and Koo et al. (2009).

In the case of physical adsorption, immobilisation may be more limited by the electrostatic forces present. For example, although the exact pI of bacteriophage 9563 is not known, phages are generally negatively charged in solutions of neutral pH [Schaldach et al., 2006]; pIs reported for phages vary from 3.9 to 7.3 but are typically below 7 [Collins et al., 2006, Dowd et al., 1998, Zerda et al., 1985]. It is also known that glass and silica surfaces are negatively charged in water [Behrens and Grier, 2001, Zerda et al., 1985]. Therefore, in water, there will be opposing electrostatic forces between phages and the glass substrate which are likely to limit

the level of immobilisation achieved by just physical adsorption. Free phages in the solution may also be repelled by immobilised phages due to their like surface charge. The presence of salts in the PBS suspension (which was actually used in experiments) is likely to promote adsorption and aggregation interactions through the formation of salt bridges [Farrah, 1982, Kessick and Wagner, 1978] and hydrophobic forces have been suggested to play a particularly important role when there is considerable electrostatic repulsion between substrate and molecules [Schijven and Hassanizadeh, 2000, van Voorthuizen et al., 2001] but the extent of this was not investigated here. However, in summary, saturation may be reached with physical adsorption at comparatively low phage coverage due to the electrostatic forces involved but the association constant between biotin and avidin may be strong enough to overcome some of this effect, resulting in improved phage immobilisation.

Silane and glutaraldehyde coupling generated one of the lowest phage immobilisation densities out of the methods tested. This could be due to poor silane layer formation, first discussed in Section 5.2.3.3. The relatively high CV value compared to some of the other immobilisation methods gives further reason to believe that phage immobilisation was inconsistent and corresponds with the variation seen in the broth culture results.

However, as discussed in Section 5.3.2 the silane and glutaraldehyde FIA results had to be obtained from images exhibiting conflicting fluorescence. This meant that images were not clear and identifying the characteristic green fluorescence was more difficult, although generally the areas of yellow/orange fluorescence were much larger that the green spots and so they could be discriminated between. However, it is possible that the computed phage density may be less accurately represented due to this abnormal fluorescence. It is not thought that the yellow/orange fluorescence is related to the phages as it was only observed on silane and glutaraldehyde treated substrates, including the control which was not exposed to phages. It was therefore concluded that the yellow/orange fluorescence originated from the silane or glutaraldehyde or a combination of both. Such autofluorescence of silanes and glutaraldehyde has been reported elsewhere [Collins and Goldsmith, 1981, Fester et

al., 2008, Raghavachari et al., 2003]. However, if the occurrence of chemical autofluorescence is to be the accepted theory then it may have been expected to see a more consistent fluorescent background to the images rather than being quite patchy. This may be further indication of an inconsistent silane/glutaraldehyde layer.

In order to put the immobilisation densities reported in Table 5.14 into perspective, a maximum possible immobilisation density was calculated for bacteriophage 9653 based on its dimensions. The mean diameter of the volume occupied by bacteriophage 9563 is 236 nm [Boonmee, 2009b]. If it is then assumed that an immobilised phage occupies a surface area of 236 nm × 236 nm then an approximate maximum immobilisation density for a monolayer of bacteriophage 9563 is calculated to be 17 phages/μm^2.

It can be seen that the immobilisation densities calculated from the FIA results are significantly less than the theoretical maximum. However, it is unrealistic to expect this maximum to be achieved due to repelling electrostatic forces arising from the similarly charged phages and steric hindrance. There is also the possibility that some competing proteins may remain after re-suspending phages. The estimated maximum value also does not take into consideration variations in phage orientation. However, it still provides a useful point of reference.

In comparison with published data, the experimental values for phage immobilisation densities compare reasonably well. Gervais et al. (2007) reported a surface density of 0.3 phages/μm^2 on a gold surface after immersion in a solution of T4 phages (10^9 PFU/ml) compared to 0.14 phages/μm^2 obtained here for the physical adsorption of bacteriophage 9563 onto glass over a similar incubation period. T4 phages also have a head and tail structure and reported dimensions are similar to that of bacteriophage 9563 [Imai et al., 1993]. As was found in this research, Gervais et al. (2007) were able to improve on physical adsorption results by utilising the biotin-avidin system. However, their reported phage density with this method was somewhat greater than that achieved here: 4.4 phages/μm^2 compared to 0.41 phages/μm^2. Possible reasons for this could lie with variations of the methods

used. Gervais et al. (2007) incubated the prepared substrates with biotinylated phages overnight and also used a carboxyl-terminated SAM to attach the avidin layer. Here, biotinylated phages were incubated with substrates for three hours and physically adsorbed B-BSA was used to anchor the biotin-avidin system. In addition to this, Gervais et al. (2007) used genetically modified phages to help in the biotinylation of phages rather than relying on direct chemical biotinylation as was used here.

Higher phage immobilisation densities have recently been reported elsewhere for other immobilisation methods. For example, Singh et al. (2009) calculated an immobilised phage density of 18 phages/μm^2. Phages were immobilised onto an amino acid (cysteine) layer on gold, activated by glutaraldehyde. Singh et al. (2009) equated this to a 37-fold improvement on physical adsorption. Conducting studies into the interactions of bacteriophage 9563 with different amino acids would be worth investigating in the future as a means of achieving comparable levels of immobilisation.

In a practical sense, it is more relevant to consider whether the phage immobilisation density would be able to capture high numbers of bacteria onto the sensor; bacteria are the biosensor's target and since they are larger in size than phages they are the governing factor for determining what an adequate phage immobilisation density is. For example, *S. aureus*, for which bacteriophage 9563 is selective, have a diameter of approximately 1 μm. For simplicity, if it is assumed that each *S. aureus* bacterium will occupy a surface area of approximately 1 μm^2, then theoretically an immobilisation density of 1 phage/μm^2 will result in a good surface coverage of bacteria assuming uniform phage distribution and that every phage captures a bacterium. Obviously this is a considerable simplification of the actual situation but it is interesting to note that the phage immobilisation density achieved with the biotin-avidin system is beginning to approach this basic requirement.

5.4 <u>Summary</u>

The research conducted into bioreceptor immobilisation revealed the subject area to be a vast and complex field which is continuously developing in order to try and

meet the requirements of systems which utilise immobilised proteins. For biosensors specifically, it is important to remember that as well as seeking a high immobilised phage density, other aspects of the immobilisation procedure are also critical such as the effect of the procedure on the sensor, the longevity of the bond between phage and substrate and the effect of the immobilisation procedure on phages. Compromises between these aspects may have to be made.

The aim of the immobilisation work presented in this chapter was to test and then compare a broad range of methods for immobilising phages onto the sensor substrate material. To the author's knowledge, there has been no such report on the direct evaluation of different methods for the immobilisation of phages despite the importance of optimising the immobilisation process for improved biosensor performance.

Immobilisation of phages onto glass and PMGI substrates by physical adsorption, corona activation, silane and glutaraldehyde coupling and the biotin-avidin system were investigated. Of these methods it was concluded that the biotin-avidin system was the most promising. Not only did this method yield the highest immobilised phage density compared to the other methods but no harsh chemicals are involved in the procedure which might damage the sensor (as was observed with the silane and glutaraldehyde method). Further to this, there is reason to believe that the orientation of the immobilised phages may be more favourable with biotin-avidin binding if it assumed that the majority of biotinylation occurs with the more protein dense phage head, rather than the smaller infecting tail. One possible drawback to the biotin-avidin approach could be desorption of phages; although the bond between biotinylated phages and NeutrAvidin is strong, the system is anchored via B-BSA which is physically adsorbed onto the substrate. In the future, this problem could be overcome by laying down the avidin layer via a SAM of an appropriate chemical, as demonstrated by Gervais et al. (2007), provided the procedure is compatible with the sensor.

The immobilisation of phages onto PMGI by corona activation was not possible under the corona settings investigated here. It was concluded that considerable time would be required to determine the appropriate parameters necessary to achieve this and so the approach was not pursued.

Chapter 6

SENSOR TESTING

In the previous chapters it was demonstrated that the proposed interdigitated microelectrode array sensor would be sensitive to the presence of bacteria through the use of a computer based model. Subsequent work then investigated immobilisation techniques for phages, proving that phages could be successfully immobilised onto sensor substrates and that some methods were better than others.

The next step was to apply the optimised immobilisation procedures to the fabricated sensors and to test the ability of the actual biosensor to detect bacteria. In the following chapter, the results of this investigation are reported, with particular focus on the performance of phages as bioreceptors. In Part I, initial experiments examining the ability of immobilised phages to enhance bacteria capture onto a substrate are presented and discussed. The results of such an investigation would help verify any changes observed in the sensor testing. Also included in Part I are the results of the post-fabrication sensor testing. A series of simple tests were carried out to characterise the sensor to ensure fabrication had been successful and that the sensor was performing as expected.

In Part II, the experimental testing of sensors is reported. Sensors, with immobilised phages, were tested with suspensions of bacteria and impedance was measured either over time (Testing Method 1) or before and after exposure to bacteria (Testing Method 2). Test parameters, including the solution used to suspend bacteria and the phage immobilisation method, were investigated.

6.1 <u>Initial Bioreceptor Evaluation</u>

It is obviously of critical importance that a bioreceptor, chosen for implementation with a biosensor device, can successfully interact with the target analyte to the extent that it increases target levels in the device's sensing region. The following experiment was devised to evaluate the performance of immobilised bacteriophage 9563 as bioreceptors for *S. aureus* 8588. It was previously shown in Chapter 5 that phages could be successfully immobilised but it was critical to ascertain whether the immobilised phages would successfully capture bacteria onto the surface of a substrate, as would be required for the detection of bacteria between sensor electrodes. Full details of the protocol and microscopy work can be found in Chapter 4, Section 4.3.5. Here, some aspects of the method are first discussed before the experimental results are presented and evaluated in Sections 6.1.2 and 6.1.3.

6.1.1 Method

Basically, the experiment involved applying a bacterial suspension onto substrates with phages immobilised by the silane and glutaraldehyde method (see Section 4.3.2.3) for 2, 5, 10 and 20 minutes, as described in Section 4.3.5. Substrates were rinsed once with PBS and then placed in methanol. The number of bacteria on treated and control substrates (without immobilised phages) were then counted and compared using phase contrast microscopy. Utilising phase contrast microscopy to detect bacteria bound to immobilised phages has previously been reported by Carnazza et al. (2007).

Rinsing the substrates with PBS was carried out to remove the excess bacteria which were not bound to phages and also for removing any debris which might reduce the clarity of the phase contrast microscope images. Substrates were also blocked with BSA prior to exposure to bacteria (as outlined in Section 4.3.5) with the aim of reducing levels of non-specific adsorption. The methanol treatment, in addition to fixing bacteria, was important for preventing eventual bacterial lysis by phages. This is critical if the results are to represent the number of bacteria captured. Note

however, that lysis will not occur during the 20 minute testing period as this is within the 25 minutes latent period for bacteriophage 9563 infection of *S. aureus* 8588 [Boonmee, 2009a]. Also, this latent period was determined at an optimal temperature for bacterial growth (37°C) whereas the experiment conducted here was at room temperature; this factor is likely to increase the phage latent period.

If the results of the experiment were to reliably represent the number of captured bacteria, it was critical that any phage-bacterium complexes were not easily removed during rinsing. Therefore, the silane and glutaraldehyde coupling technique was employed to immobilise phages as this would provide a strong covalent binding mechanism between phages and the substrate (details of the immobilisation method can be found in Chapter 4, Section 4.3.2.3). Although it was revealed in Chapter 5 that this technique yielded a comparatively low immobilised phage density, results would provide a good benchmark for predicting levels of captured bacteria with other immobilisation techniques. In addition to this, the biotin-avidin method (which was later implemented with the sensors) had not yet been fully developed.

The experiment was also repeated with immobilised antibodies, a more commonly used bioreceptor for biosensor applications. Results would act as an indicator against which phage performance could be compared. Anti-protein A antibodies were used which would bind to protein A present on the surface of *S. aureus* 8588.

Substrates with immobilised phages were incubated in a phage suspension of estimated concentration 2.4×10^9 PFU/ml. Bacterial enumeration estimated the bacterial concentrations applied to substrates with immobilised phages and antibodies to be 8.1×10^8 CFU/ml and 1.1×10^9 CFU/ml respectively (see Chapter 4, Section 4.2.2, for details on enumeration methods).

6.1.2 Results

Figure 6.1 shows examples of the phase contrast images acquired from substrates after increasing incubation times with the bacterial suspension. Images on the left of Figure 6.1 were obtained from substrates with immobilised phages (herein termed phage activated substrates) after 2, 5, 10 and 20 minutes contact time with the

bacterial suspension (Figures 6.1(a), (c), (e) and (g) respectively). Images to the right of Figure 6.1 (Figures 6.1(b), (d), (f) and (h)) were obtained from corresponding control substrates which were incubated with bacteria for 2, 5, 10 and 20 minutes respectively. Control substrates were not treated with phages but otherwise went through the same silane and glutaraldehyde immobilisation procedure as phage treated samples.

Images from phage activated substrates clearly show that, as the bacterial incubation time increased, the number of bacteria present on the substrate's surface also increased. An increase in the level of bacteria present on the control substrates is also apparent over time, however phage activated substrates consistently look to have more bacteria present than their corresponding control.
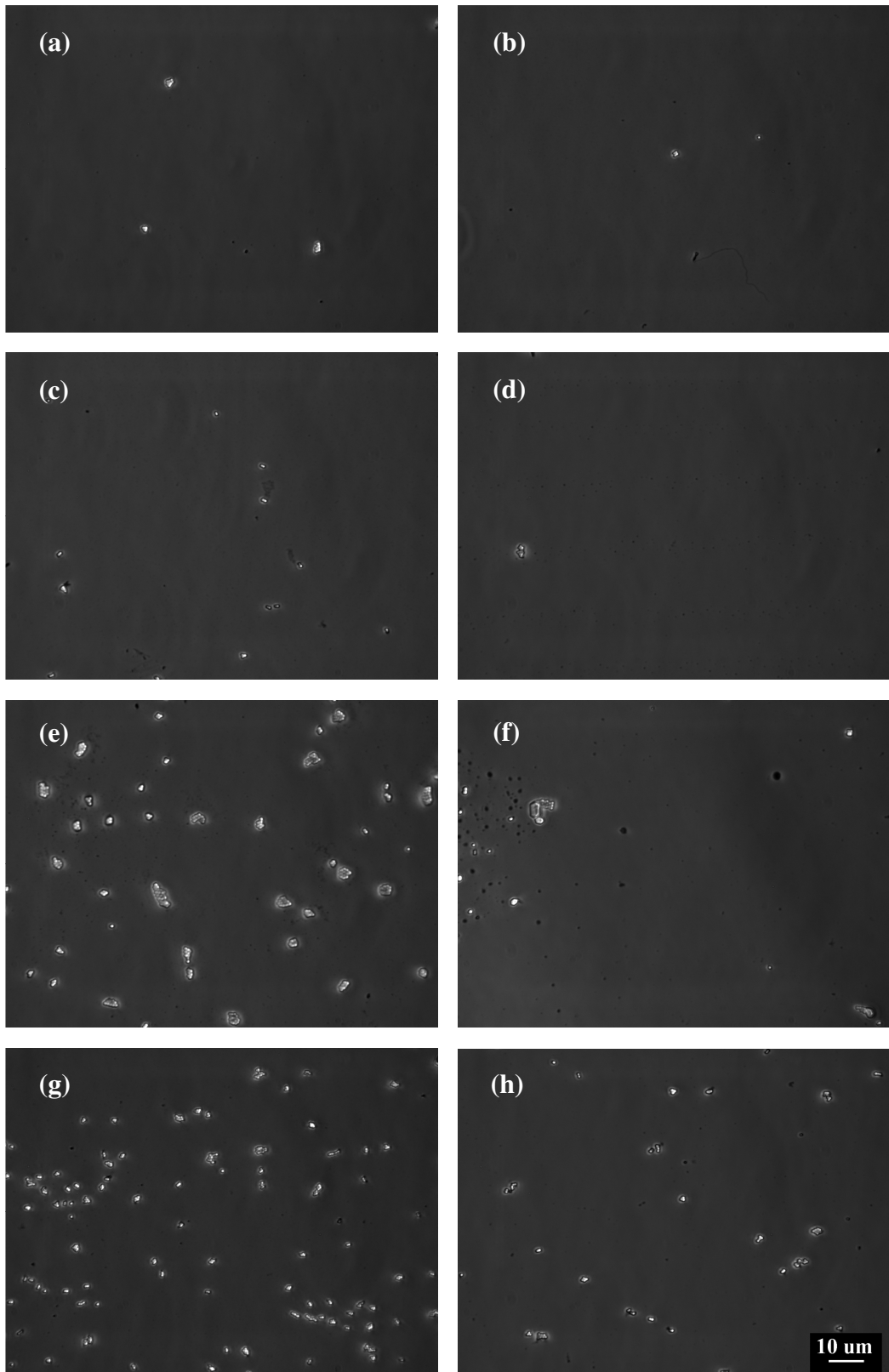
Figure 6.1. Examples of phase contrast images obtained from substrates with immobilised phages and corresponding controls (no phages) at increasing bacterial incubation times: 2 minutes, phage activated (a) and control (b); 5 minutes, phage activated (c) and control (d); 10 minutes, phage activated (e) and control (f); 20 minutes, phage activated (g) and control (h).

To confirm these observations, the average number of bacteria per image area (121.36 × 92.47 µm) was calculated for phage activated and control substrates at each incubation time. Single bacteria were easily identifiable on the images and so it was straightforward to determine the total cell count per image. The results are presented in Figure 6.2.
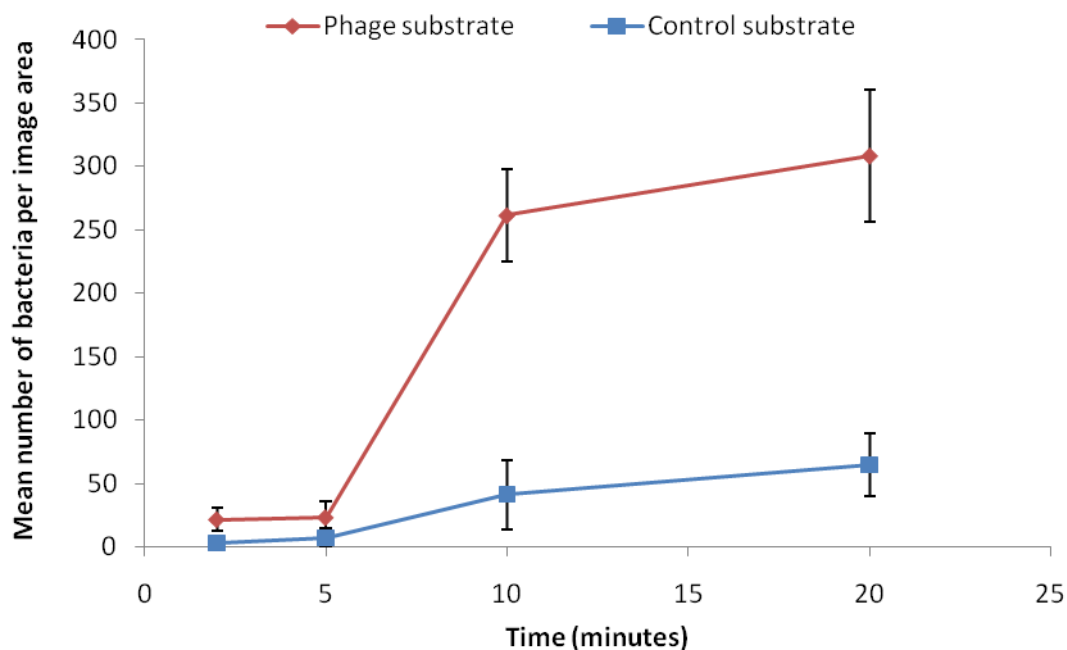
Figure 6.2. Mean number of bacteria counted per image area (121.36 × 92.47 µm) on phage activated substrates (phage substrate) after increasing incubation times with a bacterial suspension. Phages were immobilised by the silane and glutaraldehyde coupling method. Results from control substrates are also included. Control substrates underwent the same silane and glutaraldehyde treatment but were not exposed to phages. Data points show the mean and standard deviation of bacteria counts obtained from images taken at random across the substrate's surface (n = 5).

The average number of bacteria on phage activated substrates was significantly different to the control substrate at each time measurement (by two-sample t-tests, H_0: μ_1 - $\mu_2 = 0$, H_A: μ_1 - $\mu_2 \neq 0$, $\alpha = 0.05$). In addition to this, the number of bacteria captured onto the surface of phage activated substrates was significantly different over the 20 minute time period investigated; the average number of bacteria at 2 and 5 minutes was significantly different from that at 10 and 20 minutes (by the one-way ANOVA test, $\alpha = 0.05$, followed by Tukey's comparison).

194

Results obtained from substrates with immobilised antibodies ('antibody activated substrates') are shown in Figure 6.3. Results were similar to those obtained from substrates with immobilised phages: the mean number of bacteria in the image area increased with increasing incubation time with bacteria. Generally, the value for the mean number of bacteria on antibody activated substrates was greater than that of the corresponding control. The only exception to this was at 2 minutes for which the average number of bacteria was greater on the control substrate. However, a statistical analysis revealed that the difference between antibody activated and control samples was not actually significant at 2, 5 and 10 minutes (two-sample t-tests, H_0: μ_1 - μ_2 = 0, H_A: μ_1 - $\mu_2 \neq 0$, α = 0.05). This outcome is probably due to the large standard deviations obtained at each incubation time (illustrated in Figure 6.3), resulting from wide variations in bacteria counts across images.
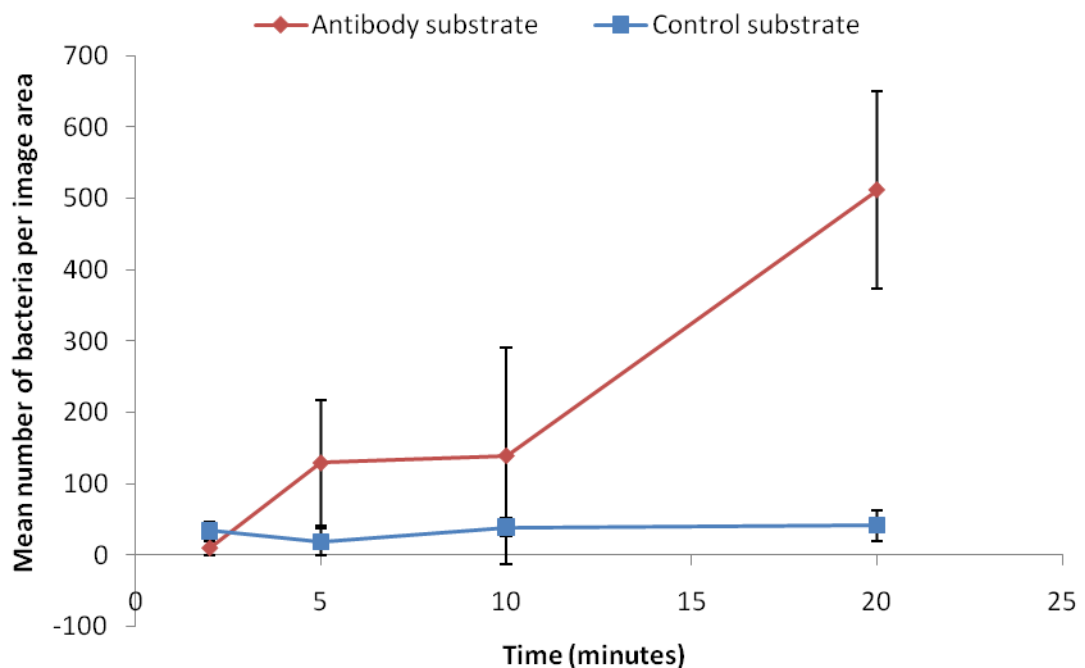
Figure 6.3. Mean number of bacteria counted per image area (121.36 × 92.47 μm) on antibody activated substrates (antibody substrate) after increasing incubation times with a bacterial suspension. Antibodies were immobilised by the silane and glutaraldehyde coupling method. Results from control substrates are also included. Control substrates underwent the same silane and glutaraldehyde treatment but were not exposed to antibodies. Data points show the mean and standard deviation of bacteria counts obtained from images taken at random across the substrate's surface (n = 5).

In Figure 6.4 the results from both bioreceptor types (phages and antibodies) are presented for comparison. Few bacteria are present on either the phage or antibody activated substrate at 2 minutes. As the bacterial incubation time increases, the mean number of bacteria per image area increased in a manner similar for both the phage and antibody activated substrate. Results from the two control substrates were also similar to each other, as would be expected. After 20 minutes, the mean number of bacteria on the antibody activated substrate was estimated to be higher than that of the phage activated substrate: approximately 512 ± 139 bacteria per image area compared to 308 ± 52 bacteria per image area.
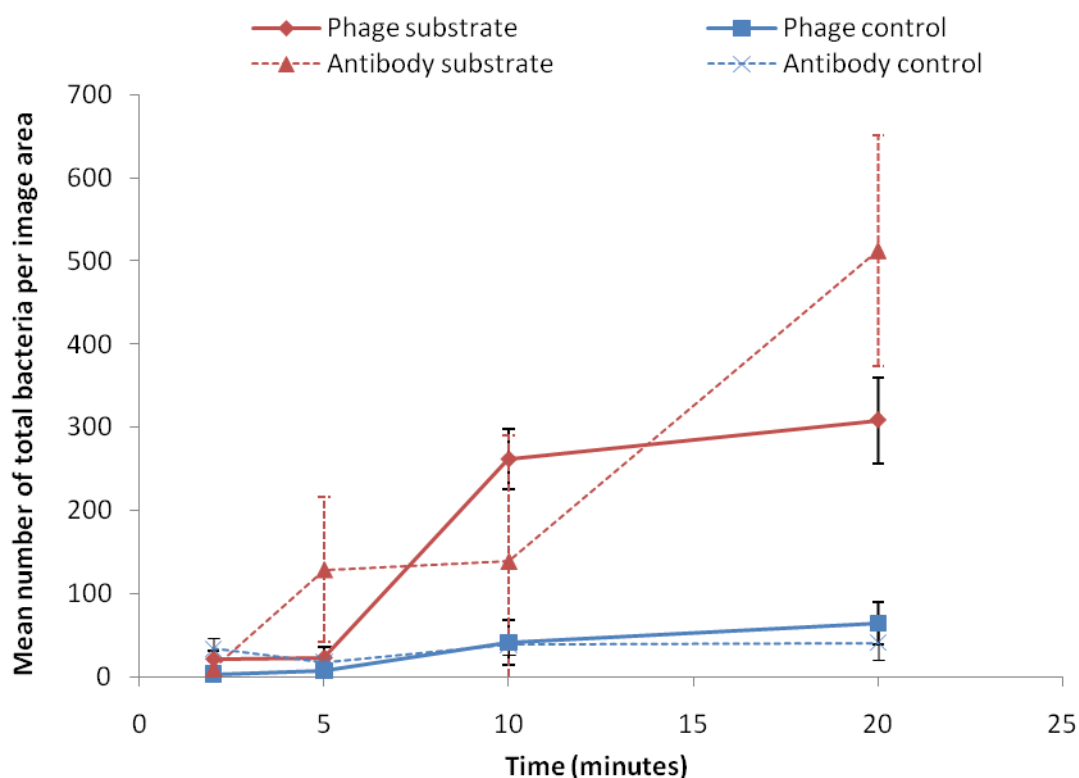
Figure 6.4. Mean number of bacteria counted per image area (121.36 × 92.47 µm) on substrates with either immobilised phages or anti-protein A antibodies after increasing incubation times with a bacterial suspension (termed phage substrate and antibody substrate respectively). Bioreceptor immobilisation was achieved through silane and glutaraldehyde coupling. Results from control substrates are also included. Control substrates underwent the same silane and glutaraldehyde treatment but were not exposed to the bioreceptors. Data points show the mean and standard deviation of bacteria counts obtained from images taken at random across the substrate's surface (n = 5).

In addition to calculating the mean number of bacteria per image, it was also decided to calculate the mean number of clusters of bacteria per image as it was noticed that bacteria were typically present on the substrate's surface in this form i.e. in groups of more than one bacterium (see Figure 6.1). The results for both phage and antibody activated substrates are shown in Figure 6.5. Note that a cluster was defined as an isolated group of bacteria (i.e. two or more bacteria in contact) but if a single bacterium was present, this was also included as one cluster in the count.
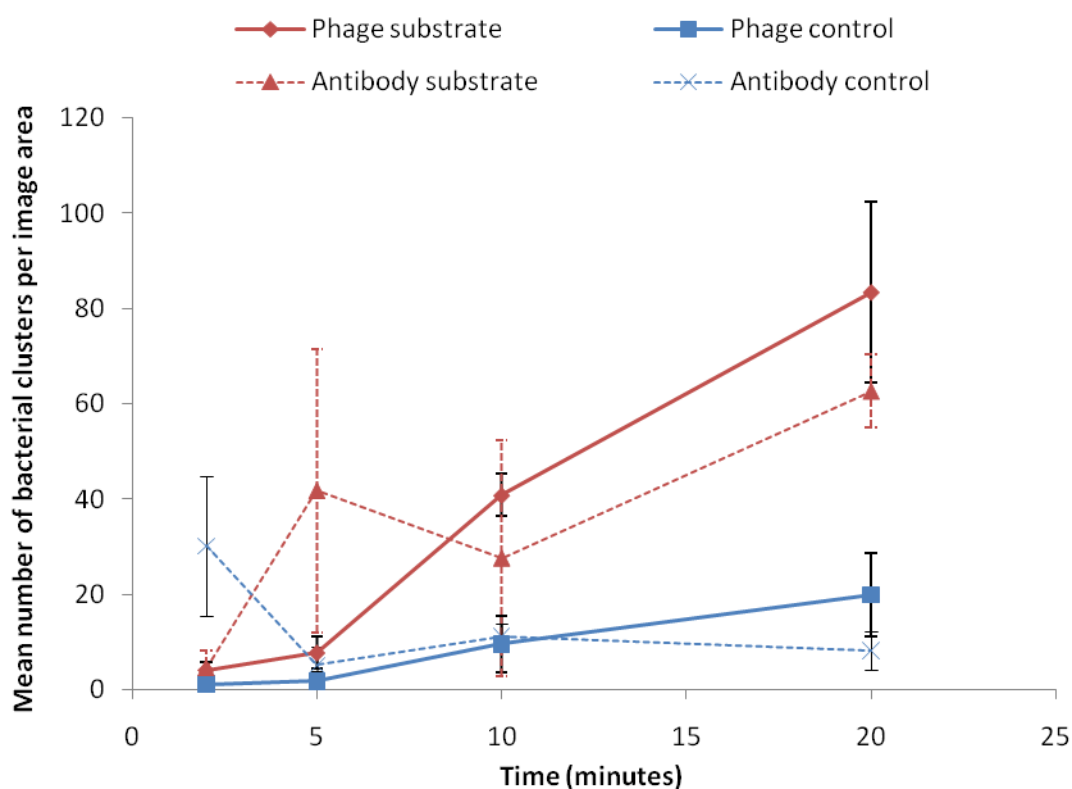
Figure 6.5. Mean number of bacterial clusters per image area (121.36 × 92.47 µm) on substrates with either immobilised phages or anti-protein A antibodies after increasing incubation times with a bacterial suspension (termed phage substrate and antibody substrate respectively). Bioreceptor immobilisation was achieved through silane and glutaraldehyde coupling. Results from control substrates are also included. Control substrates underwent the same silane and glutaraldehyde treatment but were not exposed to the bioreceptors. Data points show the mean and standard deviation of bacteria counts obtained from images taken at random across the substrate's surface (n = 5).

The cluster count results generally followed the same trend as was observed with the total bacteria count: the number of clusters on substrate surfaces (both activated and control) increased with time but typically there were more clusters present on activated substrates. Results were significantly different between phage activated and control substrates at each time interval but were only significantly between antibody activated substrates and controls at 20 minutes (based on two-sample t-tests, H_0: μ_1 - $\mu_2 = 0$, H_A: μ_1 - $\mu_2 \neq 0$, $\alpha = 0.05$). The mean number of clusters on substrates were also significantly different over the 20 minute period for both bioreceptor types (by the one-way ANOVA test, $\alpha = 0.05$). In contrast to the total bacterial count, however, Figure 6.5 shows that more clusters of bacteria are present on the phage activated substrate than the antibody activated substrate at 20 minutes; approximately 83 ± 19 compared to 62 ± 7 clusters.

6.1.3 Discussion

The results of Section 6.1.2 successfully show that immobilised bacteriophage 9563 could increase levels of *S. aureus* 8588 on a substrate surface and that bacterial levels increased over a 20 minute period. Average bacteria counts on phage activated substrates were consistently greater than that for control substrates without immobilised phages after 2, 5, 10 and 20 minutes incubation with the bacterial suspension. The low levels of non-specific attachment of bacteria on control substrates is consistent with similar published results [Bennett et al., 1997, Carnazza et al., 2007, Handa et al., 2008] therefore it was concluded that the washing step after bacteria incubation was adequate for revealing phage performance.

In terms of biosensor application, the results indicate that the presence of immobilised bacteriophage 9563 will draw *S. aureus* 8588 onto the sensor's surface and are thus suitable to perform as a bioreceptor. Further, the results suggest that applying the bacterial sample for longer (but before bacterial lysis becomes a factor) should lead to larger changes in the electrical parameters measured by the sensor due to increased levels of captured bacteria.

To be precise, the results only confirm the performance of phages immobilised via the silane and glutaraldehyde coupling method. However, the results are encouraging for other immobilisation procedures given that silane and glutaraldehyde coupling is the strongest means of immobilising a bioreceptor and therefore the most likely to cause any detrimental conformal changes to the bioreceptor and also yielded one of the lowest immobilised phage densities. Further, the performance of phages which have been immobilised by physical adsorption or the biotin-avidin method has been successfully proven elsewhere, unlike for silane and glutaraldehyde coupling. For example, Lakshmanan et al. (2007) used SEM to detect the attachment of *S. typhimurium* to the surface of a magnetoelastic sensor with physically adsorbed filamentous phages. Sensors were exposed to increasing bacterial concentrations for 20 minutes. It was found that, after washing, levels of bacteria on the sensor's surface increased with increasing bacterial concentration and control substrates without immobilised phages had negligible bacterial binding. Sun et al. (2001) immobilised phages specific to *S. enteritidis* onto magnetic beads using biotin-avidin chemistry. Results of an assay for bioluminescent bacteria showed that this approach to immobilisation improved bacteria capture compared to a control without immobilised phages. The successful interaction between biotin-avidin immobilised phages and bacteria was also reported by Gervais et al. (2007). It therefore seems reasonable to expect bacteriophage 9563 immobilised by these other methods (physical adsorption and biotin-avidin chemistry) to also successfully capture *S. aureus* 8588.

The comparison of phage and antibody performance showed them to be similar: both types of bioreceptor continuously increased the number of bacteria on the substrate's surface over the 20 minute period examined. More bacteria were present on the antibody activated substrate at 20 minutes but some of this increase may be accounted for by the slightly higher bacterial concentration of the suspension applied to antibody activated substrates (1.1×10^9 CFU/ml) compared to the suspension applied to phage activated substrates (8.1×10^8 CFU/ml). (It is worth mentioning that it would be interesting to conduct this experiment over a range of bacterial

concentrations in order to investigate the effect of concentration on captured levels of bacteria.)

Any further conclusions on the comparison of bioreceptors would not be accurate at this stage without obtaining an immobilisation density for the antibodies to compare with that for immobilised phages (as presented in Chapter 5, Section 5.3.2). Comparable numbers of bioreceptors immobilised per unit area is important for a true comparison to be made. It would also be advisable to repeat the experiment a minimum of three times to improve the reliability of the results.

In an attempt to determine the immobilisation density of anti-protein A antibodies, the FIA was applied to substrates in a similar manner as was utilised with phages; the anti-protein A antibodies were also produced in a rabbit and so would be compatible with the fluorescently tagged anti-rabbit antibodies used in the procedure. However, images obtained from antibody substrates did not show the characteristic green fluorescent spots associated with the presence of the fluorescent antibody, as previously seen in the detection of phages. It was concluded that the antibodies were too small to be detected by the microscope and imaging system used here in comparison to the considerably larger phage entities which are likely to be labelled with more fluorescent antibodies (as previously discussed in Chapter 5, Section 5.3.1.2).

Interestingly, in contrast to phage activated substrates, the mean bacteria counts on antibody activated substrates were not significantly different from control substrates at 2, 5 and 10 minutes. A contributing factor to this is likely to be the large standard deviations on the mean bacteria counts from antibody substrates (displayed in Figure 6.4). In turn, this could be indicative of a less homogenous layer of immobilised antibodies compared to phages.

In Figure 6.5 the mean number of bacterial clusters per image is reported for substrates with phage and antibody bioreceptors. This analysis was conducted as *S. aureus* strains tend to form clusters when in solution and it can not be ruled out that a

single phage may be immobilising a cluster of bacteria through its interactions with one bacterium of the cluster. Should this be the case then counting the total number of bacteria may falsely represent the ability of the treated substrates to capture bacteria by giving an overestimation. Therefore checking numbers of bacterial clusters was considered important for confirming the successful performance of bacteriophage 9563 as a bioreceptor. It was assumed that since the overnight broth culture was likely to be in the stationary phase of the growth curve (see Section 1.5) and that bacterial cells were not resuspended with nutrients for the experiment, bacterial growth was unlikely to occur over the 20 minute analysis at room temperature. Therefore the clusters were not attributed to bacterial growth.

The results of the cluster analysis were able to confirm that levels of bacteria were still significantly higher on the phage activated substrates compared to the controls. Bacterial levels also still continuously increased over 20 minutes. Interestingly, at 20 minutes the substrate with immobilised phages now had a higher level of bacteria than the antibody activated substrate based on the cluster count (approximately 83 bacterial clusters per image area compared to 62).

The results of the individual bacteria count were also used to estimate the surface coverage of bacteria. After 20 minutes, approximately 0.027 bacteria/μm^2 were present. This equates to a percentage coverage of 2.2% (for simplicity, a bacterial diameter of 1 μm was assumed for *S. aureus* [Holt et al., 2000] which is in line with estimations made from the phase contrast images of the bacteria in Figure 6.1). This value is close to some previous investigations of a similar nature. For example, Handa et al. (2008) also covalently immobilised phages through a silane coupling chemistry and exposed substrates to bacteria ($10^6 - 10^7$ CFU/ml) for 15 minutes. From the AFM images presented, the captured bacteria density was estimated to be 0.030 bacteria/μm^2. This covered approximately 4.7% of the substrate's surface area (note that the *S. typhimurium* used by Handa et al. (2008) were larger than *S. aureus*). A similar estimation was carried out with the SEM images presented by Olsen et al. (2006) who utilised physically adsorbed phages. After a 7 minute incubation period with bacteria, bacterial density was approximately 0.015 bacteria/μm^2. Significantly

higher surface coverage is evident in other literature. For example, in Carnazza et al. (2008) phase contrast images showed nearly complete surface coverage but they incubated substrates with bacteria for 2 hours which is likely to account for this notable improvement compared to the results presented here.

Finally, the number of bacteria captured onto the substrate surface was compared to the FIA results for phage immobilisation reported in Chapter 5 to ensure continuity between the results. It was found that the numbers of bacteria and bacterial clusters on phage activated substrates does not exceed the estimated number of phages immobilised by silane and glutaraldehyde coupling (0.08 phages/μm^2). The number of captured bacteria is therefore feasible if it is assumed that they have been captured by immobilised phages. It is anticipated that bacterial coverage will be improved from that calculated here with application of overnight physical adsorption or the biotin-avidin immobilisation procedure as it was reported in Chapter 5, Section 5.3.2, that both of these methods yielded a higher immobilised phage density than silane and glutaraldehyde coupling.

6.2   Post-Fabrication Sensor Analysis

It was important to verify that functioning sensors had been produced by the photolithography procedure (see Chapter 4, Section 4.4, for details on the fabrication method). This was particularly important because dimensions of 2 μm (of which some of the sensors had electrode gap sizes – see Section 3.2.2) would be approaching the fabrication limits of the photolithography method used to make the sensors [Hutson, 2008]. Several approaches were used to check each sensor. In the following sections these tests will be described and the results of the sensor functionality testing will be reported and discussed.

6.2.1   Approaches for Evaluating Sensor Functionality

A basic but essential test for evaluating sensor functionality was to measure the resistance across the sensor's electrodes using a digital multimeter (Fluke, UK). Sensors should be an open circuit, indicating that there are no connections between the electrodes. If a resistance was measured, then a voltage (15 V) was applied across

the electrodes. This often provided enough energy to physically remove the connections between electrodes by burning through points of contact (voltages higher than 15 V were avoided as this occasionally damaged the sensor). If an open circuit was not recovered following this voltage application, it was unlikely that the sensors would be recovered at all, certainly not without risking permanent damage, and so the sensor was considered unusable and discarded.

The capacitance of all open circuit sensors was then measured using a capacitance meter (Global Specialties, USA). The accuracy of the capacitance meter was verified with capacitors of known values. Capacitance data was also obtained from sensor impedance measurements collected using the equipment set-up described in Chapter 4, Section 4.5, over the frequency range 100 Hz to 10 MHz with 10 000 sample points taken. A plot of impedance values against the period of the applied signal (the reciprocal of frequency) will yield a straight line for capacitive behaviour, as demonstrated in Figure 6.6 for a sensor with 3 µm wide electrodes and 4 µm gaps.
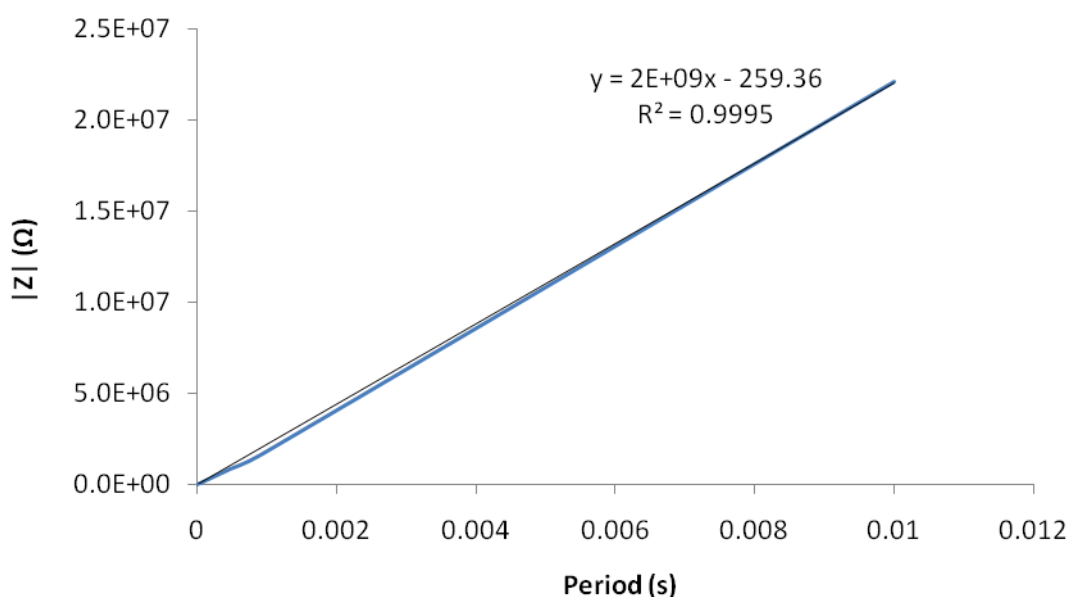
Figure 6.6. Typical plot of absolute impedance (|Z|) versus period for a sensor. A trendline is fitted to the plot in order to calculate the gradient (M) of the line. The equation of the trend line is displayed. The R^2 value indicates the closeness of the fitted trendline to the data with values approaching 1 indicating a good fit. The data was obtained from a sensor on glass with W = 3 µm and G = 4 µm.

A value of capacitance (C) can be estimated from the gradient of the straight line (M) from such a plot using the following relationship:

$$C = \frac{1}{2\pi M}$$

Sensors were also visually inspected using a standard light microscope (40× objective lens). This would provide verification of an open circuit sensor by checking for electrode connections and continuity.

6.2.2   Results and Discussion

Sensors were initially fabricated onto doped silicon wafers with a 0.3 µm silicon dioxide surface layer. Silicon wafers are widely available for use in photolithography fabrication procedures due to their applications in semiconductor technology. Whilst the semiconductor properties of the silicon wafer were not important for this particular application, silicon wafers were still considered suitable for use as a substrate for the biosensors provided that an insulating layer of silicon dioxide was present on the substrate surface. The use of silicon wafers in biosensor fabrication has been reported elsewhere [Gomez-Sjoberg et al., 2005, Radke and Alocilja, 2004, Van Gerwen et al., 1998]. Figure 6.7 shows a silicon wafer having gone through the photolithography procedure described in Chapter 4, Section 4.4.2.2, prior to wafer dicing. The 24 individual sensors can be seen. In Figure 6.8, a confocal microscope image (×40) of a section of a sensor (W = 3 µm and G = 4 µm) is presented illustrating the interdigitated electrode array. The tips of the electrode fingers of one electrode are shown in-between the electrode fingers of the second electrode. Further details on the sensor pattern and total dimensions can be found in Chapter 3, Section 3.2.2.
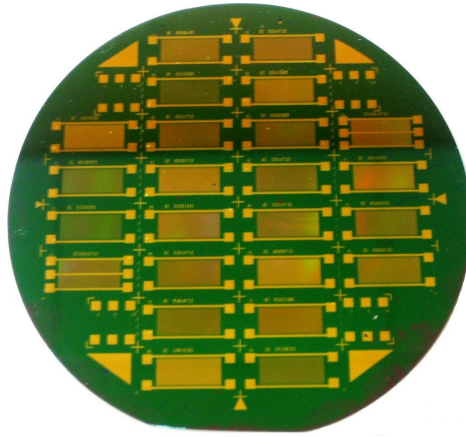
Figure 6.7. Sensor pattern on a silicon wafer after the sensor fabrication process as described in Chapter 4, Section 4.4, prior to wafer dicing.
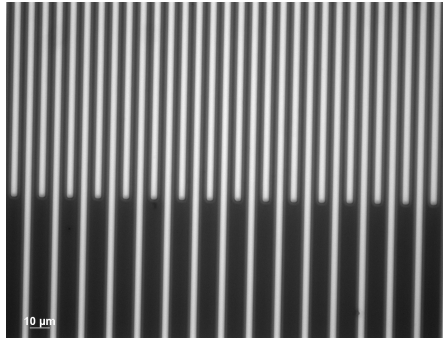
Figure 6.8. Confocal microscope image (×40) of a section of a sensor (W = 3 µm and G = 4 µm) illustrating the interdigitated electrode array. The tips of the electrode fingers of one electrode are shown, in-between the electrode fingers of the second electrode.

After fabrication, the functionality of each sensor was evaluated based on the results of the tests described in the previous section (Section 6.2.1). On average, 50% of the 24 sensors on each wafer were found to be open circuits, some requiring the voltage application to achieve this, as described previously. Of the wafers fabricated throughout the research, no sensor with a 2 µm electrode gap was successfully recovered, even after application of 15 V; the photolithography facilities utilised were obviously unable to successfully produce such small dimensions. Interestingly, problems were also encountered with sensors of larger electrode dimensions: sensors with 10 µm wide electrodes and a 4 µm gap were also not recovered but reasons for this are not as obvious. Sensors of all other dimensions (W = 3 µm, G = 4 µm;

205

W = 3 µm, G = 6 µm; W = 3 µm, G = 10 µm; W = 5 µm, G = 4 µm; W = 5 µm, G = 6 µm; W = 5 µm, G = 10 µm) were achievable however.

The requirement of a small voltage application in order to obtain an open circuit for several sensors did highlight some problems with the fabrication procedure. Microscopic inspections of sensors which were not open circuits revealed that electrode fingers were indeed connecting, as illustrated in Figure 6.9. This is likely to be a result of electrode delamination occurring during either the lift off stage of the photolithography procedure or the removal of the protective photoresist layer after wafer dicing. The delaminated electrode fingers are then crossing fixed electrodes and short circuiting the sensor. After the first attempt at sensor fabrication, all subsequent wafers were cleaned with a plasma etcher (in addition to the cleaning process outlined in Chapter 4, Section 4.4.2.2) to further improve chromium and therefore gold adhesion.
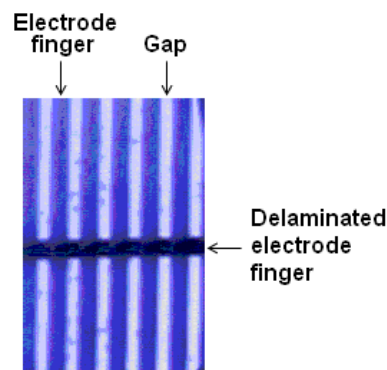
Figure 6.9. Image of a delaminated electrode finger crossing fixed electrode fingers. A standard light microscope was used with attached camera (40× objective lens).

Average capacitance values measured from open circuit sensors are displayed in Table 6.1. Values were obtained through the direct use of a capacitance meter and were also computed from impedance data as described in Section 6.2.1. It can be seen that the results from the two different approaches to measuring capacitance compared reasonably well: generally results were within 10% of each other and the same trends were observed.

Table 6.1. Capacitance of sensors with varying electrode width (W) and gap (G) combinations on a silicon substrate with a 0.3 μm silicon dioxide layer as measured by a capacitance meter. The number of pairs of electrode fingers is represented by N_P. Standard deviations on the measurements are included where possible but note that the number of each sensor recovered varied and therefore the sample size for each averaged measurement also varied. Capacitance values obtained from impedance data is also included. Analytical values obtained from two different sources are reported for comparison [Kidner et al., 2006, Olthuis et al., 1995].

W (μm)	G (μm)	N_P	Measured capacitance (pF)		Analytical Capacitance (pF)	
			Capacitance Meter	Impedance analyser	Olthuis et al. (1995)	Kinder et al. (2006)
3	4	715	1037 ± 71	1046	297	295
	6	555	895 ± 78	998	200	197
	10	385	760 ± 34	784	116	116
5	4	555	1110 ± 184	1074	277	279
	6	455	1020	1011	196	196
	10	355	855 ± 19	971	128	126

Measured capacitance values were compared to those calculated from published analytical formulae, also presented in Table 6.1. The analytical expression presented by Olthuis et al. (1995) was previously discussed in Chapter 3 where it was used to validate the ELECTRO model consisting of only one electrode pair. Olthuis et al. (1995) also presented an adapted expression which is applicable for the case of multiple electrode pairs and this was used to obtain the values listed in Table 6.1. Comparing the measured and analytical capacitance values it can be seen that measured values are consistently larger.

It should be pointed out that the expression developed by Olthuis et al (1995) was for the upper electrode space only and so capacitance was multiplied by a factor of two to include the lower electrode space, i.e. capacitance due to the substrate, and an average permittivity value was used. For simplicity, the polymer layer was ignored and the average permittivity was based on air ($\varepsilon_r \approx 1$) and the substrate material (for silicon, $\varepsilon_r \approx 12$). The analytical value, therefore, would be a slight underestimation (by approximately 7 fF based on an estimation using Equation 2.5) by not considering the presence of the polymer ($\varepsilon_r \approx 4$). Alternatively, the other extreme

could be considered by basing the average permittivity on that for the substrate and polymer layer, providing a maximum possible analytical capacitance value. However, this only raised analytical capacitance by a small factor (approximately 23%) and was still considerably smaller than the corresponding measured value.

To add confidence to the analytical results obtained from Olthuis et al. (1995), capacitance values from a second analytical expression were calculated and are also included in Table 6.1 [Kidner et al., 2006]. Kinder et al. (2006) used a different approach to obtain an analytical formula for the capacitance of an interdigitated electrode array: a fifth order polynomial expression was fitted to data generated from a finite-difference simulation whilst Olthuis et al. (1995) used conformal mapping. However, the two different approaches yielded almost identical capacitance values (both obtained based on the simplification that the polymer layer is not present). This helps to verify the discrepancy between measured and analytical values. This discrepancy is further substantiated by the fact that the two validated, independent sources for measured capacitance (the capacitance meter and impedance analyser) are so close. Overall, the results suggested that the measured values were unexpectedly high.

The high capacitance values warranted investigation and it was concluded that stray capacitance via the substrate was a likely explanation. This conclusion was reached after considering the structure of the sensor: gold electrodes are deposited on top of a thin silicon dioxide layer grown over the surface of a doped silicon wafer. It was initially assumed that the silicon dioxide layer would be thick enough to prevent any conductance below the electrodes. However, the silicon dioxide layer for this particular wafer was very thin (only $0.3 \, \mu m$) and therefore, although doped silicon is less conductive than gold, its nominal conductivity (between $0.1 – 1$ S/m [Virginia Semiconductor, 2009]) may be enough to cause stray capacitance to develop across the silicon dioxide layer. The situation is illustrated in Figure 6.10. In support of this theory, Van Gerwin et al. (1999) demonstrated that if the oxide thickness is greater than the characteristic length of the electrodes (the sum of the electrode width and gap) then stray capacitance across the oxide layer is negligible. However, this is not

the case for any of the sensors fabricated here indicating that stray capacitance can not be ignored. It should be noted that in this work, the term 'stray' capacitance is used to define the capacitance developed across the silicon dioxide layer of the substrate. The term is also used outside of this work to define other undesirable capacitive effects arising from situations such as the fringing effects at end electrodes or between wires of electronic components for example.
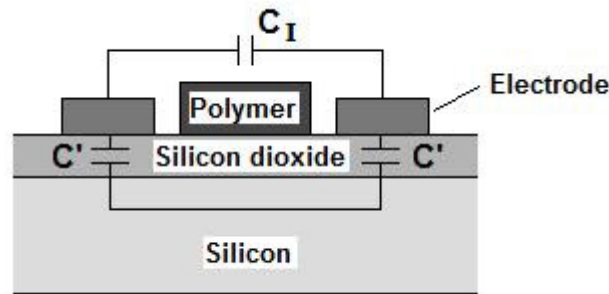
Figure 6.10. Schematic diagram of the sensor illustrating the interdigital capacitance (C_I) and also the stray capacitance (C') between the electrodes and doped silicon. Note that here C_I represents capacitance from both the upper and lower half planes.

If it is assumed that the silicon wafer is a good conductor with negligible resistance, a value for stray capacitance can be approximated by using the parallel-plate expression for capacitance as was first defined in Chapter 2 (Equation 2.5):

$$C_S = \frac{\varepsilon_r \varepsilon_0 A}{D} = \frac{\varepsilon_r \varepsilon_0 N_P L W}{2D} \qquad \textit{Equation 6.2}$$

where A is the surface area of the electrode (calculated by multiplying the electrode finger length, L, by the electrode width, W), N_P is the number of electrode pairs and D is the distance between the two conductors i.e. the thickness of the silicon dioxide layer. For a sensor with 3 μm wide electrodes and 715 electrode pairs, an approximate value for stray capacitance was calculated to be 506 pF. When this value is added to the theoretical interdigital sensor capacitance obtained from the analytical expressions (see Figure 6.10), total sensor capacitance begins to approach that of the measured value: 803 pF versus 1046 pF respectively. Some discrepancy was always likely between the analytical and measured capacitance values. For instance, the analytic expression will not take into account of any fringing effects

occurring at the edge of the outer sensor electrodes or the effects due to the presence of the main electrode track which connects the electrode fingers. Considering this, the analysis suggests that stray capacitance is a plausible explanation for the unexpectedly high measured capacitance values. It was considered possible that this stray capacitance may adversely affect the sensitivity of the sensor by masking changes in capacitance caused by the presence of bacteria.

To eliminate stray capacitance it was proposed to fabricate sensors onto a glass wafer since glass is non-conductive. A simple experiment was devised to confirm the elimination of stray capacitance. In the experiment, conductive paint was used to create two contact points (approximately 5 mm in diameter) on samples of the original silicon wafer and on a glass microscope slide. Capacitance was then measured from the contact points using the capacitance meter. As expected, it was found that a capacitance value could be measured from the silicon wafer (in the region of 100 pF) whilst zero capacitance was detected from the glass substrate. This confirmed the elimination of stray capacitance. It was therefore decided to fabricate the sensors onto a borosilicate glass wafer ($\varepsilon_r = 4.6$) sourced from IDB Technologies Ltd, UK (details in Chapter 4, Section 4.1.5).

Capacitance measurements were repeated for sensors fabricated on the glass wafer and results are reported in Table 6.2. Analytical capacitance values were re-calculated for the glass substrate using the expression described by Olthuis et al. (1995) and are included in Table 6.2 along with the measured and analytical results for the silicon substrate for comparison.

Table 6.2. Capacitance values of sensors with varying electrode width (W) and gap (G) combinations fabricated onto a glass wafer. The number of pairs of electrode fingers (N_P) for each sensor design is also included. Capacitance was measured using a capacitance meter. Analytical capacitance values for sensors were calculated from the formulae developed by Olthuis et al. (1995). Results from sensors on the silicon substrate (previously reported in Table 6.1) are also included for comparison.

W (μm)	G (μm)	N_P	Glass Substrate		Silicon Substrate	
			Measured capacitance (pF)	Analytical capacitance (pF)	Measured capacitance (pF)	Analytical capacitance (pF)
3	4	715	211	128	1037	297
	6	555	133	86	895	200
	10	385	70	50	760	116
5	4	555	214	119	1110	277
	6	455	142	84	1020	196
	10	355	70	55	855	128

As anticipated from the simple experiment carried out beforehand, Table 6.2 demonstrates that measured sensor capacitance values were reduced by fabricating the sensors onto glass and values are now much closer to predicted values (again, note that the sensor's polymer layer was ignored in calculating analytical capacitance resulting in a slight underestimation of the analytical value). The effects of stray capacitance appear to have been largely eliminated by utilising a glass substrate. The discrepancy between measured and analytical values is most likely to be due to unaccounted fringing effects and the main electrode tracks (on average analytical capacitance is 35% less than the measured value for equivalent sensors).

An interesting observation from the results of Table 6.2 was that analytical capacitance values appeared to decrease with increasing electrode widths for smaller electrode gaps. This is at odds to the measured results and basic capacitor behaviour for which capacitance generally increases with increasing electrode area (see Equation 6.2). This discrepancy could be due to reduced accuracy of the analytical equations at these smaller dimensions and their inability to account for any fringing effects.

Encouragingly, it was noticed that the capacitance measured from the double electrode array sensors (described in Chapter 3, Section 3.2.2), which are half the length of the sensors of Table 6.2 (i.e. 2 mm), had a capacitance equal to approximately half of that for the sensors with electrodes twice as long but with the same width and gap dimensions. This is consistent with expected behaviour.

The possibility of stray capacitance for sensors fabricated onto silicon wafers and its potential side effects have not been widely acknowledged in literature reporting on such sensors used for impedimetric measurements. For example, Radke and Alocilja (2004) fabricated sensors onto a silicon wafer with a 2 μm thick silicon dioxide layer. This silicon dioxide layer is thicker than that utilised here and may have sufficiently minimised stray capacitance but the thickness was not greater than the characteristic length (7 μm) as recommended by Van Gerwin et al (1999). However, Radke and Alocilja (2004) do not report the resistivity of the wafers used and if this is sufficiently high then this will also reduce the likelihood of stray capacitance.

It is also worth mentioning that predicted capacitance values could be computed from the ELECTRO modelling work. The half-wavelength computer model described in Chapter 3 was used to calculate a normalised capacitance (F/m^2) for each sensor design. An estimated sensor capacitance can be calculated by multiply the normalised capacitance by the appropriate electrode surface area. Results for sensors on a glass substrate are presented in Table 6.3. It can be seen that computed capacitance values are less than both the analytical estimation and measured values of capacitance presented in Table 6.2. A possible reason for this discrepancy could be that the results for the half-wavelength model can not be reliably scaled up to represent the full sensor; this aspect of the model was not investigated. However, the results are not overly concerning for the ELECTRO modelling work presented in Chapter 3 as absolute values of capacitance were not the focus of the investigation. Instead, general trends and the change in capacitance were under investigation to indicate sensor response and sensitivity.

Table 6.3. Sensor capacitance estimated from the ELECTRO model, described in Chapter 3, for varying electrode width (W), gap (G) and number of electrode pairs (N_P).

W (μm)	G (μm)	N_P	Sensor Capacitance (pF)
3	4	715	47
	6	555	32
	10	385	18
5	4	555	44
	6	455	31
	10	355	20

6.3   Summary of Preliminary Sensor Evaluation

Preliminary testing showed that immobilised bacteriophage 9563 significantly increased levels of *S. aureus* 8588 on the surface of a substrate. The performance of immobilised bacteriophage 9563 was found to be comparable to that of immobilised antibodies but in terms of biosensor application, phages have several practical advantages over antibodies (refer to Chapter 1, Section 1.4.5).

Post-fabrication testing of the sensors revealed unexpectedly high capacitance measurements which were attributed to significant stray capacitance across the silicon dioxide layer (between the gold electrodes and doped silicon wafer). The main concern was that this stray capacitance could affect the sensitivity of the sensor for detecting bacteria. Therefore, to eliminate this issue, sensors were fabricated onto glass wafers and it was confirmed that the resulting sensor capacitance values were more in line with those expected.

PART II

6.4 Biosensor Testing for the Detection of Bacteria

In Part I, the preliminary experiments confirmed the ability of immobilised phages to act as recognition elements for bacteria and it was ensured that fabricated sensors were functioning as expected. The next stage was to combine the bioreceptor and transducer components and to investigate the resulting impedimetric biosensor for the detection of bacteria. The results of this investigation are presented and discussed in the following sections.

6.4.1 Method

The protocols for phage immobilisation, sample preparation and sensor testing can be found in Chapter 4. The reasoning behind some of the steps in these protocols will now be discussed. Note that in the following sections, sensors with immobilised phages are termed 'activated' sensors.

Initially phages were immobilised onto sensors by physical adsorption as it was found that this method was not detrimental to the sensor and yielded one of the highest phage immobilisation densities out of the immobilisation methods investigated (see Chapter 5, Section 5.3.2). At a later stage in the study, the biotin-avidin approach was developed and was found to yield improved immobilisation densities. The biotin-avidin method was therefore also investigated with sensors. All sensor surfaces, including control sensors, were blocked with BSA before measurements. This step was carried out to reduce non-specific adsorption.

To remove debris and metabolic by-products from the cell suspension after overnight growth, bacterial cells were washed three times and were initially re-suspended in fresh 0.1% PW. It was considered important to remove the ionic species produced during bacterial growth to eliminate their effects on electrical measurements and to try and maintain a consistent suspending solution. PW (0.1%) had previously been used to re-suspend bacterial cells for impedance measurements [Radke and Alocilja,

2004]. Later, different suspending solutions (0.1% PBS and 0.1 M mannitol) were also investigated for reasons which will be addressed in subsequent sections.

It was initially decided to record impedance measurements over time (Testing Method 1). The intention was to correlate any changes in impedance to the microscopy results observed in Section 6.1 where it was shown that immobilised phages will continuously increase levels of bacteria on a substrate over at least a 20 minute period. In determining the sampling approach, the results of Section 6.1 highlighted the transient nature of the interactions occurring at the substrate surface, indicating that measurements at each time interval should be carried out quickly. On the other hand, it was desirable to cover a wide frequency range, but a large number of data points would involve a long sampling period over which duration surface interactions with bacteria could change significantly. It was therefore decided to restrict measurements to six data points over the frequency range 100 Hz to 10 MHz for initial measurements i.e. one measurement per logarithmic decade. This compromise meant that measurements at each time interval would be carried out quickly and well within the 5 minutes sampling interval, yet a large frequency range would be covered.

In later experiments the testing method was altered such that impedance measurements were recorded before and after the sensor was exposed to a bacterial suspension (Testing Method 2).

6.4.2 Results

6.4.2.1 Control Measurements

Before testing sensors with bacterial suspensions, an indication of sensor reproducibility was established by comparing impedance measurements taken from three different sensors of the same electrode topology (W = 3 µm and G = 4 µm) in air. Results are displayed in Figure 6.11. It can be seen that absolute impedance is similar for all three sensors. The average relative standard deviation was determined to be 3.3% i.e. the absolute impedance of sensors with the same electrode topology was calculated to be within 3.3% of each other. This result is also consistent with

data collected from two sensors with 5 µm wide electrodes and 6 µm gaps for which an average range of 1.9% between sensor impedance was calculated.
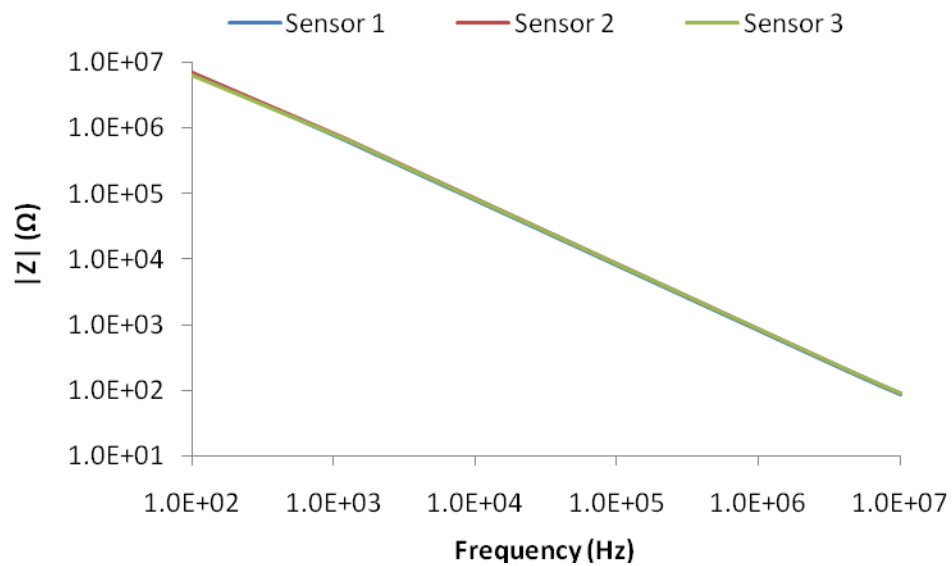
Figure 6.11. Comparison of three sensors of the same electrode topology (W = 3 µm and G = 4 µm). Absolute impedance (|Z|) is plotted against frequency. Measurements were taken in air and 10 000 sample points were taken across the frequency range (100 Hz to 10 MHz).

It was also important to establish the stability of the sensor over time so that any changes observed in data collected from an activated sensor in a suspension of bacteria could be directly attributed to the bioreceptor effect of the phages. Therefore, impedance measurements were recorded from a sensor (W = 3 µm and G = 4 µm) without immobilised phages in 0.1% PW to establish the background signal. It was found that at each frequency, there was a small consistent decrease in absolute impedance over the 60 minute period. This is illustrated in Figure 6.12 for measurements at 1 kHz which is typical of other frequencies.

216
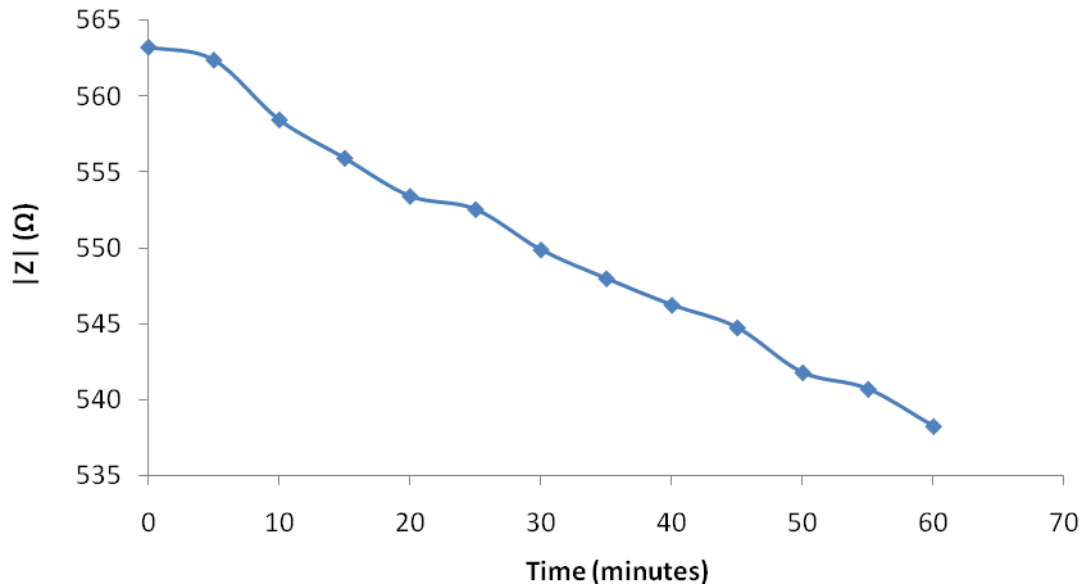
Figure 6.12. Absolute impedance (|Z|) over time at 1 kHz measured by an untreated control sensor (W = 3 µm and G = 4 µm) in 0.1% PW.

Figure 6.13 displays absolute impedance over the frequency range at 0, 30 and 60 minutes. This illustrates the decrease in absolute impedance over the 60 minute measuring period at each frequency. Changes appear to be most evident at higher frequencies. Figure 6.13 also clearly indicates that absolute impedance generally decreases with increasing frequency before reaching a plateau at high frequencies.
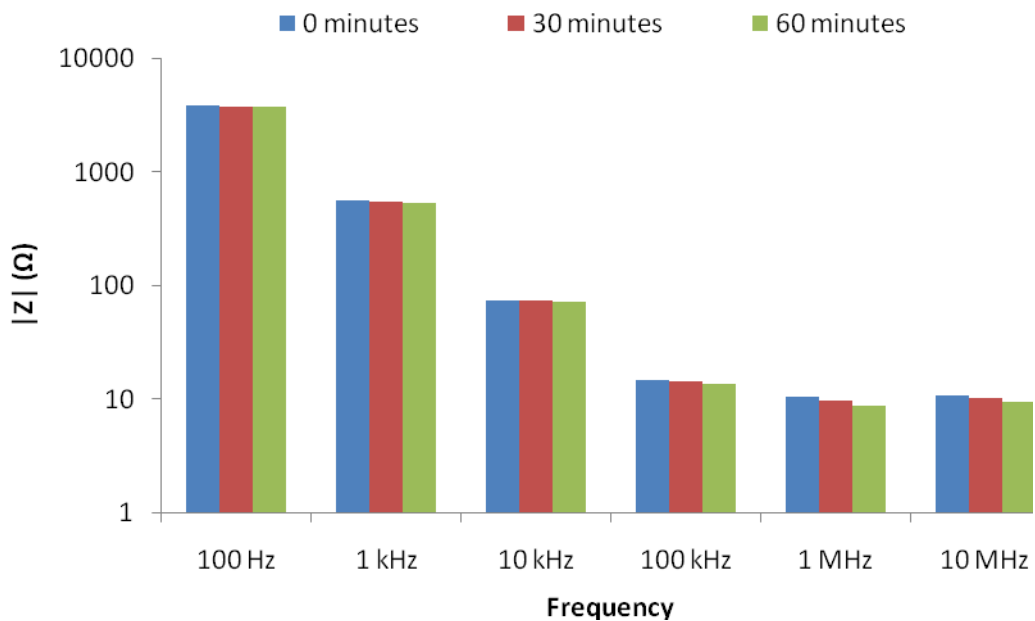
Figure 6.13. Absolute impedance (|Z|) of 0.1% PW measured by an untreated control sensor (W = 3 µm and G = 4 µm) at isolated frequencies after 0, 30 and 60 minutes.

In Figure 6.14, phase angle is also plotted for 0, 30 and 60 minutes at each frequency. It can be seen that phase angle magnitude tends to increase over time and, in a similar trend to absolute impedance, phase angle appears to be more stable at lower frequencies as larger changes in phase angle are visible at higher frequencies. Over the increasing frequency range, phase angle decreases from high negative values towards 0° and becomes positive at 10 MHz.
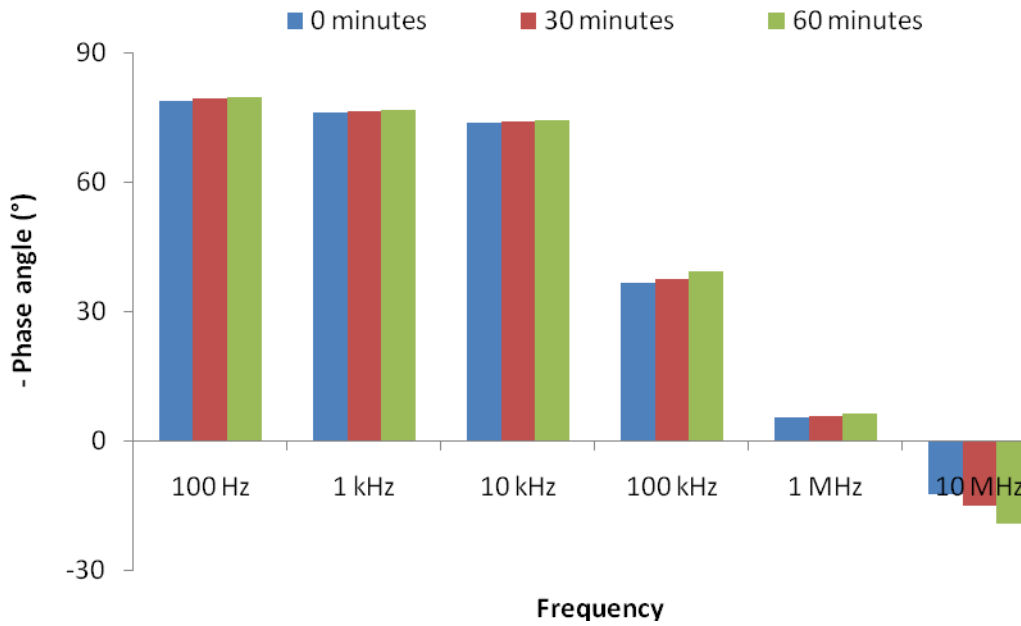
Figure 6.14. Phase angle measured by an untreated control sensor (W = 3 µm and G = 4 µm) in 0.1 % PW at isolated frequencies after 0, 30 and 60 minutes.

In this section, normalised impedance ($|Z_N|$) was defined as follows, where $|Z_t|$ is absolute impedance at time t and $|Z_0|$ is absolute impedance at t = 0:

$$|Z_N| = \frac{|Z_t|}{|Z_0|}$$
Equation 6.3

This normalised impedance was used to highlight the changes occurring overtime and at which frequencies they are most significant. Results are displayed in Figure 6.15. From the plot it can be seen that over 60 minutes, stability has still not been reached and that the maximum decrease consistently occurs at 1 MHz.
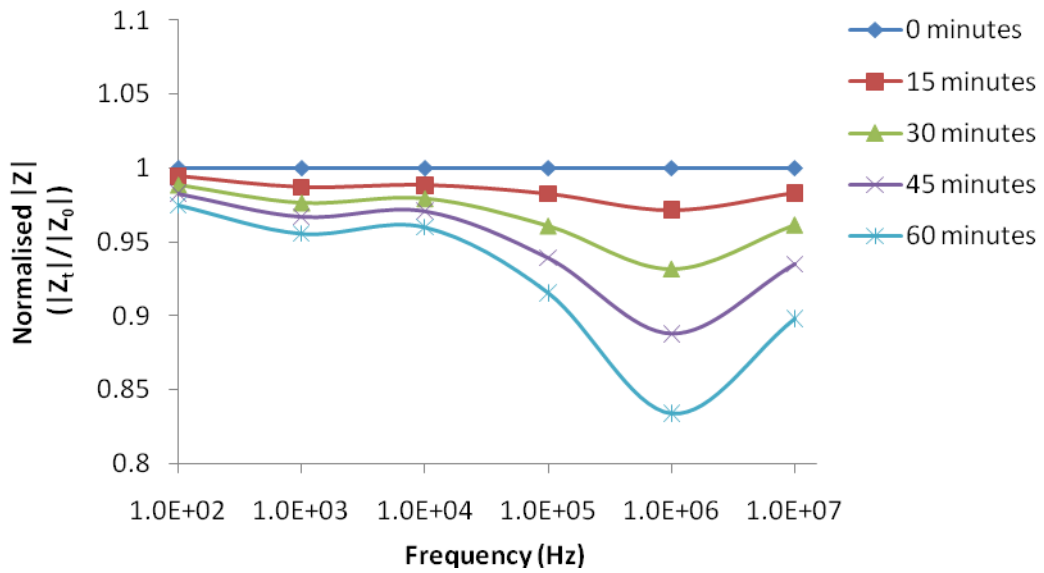
Figure 6.15. Variability of impedance measurements over time for 0.1% PW measured from an untreated control sensor. Absolute impedance at time t ($|Z_t|$) was normalised against impedance at 0 minutes ($|Z_0|$).

Figure 6.16 shows the Nyquist plot at 0 minutes and 60 minutes for the untreated sensor in 0.1% PW. The form of the Nyquist plot is similar at both times and is relatively linear in form with perhaps some evidence of a semicircle region at high frequencies.
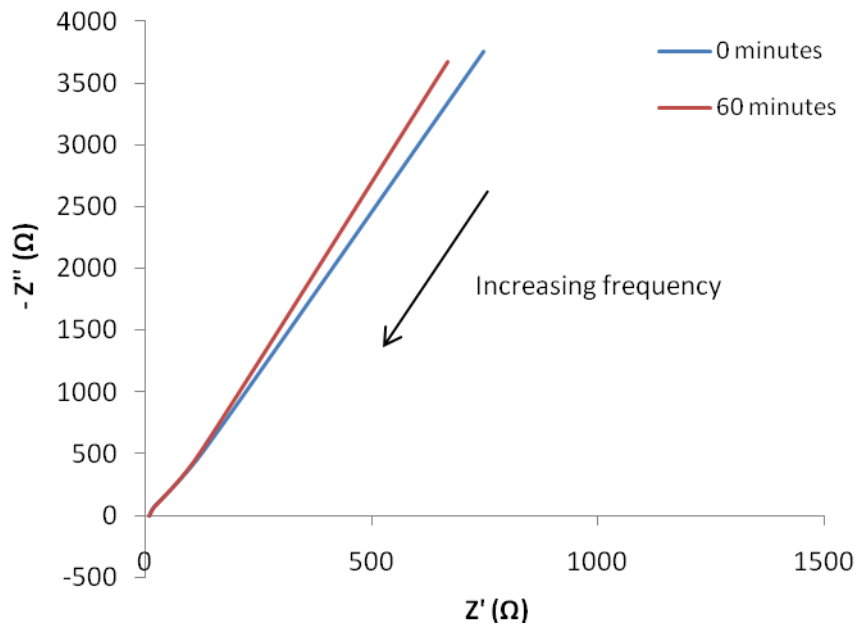
Figure 6.16. Nyquist plot for an untreated sensor (W = 3 µm and G = 4 µm) in 0.1% PW at 0 minutes and 60 minutes. The measuring frequency range was 100 Hz to 10 MHz (n = 1).

The impedance data at 0 minutes and 60 minutes for the control sensor in 0.1% PW are presented in Table 6.4.

Table 6.4. Impedance data for the control sensor (W = 3 µm and G = 4 µm) in 0.1% PW at 0 minutes and 60 minutes. Absolute impedance (|Z|), real impedance (Z') and imaginary impedance (Z'') data are presented for each measuring frequency.

Frequency (Hz)	0 minutes			60 minutes		
	|Z| (Ω)	Z' (Ω)	-Z'' (Ω)	|Z| (Ω)	Z' (Ω)	-Z'' (Ω)
10^2	3824.1	746.1	3750.7	3728.5	669.2	3668.0
10^3	563.2	134.6	546.9	538.3	124.0	523.8
10^4	74.7	21.1	71.7	71.7	19.5	69.0
10^5	14.9	12.0	8.9	13.7	10.5	8.7
10^6	10.5	10.5	1.0	8.8	8.7	1.0
10^7	10.7	10.4	-2.3	9.6	9.1	-3.2

6.4.2.2 Effect of Physically Adsorbed Bacteriophages on Sensor Impedance

Figure 6.17 shows the absolute impedance obtained from an activated sensor in a solution of 0.1% PW. Phages were immobilised by overnight physical adsorption in a phage suspension of estimated concentration 1.7×10^9 PFU/ml. Also included in Figure 6.17 is the impedance spectrum from an untreated control sensor. Measurements from both sensors were taken immediately after 0.1% PW application and both sensors were of the same electrode topology (W = 3 µm and G = 4 µm). The purpose of the plot is to illustrate the effect of the physically adsorbed phage layer on impedance. Based on the data, the immobilised phage layer appears to have caused a reduction in absolute impedance across the frequency range. Both sensors exhibit the same trend over the frequency range: absolute impedance decreases with increasing frequency until approximately 100 kHz where it begins to plateau.
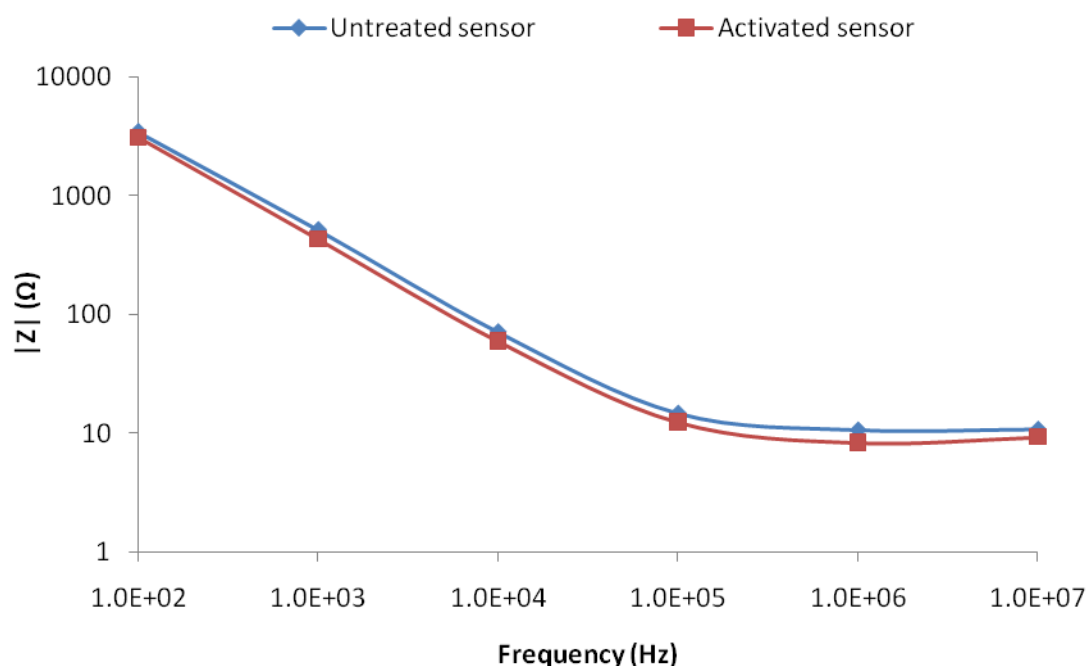
Figure 6.17. Effect of immobilised phage layer. Absolute impedance (|Z|) is plotted against frequency for an activated sensor and an untreated control sensor, both in 0.1% PW. Phages were immobilised by overnight physical adsorption in a phage suspension of approximately 1.7×10^9 PFU/ml. Both sensors were of the same electrode topology (W = 3 µm and G = 4 µm).

The absolute impedance values for the activated and untreated control sensor at each frequency are displayed in Table 6.5. Percentage differences between impedance measurements from the activated and control sensor are presented and were greater than the reproducibility error reported in Section 6.4.2.1 (3.3%). This suggests that the reduction in absolute impedance due to the phage layer is significant.

221

Table 6.5. Absolute impedance values (|Z|) for a control sensor (no immobilised phages) and an activated sensor (overnight physical adsorption) in 0.1% PW. Both sensors were of the same electrode topology (W = 3 μm and G = 4 μm). The percentage difference between measurements with respect to the control sensor are also displayed (Δ%).

Frequency (Hz)	Absolute impedance, |Z|, (Ω)		Δ%
	Control sensor	Activated sensor	
10^2	3442.38	3104.16	-9.8
10^3	513.70	432.22	-15.9
10^4	70.79	59.84	-15.5
10^5	14.57	12.45	-14.6
10^6	10.52	8.34	-20.7
10^7	10.67	9.28	-12.9

Figure 6.18 demonstrates phase angle vairation with frequency for the activated and untreated control sensor in 0.1% PW. Phase angle variations for the activated sensor follows a similar trend to that of the untreated control sensor reported in Section 6.4.2.1 with small deviations appearing at the extremes of the frequency range (100 Hz and 10 MHz). This experiment was only performed once due to time constraints.
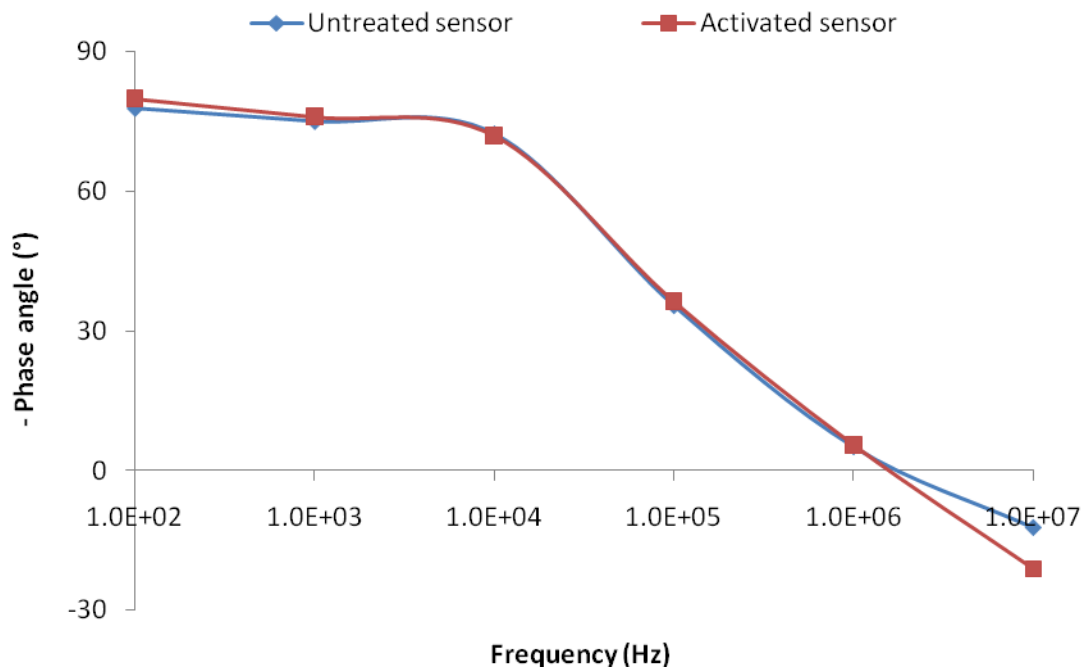
Figure 6.18. Phase angle (°) against frequency for an activated sensor and an untreated control sensor, both in 0.1% PW. Phages were immobilised by overnight physical adsorption in a phage suspension of approximately 1.7×10^9 PFU/ml. Both sensors were of the same electrode topology (W = 3 µm and G = 4 µm).

In Figure 6.19 the Nyquist plot for both the activated and untreated control sensor are presented. It can be seen that the impedance profile is close to a straight line for both the activated and control sensor with a slightly larger gradient for the activated sensor over low frequecies.
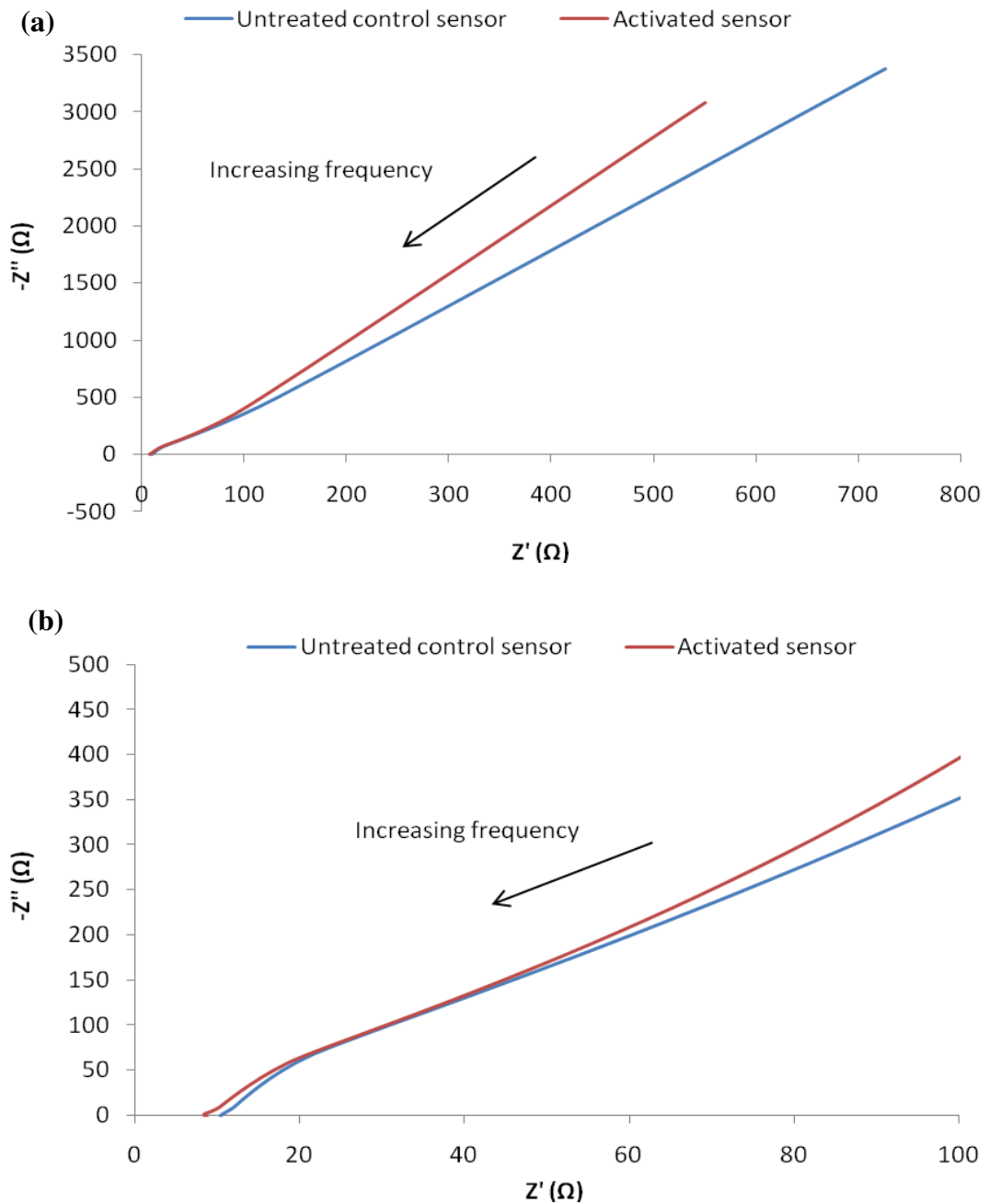
Figure 6.19. Nyquist plots for an untreated control sensor and an activated sensor in 0.1% PW. Phages were immobilised by overnight physical adsorption in a phage suspension of approximately 1.7×10^9 PFU/ml. Both sensors were of the same electrode topology (W = 3 μm and G = 4 μm). The measuring frequency range was 100 Hz to 10 MHz (n = 1). (b) Focused plot of (a) at high frequencies (10 kHz to 10 MHz).

The impedance data obtained from the untreated control sensor and the activated sensor in 0.1% PW are presented in Table 6.6.

Table 6.6. Impedance data for the untreated control sensor and activated sensor in 0.1% PW. Phages were immobilised by overnight physical adsorption. Both sensors were of the same electrode topology (W = 3 μm and G = 4 μm). Absolute impedance (|Z|), real impedance (Z') and imaginary impedance (Z'') data are presented for each measuring frequency.

Frequency (Hz)	Untreated control sensor			Activated sensor		
	$\|Z\|$ (Ω)	Z' (Ω)	-Z'' (Ω)	$\|Z\|$ (Ω)	Z' (Ω)	-Z'' (Ω)
10^2	3454.0	726.1	3376.8	313.8	550.8	3083.0
10^3	515.0	133.2	497.5	436.8	105.0	424.0
10^4	70.9	21.5	67.6	60.5	18.6	57.6
10^5	14.6	11.9	8.5	12.5	10.1	7.4
10^6	10.5	10.5	0.9	8.5	8.4	0.8
10^7	10.7	10.4	-2.3	9.4	8.8	-3.3

6.4.2.3   Detection of Bacteria – Testing Method 1

In this section, results are presented for Testing Method 1 (see Chapter 4, Section 4.5.3, for full protocol details) in which impedance measurements were recorded from an activated sensor over time. The sensor was activated by allowing overnight physical adsorption of phages onto the sensor surface. Bacteria were initially suspended in 0.1% PW. Parameters of the experiment are summarised in Table 6.7.

Table 6.7. Experimental parameters for Testing Method 1. Sensor electrode topology is displayed in terms of electrode width (W) and gap (G). For the activated sensor, phage were immobilised by overnight (O/N) physical adsorption in a suspension of phages (concentration estimated from two dilutions, each plated three times). The control sensor was not exposed to phages. Bacteria were suspended in 0.1% PW and the bacterial concentrations listed were that at the start of the experiment (t = 0 minutes). Mean concentrations are presented ± standard deviations (n = 6).

Sensor	Sensor topology (W / G μm)	Phage immobilisation method	Phage concentration (PFU/ml)	Bacteria concentration (Log_{10} CFU/ml)
Activated	3 / 4	O/N physical adsorption	1.7×10^9	8.90 ± 0.01
Control	3 / 4	N/A	N/A	8.85 ± 0.14

6.4.2.3.1 Time Dependent Impedance Changes

Figure 6.20 shows absolute impedance variation over time at 1 kHz for the activated sensor in the bacterial suspension. Also included are impedance measurements from an untreated control sensor in a bacterial suspension and a blank solution. The bacterial suspensions used with the activated and control sensors were of similar concentrations (see Table 6.7). The data demonstrates that at 1 kHz there was a slight increase in absolute impedance measured from the activated sensor in the bacterial suspension over the first 15 minutes before impedance began to decrease over time. A smaller and shorter increase was observed for the control sensor in the bacterial suspension whilst only a consistent decrease in impedance was recorded from the control sensor in the blank suspension. It was observed that the impedance of the bacterial suspension measured by the activated sensor was less than that measured by the control sensor. This could be related to the results presented in Section 6.4.2.2 where it was observed that the presence of immobilised phages led to a reduction in sensor impedance. Also, comparing the results from the control sensors with and without bacteria it is interesting to note that the presence of bacteria in 0.1% PW has led to an overall reduction in absolute impedance. This will be discussed further in Section 6.4.3.3. The trend of the results presented in Figure 6.20 was typical for low frequency measurements ($\leq$ 10 kHz).
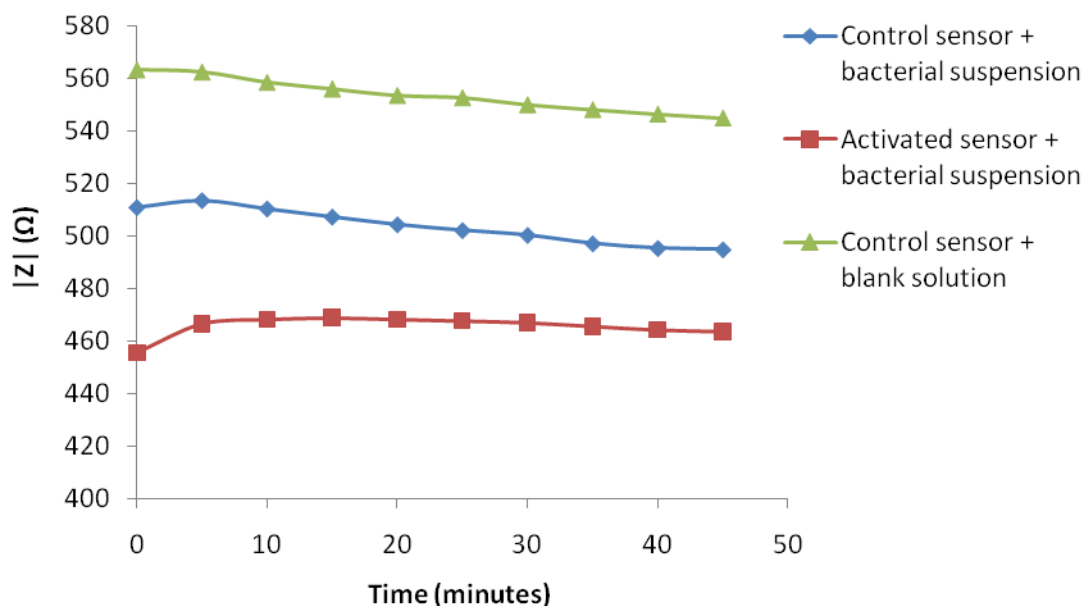
Figure 6.20. Absolute impedance (|Z|) over time measured from an activated sensor with physically adsorbed phages at 1 kHz in a bacterial suspension (8.90 ± 0.01 Log$_{10}$ CFU/ml in 0.1% PW). Results are also included for an untreated control sensor in a bacterial suspension (8.85 ± 0.14 Log$_{10}$ CFU/ml) and a blank solution (0.1% PW only).

In Figure 6.21, a corresponding plot of time dependent impedance measurements at 1 MHz is presented. A similar trend was observed at high frequencies: impedance initially increased over time followed by a consistent decrease. However, the increase in impedance was only over the first 5 minutes and at 1 MHz the control sensors' impedance in solutions with and without bacteria was more similar. The trend of the results presented in Figure 6.21 was typical for high frequency measurements ($\geq$ 100 kHz).
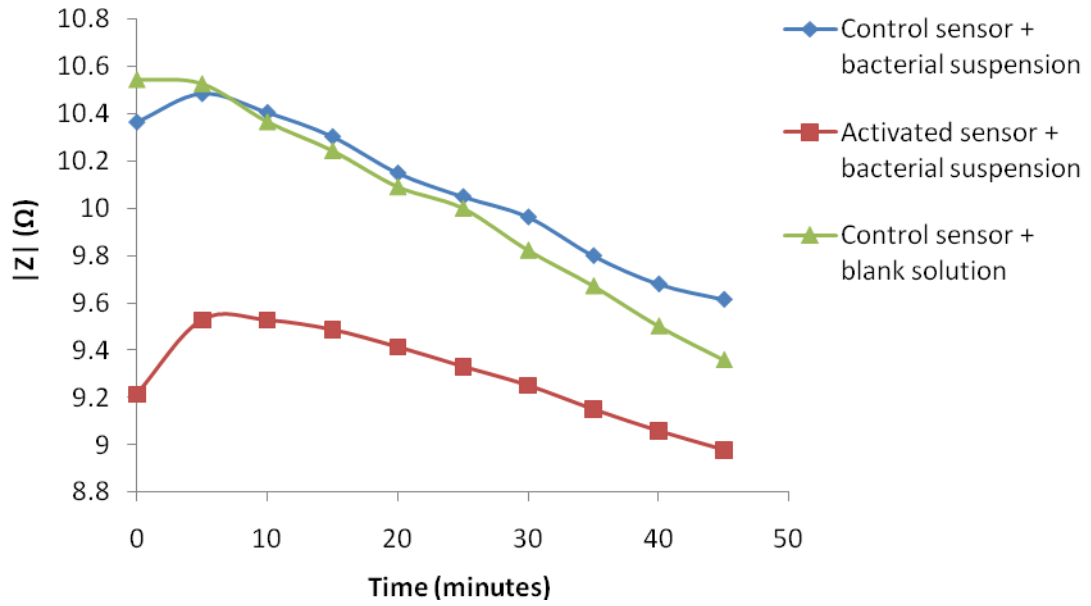
Figure 6.21. Absolute impedance (|Z|) over time measured from an activated sensor with physically adsorbed phages at 1 MHz in a bacterial suspension (8.90 ± 0.01 Log$_{10}$ CFU/ml in 0.1% PW). Results are also included for an untreated control sensor in a bacterial suspension (8.85 ± 0.14 Log$_{10}$ CFU/ml) and a blank solution (0.1% PW only).

The fact that all three sets of results eventually follow the same pattern of constant decreasing impedance suggests that some characteristic of the sensor may be dominating measurements and masking the effect of bacteria. To try and offset this, impedance measurements of bacterial suspensions from the activated and control sensor over time (|Z$_{Bacteria}$|) were normalised against the control sensor impedance measurements in 0.1% PW over time (|Z$_{Control}$|), as illustrated through the following equation:

$$\left|Z_N\right| = \frac{\left|Z_{Bacteria}\right|}{\left|Z_{Control}\right|}$$

Equation 6.4

The results for measurements at 1 kHz and 1 MHz are presented in Figure 6.22(a) and (b) respectively. At 1 kHz, normalised impedance measured from the control sensor is relatively constant over time whilst normalised impedance for the activated sensor increases, with the rate of increase reducing over time. At 1 MHz, normalised impedance increased for both the activated and control sensor in a bacterial suspension but a slightly faster rate of increase was observed for the activated sensor.

228
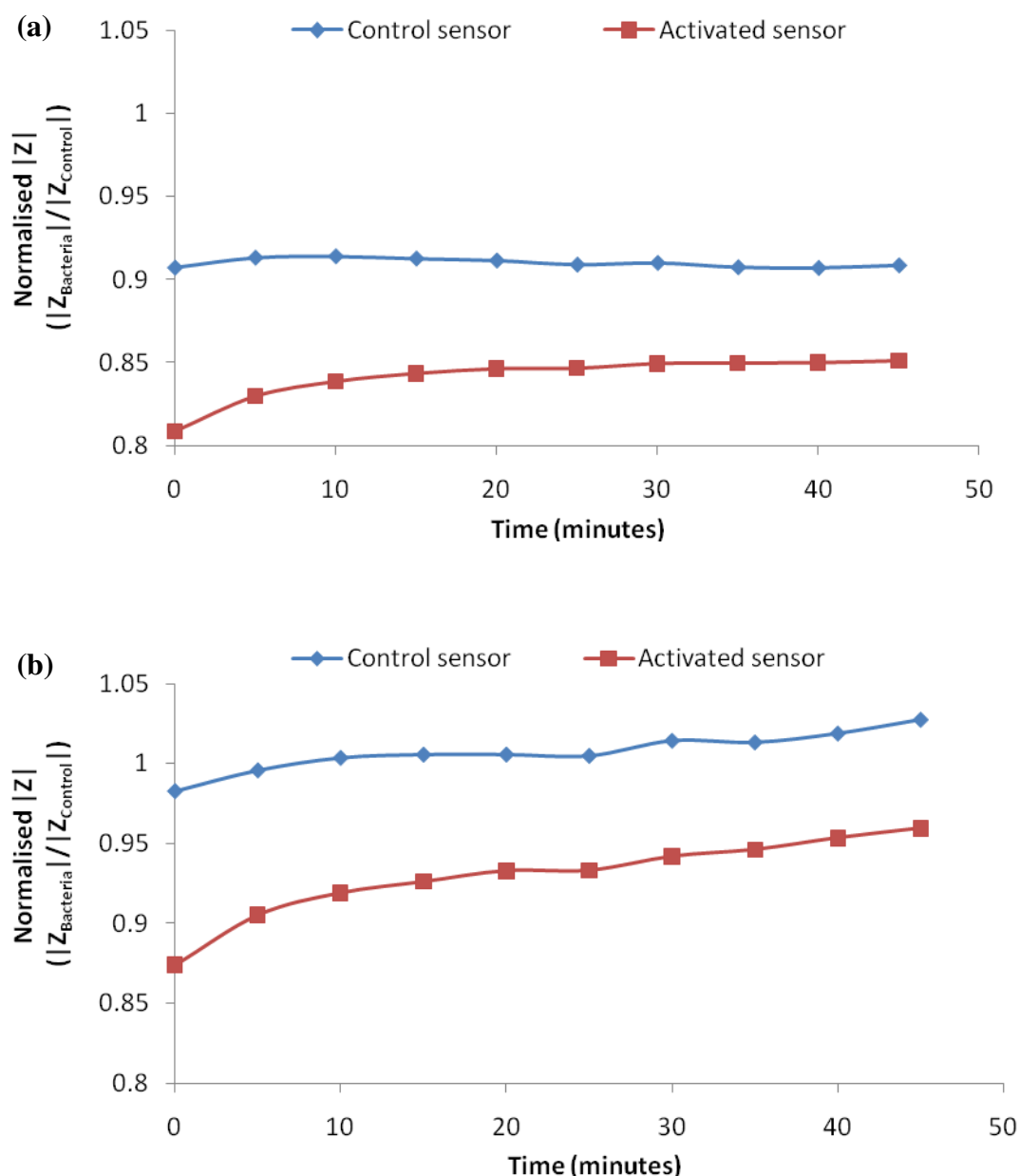
Figure 6.22. Normalised absolute impedance (normalised |Z|) variation with time at (a) 1 kHz and (b) 1 MHz for the activated and untreated control sensor in bacterial suspensions (8.90 ± 0.01 Log$_{10}$ CFU/ml and 8.85 ± 0.14 Log$_{10}$ CFU/ml respectively). Impedance values were normalised against corresponding impedance measured from an untreated sensor in 0.1% PW.

6.4.2.3.2 Frequency Spectra at Fixed Time Intervals

It is also of interest to examine the biosensor's response in the frequency domain. In this case, impedance measurements of the bacterial solution were compared to those obtained from the same biosensor with a blank solution. It should be noted that a

single measurement of the blank solution was made before application of the bacterial sample i.e. measurements were not recorded over time for the blank solution. Therefore, measurements of the bacterial suspension at each time interval are effectively being compared to blank solution measurements at t = 0 minutes.

Figure 6.23(a) shows the Bode plot of absolute impedance for the activated sensor in a suspension with and without bacteria. Impedance values for the bacterial suspension were those obtained at 15 minutes after which some of the largest changes in absolute impedance were observed (as indicated by Figure 6.20 and Figure 6.21). Figure 6.23(a) demonstrates an increase in absolute impedance due to bacteria over this frequency range. The Bode plot also demonstrates that absolute impedance decreases with increasing frequency until approximately 100 kHz at which point impedance plateaus and remains relatively constant with further increases in frequency. This was the case for measurements with both the blank and bacterial suspension.

In Figure 6.23(b) phase angle measured from the activated sensor is compared for the blank solution and bacterial suspension after 15 minutes. As with the Bode plot of absolute impedance, phase angle variations with frequency are similar for the two solutions: phase angle is close to -90° at low frequencies, decreasing towards 0° between 10 kHz and 1 MHz and then turns positive at 10 MHz. The largest difference between the bacterial suspension and the blank is observed at 10 MHz. Absolute impedance and phase angle data points, as presented in Figure 6.23, are list in Table 6.8.

(a)

(b)
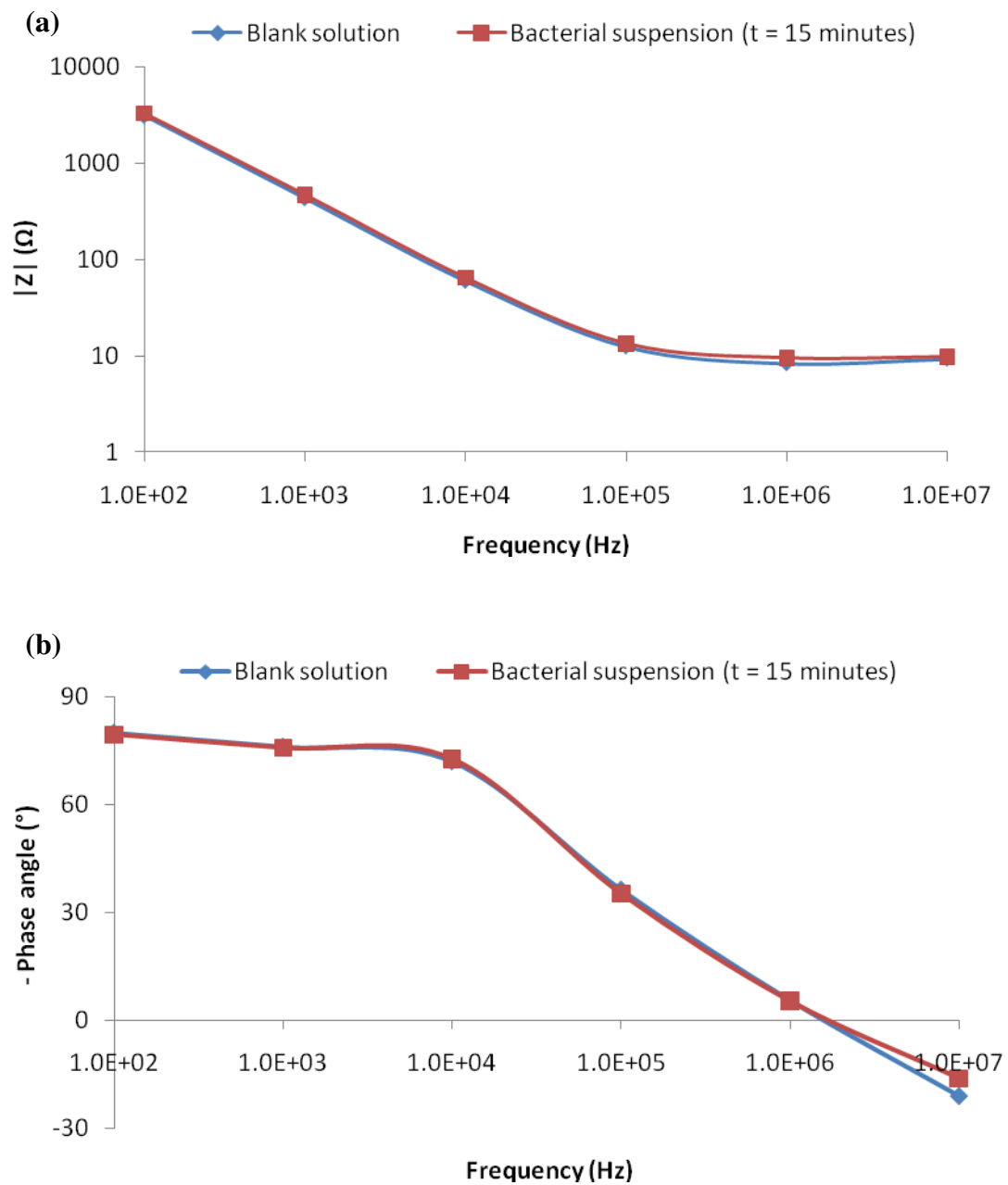
Figure 6.23. Effect of bacteria on the activated sensor. (a) Absolute impedance (|Z|) Bode plot and (b) phase angle Bode plot of a blank solution and the bacterial suspension (8.90 ± 0.01 Log$_{10}$ CFU/ml) measured from the activated sensor (phages were immobilised by overnight physical adsorption). Impedance values of the bacterial suspension are reported for 15 minutes after suspension application.

Table 6.8. Impedance (|Z|) and phase angle data (φ) measured from the activated sensor in 0.1% PW and a bacterial suspension (8.90 ± 0.01 Log_{10} CFU/ml). Phages were immobilised onto the sensor by overnight physical adsorption. Data for the bacterial suspension are reported for 15 minutes after suspension application.

Frequency (Hz)	Blank solution		Bacterial suspension	
	|Z| (Ω)	-φ (°)	|Z| (Ω)	-φ (°)
10^2	3104.2	80.0	3290.7	79.4
10^3	432.2	76.1	468.8	75.7
10^4	59.8	72.0	64.4	72.6
10^5	12.4	36.4	13.4	35.1
10^6	8.3	5.5	9.5	5.3
10^7	9.3	-21.1	9.8	-16.2

Figure 6.24 shows corresponding Bode plots for the untreated control sensor with and without bacteria. Trends for the control sensor are similar to those observed for the activated sensor in Figure 6.23. However, the difference between the solutions is generally smaller than was observed for the activated sensor. This is also demonstrated in Table 6.9 which reports the plotted data of Figure 6.24.
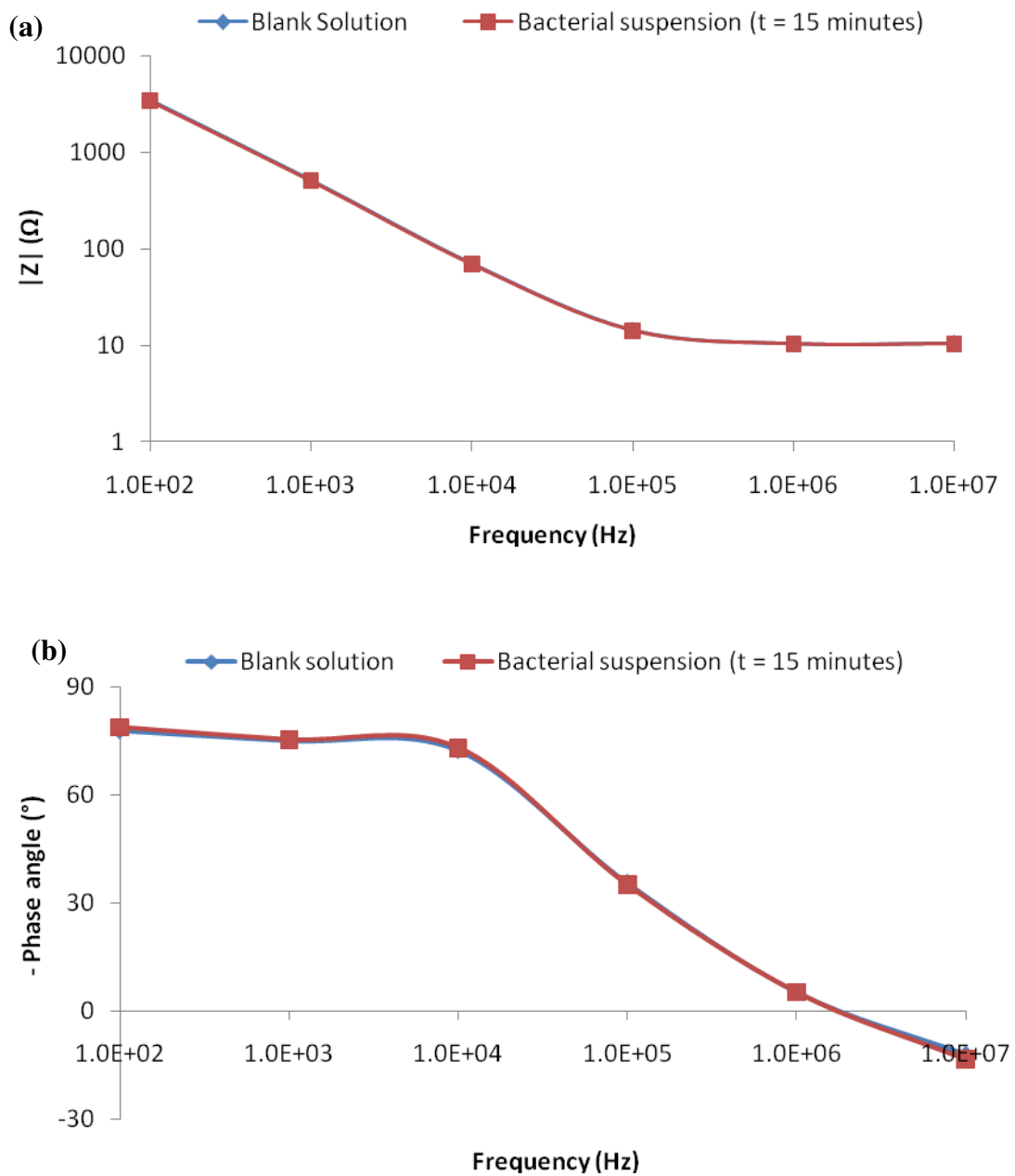
Figure 6.24. Effect of bacteria on the control sensor. (a) Absolute impedance (|Z|) Bode plot and (b) phase angle Bode plot of a blank solution and the bacterial suspension (8.85 ± 0.14 Log_{10} CFU/ml) measured from the untreated control sensor. Impedance values of the bacterial suspension are reported for 15 minutes after suspension application.

Table 6.9. Impedance (|Z|) and phase angle data (φ) measured from the control sensor in 0.1% PW and a bacterial suspension (8.85 ± 0.14 Log$_{10}$ CFU/ml). Data for the bacterial suspension are reported for 15 minutes after suspension application.

Frequency (Hz)	Blank solution		Bacterial suspension	
	|Z| (Ω)	- φ (°)	|Z| (Ω)	- φ (°)
10^2	3442.4	77.8	3430.3	78.6
10^3	513.7	75.9	507.3	75.2
10^4	70.8	72.3	69.1	73.0
10^5	14.6	35.4	14.2	35.0
10^6	10.5	5.1	10.3	5.2
10^7	10.7	-12.2	10.4	-13.4

To further illustrate the differences between solutions with and without bacteria, absolute impedance of the bacterial suspension at a particular time ($|Z_{Bacteria}|$) was normalised against absolute impedance of the control solution measurement ($|Z_{No\ bacteria}|$) taken from the same sensor, as demonstrated through the following equation for normalised impedance ($|Z_N|$):

$$|Z_N| = \frac{|Z_{Bacteria}|}{|Z_{Nobactera}|}$$

Equation 6.5

This was done for both the activated and untreated control sensor. The results obtained from the data of Figure 6.23 and Figure 6.24 (data points are listed in Table 6.8 and Table 6.9 respectively) are presented in Figure 6.25. Note that the normalised impedance quoted here differs from that of Equation 6.4 in Section 6.4.2.3.1. In Section 6.4.2.3.1, impedance of the bacterial suspensions was normalised against blank solution measurements taken from an untreated control sensor at corresponding times in order to eliminate time dependent changes related to the sensor. Here, impedance of the bacterial suspension is normalised against blank solution measurements taken from the same activated sensor at $t = 0$ in order to observe the effect of bacteria. Values for the blank solution were not available at corresponding times for the activated sensor, however if it is assumed that similar changes in background impedance would be occurring over time for both the activated and control sensors then the analysis can still be used to indicate the changes occurring due to bacteria for each sensor. Based on this assumption, the results, presented in Figure 6.25, suggest that larger changes in absolute impedance

were observed due to bacteria when immobilised phages were present on the sensor's surface. The largest change occurs around 1 MHz.
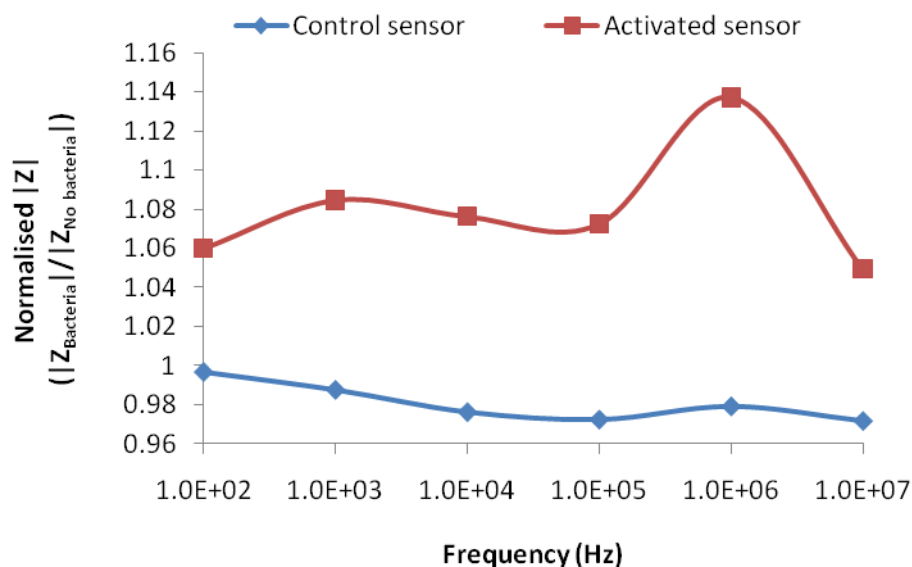
Figure 6.25. Comparison of the effect of bacteria on absolute impedance (|Z|) measured by the activated and untreated control sensor. Absolute impedance of the bacterial suspension after 15 minutes (|Z$_{Bacteria}$|) was normalised against absolute impedance of the blank solution at 0 minutes (|Z$_{No\ bacteria}$|) across the frequency range.

In Figure 6.26, normalised impedance is plotted at increasing time intervals for the activated sensor. This can be correlated to the results of Section 6.4.2.3.1 where it was found that the largest changes in absolute impedance at low frequencies (≤ 10 kHz) occurred after 15 minutes whilst at high frequencies (≥ 100 kHz) the largest changes occurred after 5 minutes (Figure 6.20 and Figure 6.21 respectively). It can also be seen from Figure 6.26 that after the first 5 minutes the system appears to be relatively stable i.e. impedance of the bacterial suspension reduces in a consistent manner compared to the blank measurement.
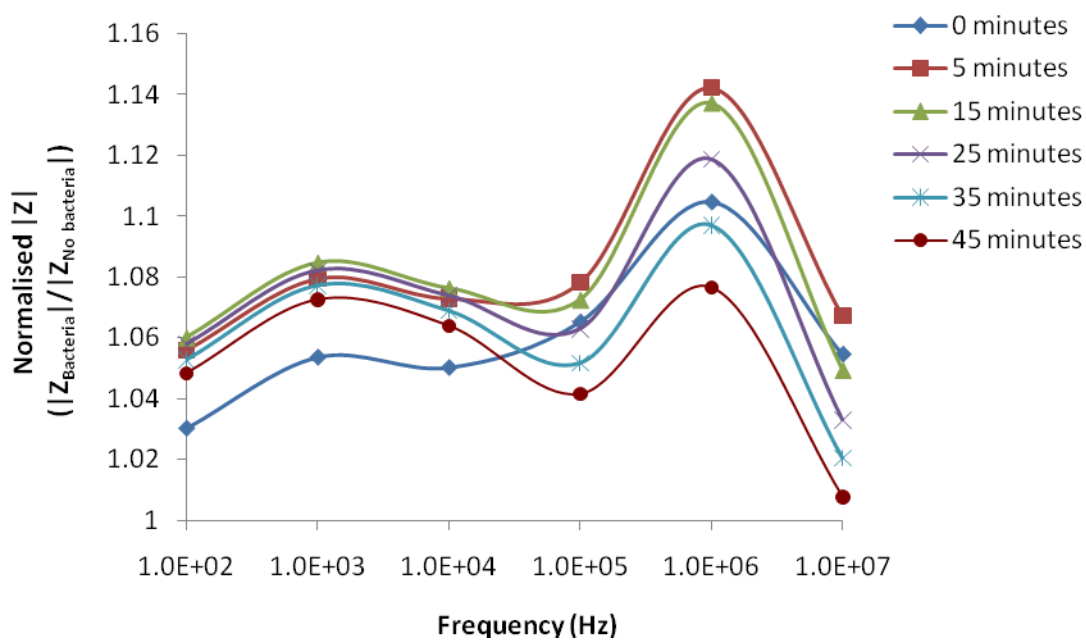
Figure 6.26. Normalised absolute impedance measured from the activated sensor at increasing time intervals. Absolute impedance of the bacterial suspension at increasing times ($|Z_{Bacteria}|$) was normalised against absolute impedance of the blank solution at 0 minutes ($|Z_{No\ bacteria}|$).

Nyquist plots comparing the control and activated sensor measurements for bacterial suspensions after 15 minutes are presented in Figure 6.27. The plots for both sensors are similar: both are relatively linear with differences between the activated and control sensor results most apparent at lower frequencies. The trend of the Nyquist plots is similar to that seen for the control sensor in the blank solution in Figure 6.19.
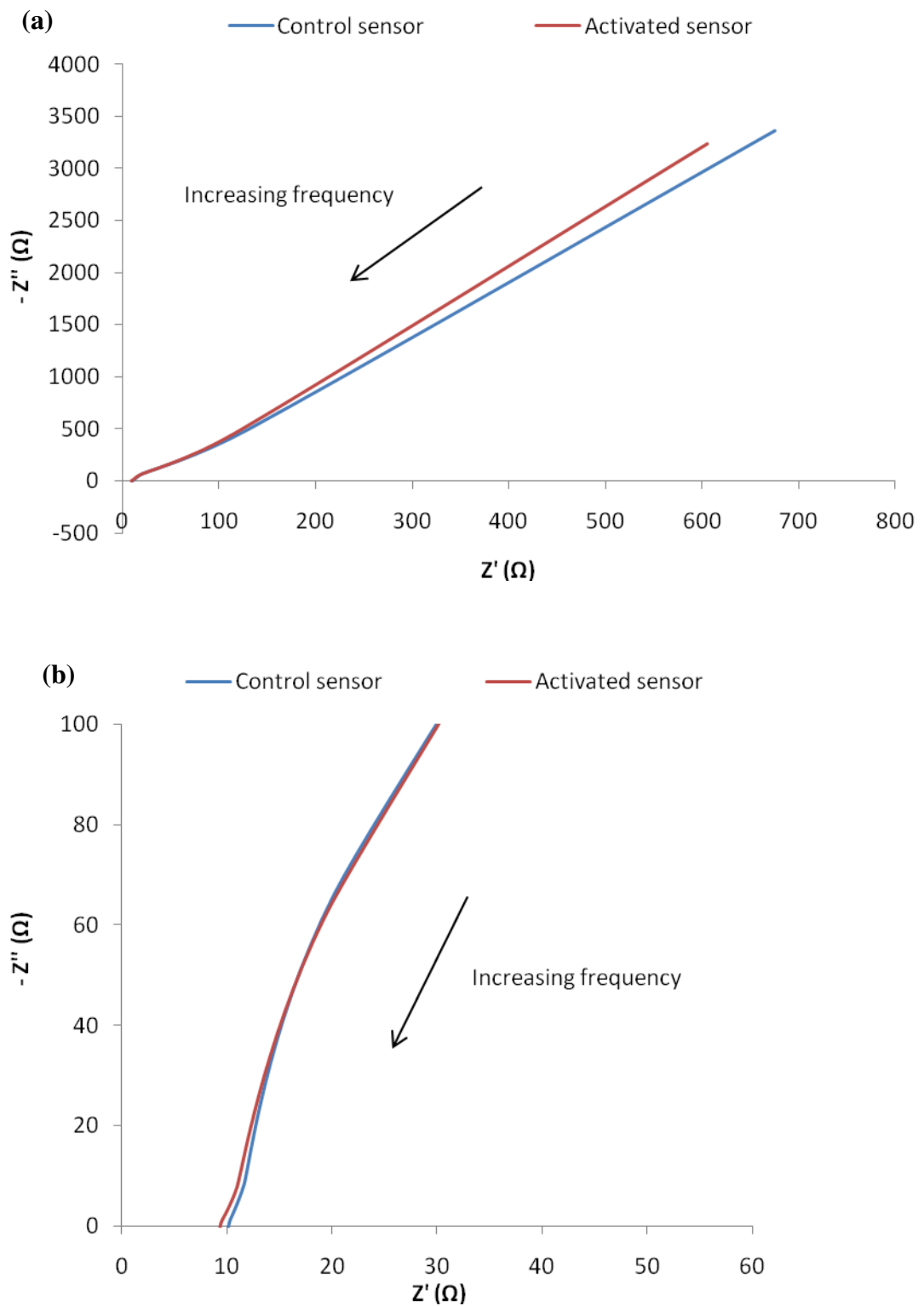
Figure 6.27. (a) Nyquist plots for the control and activated sensor in bacterial suspensions of 8.85 ± 0.14 Log$_{10}$ CFU/ml and 8.90 ± 0.01 Log$_{10}$ CFU/ml respectively after 15 minutes incubation (n = 1). Sensors were activated by physical adsorption. Z'' is the imaginary impedance and Z' is the real impedance component. The measuring frequency range was 100 Hz to 10 MHz. (b) Focused plot of (a) at high frequencies (10 kHz to 10 MHz).

237

The impedance data obtained from the control sensor and activated sensor in bacterial suspensions, upon which Figure 6.27 is based, are presented in Table 6.10.

Table 6.10. Impedance data for the control sensor and activated sensor in bacterial suspensions of 8.85 ± 0.14 Log$_{10}$ CFU/ml and 8.90 ± 0.01 Log$_{10}$ CFU/ml respectively after 15 minutes incubation. The sensor was activated by physical adsorption. Absolute impedance (|Z|), real impedance (Z') and imaginary impedance (Z'') data are presented for each measuring frequency.

Frequency (Hz)	Control sensor			Activated sensor		
	|Z| (Ω)	Z' (Ω)	-Z'' (Ω)	|Z| (Ω)	Z' (Ω)	-Z'' (Ω)
10^2	3430.3	675.7	3363.1	3290.7	604.9	3234.6
10^3	507.3	129.4	490.5	468.8	116.0	454.3
10^4	69.1	20.2	66.1	64.4	19.2	61.5
10^5	14.2	11.6	8.1	13.4	10.9	7.7
10^6	10.3	10.3	0.9	9.5	9.4	0.9
10^7	10.4	10.1	-2.4	9.8	9.4	-2.7

6.4.2.3.3 Investigation into Bacterial Growth

S. aureus can grow in 0.1% PW [Acumedia, 2004] and since bacteria were re-suspended in fresh PW (to remove metabolic by-products and bacterial debris after overnight growth in LB broth), nutrients necessary for growth would be replenished. It was assumed that the bacteria were in the stationary phase after overnight incubation and would return to the beginning of the growth curve upon re-suspension in a fresh growth medium (see Chapter 1, Section 1.5). Indeed, a small level of growth was suggested by enumerating the bacterial suspension before and after the experimental testing period using the plating method outlined in Chapter 4, Section 4.2.2.2. Results are presented in Table 6.11. The suspension was enumerated as close to the start and end of the experiment as possible covering a period of approximately 55 minutes. Although the mean concentrations were not statistically different over the testing period (paired t-test; H$_0$: $\mu_d = \mu_0 = 0$, H$_A$: $\mu_d \neq \mu_0$, $\alpha = 0.05$), an increase in concentration was observed. Conductivity can also be used to indicate bacterial growth, as was first mentioned in Chapter 1, Section 1.1.3.1; an increase in conductance is indicative of bacterial growth [Cady et al., 1978]. A conductivity meter (Model 4150, Jenway, Fisher Scientific UK) was used to measure the

conductance of the suspension before and after the experiment and results are presented in Table 6.11. It can be seen that the conductance of the bacterial suspension increased over the testing period despite a small decrease in temperature. Although the generation time for *S. aureus* is approximately 30 minutes under optimal growth temperatures (see Chapter 1, Section 1.5) and this experiment was conducted at room temperature, it may still be possible for at least one generation of bacteria to be produced over the 55 minutes.

Table 6.11. Summary of solution properties before and after testing with the activated sensor. The incubation period was approximately 55 minutes at room temperature. The concentration and conductance of the bacterial suspension in 0.1% PW are reported as well as values for the blank solution (0.1% PW only).

Solution	Bacterial concentration Log_{10} CFU/ml		Conductance (Temperature) µS	
	Start	End	Start	End
Bacterial suspension	8.90 ± 0.01	9.03 ± 0.16	1903 (27.4°C)	1959 (25.8°C)
Blank solution	< 1	< 1	1927 (26.5°C)	1927 (26.1°C)

To determine whether bacterial growth was perhaps masking or having some influence on the results presented previously in Sections 6.4.2.3.1 and 6.4.2.3.2, measurements were repeated with bacteria re-suspended in 0.1% PBS to prevent growth. Experimental parameters are listed in Table 6.12. Note that sensor topology was kept the same as previous testing in 0.1% PW.

Table 6.12. Experimental parameters for activated and untreated control sensor testing with bacteria suspended in 0.1% PBS. Sensor electrode topology is displayed in terms of electrode width (W) and gap (G). The sensor was activated by overnight (O/N) physical adsorption in a suspension of phages. Bacteria were suspended in 0.1% PBS and the bacterial concentrations listed are that at the start of the experiment (t = 0 minutes). Mean concentrations are presented ± standard deviations (n = 6).

Sensor	Sensor topology (W / G μm)	Phage immobilisation method	Phage concentration (PFU/ml)	Bacteria concentration (Log_{10} CFU/ml)
Activated	3 / 4	O/N physical adsorption	2.8×10^{10}	8.86 ± 0.09
Control	3 / 4	N/A	N/A	8.95 ± 0.09

Bacteria viability in 0.1% PBS and the prevention of growth were confirmed by enumeration and conductance measurements taken before and after the testing period. Results are presented in Table 6.13. Bacterial concentration did not significantly change over 75 minutes (paired t-test; H_0: $\mu_d = \mu_0 = 0$, H_A: $\mu_d \neq \mu_0$, $\alpha = 0.05$) suggesting adequate viability. The fact that there was a small overall decrease in both bacterial enumeration and conductance also suggests that bacteria were not growing, as expected.

Table 6.13. Bacteria suspended in 0.1% PBS. Bacterial concentration and suspension conductance are reported before and after a 75 minute static incubation period at room temperature. Mean bacterial concentrations are listed ± standard deviations (n = 6).

Suspension Parameter	Time	
	0 minutes	75 minutes
Bacterial concentration (Log_{10} CFU/ml)	8.86 ± 0.09	8.75 ± 0.15
Conductance (μS)	3280	3240

Figure 6.28 presents absolute impedance over time at 1 kHz measured from activated sensors in 0.1% PW and 0.1% PBS bacterial suspensions. It can be seen that the changes in absolute impedance recorded from suspensions of bacteria in 0.1% PBS were not larger than when testing in 0.1% PW and so results had not been improved by eliminating bacterial growth. Such results were typical of other frequencies. The

results therefore suggest that bacterial growth was not having a hugely significant effect on the impedance measurements.
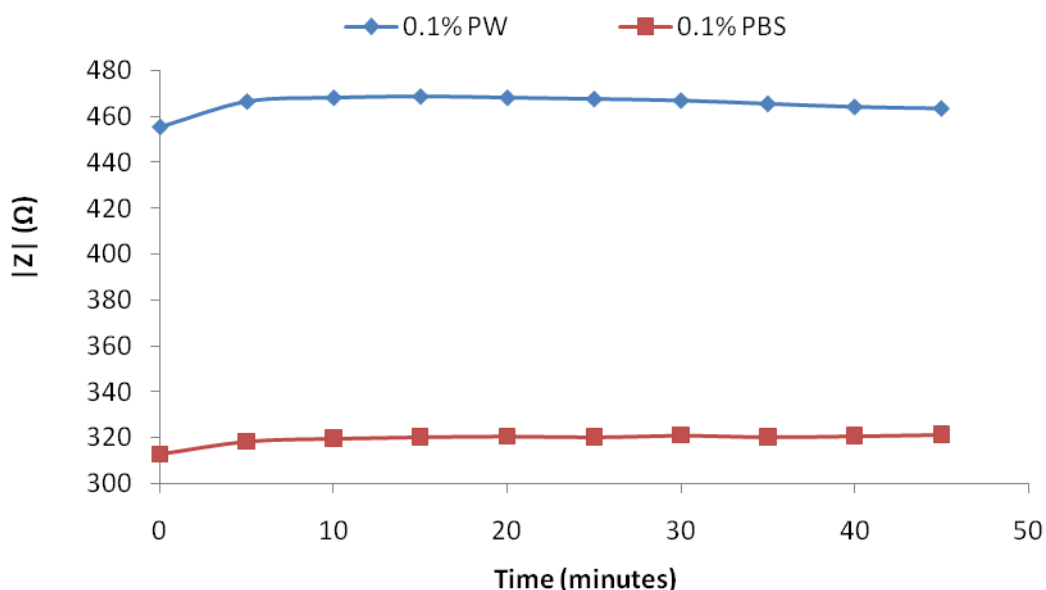
Figure 6.28. Absolute impedance (|Z|) over time measured from activated sensors with physically adsorbed phages (overnight incubation) at 1 kHz in a suspension of bacteria re-suspended in 0.1% PW (8.90 ± 0.01 Log$_{10}$ CFU/ml) and 0.1% PBS (8.86 ± 0.09 Log$_{10}$ CFU/ml).

In Figure 6.29, normalised results for measurements of bacteria in 0.1% PW and 0.1% PBS are presented based on Equation 6.5 whcih was explained in Section 6.4.2.3.2. Absolute impedance of the bacterial suspension measured by the activated sensor was normalised against the absolute impedance of the blank suspension measured from the same sensor prior to application of the bacterial sample. Results are reported at 15 minutes after bacterial sample application for both the 0.1% PW and 0.1% PBS suspending solutions. Based on this analysis, results suggest that impedance changes are smaller across the frequency range when measurements are made in 0.1% PBS.
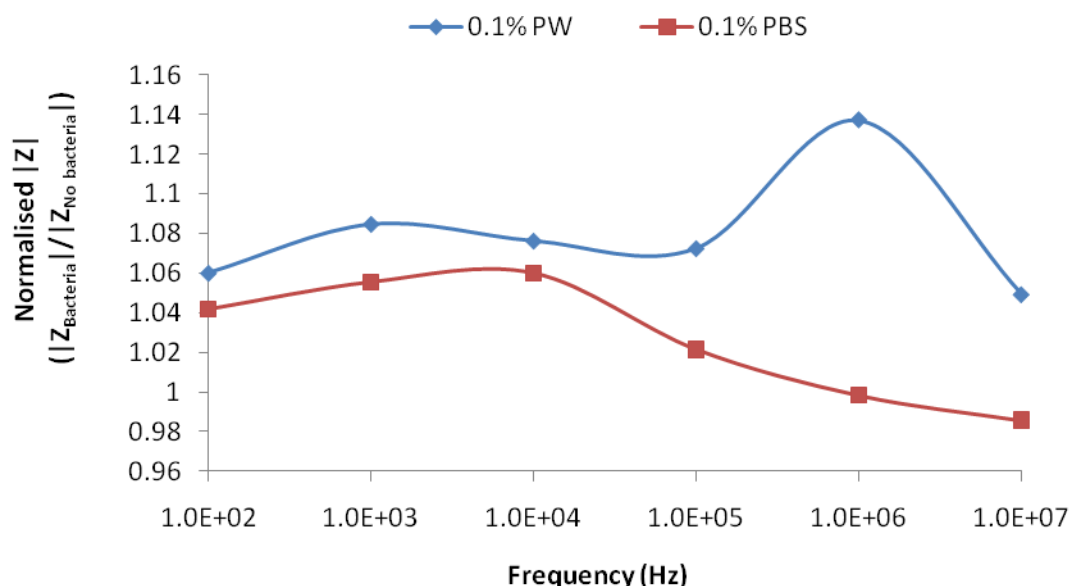
Figure 6.29. Normalised absolute impedance of bacteria suspended in 0.1% PW (8.90 ± 0.01 Log$_{10}$ CFU/ml) and 0.1% PBS (8.86 ± 0.09 Log$_{10}$ CFU/ml) measured from activated sensors (overnight physically adsorbed phages, W = 3 µm and G = 4 µm). Absolute impedance of the bacterial suspension at 15 minutes (|Z$_{Bacteria}$|) was normalised against absolute impedance of the blank solution at 0 minutes (|Z$_{No\ bacteria}$|) across the frequency range.

The absolute impedance data points on which Figure 6.29 is based are presented in Tables 6.14 and 6.15 along with the real and imaginary components of the impedance data.

Table 6.14. Impedance data for 0.1% PW and bacteria suspended in 0.1% PW after 15 minutes incubation (8.90 ± 0.01 Log$_{10}$ CFU/ml) as measured from an activated sensor (overnight physical adsorption). Absolute impedance (|Z|), real impedance (Z') and imaginary impedance (Z'') data are presented for each measuring frequency.

Frequency (Hz)	0.1% PW			Bacterial suspension		
	|Z| (Ω)	Z' (Ω)	-Z'' (Ω)	|Z| (Ω)	Z' (Ω)	-Z'' (Ω)
10^2	3104.2	541.3	3056.6	3290.7	604.9	3234.6
10^3	432.2	103.9	419.6	468.8	116.0	454.3
10^4	59.8	18.4	57.0	64.4	19.2	61.5
10^5	12.4	10.0	7.4	13.4	10.9	7.7
10^6	8.3	8.3	0.8	9.5	9.4	0.9
10^7	9.3	8.7	-3.3	9.8	9.4	-2.7

Table 6.15. Impedance data for 0.1% PBS and bacteria suspended in 0.1% PBS after 15 minutes incubation (8.86 ± 0.09 Log$_{10}$ CFU/ml) as measured from an activated sensor (overnight physical adsorption). Absolute impedance (|Z|), real impedance (Z') and imaginary impedance (Z'') data are presented for each measuring frequency.

Frequency (Hz)	0.1% PBS			Bacterial suspension		
	|Z| (Ω)	Z' (Ω)	-Z'' (Ω)	|Z| (Ω)	Z' (Ω)	-Z'' (Ω)
10^2	2100.4	379.9	2065.8	2188.1	414.5	2148.5
10^3	303.6	83.3	292.0	320.5	88.0	308.1
10^4	44.3	19.1	40.0	47.0	20.0	42.5
10^5	13.9	12.6	5.9	14.2	12.8	6.3
10^6	10.8	10.7	0.6	10.7	10.7	0.7
10^7	11.9	11.4	-3.3	11.7	11.2	-3.2

6.4.2.4 Sensitivity Test

The initial testing of the sensor had so far revealed only small changes in impedance which could be attributed to the detection of bacteria and these were considerably smaller than some published results [Kim et al., 2009, Nandakumar et al., 2008, Radke and Alocilja, 2004, Varshney et al., 2007]. In addition to this, these changes were achieved with high bacterial concentrations (in the region of 10^8 CFU/ml) leaving very little scope for the detection of lower concentrations. This was somewhat surprising considering that a number of experimental parameters applied in this work were similar to the published examples, such as sensor layout, electrode dimensions and suspending solution. Possible reasons for the differences and the generally small levels of change observed could include: too few interactions between immobilised phages and bacteria and therefore low levels of bacteria captured into the sensor's electric field or, under these measuring conditions the sensor and measuring system are not sensitive to the changes occurring.

To investigate this latter theory, a simple experiment was devised with the aim of explicitly examining the effect on impedance when an insulating material is introduced into the sensor's region of high electric field strength. The experiment involved testing an untreated sensor with a suspension of nylon beads (Orgasol, Arkema Inc., Philadelphia, USA) instead of the bacterial suspension. This simplified the suspension to just two elements: 0.1% PW and nylon. The nylon beads were of a

single dielectric permittivity which was considerably lower than that of the suspending fluid (the relative dielectric permittivities of 0.1% PW and nylon are approximately 80 and 5 respectively). Thus the complexities of the bacterial cell were eliminated. Nylon beads with a 20 μm diameter were available.

As with the bacterial suspension, measurements were recorded over time after sample application onto the sensor's electrode array. In this case however, sedimentation through gravitational effects was relied upon to form a layer of nylon beads on the sensor surface as opposed to phage capture in the case of testing with bacteria. It was visually observed from the stock suspension that the majority of the nylon beads would sediment within 5 minutes. Although the diameter of the beads was larger than that of *S. aureus*, it was expected that they would still provide sufficient coverage of the sensor's surface when used at high concentrations. Initially beads were suspended in 0.1% PW and in a later experiment they were suspended in distilled water.

6.4.2.4.1 Measurements in 0.1% Peptone Water

The concentration of the nylon beads in 0.1% PW was approximately 2×10^7 beads/ml. The resulting suspension was dense and a thick nylon layer was formed upon bead sedimentation in the preparation vessel. Absolute impedance measurements at 1 kHz for the nylon bead suspension and control (0.1% PW only) are presented in Figure 6.30 for comparison with results obtained from the activated sensor with bacteria (Figure 6.20). As with the bacterial suspension measurements, there was a small initial rise in impedance with the nylon bead suspension followed by a consistent decrease in impedance over time. However, for nylon bead measurements, absolute impedance of the particle suspension was greater than that of the blank solution as reflected by the fact that normalised impedance values for the nylon bead suspension are generally greater than 1, as shown in Figure 6.31.
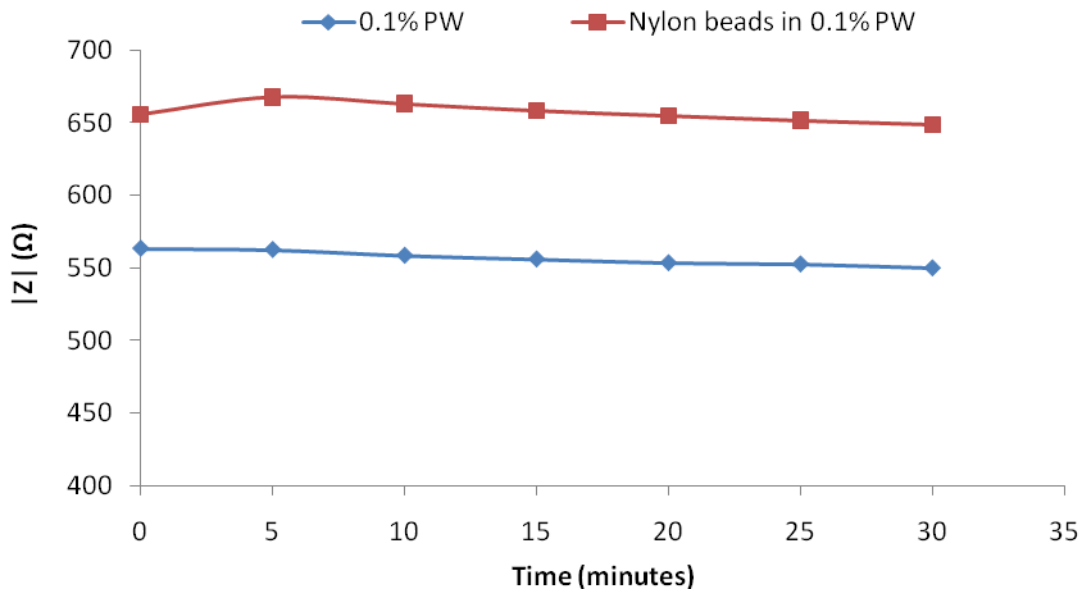
Figure 6.30. Absolute impedance (|Z|) at 1 kHz measured over time for a suspension of nylon beads (20 μm diameter) in 0.1% PW. Impedance for 0.1% PW only is also included. Sensor electrode dimensions were: W = 3 μm and G = 4 μm.

The trends observed at 1 kHz in Figure 6.30 were typical of frequencies less than and including 100 kHz. The maximum recorded increase was 1.19 times (19.3%) at 10 kHz after 5 minutes as illustrated in the normalised impedance plot of Figure 6.31 (note that only selected times are plotted for clarity). Normalisation was carried out as per Equation 6.5. At higher frequencies (1 MHz and 10 MHz), absolute impedance of a solution with and without nylon beads was almost identical over the time period analysed (normalised impedance at these frequencies was consistently close to 1). This could be indicative of poor sensitivity at these higher frequencies. This effect was not observed for the activated sensor in bacteria at 1 MHz (shown in Figure 6.22), but it must be remembered that other factors could be influencing results obtained from the activated sensor such as the phage layer and also the presence of conductive species in the solution carried over from the broth culture. Generally however, the magnitude of change observed with nylon beads in 0.1% PW appeared to be similar to those being obtained from testing with the activated sensor in bacteria (Figure 6.26).
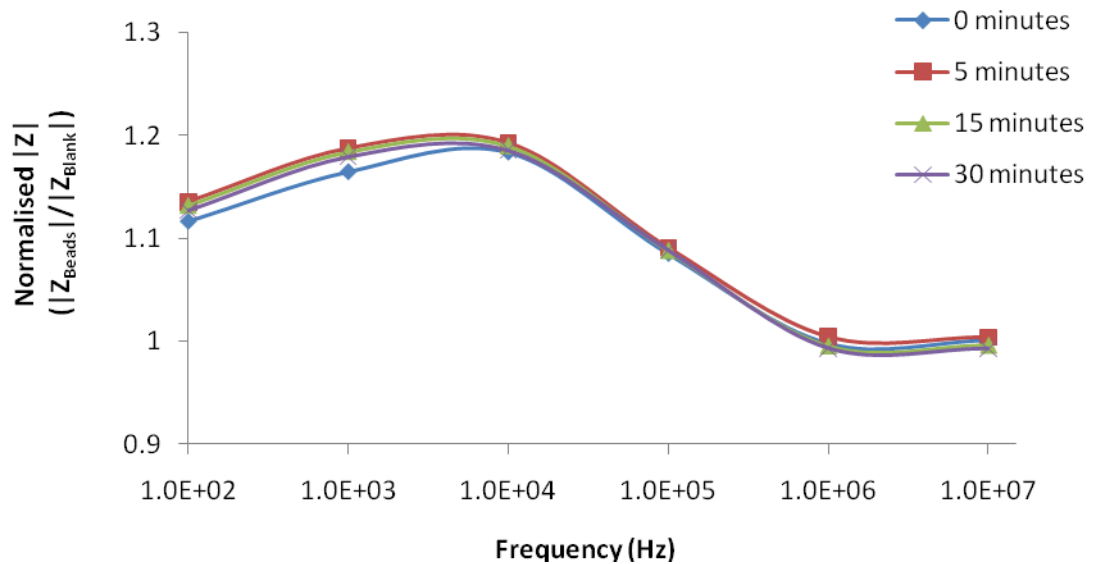
Figure 6.31. Normalised absolute impedance (normalised |Z|) at selected times over the frequency range analysed for an untreated control sensor with nylon beads suspended in 0.1% PW. Impedance values were normalised against corresponding impedance measured from an untreated sensor in 0.1% PW only.

Table 6.16 shows examples of the data collected from the sensor in 0.1% PW and the nylon bead suspension. Data points are shown for t = 5 minutes at which point some of the largest changes in normalised impedance were found.

Table 6.16. Impedance data for 0.1% PW and the nylon bead suspension in 0.1% PW after 5 minutes as measured from an untreated sensor. Absolute impedance (|Z|), real impedance (Z') and imaginary impedance (Z'') data are presented for each measuring frequency.

Frequency (Hz)	0.1% PW			Nylon bead suspension		
	|Z| (Ω)	Z' (Ω)	-Z'' (Ω)	|Z| (Ω)	Z' (Ω)	-Z'' (Ω)
10^2	3833.0	946.2	4323.9	4352.3	931.0	4251.5
10^3	562.4	172.8	650.6	667.7	171.4	645.3
10^4	74.5	24.0	87.8	88.9	23.3	85.8
10^5	14.9	12.1	10.8	16.2	12.3	10.6
10^6	10.5	10.4	1.2	10.6	10.5	1.3
10^7	10.7	10.3	-2.3	10.7	10.4	-2.3

6.4.2.4.2 Measurements in Distilled Water

Further experiments were conducted with nylon beads in distilled water to investigate suspending solutions of lower conductivity. Bead concentration was

246

again approximately 2×10^7 beads/ml. Absolute impedance measurements at 1 kHz are presented in Figure 6.32 which confirms absolute impedance values of distilled water are higher than for 0.1% PW (displayed in Figure 6.30), indicating reduced solution conductivity. A larger change in impedance over time for nylon beads suspended in distilled water is suggested by the results in Figure 6.32 and is confirmed by normalised values in Figure 6.33 which are compared to those for the nylon beads in 0.1% PW discussed in the previous section.
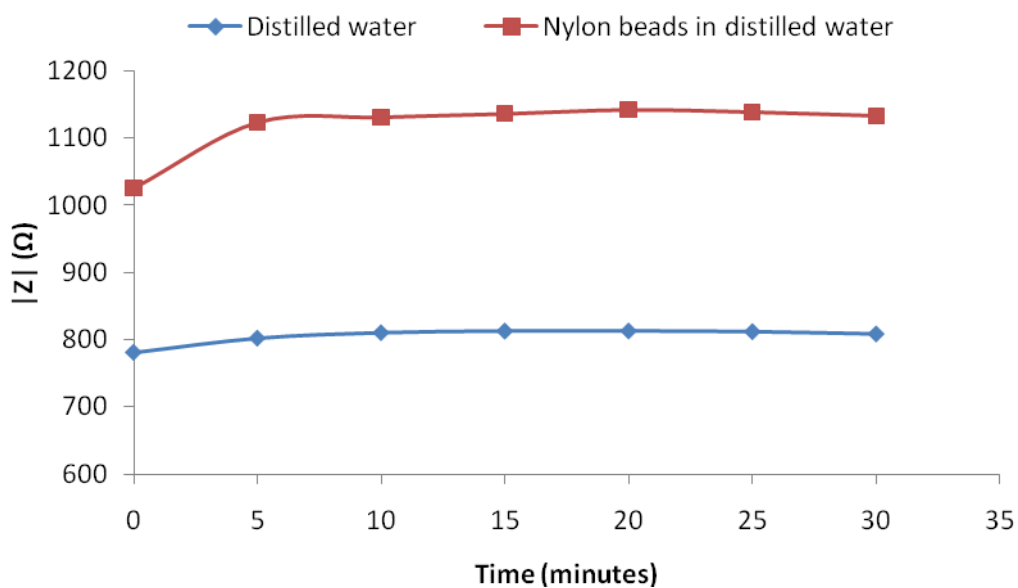
Figure 6.32. Absolute impedance (|Z|) at 1 kHz measured over time for a suspension of nylon beads (20 μm diameter) in distilled water. Impedance for distilled water only is also included. Sensor electrode dimensions were: W = 3 μm and G = 4 μm.
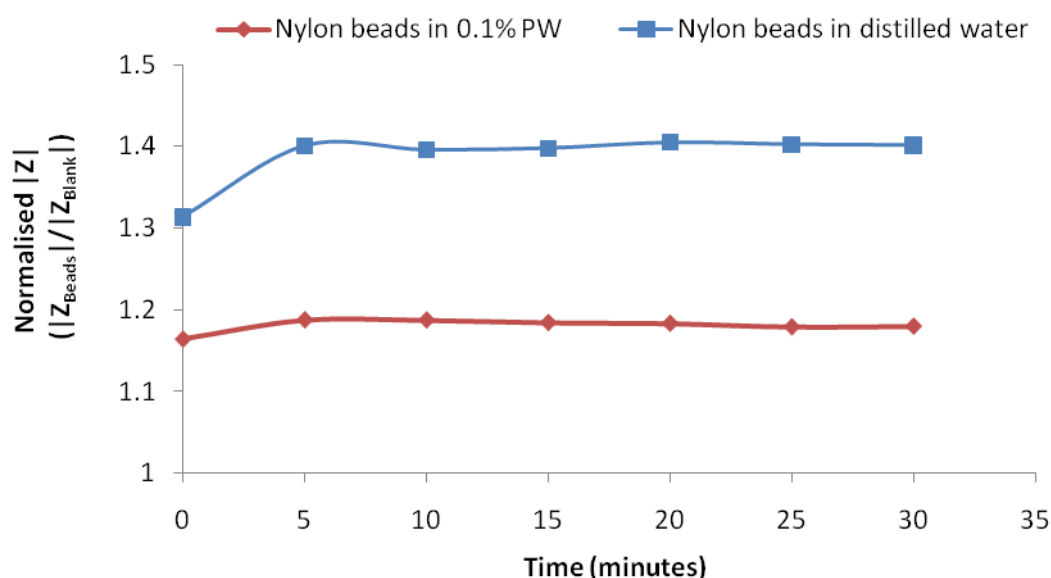
Figure 6.33. Normalised absolute impedance (normalised |Z|) over time at 1 kHz for an untreated control sensor with nylon beads suspended in 0.1% PW and distilled water. Impedance values were normalised against corresponding impedance measured from untreated sensors in their respective control solutions.

The maximum recorded increase between the solution with and without the nylon beads was larger for measurements in water than in 0.1% PW. This can be seen by comparing the normalised impedance values in Figure 6.31 for 0.1% PW to the results from distilled water testing in Figure 6.34. The maximum recorded increase in distilled water was by a factor of 4.26 at 100 kHz after 20 minutes compared to 1.19 at 10 kHz after 5 minutes. Again, at higher frequencies (10 MHz), normalised impedance was close to and often less than 1, indicating that measured impedance of the nylon bead suspension was no longer greater than the control.
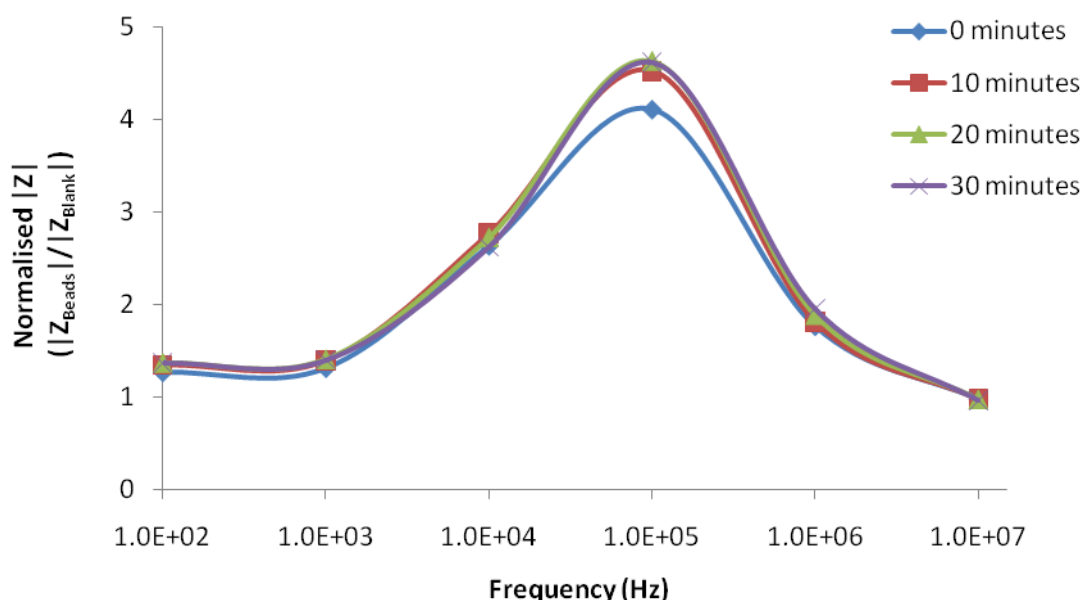
Figure 6.34. Normalised absolute impedance (normalised |Z|) at selected times over the frequency range analysed for an untreated control sensor with nylon beads suspended in distilled water. Impedance values were normalised against corresponding impedance measured from an untreated sensor in distilled water only.

Table 6.17 shows examples of the data collected from the sensor in distilled water and the nylon bead suspension in distilled water. Data points are shown for t = 30 minutes at which point some of the largest changes in normalised impedance were found.

Table 6.17. Impedance data for distilled water and the nylon bead suspension in distilled water after 30 minutes as measured from an untreated sensor. Absolute impedance (|Z|), real impedance (Z') and imaginary impedance (Z'') data are presented for each measuring frequency.

Frequency (Hz)	Distilled water			Nylon bead suspension		
	$|Z|$ (Ω)	Z' (Ω)	-Z'' (Ω)	$|Z|$ (Ω)	Z' (Ω)	-Z'' (Ω)
10^2	6102.1	1484.0	5918.9	8367.7	2148.0	8087.3
10^3	808.4	160.2	792.4	1132.8	403.3	1058.6
10^4	110.4	56.8	94.7	289.6	252.8	141.2
10^5	48.2	46.2	13.8	222.4	207.3	80.5
10^6	38.9	35.6	15.6	76.0	35.4	67.3
10^7	10.9	10.0	4.3	10.5	8.9	5.6

6.4.2.5   Detection of Bacteria – Testing Method 2

Based on the results of Testing Method 1 and the sensitivity analysis, a second approach to investigating the bioreceptor performance of immobilised phages was devised. The main changes from Testing Method 1 were as follows:

- Phages were immobilised by the biotin-avidin procedure.
- Bacteria were suspended in 0.1 M mannitol.
- Impedance was measured before and after the sensor was incubated in the bacterial suspension for 10 minutes.

Reasons for these changes will be addressed in the discussion section to follow (Section 6.4.3.6). Full details of the revised method can be found in Chapter 4, Section 4.5.3. Briefly, the activated sensor's impedance was recorded in 0.1 M mannitol before the sensor was incubated in a bacterial suspension at room temperature for 10 minutes. The sensor was then rinsed with 0.1 M mannitol and impedance measurements were repeated in 0.1 M mannitol. Two controls were carried out: a 'biotin-avidin treated' sensor which went through the biotin-avidin immobilisation procedure (as described in Chapter 4, Section 4.3.2.4.2) but was not exposed to phages and an 'untreated' control sensor which had no phage immobilisation treatment. The parameters of each experiment are summarised in Table 6.18. Note that in this section, the activated sensor is that with biotin-avidin immobilised phages and the polymer layer between electrodes was present for sensors in Testing Method 2.

Table 6.18. Experimental parameters for activated and control sensors used in Testing Method 2. Sensor electrode topology is displayed in terms of electrode width (W) and gap (G). Phages were immobilised through the biotin-avidin (B-A) immobilisation procedure for the activated sensor. The concentration of the biotinylated phage suspension used is listed (estimated from two dilutions, each plated three times). Bacteria were suspended in 0.1 M mannitol and enumerated immediately prior to the experiment. Two controls were carried out: the B-A treated control which went though the biotin-avidin immobilisation procedure only and an untreated control sensor.

Sensor	Sensor topology (W / G μm)	Sensor treatment	Phage concentration (PFU/ml)	Bacteria concentration (Log$_{10}$ CFU/ml)
Activated	3 / 10	B-A + phage	3.9×10^{10}	9.04 ± 0.12
B-A treated control	3 / 10	B-A	N/A	9.10 ± 0.15
Untreated control	5 / 10	No treatment	N/A	9.12 ± 0.15

Prior to testing, the behaviour of bacteria suspended in 0.1 M mannitol was established by enumerating a bacterial suspension before and after incubation at room temperature for 75 minutes and also by monitoring suspension conductance. Results are presented in Table 6.19. There was no significant change in concentration levels over the incubation period (paired t-test; H$_0$: $\mu_d = \mu_0 = 0$, H$_A$: $\mu_d \neq \mu_0$, $\alpha = 0.05$) but conductance did increase. The results therefore suggest that the majority of bacteria remain viable in 0.1 M mannitol for at least 75 minutes but there may be some ion release over this period.

Table 6.19. Summary of bacterial suspension in 0.1 M mannitol before and after incubation at room temperature for 75 minutes. The bacterial concentration and conductance of the bacterial suspension and a blank solution (0.1 M mannitol only) are reported.

Solution	Bacterial concentration Log$_{10}$ CFU/ml		Conductance (Temperature) μS	
	Start	End	Start	End
Bacterial suspension	9.05 ± 0.05	9.00 ± 0.07	10.20 (26.7°C)	62.60 (25.9°C)
Blank solution	< 1	< 1	4.49 (25.4°C)	18.33 (25.8°C)

Before examining the results from testing with bacteria, it is first worth comparing blank solution results obtained from the three sensors of different treatment. This is shown in Figure 6.35. Results suggest that after each treatment step (biotin-avidin treatment and then phage immobilisation), impedance increases across the measuring frequency range. Increases are most notable over the mid-frequency range (10 kHz to 1 MHz).
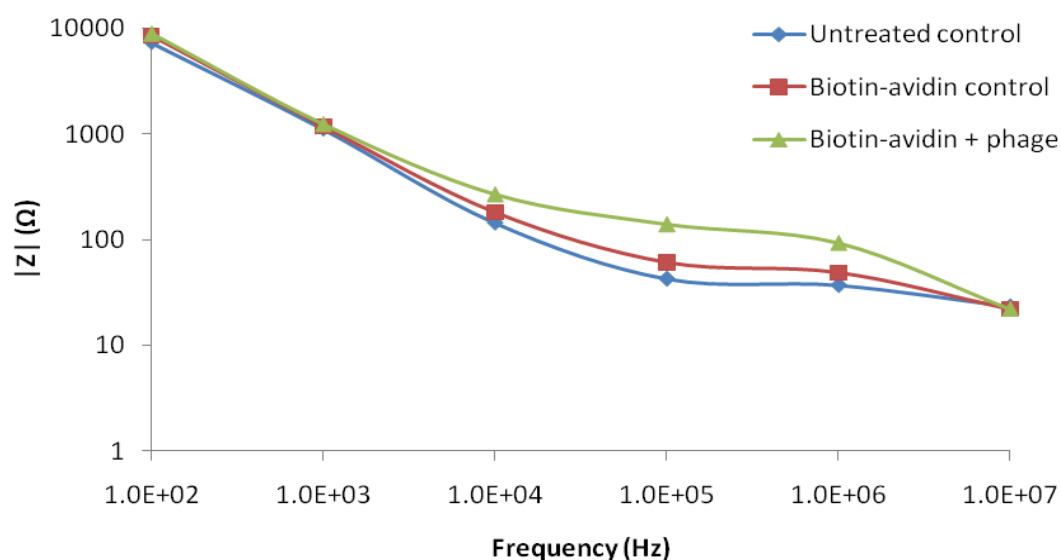
Figure 6.35. Effect of biotin-avidin immobilisation treatment on sensor impedance. Bode plot of absolute impedance (|Z|) for sensors of Testing Method 2 before testing with bacteria. Impedance was measured from: an untreated control sensor (W = 5 µm, G = 10 µm), a biotin-avidin only treated sensor (W = 3 µm, G = 10 µm) and a biotin-avidin treated sensor with phages (W = 3 µm, G = 10 µm). Measurements were carried out in 0.1 M mannitol.

Results from testing with the activated sensor are presented in Figure 6.36. Figure 6.35(a) shows a Bode plot of absolute impedance before and after the activated sensor was incubated with the bacterial suspension. A change in impedance is apparent; impedance has increased after exposure to bacteria and this is most notable at frequencies between 10 kHz and 100 kHz. A shift in phase angle was also observed, as demonstrated in Figure 6.36(b).

(a)

(b)
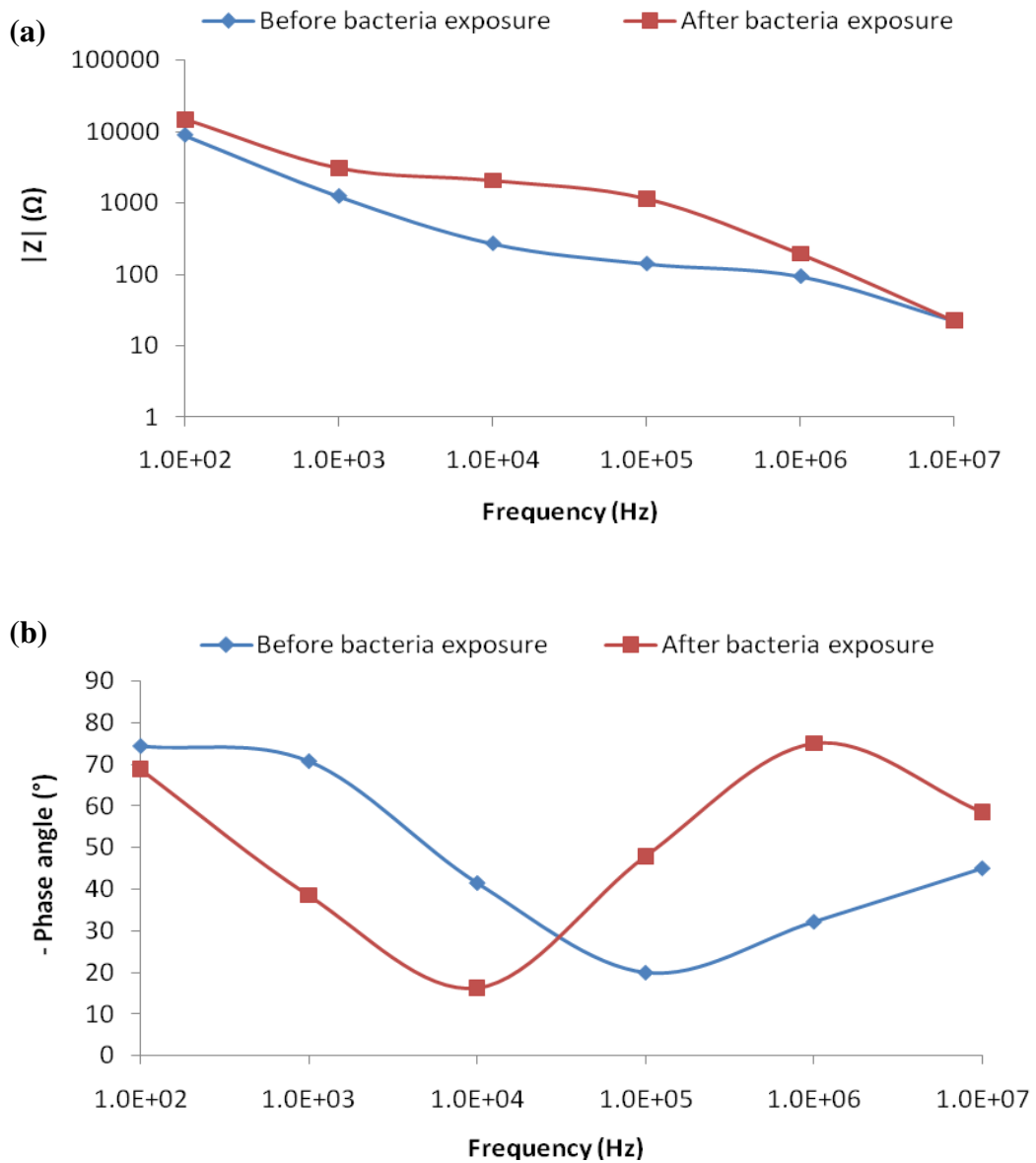
Figure 6.36. (a) Absolute impedance (|Z|) Bode plot and (b) phase angle Bode plot for an activated sensor in 0.1 M mannitol before and after 10 minutes incubation with a high concentration bacterial suspension (9.04 ± 0.12 Log10 CFU/ml). Phages were immobilised onto the sensor surface by the biotin-avidin technique.

The data points of Figure 6.36 can be found in Table 6.20.

Table 6.20. Impedance (|Z|) and phase angle data (φ) measured from the activated sensor in 0.1 M mannitol before and after 10 minutes incubation with a high concentration bacterial suspension (9.04 ± 0.12 Log10 CFU/ml). Phages were immobilised onto the sensor surface by the biotin-avidin technique.

Frequency (Hz)	Before		After	
	|Z| (Ω)	- φ (°)	|Z| (Ω)	- φ (°)
10^2	8958.7	74.4	5323.2	68.9
10^3	1246.4	70.7	3066.9	38.5
10^4	270.6	41.5	2050.9	16.3
10^5	141.0	19.9	1147.3	47.9
10^6	93.9	32.2	194.0	75.0
10^7	22.3	45.0	22.5	58.5

Although the changes in impedance observed under these conditions were encouraging, the results obtained from control experiments also showed an increase in impedance after incubation with bacteria. Indeed, larger changes in impedance were actually recorded with the control sensors. The results of the control experiments are compared to those from the activated sensor in Figure 6.37. Results are compared in terms of normalised absolute impedance ($|Z_N|$) where absolute impedance after exposure to bacteria ($|Z_{After}|$) is normalised against absolute impedance before exposure to bacteria ($|Z_{Before}|$) according to the following equation:

$$|Z_N| = \frac{|Z_{After}|}{|Z_{Before}|}$$

Equation 6.6
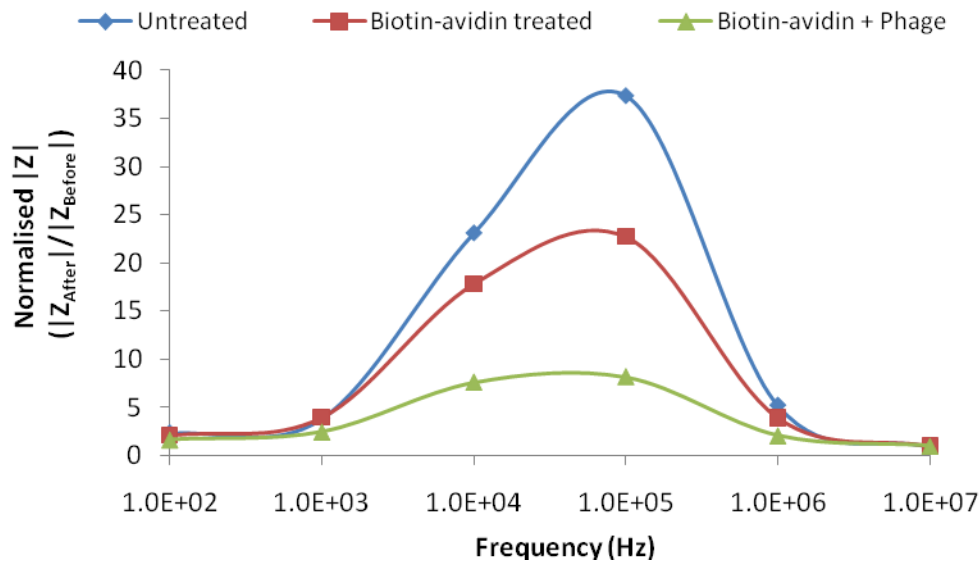
Figure 6.37. Normalised absolute impedance for Testing Method 2. An activated sensor with biotin-avidin immobilised phages was tested alongside two controls (untreated and biotin-avidin treated only). Impedance measurements after exposure to the bacterial suspension ($|Z_{After}|$) were normalised against impedance before ($|Z_{Before}|$). Measurements were taken in 0.1 M mannitol. Bacteria were suspended in 0.1M mannitol and were of similar concentrations for the activated sensor and controls (see Table 6.18). The activated and biotin-avidin treated sensors were of the same electrode topology (W = 3 µm, G = 10 µm). The untreated sensor had a slightly different electrode topology (W = 5 µm, G = 10 µm).

It should be remembered that the untreated sensor had a slightly different electrode topology to the activated and biotin-avidin treated sensor (electrodes were 2 µm wider, see Table 6.18). The effect of this on the sensor sensitivity can not be accurately accounted for with the experimental data available but the computer based modelling work in Chapter 3, Section 3.1.2.3, did suggest that sensors of larger electrode dimensions may not be as sensitive to *S. aureus*. However, the biotin-avidin treated control sensor has the same electrode topology as the activated sensor and Figure 6.37 shows that normalised impedance is still larger for this control.

Figure 6.38 shows Nyquist plots for the activated sensor before and after exposure to bacteria. A much larger semicircle portion is visible after exposure compared to before. This was also the case for both control sensors.
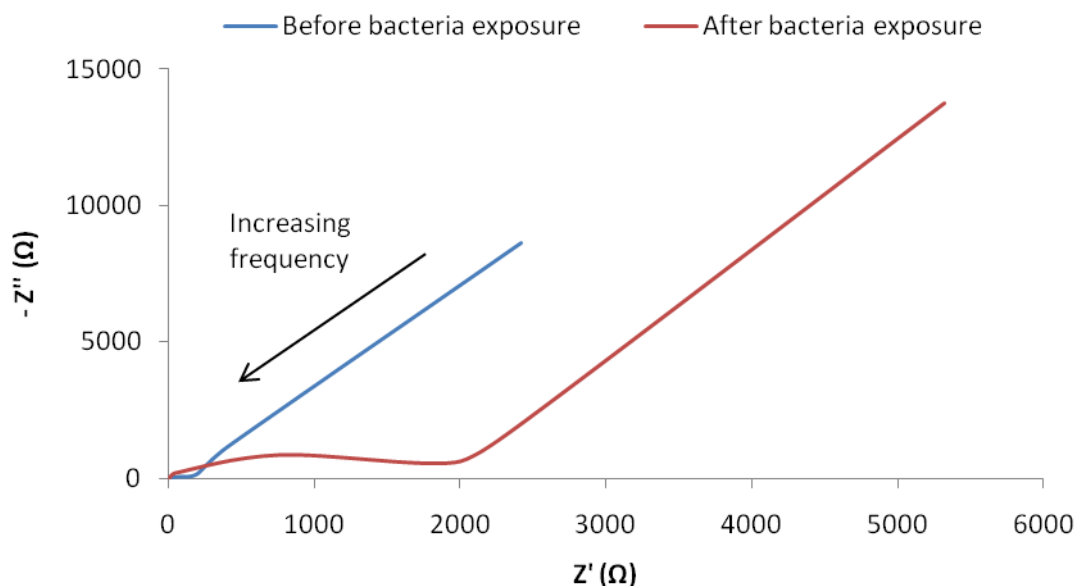
Figure 6.38. Nyquist plot showing activated sensor impedance before and after exposure to bacteria. Measurements were recorded in 0.1 M mannitol. The measuring frequency range was 100 Hz to 10 MHz (n = 1).

The impedance data, including real and imaginary components, measured from the activated sensor before and after exposure to bacteria are presented in Table 6.21.

Table 6.21. Impedance data measured from the activated sensor in 0.1 M mannitol before and after 10 minutes incubation with a high concentration bacterial suspension (9.04 ± 0.12 Log10 CFU/ml). Phages were immobilised onto the sensor surface by the biotin-avidin technique. Absolute impedance (|Z|), real impedance (Z') and imaginary impedance (Z'') data are presented for each measuring frequency.

Frequency (Hz)	Before			After		
	|Z| (Ω)	Z' (Ω)	-Z'' (Ω)	|Z| (Ω)	Z' (Ω)	-Z'' (Ω)
10^2	8958.7	2416.3	8626.7	5323.2	5323.2	13767.9
10^3	1246.4	411.4	1176.5	3066.9	2400.4	1908/8
10^4	270.6	202.7	179.2	2050.9	1968.2	576.5
10^5	141.0	132.5	48.1	1147.3	768.5	851.8
10^6	93.9	79.5	59.0	194.0	50.1	187.4
10^7	22.3	15.8	15.8	22.5	11.7	19.2

In Figure 6.39, the Nyquist plots for the sensors of different immobilisation treatment are compared after exposure to bacteria. Larger semicircle portions are evident for the control sensors.
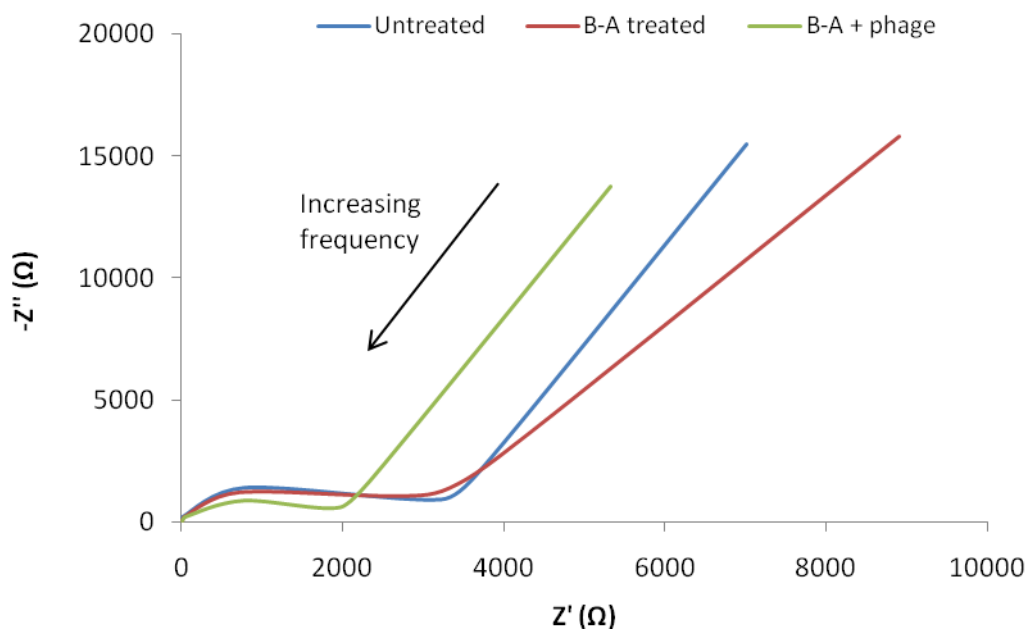
Figure 6.39. Nyquist plot showing impedance of sensors after exposure to bacteria at different stages of sensor treatment: untreated sensor, biotin-avidin treated only and biotin-avidin treated with immobilised phages. The measuring frequency range was 100 Hz to 10 MHz (n = 1).

It is also of interest to compare Nyquist plots for the three sensors at different stages of the immobilisation treatment before exposure to bacteria. Results are presented in Figure 6.40. At lower frequencies, the relationship between real (Z') and imaginary (Z'') impedance is relatively linear for all three sensors. However, at higher frequencies (illustrated on a smaller scale in Figure 6.40(b)) more significant differences are apparent and the diameter of the semicircle portion increases with each treatment step and is largest for the sensor with immobilised phages.
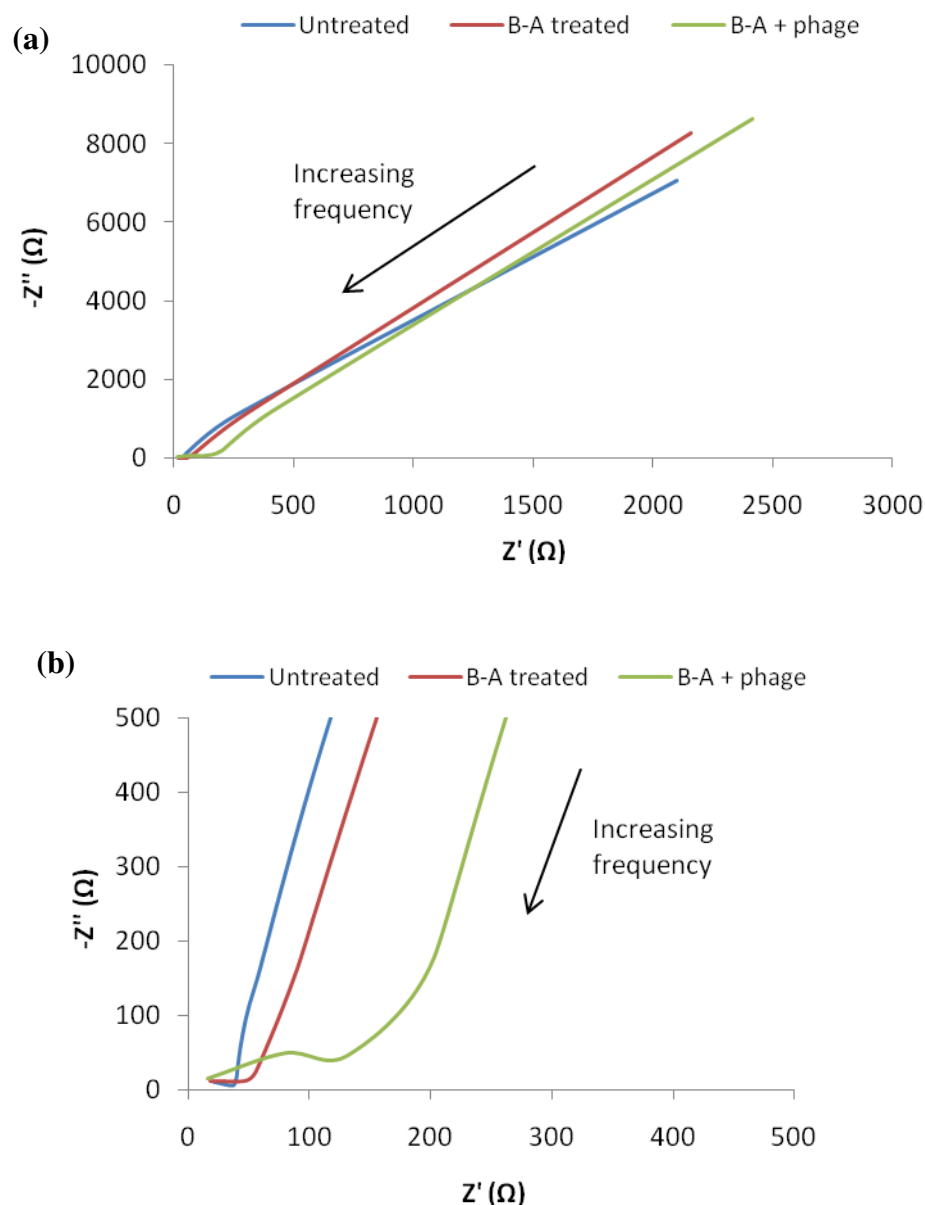
Figure 6.40. (a) Nyquist plot showing impedance of sensors before exposure to bacteria at different stages of treatment: untreated sensor, biotin-avidin treated only and biotin-avidin treated with immobilised phages (n = 1). The measuring frequency range was 100 Hz to 10 MHz. (b) Focused plot of (a) at high frequencies (10 kHz to 10 MHz).

The impedance data from the untreated sensor and the biotin-avidin treated only sensor are presented in Tables 6.22 and 6.23 respectively for comparison with Table 6.21 in which impedance data from the phage activated sensor is reported.

Table 6.22. Impedance data measured from the untreated control sensor in 0.1 M mannitol before and after 10 minutes incubation with a high concentration bacterial suspension (9.12 ± 0.15 Log10 CFU/ml). Absolute impedance (|Z|), real impedance (Z') and imaginary impedance (Z'') data are presented for each measuring frequency.

Frequency (Hz)	Before			After		
	|Z| (Ω)	Z' (Ω)	-Z'' (Ω)	|Z| (Ω)	Z' (Ω)	-Z'' (Ω)
10^2	7364.4	2100.9	7058.4	17004.3	7016.1	15489.4
10^3	1121.4	258.9	1091.1	4302.9	3729.0	2148.8
10^4	145.0	53.9	134.6	3349.2	3226.3	898.9
10^5	42.8	39.5	16.6	1599.2	801.4	1383.9
10^6	37.3	36.8	5.6	193.2	25.0	191.6
10^7	23.4	21.0	10.3	20.8	11.2	17.5

Table 6.23 Impedance data measured from the biotin-avidin treated control sensor in 0.1 M mannitol before and after 10 minutes incubation with a high concentration bacterial suspension (9.10 ± 0.15 Log10 CFU/ml). Phages were immobilised onto the sensor surface by the biotin-avidin technique. Absolute impedance (|Z|), real impedance (Z') and imaginary impedance (Z'') data are presented for each measuring frequency.

Frequency (Hz)	Before			After		
	|Z| (Ω)	Z' (Ω)	-Z'' (Ω)	|Z| (Ω)	Z' (Ω)	-Z'' (Ω)
10^2	8557.5	2157.1	8281.1	18166.9	8912.0	15830.7
10^3	1190.2	303.0	1151.0	4709.7	3920.9	2609.1
10^4	182.6	89.3	159.3	3258.3	3065.1	1105.2
10^5	61.2	56.0	24.7	1392.6	718.0	1193.3
10^6	49.0	47.4	12.4	191.5	37.2	187.8
10^7	22.0	18.4	12.1	21.7	11.5	18.4

6.4.3 Discussion

6.4.3.1 Control Measurements

Prior impedance measurements of dry sensors were used to estimate variability across different sensors of the same electrode topology. A relative standard deviation of 3.3% suggests that sensor fabrication was reproducible. When comparing data from different sensors, differences in the results would have to exceed this value in

order to be considered significant and this was largely found to be the case, as will be discussed in the following sections.

When measurements were made in a control solution of 0.1% PW, it was found that there was a small consistent decrease in absolute impedance over time at each frequency analysed. An example of this was shown in Figure 6.12 for measurements at 1 kHz. This trend appeared to be a characteristic of the system under these conditions as it featured at some stage in all impedance measurements made in 0.1% PW, with or without bacteria present. It was observed that the change in absolute impedance over time was frequency dependent and the largest changes occurred at 1 MHz, as shown in Figure 6.15.

Time dependent variations in electrical measurements have previously been reported for simple electrodes in an electrolyte. For example, Moulton et al. (2004) stated that when determining the open circuit potential of their three electrode cell in 0.2 M PBS (the working electrode was gold), steady state was not achieved until after approximately 120 minutes. Typically an increase in impedance over time is reported [Moulton et al., 2004, Omanovic and Roscoe, 1999, Yang et al., 2003]. This has been attributed to the adsorption of proteins and other compounds onto the surface of the electrodes which hinder electron transfer and decrease electrode capacitance therefore increasing measured impedance. In opposition to this, a decrease in impedance over time was suggested in the control results presented by Oliver et al. (2006) in which impedance was measured from gold electrodes in a bacterial growth media (brain heart infusion media). Reasons for the trend were not discussed.

Here, impedance was found to consistently decrease over time. Possible explanations for the results observed will now be discussed. Firstly, returning to the work of Moulton et al. (2004), it was reported that no faradaic processes occurred for their electrode system in 0.2 M PBS at low applied voltages (between -200 mV and 700 mV) and only double layer charging was observed. Since the voltage applied here was also small (50 mV) it was anticipated that faradaic reactions involving ionic species present in 0.1% PW would also be minimal or avoided and therefore the

changes observed were likely to be due to non-faradaic electrode reactions or changes in the bulk solution. Given that measurements were taken in freshly prepared sterile media, properties of the bulk solution should be fairly constant. Therefore non-faradaic reactions seem the most likely cause of the time dependent decrease in impedance.

As discussed in Chapter 2, non-faradaic processes are complex. They can result from the adsorption and desorption of species on the electrode surface. Since every sensor was incubated with BSA for 30 minutes immediately prior to measurements in order to minimise non-specific adsorption [Huang et al., 2003], it is possible that some desorption of BSA may occur as the sensor equilibrates to the new environment (0.1% PW instead of PBS in which BSA was suspended). It was mentioned previously that adsorption has been found to cause an increase in impedance over time and so it is logical to conclude that desorption will result in the opposite effect. Based on this, desorption of BSA may be responsible for the changes in impedance observed here, or at least contribute towards them. In further support of this theory, it was noticed that when testing sensors in 0.1% PBS (Section 6.4.2.3.3), the impedance decrease was not as significant, as demonstrated in Figure 6.28. This perhaps indicates that desorption of BSA was not dominating measurements under these conditions as the sensor had not been subjected to as big a change in its external environment compared to the sensor placed in 0.1% PW. Instead, the adsorption of compounds in the PBS solution may now have more of an influence on impedance.

Another possible explanation for the constant decrease in impedance in the control results could be electrode delamination. During fabrication it was observed that gold electrode fingers would sometimes delaminate from the substrate suggesting that for some sensors there was poor adherence between the electrodes and the substrate. If this is the case for the sensors being tested then electrode seepage could be occurring during measurements i.e. solution could be entering gaps between the electrode and substrate around the electrode edges. This will effectively increase the electrode area

and lead to non-faradaic reactions which will alter impedance over time as the sensor adjusts to the wet conditions [Mirtaheri et al., 2005].

For the work carried out here, further investigations would be required to accurately determine the source of the time dependent impedance variations. It could be that if measurements had been extended over a longer period of time, a steady state may have been reached. However, for the results obtained it was decided to normalise the impedance measured from sensors against these control results with the aim of eliminating the electrode effects and revealing information on the effects of bacteria on sensor impedance over time.

In terms of the Nyquist plot, the profile of the control results appears to be of a large arc shape. There is perhaps some evidence of a small semicircle region at high frequencies which could be attributed to either the presence of the BSA layer or perhaps some faradaic reactions, although this latter explanation seems less likely at the low voltage applied. The results are similar to the control results presented by Moulton et al. (2004) in which impedance measurements were recorded for a gold sensor in 0.2 M PBS. Over the 60 minute testing period, a change in the Nyquist plot was observed at low frequencies (Figure 6.16) which could be attributed to changes in electron transfer resistance as the electrode surface equilibrates to its environment [Oliver et al., 2006].

6.4.3.2   Effect of Immobilised Bacteriophage Layer on Sensor Impedance

In the case of activated sensors it was assumed that phage immobilisation, either by physical adsorption or via biotin-avidin chemistry, was successful based on the immobilisation work presented in Chapter 5. Immobilised phage densities on the sensor surface were assumed to be similar to those reported from testing on the substrate material (Chapter 5, Section5.3.2).

The results presented in Sections 6.4.2.2 and 6.4.2.5 respectively showed that physically adsorbed phages caused a decrease in absolute impedance across the measured frequency range whilst phages immobilised by the biotin-avidin layer had the opposite effect and caused an increase in impedance. Although this discrepancy

was unexpected, viable theories can be put forward to explain it. These theories will now be discussed by first examining the physical adsorption results.

It is expected that phages will physically adsorb onto the gold electrodes as well as the substrate between electrodes [Lakshmanan et al., 2007, Olsen et al., 2006]. It was mentioned previously that the adsorption of proteins onto a gold electrode surface has been found to cause a decrease in electrode capacitance and an increase in electron transfer resistance, resulting in an overall increase in impedance [Moulton et al., 2004] and it has previously been reported by Yang et al. (2006) that covalently immobilised phages on a gold electrode resulted in an increase in electrode resistance across the frequency range 0.1 Hz to 100 kHz (less of a change was found in the region of 1 MHz). Therefore, an increase in absolute impedance instead of a decrease may have been expected here when phages were allowed to physically adsorb onto the sensor surface. Further to this, the decrease in impedance was considered significant as the percentage change between the activated and control sensor at each frequency (listed in Table 6.5) was greater than the 3.3% sensor reproducibility error reported in Section 6.4.2.1.

The result suggests that the presence of phages cannot be considered simply in terms of their effects on electrode capacitance and electron transfer resistance and that other processes are having an effect as well. One possible explanation for the results could be the retention of conductive species across the phage layer. In the physical adsorption process, phages were suspended in PBS and sensors were subsequently washed only three times. Therefore, ions from the phage suspension, including salts, may be retained on the surface of the sensor which could explain the reduced impedance observed. Less ion retention may be expected on samples with biotin-avidin immobilised phages as they were washed 10 times.

Nyquist plots are also useful for evaluating the effect of surface treatments such as adsorption [Moulton et al., 2004, Omanovic and Roscoe, 1999, Shabani et al., 2008]. The Nyquist plots for the sensors with and without physically adsorbed phages were similar (shown in Figure 6.19); the main difference between the results was observed

at low frequencies where the gradient of the activated data was seen to be larger than that for the control sensor. As outlined in Section 2.5 of Chapter 2, the linear portion of a Nyquist plot at low frequencies is characterised by slow electrode processes, such as diffusion. The results therefore indicate that the adsorbed phages could be having an effect on these diffusion processes; most likely they could be hindering diffusion across the electrode/electrolyte double layer. The results of the Nyquist plot at low frequencies are consistent with those presented by Moulton et al. (2004) who tested gold electrodes before and after exposure to antibodies in PBS and also Shabani et al. (2008) who covalently immobilised phages onto carbon micro-electrode arrays. A small difference between the activated and control sensor was also observed in the Nyquist plot at high frequencies: the real axis intercept of the activated sensor data was less than that for the control data. This intercept represents the solution resistance (as defined in Chapter 2, Section 2.5). The results therefore suggest that solution resistance was lower for measurements with the activated sensor. This could be related to increased conductivity due to the presence of retained salts as discussed previously.

In the case of phage immobilisation via biotin-avidin, the effects of the immobilisation process were much more evident than with physical adsorption (note that measurements were made in different solutions which may account for some of this difference). In Figure 6.35 it was shown that absolute impedance increased due to the biotin-avidin layer and then again after phage immobilisation. Changes were most notable over mid-frequency ranges (10 kHz to 1 MHz) and were greater than the reproducability error. This outcome is more in line with the expected effect of an immobilised phage layer. It is likely that, although the technique was optimised for the glass substrate, the biotin-avidin and phage layers were also present on the gold electrodes and as a result, electron transfer resistance at the electrodes increased and electrode capacitance decreased leading to an overall increase in impedance. This theory corresponds well with the changes in phase angle presented in Figure 6.41: after each treatement, capacitive effects at low frequencies were seen to decreases and as frequency increased, increased resistive effects became more apparant. It is acknoweldged that there is some inaccuracy in including the untreated sensor in the

comparison as it was of a slightly different electrode topology (see Table 6.18). However, consistent effects were still observed between identical sensors (biotin-avidin control and the activated sensor).
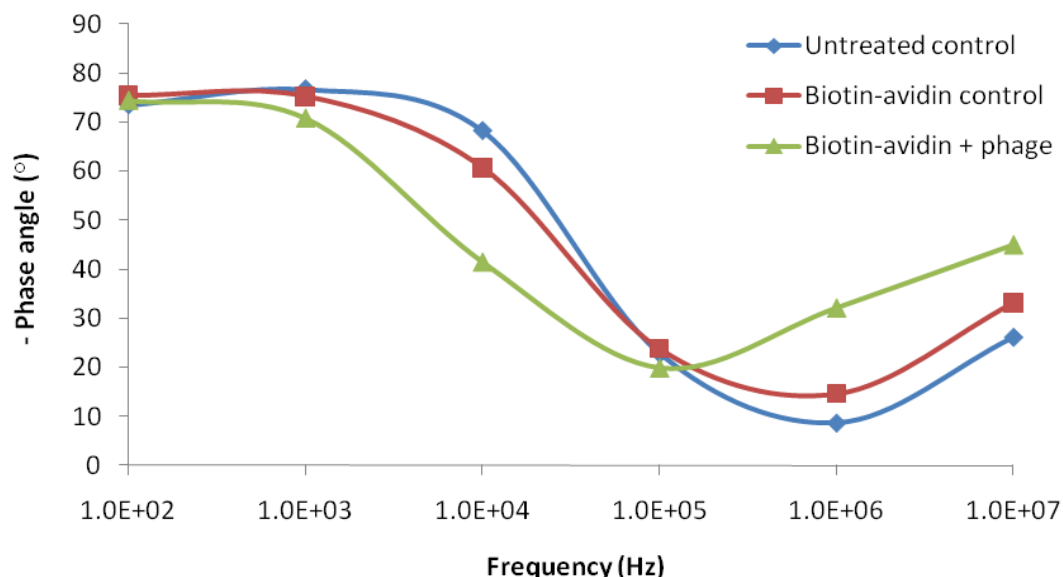
Figure 6.41. Bode plot of phage angle for sensors of Testing Method 2 before testing with bacteria. Impedance was measured from an untreated control sensor (W = 5 µm, G = 10 µm), a biotin-avidin only treated sensor (W = 3 µm, G = 10 µm) and a biotin-avidin treated sensor with phages (W = 3 µm, G = 10 µm). Measurements were carried out in 0.1 M mannitol.

A more defined semicircle region was present in the Nyquist plots for sensors with biotin-avidin immobilised phages (Figure 6.40) compared to that for physically adsorbed phages (Figure 6.19). This semicicle region is a typical characteristic of impedance measurements of biological material at high frequencies [Schwan, 1957]. It was observed that the diameter of the semicircle portion increased after consequative stages of the biotin-avidin immobilisation treatment. This confirms that electron transfer resistance increased with increasing stages of the immobilisation treatment (in Chapter 2, Section 2.5, it was described that by extending the semicircle to the x-axis, an indication of the electron transfer resistance can be obtained). This is consistent with results presented by Lasseter et al. (2004) who obseved an increase in semicircle diameter upon avidin binding to biotin immobilised onto a gold electrode. Yang et al. (2004b) and Shabani et al. (2008) also

demonstrated similar results when covalently immobilising antibodies and phages onto micro-electrode arrays respectively.

The lack of a clearly defined semicricle region in the Nyquist plot for physically adsorpbed phages could be attributed to the lower phage density levels compared to the biotin-avidin immobilisation technique as revealed in Chapter 5. Further to this, there is the multi layer nature of the biotin-avidin approach which is likely to lead to a more significant effect (i.e. the B-BSA layer, avidin and then biotinylated phages). The addition of a redox probe to the solution might have revealed a more distinct semicircle region in the results for the physically adorbed phages as was found by Moulton et al. (2004) for their testing of antibody adsorption onto gold electrodes.

A final point worth considering is the fact that phages had been stored in SM which contains gelatin (see Chapter 4, Section 4.1.3). Although the phages were washed three times with PBS, some gelatin is likely to remain and interact with the phage proteins and this could have an effect on the impedance observed and would be worth investigating.

6.4.3.3 Testing Method 1

As previously stated, it was decided to conduct initial bacterial detection measurements over time to try and relate impedance changes to bacterial capture levels obtained in the microscopy work of Section 6.1. Measurements were initially carried out in 0.1% PW as this suspending solution had previously been used by Radke and Alocilja (2004) who had implemented a sensor of similar topology with immobilised antibodies for bacterial detection. Comparisons could therefore be made with their work. Phages were immobilised by physical adsorption for Testing Method 1 due to the high immobilisation yield compared to other techniques and its mild nature (the biotin-avidin approach had not yet been developed at this stage).

It should be pointed out that care was taken to maintain consistency across comparable experiments by ensuring that certain variables remained constant, or as close to each other as reasonably possible. For example, bacterial suspensions were prepared in the same manner for each experiment and so were typically of similar

concentrations, in the same stage of the growth curve (lag phase – see Chapter 1, Section 1.5) and were used after the same acclimatisation period at room temperature (10 minutes). It was therefore anticipated that the different suspensions used would not contribute greatly to the outcome of experiments. Sensors of similar topology were also used when experiments were to be compared. Such measures were carried out to ensure that the results presented in Section 6.4 would reflect the detection of bacteria.

It is first worth discussing the observation that for the control sensor, the absolute impedance of the bacterial suspension was generally measured to be less than that of the control solution without bacteria (see Figure 6.20). This was especially notable at low frequencies (≤ 10 kHz) where differences between solutions with and without bacteria were greater than the 3.3% reproducibility error. This is not too surprising as it is reasonable to expect some conductive species to be transferred to the bacterial re-suspension from the broth culture despite the washing steps. Also, some ion leakage from the bacterial cells may occur upon re-suspension into fresh 0.1% PW. Both of these factors will result in a slightly more conductive external solution for the bacterial re-suspension and therefore reduced impedance. The results are in line with conductance measurements (Table 6.11) which showed the conductance of the bacterial suspension to exceed that of the blank solution over the 75 minutes testing period.

Similarly, the magnitude of absolute impedance measured from the activated sensor in a bacterial suspension was less than that for the control sensor in a bacterial suspension over the entire frequency range (see Figure 6.20 and also Figure 6.21). Differences were generally greater than the 3.3% reproducibility error. At times close to 0 minutes, this observation was expected as it was previously established in Section 6.4.2.2 that the physically adsorbed phage layer reduces sensor impedance. Therefore, assuming all other variables were the same for each sensor and that bacteria had not yet had time to interact with phages, the results are logical. Over time, it was expected to see changes in the activated sensor's impedance which could be correlated to the microscopy results of Section 6.1 where it was found that

numbers of bacteria captured onto a surface with immobilised phages increased. In addition to this it was expected that these changes in impedance would be significantly larger than any changes obtained from the control sensor. However, although impedance measured from the activated sensor initially increased over the first 5 to 15 minutes and changes appeared to be larger than that for the control sensor, absolute impedance soon began to follow the trend observed in the control results and consistently decreased with time. This made interpretation of the results difficult for establishing the bioreceptor performance of the phage layer. It was therefore decided to normalised values against the results from the control sensor in the blank solution. The aim of this approach was to effectively eliminate this background change in impedance and hopefully reveal the effect of the phage layer.

The normalised impedance results did reveal a difference between the activated and control sensor, examples of which were presented in Figure 6.22. When the background impedance is taken into consideration, control sensor impedance is relatively constant over time whilst the impedance of the activated sensor increased. This was the trend at low frequencies. At higher frequencies (100 kHz and 1 MHz), an increase in impedance was also observed with the control sensor but the increase for the activated sensor was larger. These results were quantitatively confirmed by calculating the percentage change in normalised impedance over the duration of the experiment for the activated and control sensor at each frequency. Results are listed in Table 6.24.

Table 6.24. Percentage change (Δ%) in normalised absolute impedance over 45 minutes for the control sensor and activated sensor in a bacterial suspension. Sensors were of the same electrode topology (W = 3 μm and G = 4 μm) and in the case of the activated sensor, phages were immobilised by overnight physical adsorption. Bacterial suspensions were of similar concentrations (see Table 6.7).

Frequency (Hz)	Δ% in normalised |Z| over 45 minutes	
	Control sensor	Activated sensor
10^2	-1.0	3.5
10^3	0.2	5.2
10^4	-1.2	4.3
10^5	1.0	4.1
10^6	4.5	9.8
10^7	-1.0	2.2

The constant increase in normalised impedance observed for the activated sensor and the overall larger change in normalised impedance over the duration of the experiment compared to the control sensor suggests that the presence of the phage layer is responsible for this effect. It could be argued that the difference may be due to changes occurring within the phage layer as, due to the limited supply of sensors, impedance was not measured over time for the activated sensor in a blank solution (such measurements may have also helped established the stability of the phage layer). However, in combination with the microscopy work in Section 6.1, it seems more plausible that phages have performed as previously demonstrated and interacted with bacteria thereby specifically drawing them into the sensors electric field. If this is taken to be the case then it can be surmised from the results that bacteria have caused an increase in impedance. It can also be ruled out that the changes seen are due to bacterial growth as this would have resulted in a decrease in impedance [Cady et al., 1978]. The effects of bacterial growth are discussed further in the following section.

In addition to measuring impedance changes over time, the impedance of the bacterial suspension was also compared to that of a blank solution measured from the same activated sensor before bacteria application. Results were compared in Bode plots for the bacterial sample at 15 minutes (Figure 6.23), before impedance began to

decrease across all frequencies. An increase in impedance due to the bacterial suspension was observed, as confirmed by the normalised plot of Figure 6.25. Changes were larger than those observed for the control sensor for which a small decrease typically occurred. This is consistent with the computer aided modelling results of Chapter 3 from which it was predicted that the presence of bacteria in the sensor's electric field would result in a reduction in dielectric capacitance when measurements are made in a water based medium which in turn would cause an increase in impedance.

The experimental results are also in agreement with some published data. For example, Radke and Alocilja (2004) reported on a micro-scaled interdigitated gold electrode array with immobilised antibodies for the detection of bacteria. Sensors were immersed in bacterial suspensions of different concentration for 2 minutes. Impedance was found to increase in direct proportion to the concentration of the bacterial suspension. This was attributed to increased levels of bacteria attaching to the sensor surface which was confirmed by scanning electron microscopy. They also reported that impedance increased the longer the sensor was incubated with the sample. The reported change in impedance due to bacteria was substantial. For example, at 1 kHz the impedance of the blank solution was 328 Ω; after incubation with a bacterial suspension of 10^7 CFU/ml impedance was 71 868 Ω. Impedance therefore increased by a factor of 219. Surprisingly, Radke and Alocilja (2004) did not conduct measurements with a control sensor (a sensor without immobilised antibodies). The results obtained from increasing bacterial concentrations could therefore be due to bulk effects and the non-specific attachment of bacteria, although in later papers published by the group, specificity work was carried out which to some extent indicated the bioreceptor performance of immobilised antibodies [Radke and Alocilja, 2005b].

Varshney et al. (2007) have also developed an impedimetric biosensor for the detection of bacteria which utilises a gold interdigitated micro-electrode array. Instead of implementing immobilised bioreceptors to capture bacteria, the group added magnetic nanoparticle-antibody conjugates to the sample prior to detection

and used a magnetic field and then microfluidics to concentrate and collect bacteria in the active area of the sensor (a few microns above the surface of the electrodes). The group reported impedance to increase a maximum of 2.6 times at 16 kHz when a test solution of 8.4×10^7 CFU/ml was used compared to a blank control. The smaller increase in the results of Varshney et al. (2007) compared to Radke and Alocilja (2004) could be attributed to the different approaches to applying the bacterial sample: Varshney et al. (2007) used a fluid flow system at a rate of 10 µl/min with bacteria suspended in 0.1 M mannitol whilst Radke and Alocilja (2004) immersed the sensor into the sample (bacteria were suspended in a mixed solution of 0.1% PW and phosphate buffer). Other recent examples of published biosensor literature reporting an increase in impedance due to the presence of bacteria include de la Rica et al. (2009), Kim et al. (2009) and Nandakumar et al. (2008).

The changes detected with the present sensor, although in agreement with some published data in terms of indicating an increase in impedance due to bacteria, were considerably smaller than those reported in the literature in terms of magnitude. For example, at 1 kHz impedance due to bacteria increased a maximum 1.08 times compared to a factor of 219 reported by Radke and Alocilja (2004). The results presented here are probably a slight underestimation for the sensor as impedance measurements of the bacterial suspension at t = 15 minutes had to be compared to the blank measurements at t = 0 minutes. However, correcting this inconsistency is unlikely to lead to large improvements. The maximum increase in impedance for the present sensor was recorded at 1 MHz after 5 minutes when impedance increased 1.14 times due to bacteria, as shown in Figure 6.26. Changes in impedance were consistently found to be greatest at 1 MHz at each time interval when monitored over time (see Table 6.24). This was surprising as it had been expected that current would begin to penetrate the bacterial cell membrane at high frequencies at which point the bacterial cells no longer behave as insulating particles [Grimnes and Martinsen, 2000]. Experimental results in published works also conformed to this theory [de la Rica et al., 2009, Radke and Alocilja, 2004, Varshney et al., 2007]. The effects at high frequency will be discussed further in Section 6.4.3.5.

The work of Shabani et al. (2008) is perhaps particularly noteworthy as they also implemented immobilised phages as bioreceptors with an impedimetric sensor. Shabani et al. (2008) report an initial increase in impedance shift of approximately 1.9×10^4 Ω but they did not quote the measuring frequency. The largest changes observed here for Testing Method 1 were more in the region of 10 Ω. Possible reasons as to why the changes observed in this work were lower than that reported by Shabani et al. could include differences in: sensor layout and construction, the suspending solution and immobilisation method (Shabani et al. used a three-carbon electrode setup, bacteria were suspended in SM buffer and phages were immobilised through covalent chemical coupling).

Interestingly, Shabani et al. (2008) also investigated using the lytic effect of phages to detect bacteria which was a consideration with the sensor investigated in this work. Upon lysis of bacteria, the intercellular contents will be released. This will include conductive ionic species and should cause a local increase in conductivity and therefore a reduction in impedance. Indeed, after 20 minutes of sensor incubation with the bacterial suspension, Shabani et al. (2008) reported a distinct reduction in impedance (after an initial increase in impedance) which they attributed to lysis of the captured bacteria. Lysis was confirmed with fluorescent microscopy. Such a distinctive reduction in impedance was not observed in the results obtained with the present sensor. A possible reason for this may be that levels of captured bacteria were too low to illicit a response more significant than the background decrease in impedance shown to occur with the sensors. Another consideration is that the bacterium-phage interaction is taking place at room temperature i.e. at a temperature lower than optimal conditions for bacterial growth (37°C) and so it was anticipated that lysis would occur after an extended latent period (longer that the 25 minutes at optimal conditions), perhaps outside the 45 minute testing period.

A potentially significant difference between the work carried out here and some of the literature mentioned (Radke and Alocilja (2004) and Shabani et al. (2008)) is the bacterial species used. Whilst *S. aureus* was used in the work here, Radke and Alocilja (2004) and Shabani et al. (2008) used *E. coli* and there are some significant

differences between these bacterial species which could be influencing results. For example, *E. coli* are not as prone to forming clusters of bacteria like *S. aureus* do. *E. coli* are also cylindrical in shape compared to the spherical shape of *S. aureus*. These differences may be contributing to the differences observed between biosensor performances.

The analysis of the present sensor focused primarily on monitoring changes in impedance (over time and between solutions with and without bacteria) and comparing the changes obtained with published results. Making a reliable comparison of the magnitude of absolute impedance would be difficult due to the different treatments applied to sensors and varying bacterial strains used across the literature. However, it was interesting to note that the magnitude of impedance obtained here was close to values reported by Radke and Alocilja (2004) who also carried out testing in 0.1% PW based solutions. For example, at 1 kHz the absolute impedance value for the blank solution measured by their activated sensor was 328 Ω which compared well with the blank solution measurement made from the activated sensor investigated here (455 Ω).

The Nyquist plots of the control and activated sensor after 15 minutes also showed only a small difference between the sensors with and without phages and were similar to the control and activated senor results without bacteria in Figure 6.19. Of most significance perhaps was the fact that there was no clear difference at high frequencies where a more defined semicircle portion in the activated sensor results might have indicated the presence of captured bacteria. These semicircular regions were present in Nyquist plots presented by Radke and Alocilja (2004). The results found here, in combination with the small changes in absolute impedance, suggest that only low levels of bacteria were captured by the sensors.

The limits of detection being achieved by recently developed biosensors are in the region of 10^2 CFU/ml [de la Rica et al., 2009, Nandakumar et al., 2008, Varshney et al., 2007]. Based on the results obtained with Testing Method 1, it was concluded that the existing biosensor, although able to indicate the presence of bacteria within

273

15 minutes when applied in high concentrations (10^8 CFU/ml), would not be sensitive enough under the present conditions if low levels of bacteria are to be detected. The changes due to bacteria were small and appear to eventually be dominated by the residual electrode effects identified in the control work. Possible reasons for the lack of sensitivity were considered and included: bacterial growth; the measurement conditions (such as the impedance of the suspending solution and the testing method); and/or too few interactions between bacteria and phages due to low levels of immobilised phages. The subsequent experimental work was designed to investigate some of these factors with a view to improving sensor sensitivity.

6.4.3.4 Effect of Bacterial Growth

In Testing Method 1, the enumeration of the bacterial suspension before and after the experiment suggested that some bacterial growth was occurring (Table 6.11). It was assumed that, having been re-suspended from an overnight broth into a fresh medium containing nutrients (0.1% PW), the bacteria would enter the lag phase of the growth curve (refer to Chapter 1, Section 1.5). Although temperature conditions were not optimal, some slow bacterial growth might be expected as it is known that *S. aureus* can grow in 0.1% PW [Acumedia, 2004]. It is also known that bacterial growth results in a decrease in impedance which is consistent with the increase in conductance measured from the bacterial suspension, also reported in Table 6.11 [Cady et al., 1978, Eden and Eden, 1984, Ur and Brown, 1975].

In light of this, it could be that effects arising from slow bacterial growth could be having a detrimental effect on the detection of bacteria and may also be contributing to the decrease in impedance over time for bacterial suspensions. The effects of bacterial growth on impedance measurements were explored by repeating the experiment of Testing Method 1 with bacteria re-suspended in 0.1% PBS. Bacteria were not expected to grow in 0.1% PBS due to the lack of nutrients available, thus bacteria were likely to remain in the stationary phase of the growth curve after the previous overnight incubation. A 10 fold dilution of PBS was used to yield a 0.1% PBS solution. This reduced salt conductivity and produced a suspending solution of similar conductance to 0.1% PW. Prevention of bacterial growth was confirmed through enumeration and conductance measurements of the bacterial

suspension before and after 75 minutes incubation at room temperature (Table 6.13). Since there was no significant difference in the enumeration results, bacteria viability in 0.1% PBS over this period of time was also confirmed.

The results of testing in 0.1% PBS, however, did not reveal any improvement on the results obtained in 0.1% PW, as indicated by Figure 6.28. In fact, the plot of normalised impedance for measurements in 0.1% PW and 0.1% PBS in Figure 6.29 revealed there to be comparatively smaller changes in 0.1% PBS. This is despite the 0.1% PBS sensor being incubated with a higher phage concentration during sensor activation (Table 6.12). This suggests that bacterial growth was not having a detrimental effect on impedance measurements over the testing period investigated.

6.4.3.5 Nylon Bead Testing

As outlined in Section 6.4.2.4, a sensitivity test was devised to further investigate the performance of the sensor. The experiment, which involved testing an untreated sensor with a suspension of nylon beads, was designed to eliminate experimental variables such as the phage layer and bacteria and to simply test the sensor's response to the presence of insulating particles in the sensor's electric field. Initially, the beads were suspended in the original test solution (0.1% PW). The beads were observed to naturally sediment over time through gravitational effects. It was intended to use a nylon bead suspension of higher percentage volume than the bacterial suspension in order to try and ensure a response from the sensor. At a concentration of approximately 2×10^7 beads/ml, the percentage volume occupied by the beads was estimated to be 8.4%. The estimated percentage volume for a bacterial suspension of 8×10^8 CFU/ml, as was typically applied in sensor testing, was 0.04%.

The results of the nylon bead testing in 0.1% PW, displayed in Figure 6.30 and Figure 6.31, showed that the nylon beads caused an increase in absolute impedance with respect to the blank solution. The maximum increase was by a factor of 1.19 at 10 kHz obtained after 5 minutes (Figure 6.31). This is close to normalised impedance values obtained from the activated sensor with bacteria when absolute impedance was normalised against the blank solution impedance measured by the activated sensor (Figure 6.26). In terms of analysing impedance changes over time, the largest

increase in impedance for the nylon bead suspension was over the first 5 minutes but due to the relatively fast sedimentation of the nylon beads it was accepted that analysing temporal effects is perhaps not a practical approach.

At high frequencies (1 MHz and 10 MHz), it can be seen from Figure 6.31 that the impedance values of solutions with and without the nylon beads were comparable. This could be indicative of poor sensor sensitivity at frequencies of and above 1 MHz. If this is the case however, it is even more surprising that the maximum increase in impedance due to bacteria in Testing Method 1 was found to be at 1 MHz, as reported in Section 6.4.2.3.2. Since this result did not correspond with the expected behaviour of impedance measurements of bacteria [Grimnes and Martinsen, 2000] (as first mentioned in Section 6.4.3.3) or with results in published literature [de la Rica et al., 2007, Radke and Alocilja, 2004, Varshney et al., 2007] it is considered that experimental results in this high frequency region (1 MHz to 10 MHz) should be treated cautiously.

In agreement with this, it was noticed that phase angle measurements of the nylon bead suspension turned positive at 10 MHz; a trend which was also exhibited with activated sensor measurements of the bacterial suspensions (Figure 6.23(b)). This indicates the onset of some inductive behaviour, possibly due to inductance of the sensor and connecting wires [Katz and Willner, 2003], and could explain the results being obtained in this high frequency region.

The nylon bead test was repeated with the beads suspended in distilled water to investigate whether carrying out measurements in a solution of lower conductivity could improve sensitivity. In this case, larger changes in impedance were observed compared to measurements in 0.1% PW, as demonstrated in Figure 6.33. The maximum increase was by a factor of 4.26 after 20 minutes (Figure 6.34). Interestingly, the variation of normalised impedance with frequency also appears to be dependent upon the suspending solution used. By comparing Figure 6.31 and Figure 6.34, the peaks relating to maximum changes in impedance occur at different frequencies for each solution: 10 kHz in 0.1% PW and 100 kHz in distilled water.

However, at high frequencies (above 1 MHz), normalised values close to 1 were seen for both solutions and, for distilled water, impedance of the suspension with nylon beads was now less than that without beads. This furthers the notion of reduced sensitivity and unreliable measurements at high frequencies.

The changes obtained with distilled water were closer to literature results, certainly those reported by Varshney et al. (2007) in which impedance increased 2.6 times when testing was conducted with a sample of high bacterial concentration in 0.1 M mannitol (a relatively low conductivity solution). The larger changes obtained in distilled water could be due to improved sensitivity of the sensor system when higher background impedances are used as the impedance of distilled water is higher than that of 0.1% PW, as illustrated by comparing Figure 6.30 and Figure 6.32, although there was again very little difference at 10 MHz. (This theory may also be responsible for the smaller changes obtained in 0.1% PBS compared to 0.1% PW reported in Section 6.4.2.3.3.) Another possible explanation could be the reduction of any electrochemical effects or other electrode processes due to conductive species, peptides and other molecules present in 0.1% PW. Based on the nylon bead testing results, it was decided to carry out bacterial testing in a solution of lower conductivity, the results of which are discussed in the following section.

6.4.3.6 Testing Method 2

The nylon bead testing revealed improved sensitivity when measurements were carried out in distilled water. However, water was not considered a suitable suspending solution for bacteria as pure water can cause osmosis and ion leakage across the bacterial cell membrane which can eventually result in cell lysis [Lodish et al., 2000]. Therefore a more suitable low conductivity solution was sought.

Mannitol is a sugar alcohol and is the main ingredient of mannitol salt agar in which *S. aureus* can grow. Mannitol solution (0.1 M) had previously been used to re-suspend bacteria for electrical based bacterial detection investigations and so was considered here [Suehiro et al., 1999, Varshney et al., 2007]. Conductance measurements confirmed its low conductivity compared to 0.1% PW, as illustrated by comparing Table 6.11 and Table 6.19. The behaviour of bacteria in

0.1 M mannitol was first monitored by enumerating bacterial re-suspensions before and after a 75 minutes incubation period at room temperature and also by measuring conductance over this period. It was expected that any bacterial growth would be minimal as although *S. aureus* can grow in mannitol salt agar, 0.1 M mannitol consists of mannitol only and not the other ingredients of mannitol salt agar (such as salts and peptones) which are favourable for growth. The results, displayed in Table 6.10, showed only a very small reduction in bacterial levels which was not statistically significant. This suggests that bacteria are not growing but remain viable over 75 minutes. There was a rise in conductance which, if due to bacterial growth and/or cell lysis, effects were not significant enough to be reflected in the bacterial counts. Based on this analysis, 0.1 M mannitol was considered a suitable suspending solution for bacteria. Surprisingly however, there was also a notable increase in the conductivity of 0.1 M mannitol without bacteria. This was unexpected and at present can not be accounted for as there was no corresponding temperature change which might explain the observation. The results warrant further investigation in order to understand the trend.

In addition to changing the suspending solution, other experimental parameters were altered with a view to improving results in Testing Method 2. Phages were immobilised via biotin-avidin chemistry which was shown to yield a higher immobilised phage density than physical adsorption used previously (see Chapter 5). The testing method was also altered; instead of monitoring a sample over time, impedance was measured before and after 10 minutes incubation in a bacterial suspension. Bacteria were not expected to immediately enter the exponential phase of the growth curve and were thus not expected to be growing. In addition to this, preparation and testing of the solution was within the 30 minute generation time for *S. aureus* (refer to Chapter 1, Section 1.5). Impedance measurements were carried out in fresh 0.1 M mannitol to provide a consistent background and to highlight any effects due to the presence of bacteria on the surface of the sensor by eliminating bulk effects from the bacterial suspension. Due to time constraints and a limited supply of sensors available, these aspects could not be investigated individually and were changed concurrently for Testing Method 2.

The results obtained from Testing Method 2 showed a much larger change in absolute impedance due to bacteria than those obtained from Testing Method 1. Results were presented in the form of Bode plots for the activated sensor in Figure 6.35 and show a clear difference between impedance measured before and after exposure to bacteria. Differences were most evident between 10 kHz and 100 kHz where the absolute impedance after incubation with bacteria was greater than before exposure to bacteria. Three distinct regions are identifiable from the Bode plots. At low frequencies, impedance decreases with increasing frequencies and phase angle values are close to -90°, indicative of capacitive behaviour. Over mid-range frequencies, impedance levels off and phase angle values decrease towards 0° which is more in line with resistive behaviour. At high frequencies, impedance begins to decrease again and phase angle values rise and so the sensor becomes capacitive again. The presence of bacteria appears to alter features of these regions, most notably in the resistive region. The trends are consistent with results published elsewhere for impedimetric biosensors for the detection of bacteria which were first discussed in Section 6.4.3.3 [de la Rica et al., 2009, Kim et al., 2009, Nandakumar et al., 2008, Radke and Alocilja, 2004, Varshney et al., 2007].

A common tool used to analyse impedance data is ECM. The theory behind ECM was introduced in Chapter 2. ECM was attempted with the data collected in Testing Method 2 using the software Zview 2 (Scribner Associates Inc, Solartron Analytical, Hampshire, UK). However, since only six data points were available across the frequency range, results from the ECM were not considered reliable. Instead, the ECM work carried out by other research groups developing similar biosensors was used to help analyse the trends observed here. For example, one of the most common and simplest circuit models found to accurately represent biosensors for the detection of bacteria consists of a capacitor-resistor-capacitor series combination in parallel with a capacitor, as illustrated in Figure 6.42. This model was successfully used by the research groups of Kim et al. (2009), Radke and Alocilja (2005a), Varshney et al. (2007) and Yang et al. (2004b) to represent data obtained from impedimetric sensors used to detect bacteria.
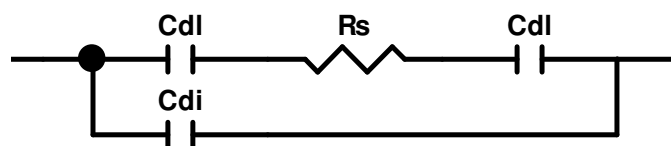
Figure 6.42. A frequently used equivalent circuit of an impedimetric biosensor. C_{dl} is the double layer capacitance, R_S is the bulk solution resistance and C_{di} is the dielectric capacitance of the solution.

The two double layer capacitors (C_{dl}) represent the capacitance for each electrode, in between which is the bulk medium resistance (R_S). Varshney et al. (2007) used CPEs to describe double layer capacitance, as is often used when modelling electrode behaviour (reasons for this were mentioned in Chapter 2, Section 2.5). The use of a CPE in an equivalent circuit model would also likely be suitable for representing the data collected in this work as the straight line portions in Nyquist plots were always at an angle less than 90° to the real axis and not perpendicular (refer to Chapter 2, Figure 2.13). The parallel capacitive component is said to represent the dielectric capacitance of the solution (C_{di}). The dielectric capacitance of the substrate appears to be largely ignored in the literature, presumably because it is so much smaller than that of the solution due to its comparatively low dielectric permittivity.

Based on the equivalent circuit of Figure 6.42, the three regions of the Bode plot identified previously can be described in terms of system parameters. At low frequencies, current is not able to pass through the C_{di} branch and the double layer capacitance dominates the signal whilst over mid frequency ranges bulk resistance becomes the main contributor to impedance. At higher frequencies, current will flow through the dielectric branch and the dielectric capacitance of the medium dominates the impedance signal.

Whilst values for circuit parameters can not be calculated with the data available here, the results can still be discussed in a qualitative manner in terms of the identified parameters by relating results to those of similar published work [Kim et al., 2009, Radke and Alocilja, 2005a, Varshney et al., 2007, Yang et al., 2004b]. For example, the largest changes observed for the activated sensor after exposure to

bacteria were over mid-range frequencies in the plateau region. Therefore, based on the proposed circuit of Figure 6.42 and previously published work, the main changes due to bacteria appear to be a result of changes in the bulk resistance (R_S). This is not surprising based on the theory of Chapter 2, Section 2.3.1, where it was discussed that a bacterium can be considered as a dielectric and that at lower frequencies current cannot penetrate the cell membrane and thus bacteria act as insulating particles. At higher frequencies, it is anticipated that current will begin to penetrate the cell membrane and the conductivity of the cell cytoplasm will have an effect. Varshney et al. (2007) also reported greatest changes in impedance due to bacteria in this resistive region and estimated a 95% increase in R_S based on ECM.

At lower frequencies, double layer capacitance dominates measurements based on the equivalent circuit and less of a change was observed in the results from the activated sensor. There was a small increase in impedance due to bacteria which would correspond with a decrease in C_{dl} according to Equation 2.9. This is again consistent with the results found by Varshney et al. (2007) who reported a 10% decrease in C_{dl}. This decrease in C_{dl} is likely to be a result of changes in the electrode double layer occurring due to the presence of bacteria. As bacteria become attached to the electrode, the area and thickness of the double layer will be altered. As previously mentioned, the adsorption of proteins onto electrodes has been found to result in a decrease in electrode capacitance [Luong et al., 2001, Moulton et al., 2004, Yang et al., 2003].

At high frequencies, again only a small change in impedance was observed from the activated sensor. Generally impedance was greater after exposure to bacteria but at 10 MHz the impedance of solutions with and without bacteria converged. The small increase in impedance due to bacteria is again consistent with the results of Varshney et al. (2007) who reported a 7.2% decrease in C_{di}. The decrease in dielectric capacitance is also consistent with the modelling work presented in Chapter 3 (although it should be remembered that the modelling work was based on a DC analysis). In addition to this, electric field theory for bacterial suspensions (Chapter 2, Section 2.3.1) suggests that at high frequencies, current begins to

penetrate the cell membrane. A decrease in capacitance is therefore conceivable when it is considered that the overall permittivity of bacteria is lower than that of the surrounding solution [Markx and Davey, 1999]. The convergence of the results at 10 MHz was not surprising as this had previously been seen in the nylon bead testing where it was concluded that measurements at this frequency were not reliable due to the development of inductive parameters. Another plausible reason for the convergence at higher frequencies could be the dominance of water dipole relaxations (discussed in Chapter 2, Section 2.3.1), though typically this phenomenon occurs closer to 25 MHz [Rigaud et al., 1996] and so such effects might have been expected at higher frequencies still.

Absolute impedance values were generally one order of magnitude larger for 0.1 M mannitol compared to 0.1% PW. Interestingly, it was observed that the impedance spectra collected in solutions of low conductance (0.1 M mannitol) were of a slightly different form to those collected in solutions of higher conductance (0.1% PW). Over the frequency range analysed, in solutions of higher conductance, the second capacitive region was not exhibited. This is consistent with the results of Yang (2008) who reported on the impedance of low and high conductivity solutions (distilled water and PBS respectively) as measured by a gold interdigitated microelectrode array. It appears that by carrying out measurements in the lower conductivity medium the resistive region of the Bode plot has shifted to a slightly lower frequency range (10 kHz to 100 kHz instead of 100 kHz to 10 MHz) where the sensor appears to be more sensitive to changes in the bulk solution.

The Nyquist plot also indicated the presence of bacteria on the sensor surface. Figure 6.38 shows a much larger semicircle diameter at high frequencies after exposure to bacteria compared to measurements before. As discussed in Section 6.4.3.2, this is likely to correspond to the presence of bacteria on and in between electrodes, preventing the passage of conductive species to electrodes and therefore increasing electron transfer resistance. The Nyquist plots are consistent with previously published works on biosensors used to detect bacteria [Radke and Alocilja, 2004, Shabani et al., 2008, Yang et al., 2004a].

The plot of normalised impedance in Figure 6.37 revealed that the maximum increase in impedance for the activated sensor occurred at approximately 40 kHz and was by an estimated factor of 8.5. However, despite the clear increase in impedance obtained with the activated sensor in Testing Method 2, the specific detection of bacteria by the immobilised phage layer was not confirmed because large changes in impedance after bacteria exposure were also found for the control sensors. This is illustrated in Figure 6.37 from which it was estimated that the maximum normalised impedance values for the untreated and biotin-avidin treated sensors were 38 (at 80 kHz) and 23.5 (at 6.5 kHz) respectively. The results suggest that bacteria are present on the surface of sensors after 10 minutes incubation with the bacterial sample regardless of the sensor's surface treatment and despite the subsequent washing step and prior surface blocking with BSA. In addition to this, the increase in impedance was actually seen to be larger for the control sensors than the activated sensor.

The larger semicircle portions in the Nyquist plots for the control sensors also suggests higher levels of bacteria are present on the control sensors (Figure 6.39). As discussed for the activated sensor, an increase in the semicircle diameter indicates increased electron transfer resistance probably due to increased levels of bacteria present on the sensor surface. The results therefore disagree with the microscopy work of Section 6.1 which showed a significant increase in the number of bacteria on glass substrates with immobilised phages compared to control substrates without phages. The high levels of bacteria on control sensors are obviously undesirable and eliminating this would be of primary importance in future work. As first mentioned in Section 6.4.3.3, some groups investigating the performance of bioreceptors immobilised onto interdigitated biosensors did not include a control sensor without bioreceptors in their publications, for example Radke and Alocilja (2004) and Kim et al (2009). Radke and Alocilja (2004) also did not incorporate a blocking step into sensor preparation to prevent non-specific adsorption of particles. A control sensor is considered important in verifying the performance of the bioreceptor and, as highlighted in the work presented here, it can be possible to obtain the desired sensor

response without the presence of the bioreceptor. Therefore there is some uncertainty over the validity of the claims in publications without suitable controls.

To explain the results of the control sensors it would have been logical to conclude that the washing step after bacterial incubation had not been adequate in removing excess bacteria which were non-specifically bound on the sensor surface. However, the washing step was the same as that applied in the microscopy work and so whilst further washing may improve the results if the experiment were to be repeated, it had been expected that the procedure would be adequate based on this previous work. Alternative possible explanations for the results were therefore explored.

The larger changes in impedance were found to correspond with slight differences in bacterial concentrations. As seen from Table 6.18, the highest bacterial concentration was applied to the untreated sensor which also exhibited the largest change in impedance. However, the differences between the mean concentrations of the bacterial suspensions were not found to be significant (by the one-way ANOVA test, $\alpha = 0.05$, followed by Tukey's comparison) and so this is unlikely to wholly account for the results observed. The slightly different electrode dimensions of the untreated sensor, although worth acknowledging, are also unlikely to fully account for the larger changes in impedance as the computer based modelling work of Chapter 3 suggested that sensors with electrodes of larger width (as is the case for the untreated sensor compared to the activated sensor) are less likely to be sensitive for detecting *S. aureus*. In addition to this, the biotin-avidin treated control sensor showed larger changes in impedance than the activated sensor with identical sensor topologies.

It is worth considering the work of Suehiro et al. (1999) at this stage. It was mentioned in Chapter 1 that conflicting results have been reported in the literature for the effect of bacteria on impedance. Thus far, literature reporting an increase in impedance due to bacteria present in the electric field of interdigitated microelectrode arrays have been considered as this was the trend discovered in Testing Method 1. On the other hand, Suehiro et al. (1999) indicated a decrease in impedance due to the presence of bacteria between electrodes.

Reasons for this discrepancy are not immediately clear but could be explained by the different detection techniques. Suehiro et al. (1999) used DEP (sometimes in combination with immobilised antibodies [Suehiro et al., 2006]) to capture bacteria between electrodes and in doing so chains of bacteria were formed which connected the electrodes (see Chapter 1, Section 1.2.2 for more details). It was reported that conductance and capacitance increased over time due to cell pearl chain formation. Reasons for this were not discussed in detail but the changes could be related to the surface conductivity of touching bacteria. It has been reported that the cell wall of bacteria have a relatively high conductivity (0.4 S/m) [Carstensen, 1967, Carstensen and Marquis, 1986]. This was first discussed in Chapter 1, Section 1.3.1. If bacteria are touching and in connection with the electrodes then a conductive pathway is provided which may be responsible for the increased conductance. Lu et al. (2008) reported increases in current with increasing numbers of bacteria connecting interdigitated electrodes after the sensor had been dried and this also infers a decrease in impedance due to the presence of bacteria connecting electrodes. In contrast to this approach, Radke and Alocilja used immobilised antibodies to capture bacteria between electrodes whilst Varshney et al. (2007) concentrated bacteria into an area above the sensor and so they will not necessarily form ordered pearl chain arrays between electrodes.

Based on this, it is proposed that two opposing mechanisms could be playing a role in determining the impedance due to the presence of bacteria between electrodes: the case where bacteria are insulated entities between the electrodes and cause a general increase in impedance and the case where bacteria connect with each other and the electrodes to form a conductive pathway which reduces impedance between electrodes. Applying this theory to the results found in this work could explain why smaller changes were observed from the activated sensor. For example, more bacteria could be present on the surface of the activated sensor, as expected, but so much so that chains of bacteria begin to form, connecting electrodes and resulting in an opposing effect on impedance. This is especially relevant to the case of *S. aureus* as they tend to form clusters.

Another potentially significant difference between the approaches of Radke and Alocilja (2004) and Suehiro et al. (1999) was the voltages used. Generally, when performing impedance measurements with EIS, relatively low voltages are applied (typically 50 – 100 mV [Radke and Alocilja, 2004, Varshney et al., 2007]). However, larger voltages are necessary to manipulate bacteria through DEP, for example Suehiro et al. (1999) used 10.7 V peak-to-peak. This in turn results in the application of different electric fields and it is known that electric field strength can have an important effect on cell membranes [Zimmermann and Neil, 1996]. For example, for electric field strengths in the region of 12 – 20 kV/cm, electropermeabilisation of the bacterial cell membrane can occur which can lead to the transfer of species, such as ions, across the cell membrane [Taketo, 1996]. For even higher electric fields, the cell membrane begins to irreversibly break down and cell lysis can occur [MacGregor et al., 2000]. These events could have an effect on measured conductivity and impedance. Therefore, whilst such electric field strengths are unlikely to be generated with microelectrodes when low voltages are applied (for example, the electric field strength generated by applying 50 mV across a 4 μm gap, as in the work of this study and also Radke and Alocilja (2004), is 0.13 kV/cm), they may be a consideration for larger voltages. The electric field strength for the case of Suehiro et al. (1999) was calculated to be in the region of 7.6 kV$_{rms}$/cm based on the voltage applied and the electrode gap. Although this value is considerably larger than that generated in works not using DEP, it is still outside of the quoted electropermeabilisation range. However, electropermeabilisation is ultimately dependent on the voltage induced across the cell membrane which in turn is dependent upon factors such as the treatment conditions, suspending medium parameters and also bacterial parameters and so electropermeabilisation can not be explicitly ruled out. Further investigation would be required in order to establish whether electropermeabilisation could be contributing to the results observed in Suehiro et al. (1999). Interestingly, Suehiro's research group later successfully investigated the possibility of utilising the electropermeabilisation of bacterial cells in combination with their DEP system to improve bacterial detection and in this case even higher voltages were used (20 V peak-to-peak) [Suehiro et al., 2005].

Returning to the work carried out in this study, another possible explanation for the smaller changes in impedance obtained from the activated sensor compared to control sensors without immobilised phages could be related to ion efflux occurring during phage-bacterium interactions as has been reported by Boulanger and Letellier (1988, 1992) and Glenn and Duckworth (1980). If ion efflux is significant, its effect may be sufficient to cause a reduction in impedance.

One final consideration is the fact that *S. aureus* are capable of secreting enzymes and toxins (such as enterotoxin as mentioned in Chapter 1, Section 1.5). The addition of these proteins may be influencing the impedance signal. Notably, proteases are secreted by *S. aureus* which break down proteins. This will be a consideration with regards to the BSA and phage layer on the sensor surface. Further work would be required to investigate the possible effect of secreted enzymes and toxins in order to establish the extent to which this may be a factor.

The theories discussed here are speculative. The fact that conflicting effects have been reported in the literature but have not been addressed highlight the complexities of this field and suggest that the fundamental effects of bacteria on biosensor impedance require further investigation and collaboration.

Overall however, the results have shown that the combination of reducing the conductivity of the suspending solution, increasing immobilised phage levels and carrying out measurements in a constant and controlled background solution have improved the sensitivity of the sensor.

6.5   Summary of Biosensor Testing

In Part I it was shown that immobilised phages increased the level of target bacteria captured onto a substrate surface. Electrical characteristics of the fabricated sensor were then discussed and it was reported that a concerning level of stray capacitance across the thin oxide layer was present when doped silicon substrates were used. This

stray capacitance was reduced by fabricating sensors onto glass substrates which were used in subsequent sensor fabrication and testing.

In Part II the results of the biosensor testing were reported. It was found that when bacterial detection was attempted with physically adsorbed phages and a high concentration of bacteria suspended in a solution of relatively high conductance (Testing Method 1), small increases in impedance could be detected within 15 minutes. Larger changes were obtained with activated sensors than control sensors (without immobilised phages) and so the results could be attributed to immobilised phages performing as bioreceptors.

To try and improve on these initial results, several variables were altered in Testing Method 2. It was found that larger changes in impedance due to bacteria could be obtained when phages were immobilised by the biotin-avidin technique (shown to yield a higher immobilised phage density in Chapter 5) and when discrete measurements were taken in a medium of lower conductivity before and after a 10 minute exposure to bacteria. However, under these conditions, larger changes were observed with control sensors, indicating that specific bacterial detection with immobilised phages had not been achieved. It is acknowledged that the lack of repeated experiments is a limitation to the work presented here and that performing experiments at least three times would help to establish trends and add confidence to the outcomes from this work. However, due to limited resources and time this was not possible.

In conclusion of the biosensor testing work, it was proposed that opposing mechanisms could be playing a role in determining the impedance changes due to bacteria depending on the level of bacteria captured between electrodes and as a result of the inherent structure of bacteria. It is clear that further detailed investigations into the area of impedimetric bacterial detection are required in order to confirm this theory and clarify conflicting published results. This could then lead to the advances in impedimetric detection necessary for it to become a sensitive rapid bacterial detection method.

Chapter 7

CONCLUSIONS AND FUTURE WORK

As discussed in Chapter 1, biosensors are showing promise in the field of rapid bacterial detection but are presently not yet capable of adequate sensitivity levels. In this study, a phage based interdigitated microelectrode array impedimetric biosensor was investigated for improved performance. The research comprised of three main areas of work: a computer based analysis to allow optimisation of the biosensor; an investigation and comparison of immobilisation methods for phages; and an experimental investigation of the phage based impedimetric biosensor. The following chapter will summarise each area of work and outline the main findings before coming to an overall conclusion. Also included in this chapter are some recommendations for future work.

7.1 <u>Conclusions</u>

7.1.1 Computer Based Modelling

A review of the literature revealed there to be very few reports on the use of CAE in biosensor development. Therefore a computer based model of the impedimetric biosensor was created in order to investigate the sensor's response to bacteria and to optimise biosensor design. The intention was to apply optimisation results to the actual biosensor design in order to improve biosensor performance.

A two-dimensional electrostatic model was developed based on a simplified model of *S. aureus* from which the following conclusions were drawn:

- The sensor was sensitive to the presence of bacteria and results were in line with some previously published experimental results.
- Saturation was observed when increasing layers of bacteria were introduced on top of the sensor; more than four layers did not result in further changes in capacitance.

- Improved sensitivity can be achieved through optimising sensor topology to the dimensions of the target bacteria. It was discovered that maximum sensitivity for detecting spherical bacteria 1 µm in diameter (modelled on *S. aureus*) was achieved with 3 µm wide electrodes and a 4 µm electrode gap.

- Properties of the external medium are important in defining the sensor's sensitivity; results suggested that conducting measurements in low permittivity media will lead to improvements in sensitivity.

Overall, the computer based model was a useful tool for investigating biosensor performance and could lead to significant improvements in biosensor performance. Results from this study were heeded in the design of the actual sensor and consequently several different sensor topologies were included for fabrication, the intention of which was to confirm, through experiments, that improved sensitivity can be achieved by optimising sensor topology for the target bacteria dimensions. However, due to time constraints and the development of some unexpected results (discussed in Section 7.1.3), this could not be carried out.

7.1.2 Bacteriophage Immobilisation

It is commonly acknowledged by experts that the bioreceptor immobilisation step plays an important role in determining the performance of a biosensor. For this reason, a broad selection of immobilisation methods were compared for the immobilisation of phages, such a study had not been performed previously. A FIA was successfully developed within this study to provide a quantitative means of comparing the immobilisation techniques.

Results showed that phage immobilisation densities varied significantly depending on the immobilisation method used. Of the immobilisation methods tested, immobilisation via biotin-avidin was found to be most suitable compared to physical adsorption, corona activation and covalent attachment via silane and glutaraldehyde. This conclusion was reached by considering not only phage immobilisation densities but also the physical effects of the immobilisation procedure on the sensor and its effect on phage activity. In the case of the biotin-avidin immobilisation procedure

implemented in this study, the method yielded the highest immobilised phage density, was relatively mild compared to other processes in terms of its potential side-effects on the sensor and optimisation was possible such that good levels of phage activity were retained after treatment. The results of the phage immobilisation investigation were used to guide the development of the actual biosensor.

7.1.3 Biosensor Investigation

In terms of successfully implementing the proposed biosensor, it was important to first demonstrate the ability of immobilised bacteriophage 9563 to perform as a bioreceptor, i.e. to capture bacteria onto a surface. Work undertaken in this study has shown that immobilised bacteriophage 9563 significantly increased the level of bacteria (*S. aureus* 8588) present on substrates and that levels of bacteria increased with increasing incubation time up to 20 minutes. The results were comparable to those obtained with immobilised antibodies but it is anticipated that the implementation of phage based bioreceptors will provide desirable benefits such as improved stability and low cost production, as previously listed in Chapter 1, Section 1.4.5.

Prior to immobilising phages onto the sensors, standard post-fabrication inspections of the sensors revealed that sensor capacitance was significantly higher than analytical predictions. This behaviour was determined to be caused by the presence of stray capacitance across the silicon dioxide layer of the sensor's substrate due to conduction through the doped silicon underneath. Following this discovery, sensors were fabricated onto glass wafers to avoid this stray capacitance masking impedance changes due to bacteria. The stray capacitance was shown to have been eliminated on glass substrates. This finding is important as the effects of stray capacitance on sensor sensitivity could be significant and indicates that care should be taken when developing sensors on doped semiconductor wafers.

In the initial testing of the biosensors, impedance was monitored over time (Testing Method 1). This approach was used because increasing levels of bacteria were expected to be captured onto the sensor's surface based on the bioreceptor testing results mentioned previously. It therefore seemed logical to expect corresponding

impedance changes. However, only a very small increase in impedance was detected (within 15 minutes), which was considerably less than published results obtained with similar biosensors.

In order to improve on the results observed in Testing Method 1, several variables were altered concurrently for Testing Method 2: the immobilised phage density was increased by immobilising phages with the biotin-avidin technique rather than physical adsorption; bacteria were suspended in a solution of lower conductance; and discrete impedance measurements before and after a 10 minute exposure to bacteria were compared rather than continuously monitoring impedance of the bacterial suspension. This successfully led to increased changes in impedance: impedance was found to increase by a factor of 8.5 due to the presence of bacteria under the conditions of Testing Method 2, compared to a factor of 1.14 with Testing Method 1. This could be a result of increased numbers of captured bacteria due to increased levels of immobilised phages with the biotin-avidin technique and/or the altered measuring conditions (lowered background conductivity and discrete measurements).

However, for Testing Method 2, it was found that larger changes were observed with the control sensors than with the phage activated sensor. This result suggests that there were high levels of non-specific bacterial binding and that selectivity had not been achieved. This was surprising considering that it had previously been shown that immobilised phages significantly increased levels of bacteria on a substrate compared to a surface without phages. Based on this, it is speculated that two opposing mechanisms may be occurring when bacteria are present in the inter-electrode space of microelectrodes: one mechanism which applies when bacteria are present between the electrodes as isolated entities and leads to an increase in impedance due to the insulating properties of the cell membrane; the other mechanism, which occurs at higher bacterial concentrations, lowers the measured impedance due to the presence of lower impedance channels formed by contact between the conductive cell walls as chains of bacteria developed between the electrodes. This theory could also explain the conflicting literature in this area and is particularly relevant for cluster forming bacteria such as *S. aureus* which was

investigated here. Indeed, it is surprising that the discrepancies that exist in the experimental data in the literature (detailed in Chapters 1 and 6) have not been more widely acknowledged and discussed. Substantial experimental work would be required to investigate this theory further, as discussed in the following future works section (Section 7.2).

Due to time limitations, it was not possible to progress the experimental testing of the biosensor as far as intended. Thus, although the initial studies of this sensor are promising, it is not possible to definitively conclude whether the phage based impedimetric biosensor presented here is an improvement on present biosensor technology from the data collected in this study; continued investigation is required. In particular, it was stated that one of the main objectives of this study was to develop a rapid detection system. In terms of the detection times achieved in this work, bacteria were detected within 10 to 15 minutes when concentrations of 10^8 CFU/ml were applied. However, lower concentrations could not be investigated in the time available and so the limit of detection for the sensor can not be established. It is obviously important to be able to detect much lower concentrations than 10^8 CFU/ml, ideally in the region of 1 to 10 CFU/ml. Whether such detection limits could be achieved with the present sensor and still within 15 minutes (i.e. without a pre-enrichment step) would need to be determined with further experimental work.

The study has also shown that the factors effecting the detection of bacteria using an impedimetric biosensor are more complex than have been reported in the literature published to date. It has revealed that there are a large number of variables involved which have yet to be fully explored in biosensor research. These variables include: the bacterial suspending solution, bioreceptor immobilisation procedure, voltage applied and bacterial sample application procedure. It is proposed that an in-depth investigation of these variables be conducted in order to gain a better understanding of impedimetric bacterial detection. This seems critical if present biosensor technology is to be exploited.

7.2 <u>Future work</u>

In this section, possible future work is outlined.

- First, it is suggested that the true effect of bacteria on impedance, measured from a typical impedimetric microelectrode biosensor, should be addressed in order to clarify the conflicting experimental results observed in this study and in the published literature. Reproducible experiments are required which will provide unequivocal results and determine conditions and parameters which affect impedance measurements. It is suggested that a systematic investigation be carried out with an impedimetric sensor, investigating variables individually. Such variables would include: bacterial concentration; the suspending medium; voltage; the bioreceptor immobilisation method; the measuring approach (for example, sample application technique and the level of washing incorporated); and the bacterial species.

- The computer based model should be expanded by incorporating the effects of conductivity and by constructing a periodic three-dimensional model. This would provide a more complete and advanced analysis which may prove particularly useful for investigating the theory that chains of bacteria, formed between electrodes, will decrease impedance (as discussed previously). In addition to this, the effects of AC potential signals should also be analysed in order to investigate optimal measuring frequencies.

- Improving bioreceptor immobilisation could be key to achieving adequate sensor sensitivity. Therefore the analysis of immobilisation methods for phages should be expanded further by including other established and novel immobilisation techniques in the study. In addition to the parameters investigated here, in future the selection of the appropriate immobilisation method should also be highlighted through the investigation and comparability of the stability of phages (immobilised by different techniques) over extended periods of time i.e. in the order of months.

- The non-specific binding of bacteria to sensors (as suggested in the control results of Testing Method 2) must be addressed if the present sensor is to represent a viable option for rapid bacterial detection. It is suggested that the

procedure for applying the bacterial sample be carefully examined – more thorough rinsing may be required after incubation with the bacterial sample.

- The detection limit of the sensor should be determined by testing it with decreasing bacterial concentrations. Also, due to time restrictions, the results of the modelling work could not be confirmed experimentally. It would therefore be useful to confirm that improved sensitivity can indeed be achieved by optimising sensor topology for specific target bacteria dimensions. Similarly, it would be of interest to investigate performing measurements in low permittivity media, as this was also identified as a potential approach to improving sensor sensitivity. Finally, the double electrode array sensor format described in Chapter 3, Section 3.2.2, remains to be tested in order to establish whether such a system would be an improvement on the standard interdigitated array format.

- In Chapter 3, Section 3.2.3, the role that platinum electrodes may play in improving sensor sensitivity through reduced polarisation effects was discussed [Schwan, 1966]. Therefore, it may prove useful to investigate platinising the gold electrodes of the sensor in future testing. Alternative electrode structures could also be investigated, such as an interdigitated castellated microelectrode geometry, which could prove to be more sensitive if regions of high electric field strength are better located in relation to the immobilised phage layer.

List of Publications

Webster, M. S., Timoshkin, I. V., MacGregor, S. J., Mattey, M. Computer aided modelling of an interdigitated microelectrode array impedance biosensor for the detection of bacteria. *IEEE Transactions on Dielectrics and Electrical Insulation*, 16 (2009), 1356-1363.

Webster, M. S., Timoshkin, I. V., MacGregor, S. J., Mattey, M. Analysis of the sensitivity of an impedimetric biosensor for the detection of bacteria. Proceedings of the IEEE Conference on Electrical Insulation and Dielectric Phenomena, Virginia Beach, USA, October 2009.

References

Acumedia, N. C. (2004) Peptone Water Product Information Sheet. PI 7365, Rev 01, 11/17/04.

Albuquerque, P., Mendes, M. V., Santos, C. L., Moradas-Ferreira, P. & Tavares, F. (2009) DNA signature-based approaches for bacterial detection and identification. *Science of the Total Environment,* 407**,** 3641-3651.

Asami, K., Hanai, T. & Koizumi, N. (1980) Dielectric Approach to Suspensions of Ellipsoidal Particles Covered with a Shell in Particular Reference to Biological Cells. *Japanese Journal of Applied Physics,* 19**,** 359-365.

Baeumner, A. J., Cohen, R. N., Miksic, V. & Min, J. H. (2003) RNA biosensor for the rapid detection of viable *Escherichia coli* in drinking water. *Biosensors & Bioelectronics,* 18**,** 405-413.

Bai, W., Zhao, K. S. & Asami, K. (2006) Dielectric properties of *E. coli* cell as simulated by the three-shell spheroidal model. *Biophysical Chemistry,* 122**,** 136-142.

Balasubramanian, S., Sorokulova, I. B., Vodyanoy, V. J. & Simonian, A. L. (2007) Lytic phage as a specific and selective probe for detection of *Staphylococcus aureus* - A surface plasmon resonance spectroscopic study. *Biosensors and Bioelectronics,* 22**,** 948-955.

Bardea, A., Katz, E. & Willner, I. (2000) Probing antigen-antibody interactions on electrode supports by the biocatalyzed precipitation of an insoluble product. *Electroanalysis,* 12**,** 1097-1106.

Behrens, S. H. & Grier, D. G. (2001) The charge of glass and silica surfaces. *Journal of Chemical Physics,* 115**,** 6716-6721.

Bell, E. L. (2008) Sequencing of bacteriophage 9563 genome. Unpublished Work. University of Strathclyde.

Bennett, A. R., Davids, F. G. C., Vlahodimou, S., Banks, J. G. & Betts, R. P. (1997) The use of bacteriophage-based systems for the separation and concentration of *Salmonella. Journal of Applied Microbiology,* 83**,** 259-265.

Berezhetskyy, A. (2007) Development of conductiometric biosensor based on alkaline phosphatase for the quality control of water. Lyon, Claude Bernard University.

Berkenpas, E., Millard, P. & Cunha, M. P. D. (2006) Detection of *Escherichia coli* O157:H7 with langasite pure shear horizontal surface acoustic wave sensors. *Biosenosrs and Bioelectronics,* 21**,** 2255-2262.

Beveridge, T. J. & Graham, L. L. (1991) Surface-layers of bacteria. *Microbiological Reviews,* 55**,** 684-705.

Bhatia, S. K., Shriverlake, L. C., Prior, K. J., Georger, J. H., Calvert, J. M., Bredehorst, R. & Ligler, F. S. (1989) Use of thiol-Terminal silanes and heterobifunctional crosslinkers for immobilization of antibodies on silica surfaces. *Analytical Biochemistry,* 178**,** 408-413.

Bickerstaff, G. F. (1997) *Immobilization of Enzymes and Cells*, Totowa, New Jersey, Humana Press Inc..

Blais, B. W., Leggate, J., Bosley, J. & Martinez-Perez, A. (2004) Comparison of fluorogenic and chromogenic assay systems in the detection of *Escherichia coli* O157 by a novel polymyxin-based ELISA. *Letters in Applied Microbiology,* 39**,** 516-522.

Boehm, D. A., Gottlieb, P. A. & Hua, S. Z. (2007) On-chip microfluidic biosensor for bacterial detection and identification. *Sensors and Actuators B-Chemical,* 126**,** 508-514.

Bolton, F. J. (1990) An investigation of indirect conductimetry for detection of some food-borne bacteria. *Journal of Applied Bacteriology,* 69**,** 655-661.

Bonini, F., Piletsky, S., Turner, A. P. F., Speghini, A. & Bossi, A. (2007) Surface imprinted beads for the recognition of human serum albumin. *Biosensors & Bioelectronics,* 22**,** 2322-2328.

Boonmee, W. (2009a) Latent period for *S. aureus* 8588 infected with bacteriophage 9563. Unpublished Work. The University of Strathclyde.

Boonmee, W. (2009b) Size of bacteriophage 9563 as estimated from Nanosight. Unpublished Work. The University of Strathclyde.

Boulanger, P. & Letellier, L. (1988) Characterization of ion channels involved in the penetration of phage T4 DNA into *Escherichia coli* cells. *Journal of Biological Chemistry,* 263**,** 9767-9775.

Boulanger, P. & Letellier, L. (1992) Ion channels are likely to be involved in the two steps of phage T5 DNA penetration into *Escherichia coli* cells. *The Journal of Biological Chemistry,* 267**,** 3168-3172.

Bremer, P. J., Fletcher, G. C. & Osborne, C. (2004) *Staphylococcus aureus*. Christchurch, New Zealand Institute for Crop and Food Research Limited.

Buerk, D. G. (1993) *Biosensors. Theory and Applications,* Lancaster, Pennsylvania, Technomic Publishing Compancy, Inc.

Byrne, B., Stack, E., Gilmartin, N. & O'kennedy, R. (2009) Antibody-based sensors: principles, problems and potential for detection of pathogens and associated toxins. *Sensors,* 9**,** 4407-4445.

Cady, P. (1975) Rapid automated bacterial identification by impedance measurement. IN HEDEN, C.-G. & ILLENI, T. (Eds.) *New Approaches to the identification of microorganisms.* John Wiley & Sons.

Cady, P., Dufour, S. W., Shaw, J. & Kraeger, S. J. (1978) Electrical impedance measurements: rapid method for detecting and monitoring mircroorganisms. *Journal of Clinical Microbiology,* 7**,** 265-272.

Campbell, R. M., Crichton, B. H., Fouracre, R. A., Timoshkin, I. V. & Given, M. J. (2006) Evaluation of induced voltage on biological cell membranes. *Proceedings of the 27th International Power Modulator Symposium and 2006 High Voltage Workshops***,** 502-505.

Cao, L. (2006) *Carrier-bound Immobilized Enzymes: Principles, Applications and Design*, Weinheim, Wiley.

Carnazza, S., Gioffre, G., Felici, F. & Guglielmino, S. (2007) Recombinant phage probes for *Listeria monocytogenes*. *Journal of Physics-Condensed Matter,* 19.

Carr, P. W. & Bowers, L. D. (1980) *Immobilized enzymes in analytical and clinical chemistry,* New York, John Wiley & Sons.

Carstensen, E. L. (1967) Passive electrical properties of microorganisms. II. Resistance of the bacterial membrane. *Biophysics Journal,* 7**,** 493-503.

Carstensen, E. L., H. A. Cox, J., Mercer, W. B. & Natale, L. A. (1965) Passive electrical properties of microorganisms. I. Conductivity of *Escherichia coli* and *Micrococcus lysodeikticus*. *Biophysics Journal,* 5**,** 289-300.

Carstensen, E. L. & Marquis, R. E. (1986) Passive electrical properties of microorganisms. III. Conductivity of isolated bacterial cell walls. *Biophysics Journal,* 8**,** 536-548.

Castellarnau, M., Errachid, A., Madrid, C., Juarez, A. & Samitier, J. (2006) Dielectrophoresis as a tool to characterize and differentiate isogenic mutants of *Escherichia coli*. *Biophysical Journal,* 91**,** 3937-3945.

Centers for Disease Control and Prevention (2002) *Staphylococcus aureus* resistant to vancomycin: United States, 2002. *Morbidity and Mortality Weekly Report,* 51**,** 565-567.

Chan, C. M., Ko, T. M. & Hiraoka, H. (1996) Polymer surface modification by plasmas and photons. *Surface Science Reports,* 24**,** 3-54.

Chemburu, S., Wilkins, E. & Abdel-Hamid, I. (2005) Detection of pathogenic bacteria in food samples using highly-dispersed carbon particles. *Biosenosrs and Bioelectronics,* 21**,** 491-499.

Chen, I. J. & Lindner, E. (2007) The stability of radio-frequency plasma-treated polydimethylsiloxane surfaces. *Langmuir,* 23**,** 3118-3122.

Clark, J. R. & March, J. B. (2006) Bacteriophages and biotechnology: vaccines, gene therapy and antibacterials. *Trends in Biotechnology,* 24**,** 212-218.

Collins, J. S. & Goldsmith, T. H. (1981) Spectral properties of fluorescence induced by glutaraldehyde fixation. *Journal of Histochemistry & Cytochemistry,* 29**,** 411-414.

Collins, K. E., Cronin, A. A., Rueedi, J., Pedley, S., Joyce, E., Humble, P. J. & Tellam, J. H. (2006) Fate and transport of bacteriophage in UK aquifers as surrogates for pathogenic viruses. *Engineering Geology,* 85**,** 33-38.

Cras, J. J., Rowe-Taitt, C. A., Nivens, D. A. & Ligler, F. S. (1999) Comparison of chemical cleaning methods of glass in preparation for silanization. *Biosensors & Bioelectronics,* 14**,** 683-688.

Creager, S. E. & Wooster, T. T. (1998) A new way of using ac voltammetry to study redox kinetics in electroactive monolayers. *Analytical Chemistry,* 70**,** 4257-4263.

Croci, L., Delibato, E., Volpe, G., De Medici, D. & Palleschi, G. (2004) Comparison of PCR, electrochemical enzyme-linked immunosorbent assays, and the standard culture method for detecting *Salmonella* in meat products. *Applied and Environmental Microbiology,* 70**,** 1393-1396.

Davey, C. L. & Kell, D. B. (1995) *The low-frequency dielectric properties of biological cells,* Zurisch, Birkauser.

De La Rica, R., Baldi, A., Fernandez-Sanchez, C. & Matsui, H. (2009) Selective detection of live pathogens via surface-confined electric field perturbation on interdigitated silicon transducers. *Analytical Chemistry,* 81**,** 3830-3835.

Deisingh, A. K. & Thompson, M. (2004) Biosensors for the detection of bacteria. *Canadian Journal of Microbiology,* 50**,** 69-77.

Department of Health (2006) Screening for methicillin-resistant *Staphylococcus aureus* (MRSA) colonisation: A strategy for HNS trusts: a summary of best practice.

Dézenclos, T., Ascon-Cabrera, M., Ascon, D., Lebeault, J.-M. & Pauss, A. (1994) Optimisation of the indirect impedancemetry technique; a handy technique for microbial growth measurement. *Applied Microbiology and Biotechnology,* 42**,** 232-238.

Dobozi-King, M., Seo, S., Kim, J. U., Young, R., Cheng, M. & Kish, L. B. (2005) Rapid detection and identification of bacteria: Sensing of phage-triggered ion cascade (SEPTIC). *Journal of Biological Physics and Chemistry,* 5**,** 3-7.

Dong, J. P., Wang, A. F., Ng, K. Y. S. & Mao, G. Z. (2006) Self-assembly of octadecyltrichlorosilane monolayers on silicon-based substrates by chemical vapor deposition. *Thin Solid Films,* 515**,** 2116-2122.

Dowd, S. E., Pillai, S. D., Wang, S. Y. & Corapcioglu, M. Y. (1998) Delineating the specific influence of virus isoelectric point and size on virus adsorption and transport through sandy soils. *Applied and Environmental Microbiology,* 64**,** 405-410.

EARSS (2004) European Antimicrobial Resistance Surveillance System (EARSS) Annual Report 2004.

Eden, G. & Eden, R. (1984) Enumeration of microorganisms by their dynamic AC conductive patterns. *IEEE Transactions on Biomedical Engineering,* 31**,** 1984.

Edgar, R., Mckinstry, M., Hwang, J., Oppenheim, A. B., Fekete, R. A., Giulian, G., Merril, C., Nagashima, K. & Adhya, S. (2006) High-sensitivity bacterial detection using biotin-tagged phage and quantum-dot nanocomplexes. *Proceedings of the National Academy of Sciences of the United States of America,* 103**,** 4841-4845.

Einolf, C. W. J. & Carstensen, E. L. (1969) Passive electrical properties of microorganisms IV. Studies of the protoplasts of *Micrococcus lysodeikticus*. *Biophysical Journal,* 9**,** 634-643.

Elsholz, B., Nitsche, A., Achenbach, J., Ellerbrok, H., Blohm, L., Albers, J., Pauli, G., Hintsche, R. & Worl, R. (2009) Electrical microarrays for highly sensitive detection of multiplex PCR products from biological agents. *Biosensors & Bioelectronics,* 24**,** 1737-1743.

Ercole, C., Gallo, M. D., Mosiello, L., Baccella, S. & Lepidi, A. (2003) *Escherichia coli* detection in vegetable food by a potentiometric biosensor. *Sensors and Actuators B,* 91**,** 163-168.

Ercole, C., Gallo, M. D., Pantalone, M., Santucci, S., Mosiello, L., Laconi, C. & Lepidi, A. (2002) A biosensor for *Escherichia coli* based on a potentiometric alternating biosensing (PAB) transducer. *Sensors and Actuators B,* 83**,** 48-52.

Eriksson, E. & Aspan, A. (2007) Comparison of culture, ELISA and PCR techniques for *Salmonella* detection in faecal samples for cattle, pig and poultry. *BMC Veterinary Research,* 3.

Farley, J., Stamper, P. D., Ross, T., Speser, S., Cai, M. & Carroll, K. C. (2007) Comparison of the IDI-MRSA^{TM} assay to culture using BBL^{TM} CHROMagar^{TM} MRSA for detection of MRSA from nasal surveillance cultures in an at-risk population. *Abstracts of the General Meeting of the American Society for Microbiology,* 107**,** 203.

Farrah, S. R. (1982) Chemical factors influencing adsorption of bacteriophage-Ms2 to membrane filters. *Applied and Environmental Microbiology,* 43**,** 659-663.

FDA (2004) *Bad Bug Book:Foodborne Pathogenic Microorganisms and Natural Toxins Handbook,* McLean, Virginia, International Medical Publishing, Inc.

Ferris, C. D. (1974) *Introduction to Bioelectrodes,* New York, Plenum Press.

Fester, T., Berg, R. H. & Taylor, C. G. (2008) An easy method using glutaraldehyde-introduced fluorescence for the microscopic analysis of plant biotrophic interactions. *Journal of Microscopy-Oxford,* 231**,** 342-348.

Foods Standard Agency (2009) Annual Report of the Chief Scientist 2008/9.

Fricke, H. (1925) A mathematical treatment of the electric conductivity and capacity of disperse systems ii. The capacity of a suspension of conducting spheroids surrounded by a non-conducting membrane for a current of low frequency. *Physical Review,* 26**,** 678.

Fricke, H. (1953) Relation of the permittivity of biological cell suspensions to fractional cell volume. *Nature,* 172**,** 731-2.

Fricke, H., Schwan, H. P., Li, K. & Bryson, V. (1956) A dielectric study of the low-conductance surface membrane in *E. coli. Nature,* 177**,** 134-5.

Fu, Z., Rogelj, S. & Kieft, T. L. (2005) Rapid detection of *Escherichia coli* O157:H7 by immunomagnetic separation and real-time PCR. *International Journal of Food Microbiology,* 99**,** 47-57.

Gehring, A. G., Irwin, P. L., Reed, S. A., Ttu, S.-I., Andreotti, P. E., Akhavan-Tafti, H. & Handley, R. S. (2004) Enzyme-linked immunomagnetic chemiluminescent detection of *Escherichia coli* O157:H7. *Journal of Immunological Methods,* 293**,** 97-106.

Gehring, A. G., Patterson, D. L. & Tu, S.-I. (1998) Use of a light-addressable potentiometric sensor for the detection of *Escherichia coli* O157:H7. *Analytical Biochemistry,* 258**,** 293-298.

German, G. J., Mirsa, R. & Kropinski, A. M. (2006) The T1-like bacteriophages. IN CALENDAR, R. (Ed.) *The bacteriophages.* 2nd ed. New York, Oxford University Press.

Gervais, L., Gel, M., Allain, B., Tolba, M., Brovko, L., Zourob, M., Mandeville, R., Griffiths, M. & Evoy, S. (2007) Immobilization of biotinylated bacteriophages on biosensor surfaces. *Sensors and Actuators B-Chemical,* 125**,** 615-621.

Glenn, J. & Duckworth, D. H. (1980) Ion fluxes during T5 bacteriophage infection of *Escherichia coli. Archieves of Biochemistry and Biophysics,* 201**,** 576-585.

Gomez-Sjoberg, R., Morisette, D. T. & Bashir, R. (2005) Impedance microbiology-on-a-chip: microfluidic bioprocessor for rapid detection of bacterial metabolism. *Journal of Microelectromechanical Systems,* 14**,** 829-838.

Goodridge, L. & Abedon, S. T. (2003) Bacteriophage biocontrol and bioprocessing: Application of phage therapy to industry. *SIM News,* 53**,** 254-262.

Goodridge, L., Chen, J. & Griffiths, M. (1999) Development and characterization of a fluorescent-bacteriophage assay for detection of *Escherichia coli* O157:H7. *Applied and Environmental Microbiology,* 65**,** 1397-1404.

Goodridge, L. & Griffiths, M. (2002) Reporter bacteriophage assays as a means to detect foodborne pathogenic bacteria. *Food Research International,* 35**,** 863-870.

Gorman, S. P., Scott, E. M. & Russell, A. D. (1980) Anti-microbial activity, uses and mechanism of action of glutaraldehyde. *Journal of Applied Bacteriology,* 48**,** 161-190.

Green, N. M. (1963) Avidin. 1. The use of (14-C)biotin for kinetic studies and for assay. *Biochemical Journal,* 89**,** 585-91.

Grimnes, S. & Martinsen, O. G. (2000) *Bioimpedance and bioelectricity basics,* London, Academic Press.

Hafeman, D. G., Parce, J. W. & Mcconnell, H. M. (1988) Light-addressable potentiometric sensor for biochemical systems. *Science,* 240**,** 1182-1185.

Hahm, B. K. & Bhunia, A. K. (2006) Effect of environmental stresses on antibody-based detection of *Escherichia coli* O157:H7, *Salmonella enterica* serotype *Enteritidis* and *Listeria monocytogenes. Journal of Applied Microbiology,* 100**,** 1017-1027.

Hammond, P. (1997) *Electromagnetism for engineers: an introductory course*, Oxford, Oxford Science Publications.

Han, J. H., Heinze, B. C. & Yoon, J. Y. (2008) Single cell level detection of *Escherichia coli* in microfluidic device. *Biosensors & Bioelectronics,* 23**,** 1303-1306.

Handa, H., Gurczynski, S., Jackson, M. P., Auner, G., Walker, J. & Mao, G. (2008) Recognition of *Salmonella typhimurium* by immobilized phage P22 monolayers. *Surface Science,* 602**,** 1392-1400.

Hao, R. Z., Wang, D. B., Zhang, X. E., Zuo, G. M., Wei, H. P., Yang, R. F., Zhang, Z. P., Cheng, Z. X., Guo, Y. C., Cui, Z. Q. & Zhou, Y. F. (2009) Rapid detection of *Bacillus anthracis* using monoclonal antibody functionalized QCM sensor. *Biosensors & Bioelectronics,* 24**,** 1330-1335.

Health Protection Agency (2009) Quarterly Report for *C. difficle* infections - April 2007 to June 2009.

Holland, F. (2010) Prevention and treatment of wound and systematic methicillin Resistant *Staphyloccocus aureus* (MRSA) infection by immobilised bacteriophage in a rat model. *SIPBS*. Glasgow, University of Strathclyde.

Holt, G. H., Krieg, N. R., Sneath, P. H. A., Staley, J. T. & Williams, S. T. (2000) *Bergey's manual of determinative bacteriology,* Philadelphia, Lippincott Williams and Wilkins.

Huang, T. T., Sturgis, J., Gomez, R., Geng, T., Bashir, R., Bhunia, A. K., Robinson, J. P. & Ladisch, M. R. (2003) Composite surface for blocking bacterial adsorption on protein biochips. *Biotechnology and Bioengineering,* 81**,** 618-624.

Huang, Y., Holzel, R., Pethig, R. & Wang, X. B. (1992) Differences in the AC electrodynamics of viable and non-viable yeast cells determined through combined dielectrophoresis and electrorotation studies. *Phys Med Biol,* 37**,** 1499-517.

Huletsky, A., Giroux, R., Rossbach, V., Gagnon, M., Vaillancourt, M., Bernier, M., Gagnon, F., Truchon, K., Bastien, M., Picard, F. J., Van Belkum, A., Ouellette, M., Roy, P. H. & Bergeron, M. G. (2004) New real-time PCR assay for rapid detection of methicillin-resistant *Staphylococcus aureus* directly from specimens containing a mixture of *staphylococci. Journal of Clinical Microbiology,* 42**,** 1875-1884.

Hutson, D. (2008) Fabrication limits of the photolithography equipment at the Univesity of Strathclyde. Personal Communication.

Imai, K., Yoshimura, K., Tomitori, M., Nishikawa, O., Kokawa, R., Yamamoto, M., Kobayashi, M. & Ikai, A. (1993) Scanning tunneling and atomic-force microscopy of T4-bacteriophage and tobacco mosaic-virus. *Japanese Journal of Applied Physics Part 1-Regular Papers Short Notes & Review Papers,* 32**,** 2962-2964.

Integrated Engineering Software (2001) ELECTRO 2D/RS. 6.2 ed.

Integrated Engineering Software (2009) ELECTRO product sheet.

Israel, D., Barry, W. H., Edell, D. J. & Mark, R. G. (1984) An array of microelectrodes to stimulate and record from cardiac-cells in culture. *American Journal of Physiology,* 247**,** H669-H674.

Ivnitski, D., Abdel-Hamid, I., Atanasov, P. & Wilkins, E. (1999) Biosensors for detection of pathogenic bacteria. *Biosensors and Bioelectronics,* 14**,** 599-624.

Jouy, E., Proux, K., Humbert, F., Rose, V., Lalande, F., Houdayer, C., Picault, J. P. & Salvat, G. (2005) Evaluation of a French ELISA for the detection of *Salmonella enteritidis* and *Salmonella typhimurium* in flocks of laying and breeding hens. *Preventive Veterinary Medicine,* 71**,** 91-103.

Katz, E. & Willner, I. (2003) Probing biomolecular interactions at conductive and semiconductive surfaces by impedance spectroscopy: routes to impedimetric immunosensors, DNA-sensors, and enzyme biosensors. *Electroanalysis,* 15**,** 913-947.

Kessick, M. A. & Wagner, R. A. (1978) Electrophoretic mobilities of virus adsorbing filter materials. *Water Research,* 12**,** 263-268.

Kidner, N. J., Homrighaus, Z. J., Mason, T. O. & Garboczi, E. J. (2006) Modeling interdigital electrode structures for the dielectric characterization of electroceramic thin films. *Thin Solid Films,* 496**,** 539-545.

Kierstan, M. P. J. & Coughlan, M. P. (1991) Immobilization of protein by noncovalent procedures: principles and applications. IN TAYLOR, R. F. (Ed.) *Protein immobilization: fundamentals and applications.* 1st ed. New York, Marcel Dekker, Inc.

Kim, G., Moon, J. H., Hahm, B. K., Morgan, M., Bhunia, A. & Om, A. S. (2009) Rapid detection of *Salmonella enteritidis* in Pork Samples with impedimetric biosensor: effect of electrode spacing on sensitivity. *Food Science and Biotechnology,* 18**,** 89-94.

Koo, O. K., Liu, Y. S., Shuaib, S., Bhattacharya, S., Ladisch, M. R., Bashir, R. & Bhunia, A. K. (2009) Targeted capture of pathogenic bacteria using a mammalian cell receptor coupled with dielectrophoresis on a biochip. *Analytical Chemistry,* 81**,** 3094-3101.

Kutter, E. & Sulakvelidze, A. (2004) *Bacteriophages: Biology and Applications*, Boca Raton, CRC Press.

Lakdawala, V., Noel, M. M., Basappa, P. & Jambula, A. (2008) Optimization of complex electrode system for use in electrical measurements. *Conference Record of the 2008 IEEE International Symposium on Electrical Insulation, Vols 1 and 2*, 308-311.

Lakshmanan, R. S., Guntupalli, R., Hu, J., Kim, D. J., Petrenko, V. A., Barbaree, J. M. & Chin, B. A. (2007) Phage immobilized magnetoelastic sensor for the detection of *Salmonella typhimurium*. *Journal of Microbiological Methods,* 71**,** 55-60.

Lasseter, T. L., Cai, W. & Hamers, R. J. (2004) Frequency-dependent electrical detection of protein binding events. *Analyst,* 129**,** 3-8.

Lazcka, O., Del Campo, F. J. & Munoz, F. X. (2007) Pathogen detection: a perspective of traditional methods and biosensors. *Biosensors & Bioelectronics,* 22**,** 1205-1217.

Lee, N. Y., Yang, Y., Kim, Y. S. & Park, S. (2006) Microfluidic immunoassay platform using antibody-immobilized glass beads and its application for detection of *Escherichia coli* O157:H7. *Bulletin of the Korean Chemical Society,* 27**,** 479-483.

Lee, T. M.-H. & Hsing, I.-M. (2006) DNA-based bioanalytical microsystems for handheld device applications. *Analytica Chimica Acta,* 556**,** 26-37.

Leonard, P., Hearty, S., Brennan, J., Dunne, L., Quinn, J., Chakraborty, T. & O'kennedy, R. (2003) Advances in biosenors for detection of pathogens in food and water. *Enzyme and Microbial Technology,* 32**,** 2-13.

Li, X. B. B., Larson, S. D., Zyuzin, A. S. & Mamishev, A. V. (2006) Design principles for multichannel fringing electric field sensors. *IEEE Sensors Journal,* 6**,** 434-440.

Lim, D. V., Simpson, J. M., Kearns, E. A. & Kramer, M. F. (2005) Current and developing technologies for monitoring agents of bioterrorism and biowarfare. *Clinical Microbiology Reviews,* 18**,** 583-607.

Lin, Y. H., Chen, S. H., Chuang, Y. C., Lu, Y. C., Shen, T. Y., Chang, C. A. & Lin, C. S. (2008) Disposable amperometric immunosensing strips fabricated by Au nanoparticles-modified screen-printed carbon electrodes for the detection of foodborne pathogen *Escherichia coli* O157:H7. *Biosensors & Bioelectronics,* 23**,** 1832-1837.

Lodish, H., Berk, A., Zipursky, S. L., Matsudaira, P., Baltimore, D. & Darnell, J. (2000) *Molecular cell biology,* New York, W. H. Freeman and Company.

Lu, Y. C., Chuang, Y. S., Chen, Y. Y., Shu, A. C., Hsu, H. Y., Chang, H. Y. & Yew, T. R. (2008) Bacteria detection utilizing electrical conductivity. *Biosensors & Bioelectronics,* 23**,** 1856-1861.

Luong, J. H. T., Habibi-Rezaei, M., Meghrous, J., Xiao, C., Male, K. B. & Kamen, A. (2001) Monitoring motility, spreading, and mortality of adherent insect cells using an impedance sensor. *Analytical Chemistry,* 73**,** 1844-1848.

MacGregor, S. J., Farish, O., Fouracre, R., Rowan, N. J. & Anderson, J. G. (2000) Inactivation of pathogenic and spoilage microorganisms in a test liquid using pulsed electric fields. IEEE *Transactions on Plasma Science,* 28**,** 144-149.

Maillard, J. Y., Beggs, T. S., Day, M. J., Hudson, R. A. & Russell, A. D. (1996) The effect of biocides on proteins of *Pseudomonas aeruginosa* PAO bacteriophage F116. *Journal of Applied Bacteriology,* 80**,** 291-295.

Mamishev, A. V., Du, Y., Lesieutre, B. C. & Zahn, M. (1999) Development and applications of fringing electric field dielectrometry sensors and parameter estimation algorithms. *Journal of Electrostatics,* 46**,** 109-123.

Manesse, M., Stambouli, V., Boukherroub, R. & Szunerits, S. (2008) Electrochemical impedance spectroscopy and surface plasmon resonance studies of DNA hybridization on gold/SiOx interfaces. *Analyst,* 133**,** 1097-1103.

Mao, X., Yang, L., Su, X.-L. & Li, Y. (2006) A nanoparticle amplification based quartz crystal microbalance DNA sensor for detection of *Escherichia coli* O157:H7. *Biosensors and Bioelectronics,* 21**,** 1178-1185.

Markx, G. H. & Davey, C. L. (1999) The dielectric properties of biological cells at radiofrequencies: applications in biotechnology. *Enzyme and Microbial Technology,* 25**,** 161-171.

Matsuzaki, S., Rashel, M., Uchiyama, J., Sakurai, S., Ujihara, T., Kuroda, M., Ikeuchi, M., Tani, T., Fujieda, M., Wakiguchi, H. & Imai, S. (2005) Bacteriophage therapy: a revitalized therapy against bacterial infectious diseases. *Journal of Infection and Chemotherapy* 11**,** 211-219.

Mattey, M. (2005a) Data on an investigation into bacteriophage 9563 immobilisation. Unpublished Work. University of Strathclyde.

Mattey, M. (2005b) De-activation of adsorbed phages compared to free phages. Unpublished Work. University of Strathclyde.

McGrath, S. & Sinderen, D. V. (2007) *Bacteriophage: genetics and molecular biology*, Norfolk, Caister Academic Press

McNerney, R., Wilson, S. M., Sidhu, A. M., S.Harley, V., Suwaidi, Z. A., Nye, P. M., Parish, T. & Stoker, N. G. (1998) Inactivation of mycobacteriophage D29 using ferrous ammonium sulphate as a tool for the detection of viable *Mycobacterium smegmatis* and *M. tuberculosis. Research in Microbiology,* 149**,** 487-495.

Meadows, D. (1996) Recent developments with biosensing technology and applications in the pharmaceutical industry. *Advanced Drug Delivery Reviews,* 21**,** 179-189.

Merlino, J., Leroi, M., Bradbury, R., Veal, D. & Harbour, C. (2000) New chromogenic identification and detection of *Staphylococcus aureus* and methicillin-resistant *S. aureus. Journal of Clinical Microbiology,* 38**,** 2378-2380.

Mirtaheri, P., Grimnes, S. & Martinsen, O. G. (2005) Electrode polarization impedance in weak NaCl aqueous solutions. *IEEE Transactions on Biomedical Engineering,* 52**,** 2093-2099.

Mittelmann, A. S., Ron, E. Z. & Rishpon, J. (2002) Amperometric quantification of total coliforms and specific detection of *Escherichia coli. Analytical Chemistry,* 74**,** 903-907.

Mohr, A., Finger, W., Fohr, K. J., Gopel, W., Hammerle, H. & Nisch, W. (1996) Performance of a thin film microelectrode array for monitoring electrogenic cells in vitro. *Sensors and Actuators B-Chemical,* 34**,** 265-269.

Montelius, L., Tegenfeldt, J. O. & Ling, T. G. I. (1995) Fabrication and characterization of a nanosensor for admittance spectroscopy of biomolecules. *Journal of Vacuum Science & Technology a-Vacuum Surfaces and Films,* 13**,** 1755-1760.

Montenegro, M. I., Queiros, M. A. & Daschbach, J. L. (1990) *Microelectrodes: theory and applications,* Alvo, Portugal, Kluwer Acedemic Publishers.

Mosier-Boss, P. A., Lieberman, S. H., Andrews, J. M., Rohwer, F. L., Wegley, L. E. & Breitbart, M. (2003) Use of fluorescently labeled phage in the detection and identification of bacterial species. *Applied Spectroscopy,* 57**,** 1138-1144.

Moulton, S. E., Barisci, J. N., Bath, A., Stella, R. & Wallace, G. G. (2004) Studies of double layer capacitance and electron transfer at a gold electrode exposed to protein solutions. *Electrochimica Acta,* 49**,** 4223-4230.

Muhammad-Tahir, Z. & Alocilja, E. C. (2003) A conductometric biosensor for biosecurity. *Biosensors and Bioelectronics,* 18**,** 813-819.

Nam, K. T., Kim, D. W., Yoo, P. J., Chiang, C. Y., Meethong, N., Hammond, P. T., Chiang, Y. M. & Belcher, A. M. (2006) Virus-enabled synthesis and assembly of nanowires for lithium ion battery electrodes. *Science,* 312**,** 885-888.

Nandakumar, V., La Belle, J. T., Reed, J., Shah, M., Cochran, D., Joshi, L. & Alford, T. L. (2008) A methodology for rapid detection of *Salmonella typhimurium* using label-free electrochemical impedance spectroscopy. *Biosensors & Bioelectronics,* 24**,** 1039-1042.

Nanduri, V., Bhunia, A. K., Tu, S. I., Paoli, G. C. & Brewster, J. D. (2007a) SPR biosensor for the detection of *L. monocytogenes* using phage-displayed antibody. *Biosensors & Bioelectronics,* 23**,** 248-252.

Nanduri, V., Sorokulova, I. B., Samoylov, A. M., Simonian, A. L., Petrenko, V. A. & Vodyanoy, V. (2007b) Phage as a molecular recognition element in biosensors immobilized by physical adsorption. *Biosensors & Bioelectronics,* 22**,** 986-992.

Neufeld, T., Schwartz-Mittelmann, A., Biran, D., Ron, E. Z. & Rishpon, J. (2003) Combined phage typing and amperometric detection of released enzymatic activity for the specific identification and quantification of bacteria. *Analytical Chemistry,* 75**,** 580-585.

New Zealand Food Safety Authority (2001) *Staphylococcus aureus*. Prepared for the New Zealand Ministry of Health by the Institute of Environmental Science and Research Limited.

Office for National Statistics (2008) Deaths involving MRSA and *Clostridium difficile* by communal establishment: England and Wales, 2001-06.

O'Flaherty, S., Ross, R. P., Meaney, W., Fitzgerald, G. F., Elbreki, M. F. & Coffey, A. (2005) Potential of the polyvalent anti-*Staphylococcus* bacteriophage K for control of antibiotic-resistant *Staphylococci* from hospitals. *Applied and Environmental Microbiology,* 71**,** 1836-1842.

Oh, B.-K., Lee, W., Chun, B. S., Bae, Y. M., Lee, W. H. & Choi, J.-W. (2005) The fabrication of protein chip based on surface plasmon resonance for detection of pathogens. *Biosenosrs and Bioelectronics,* 20**,** 1847-1850.

Oliver, L. M., Dunlop, P. S. M., Byrne, J. A., Blair, I. S., Boyle, M., Mcguigan, K. G. & Mcadams, E. T. (2006) An impedimetric sensor for monitoring the growth of *Staplylococcus epidermidis. 2006 28th Annual International Conference of the IEEE Engineering in Medicine and Biology Society, Vols 1-15.* New York, IEEE.

Olsen, E. V., Sorokulova, I. B., Petrenko, V. A., Chen, I.-H., Barbaree, J. M. & Vodyanoy, V. J. (2006) Affinity-selected filamentous bacteriophage as a probe for acoustic wave biodetectors of *Salmonella typhimurium. Biosenosrs and Bioelectronics,* 21**,** 1434-1442.

Olthuis, W., Streekstra, W. & Bergveld, P. (1995) Theoretical and experimental-determination of cell constants of planar-interdigitated electrolyte conductivity sensors. *Sensors and Actuators B-Chemical,* 24**,** 252-256.

Omanovic, S. & Roscoe, S. G. (1999) Electrochemical studies of the adsorption behavior of bovine serum albumin on stainless steel. *Langmuir,* 15**,** 8315-8321.

O'Neill, R. D., Chang, S. C., Lowry, J. P. & Mcneil, C. J. (2004) Comparisons of platinum, gold, palladium and glassy carbon as electrode materials in the design of biosensors for glutamate. *Biosensors & Bioelectronics,* 19**,** 1521-1528.

Owens, J. D., Thomas, D. S., Thompson, P. S. & Timmerman, J. W. (1989) Indirect conductimetry: a novel approach to the conductimetric enumeration of microbial populations. *Letters in Applied Microbiology,* 9**,** 245-249.

Palchetti, I. & Mascini, M. (2008) Electroanalytical biosensors and their potential for food pathogen and toxin detection. *Analytical and Bioanalytical Chemistry,* 391**,** 455-471.

Pancrazio, J. J., Whelan, J. P., Borkholder, D. A., Ma, W. & Stenger, D. A. (1999) Development and application of cell-based biosensors. *Annals od Biomedical Engineering,* 27**,** 697-711.

Parkinson, G. & Pejcic, B. (2005) Using biosensors to detect emerging infectious diseases. The Australia Biosecurity Cooperative Research Centre.

Pathirana, S. T., Barbaree, J., Chin, B. A., Hartell, M. G., Neely, W. C. & Vodyanoy, V. (2000) Rapid and sensitive biosensor for *Salmonella. Biosensors and Bioelectronics,* 15**,** 135-141.

Pavlin, M. & Miklavcic, D. (2003) Effective conductivity of a suspension of permeabilized cells: a theoretical analysis. *Biophysical Journal,* 85**,** 719-729.

Penrod, S. L., Olson, T. M. & Grant, S. B. (1996) Deposition kinetics of two viruses in packed beds of quartz granular media. *Langmuir,* 12**,** 5576-5587.

Peruski, A. H. & Peruski, L. F. (2003) Immunological methods for detection and identification of infectious disease and biological warfare agents. *Clinical and Diagnostic Laboratory Immunology,* 10**,** 506-513.

Petrenko, V. A. & Vodyanoy, V. J. (2003) Phage display for detection of biological threat agents. *Journal of Microbiological Methods,* 53**,** 253-262.

Petty, N. K., Evans, T. J., Fineran, P. C. & Salmond, G. P. C. (2007) Biotechnological exploitation of bacteriophage research. *Trends in Biotechnology,* 25**,** 7-15.

Pierce Biotechnology Inc. (2006) EZ-Link® Sulfo-NHS-Biotinylation Kit Instructions. Product number 21425 (1775.2).

Plueddemann, E. P. (1991) *Silane Coupling Agents,* New York, Plenum Press.

Potter, E. C. (1961) *Electrochemistry: principles and applications*, London, Cleaver-Hume Press.

Price, C. P. & Newman, D. J. (1997) *Principles and practice of immunoassay,* London, Macmillan Reference Ltd.

Quinn, C., Ward, J., Griffin, M., Yearsley, D. & Egan, J. (1995) A comparison of conventional culture and 3 rapid methods for the detection of *Salmonella* in poultry feeds and environmental-samples. *Letters in Applied Microbiology,* 20**,** 89-91.

Radke, S. M. & Alocilja, E. C. (2004) Design and fabrication of a microimpedance biosensor for bacterial detection. *IEEE Sensors Journal,* 4**,** 434-440.

Radke, S. M. & Alocilja, E. C. (2005a) A high density microelectrode array biosensor for detection of *E. coli* O157:H7. *Biosensors and Bioelectronics,* 20**,** 1662-1667.

Radke, S. M. & Alocilja, E. C. (2005b) A microfabricated biosensor for detecting foodborne bioterrorism agents. *IEEE Sensors Journal,* 5**,** 744-750.

Raghavachari, N., Bao, Y. P., Li, G. S., Xie, X. Y. & Muller, U. R. (2003) Reduction of autofluorescence on DNA microarrays and slide surfaces by treatment with sodium borohydride. *Analytical Biochemistry,* 312**,** 101-105.

Raicu, V., Raicu, G. & Turcu, G. (1996) Dielectric properties of yeast cells as simulated by the two-shell model. *Biochimica et Biophysica Acta-Bioenergetics,* 1274**,** 143-148.

Rigaud, B., Morucci, J.-P. & Chauveau, N. (1996) Bioelectrical impedance techniques in medicine. Part I: bioimpedance measurement. Second section: impedance spectrometry. *Critical Reviews in Biomedical Engineering,* 24**,** 257-351.

Rogers, K. R. & Mascini, M. (1998) Biosensors for field analytical monitoring. *Field Analytical Chemistry and Technology,* 2**,** 317-331.

Rompré, A., Servais, P., Baudart, J., De-Roubin, M.-R. & Laurent, P. (2002) Detection and enumeration of coliforms in drinking water: current methods and emerging approaches. *Journal of Microbiological Methods,* 49**,** 31-54.

Rowe-Taitt, C. A., Golden, J. P., Feldstein, M. J., Cras, J. J., Hoffman, K. E. & Ligler, F. S. (2000) Array biosensor for detection of biohazards. *Biosensors and Bioelectronics,* 14**,** 785-794.

Rudi, K., Nogva, H. K., Moen, B., Nissen, H., Bredholt, S., Moretro, T., Naterstad, K. & Holck, A. (2002) Development and application of new nucleic acid-based technologies for microbial community analyses in foods. *International Journal of Food Microbiology,* 78**,** 171-180.

Sapsford, K. E. & Ligler, F. S. (2004) Real-time analysis of protein adsorption to a variety of thin films. *Biosensors & Bioelectronics,* 19**,** 1045-1055.

Schaldach, C. M., Bourcier, W. L., Shaw, H. F., Viani, B. E. & Wilson, W. D. (2006) The influence of ionic strength on the interaction of viruses with charged surfaces under environmental conditions. *Journal of Colloid and Interface Science,* 294**,** 1-10.

Schijven, J. F. & Hassanizadeh, S. M. (2000) Removal of viruses by soil passage: overview of modeling, processes, and parameters. *Critical Reviews in Environmental Science and Technology,* 30**,** 49-127.

Schmelcher, M. & Loessner, M. J. (2008) Bacteriophage: powerful tools for the detection of bacterial pathogens. IN ZOUROB, M., ELWARY, S. & TURNER, A. (Eds.) *Principles of bacterial detection: biosensors, recognition receptors and microsystems.* New York, Springer.

Schoenbach, K. H., Peterkin, F. E., Alden, R. W. & Beebe, S. J. (1997) The effect of pulsed electric fields on biological cells: experiments and applications. *IEEE Transactions on Plasma Science,* 25**,** 284-292.

Schuenck, R. P., Lourenco, M. C. S., Iiiorio, N. L. P., Ferreira, A. L. P., Nouer, S. A. & Santos, K. R. N. (2006) Improved and rapid detection of methicillin-resistant *Staphylococcus aureus* nasal carriage using selective broth and multiplex PCR. *Research in Microbiology,* 157**,** 971-975.

Schwan, H. P. (1957) *Electrical Properties of Tissue and Cell Suspensions,* New York, Acadmeic Press Inc.

Scott, H. & Mattey, M. (2003) Immobilisation and Stabilisation of Virus. WO 03/093462 A2.

Scouten, W. H., Luong, J. H. T. & Brown, R. S. (1995) Enzyme or protein immobilization techniques for application in biosensor design. *Trends in Biotechnology,* 13.

Serwer, P., Hayes, S. J., Lieman, K. & Griess, G. A. (2007) In situ fluorescence microscopy of bacteriophage aggregates. *Journal of Microscopy-Oxford,* 228**,** 309-321.

Shabani, A., Zourob, M., Allain, B., Marquette, C. A., Lawrence, M. F. & Mandeville, R. (2008) Bacteriophage-modified microarrays for the direct impedimetric detection of bacteria. *Analytical Chemistry,* 80**,** 9475-9482.

Shen, Z., Huang, M., Xiao, C., Zhang, Y., Zeng, X. & Wang, P. G. (2007) Nonlabeled quartz crystal microbalance biosensor for bacterial detection using carbohydrate and lectin recognitions. *Analytical Chemistry,* 79**,** 2312-2319.

Shriver-Lake, L. C., Gammeter, W. B., Bang, S. S. & Pazirandeh, M. (2002) Covalent binding of genetically engineered microorganisms to porous glass beads. *Analytica Chimica Acta,* 470**,** 71-78.

Silley, P. & Forsythe, S. (1996) Impedance microbiology-a rapid change for microbiologists. *Journal of Applied Bacteriology,* 80**,** 233-243.

Simpkins, B. S., Mccoy, K. M., Whitman, L. J. & Pehrsson, P. E. (2007) Fabrication and characterization of DNA-functionalized GaN nanowires. *Nanotechnology,* 18.

Singh, A., Glass, N., Tolba, M., Brovko, L., Griffiths, M. & Evoy, S. (2009) Immobilization of bacteriophages on gold surfaces for the specific capture of pathogens. *Biosensors & Bioelectronics,* 24**,** 3645-3651.

Singh, A. K., Flounders, A. W., Volponi, J. V., Ashley, C. S., Wally, K. & Schoeniger, J. S. (1999) Development of sensors for direct detection of organophosphates. Part I: immobilization, characterization and stabilization of acetylcholinesterase and organophosphate hydrolase on silica supports. *Biosensors & Bioelectronics,* 14**,** 703-713.

Sipehia, R., Chawla, A. S., Daka, J. & Chang, T. M. S. (1988) Immobilization of enzymes on polypropylene bead surfaces by anhydrous ammonia gaseous plasma technique. *Journal of Biomedical Materials Research,* 22**,** 417-422.

Skurnik, M., Strauch, E. (2006) Phage therapy: facts and fiction. *International Journal of Medical Microbiology*, 296, 5-14.

Smith, G. P. (1985) Filamentous fusion phage - novel expression vectors that display cloned antigens on the virion surface. *Science,* 228**,** 1315-1317.

Song, X., Zhai, J., Wang, Y. & Jiang, L. (2006) Self-assembly of amino-functionalized monolayers on silicon surfaces and preparation of superhydrophobic surfaces based on alkanoic acid dual layers and surface roughening. *Journal of Colloid and Interface Science,* 298**,** 267-273.

Sorokulova, I. B., Olsen, E. V., Chen, I. H., Fiebor, B., Barbaree, J. M., Vodyanoy, V. J., Chin, B. A. & Petrenko, V. A. (2005) Landscape phage probes for *Salmonella typhimurium*. *Journal of Microbiological Methods,* 63**,** 55-72.

SPEERS, D. J., OLMA, T. R. & GILBERT, G. L. (1998) Evaluation of four methods for rapid identification of *Staphylococcus aureus* from blood cultures. *Journal of Clinical Microbiology,* 36, 1032-1034.

Squirrell, D. J., Price, R. L. & Murphy, M. J. (2002) Rapid and specific detection of bacteria using bioluminescence. *Analytica Chimica Acta,* 457, 109-114.

Srinivasan, B., Tung, S., Li, Y. & Varshney, M. (2006) Simulation of an electrical impedance based microfluidic biosensor for detection of *E. coli* cells. *Proceedings of the COMSOL Users Conference.* Boston.

Stefan, R.-I., Staden, J. F. K. V. & Aboul-Enein, H. Y. (2000) Immunosensors in clinical analysis. *Fresenius Journal of Analytical Chemistry,* 366, 659-668.

Stewart, G. N. (1899) The changes produced by the growth of bacteria in the molecular concentration and electrical conductivity of culture media. *Journal of Experimental Medicine,* 4, 235-243.

Stulik, K., Amatore, C., Holub, K., Marecek, V. & Kutner, W. (2000) Microelectrodes. Definitions, characterisation, and applications. *Pure and Applied Chemistry,* 72, 1483-1492.

Su, X.-L. & Li, Y. (2005) A QCM immunosensor for *Salmonella* detection with simultaneous measurements of resonant frequency and motional resistance. *Biosensors and Bioelectronics,* 21, 840-848.

Suehiro, J., Hatano, T., Shutou, M. & Hara, M. (2005) Improvement of electric pulse shape for electropermeabilization-assisted dielectrophoretic impedance measurement for high sensitive bacteria detection. *Sensors and Actuators B-Chemical,* 109, 209-215.

Suehiro, J., Ohtsubo, A., Hatano, T. & Hara, M. (2006) Selective detection of bacteria by a dielectrophoretic impedance measurement method using an antibody-immobilized electrode chip. *Sensors and Actuators B-Chemical,* 119, 319-326.

Suehiro, J., Yatsunami, R., Hamada, R. & Hara, M. (1999) Quantitative estimation of biological cell concentration suspended in aqueous medium by using dielectrophoretic impedance measurement method. *Journal of Physics D-Applied Physics,* 32, 2814-2820.

Sugimura, H., Hozumi, A., Kameyama, T. & Takai, O. (2002) Organosilane self-assembled monolayers formed at the vapour/solid interface. *Surface and Interface Analysis,* 34, 550-554.

Sun, W., Brovko, L. & Griffiths, M. (2001) Use of bioluminescent *Salmonella* for assessing the efficiency of constructed phage-based biosorbent (Reprinted from Journal Industrial Microbiology & Biotechnology, vol 25, pg 273-275, 2000). *Journal of Industrial Microbiology & Biotechnology,* 27, 126-128.

Swaminathan, B. & Feng, P. (1994) Rapid detection of food-borne pathogenic bacteria. *Annual Review of Microbiology,* 48, 401-426.

Taketo, A. (1996) Electrotransformation of bacteria. IN ZIMMERMANN, U. & NEIL, G. A. (Eds.) *Electromanipulation of Cells.* Boca Raton, Florida, CRC Press, Inc.

Tanji, Y., Furukawa, C., Na, S.-H., Hijikata, T., Miyanaga, K. & Unno, H. (2004) *Escherichia coli* detection by GFP-labeled lysozyme-inactivated T4 bacteriophage. *Journal of Biotechnology,* 114**,** 11-20.

Timoshkin, I. V., Macgregor, S. J., Fouracre, R. A., Crichton, B. H. & Anderson, J. G. (2006a) Transient electrical field across cellular membranes: pulsed electric field treatment of microbial cells. *Journal of Physics D-Applied Physics,* 39**,** 596-603.

Timoshkin, I. V., Macgregor, S. J., Fouracre, R. A., Given, M. J. & Anderson, J. G. (2006b) Forces acting on biological cells in external electrical fields. *2006 Annual Report Conference on Electrical Insulation and Dielectric Phenomena***,** 676-679.

Torrey, S. (1983) *Enzyme technology preparation, purification, stabilization, immobilization: recent advances,* New Jersey, Noyes Pubns.

Turner, A. P. F., Isao, K. & Wilson, G. S. (1990) *Biosensors: fundamentals and applications,* New York, Oxford University Press.

Uithoven, K. A., Schmidt, J. C. & Ballman, M. E. (2000) Rapid identification of biological warfare agaents using an instrument employing a light addressable potentiometric sensor and a flow-through immunofiltration-enzyme assay system. *Biosensors and Bioelectronics,* 14**,** 761-770.

Ur, A. & Brown, F. J. (1975) *Monitoring of Bacterial Activity by Impedance Measurements,* New York, John Wiley & Sons.

Van Gerwen, P., Laureyn, W., Laureys, W., Huyberechts, G., De Beeck, M. O., Baert, K., Suls, J., Sansen, W., Jacobs, P., Hermans, L. & Mertens, R. (1998) Nanoscaled interdigitated electrode arrays for biochemical sensors. *Sensors and Actuators B-Chemical,* 49**,** 73-80.

Van Voorthuizen, E. M., Ashbolt, N. J. & Schafer, A. I. (2001) Role of hydrophobic and electrostatic interactions for initial enteric virus retention by MF membranes. *Journal of Membrane Science,* 194**,** 69-79.

Varshney, M. & Li, Y. B. (2007) Interdigitated array microelectrode based impedance biosensor coupled with magnetic nanoparticle-antibody conjugates for detection of *Escherichia coli* O157:H7 in food samples. *Biosensors & Bioelectronics,* 22**,** 2408-2414.

Varshney, M. & Li, Y. B. (2008) Double interdigitated array microelectrode-based impedance biosensor for detection of viable *Escherichia coli* O157:H7 in growth medium. *Talanta,* 74**,** 518-525.

Varshney, M. & Li, Y. B. (2009) Interdigitated array microelectrodes based impedance biosensors for detection of bacterial cells. *Biosensors & Bioelectronics,* 24**,** 2951-2960.

Varshney, M., Li, Y. B., Srinivasan, B. & Tung, S. (2007) A label-free, microfluidics and interdigitated array microelectrode-based impedance biosensor in combination with nanoparticles immunoseparation for detection of *Escherichia coli* O157:H7 in food samples. *Sensors and Actuators B-Chemical,* 128**,** 99-107.

Verkade, E., Elberts, S., Verhulst, C. & Kluytmans, J. (2009) Performance of Oxoid Brilliance[TM] MRSA medium for detection of methicillin-resistant *Staphylococcus aureus*: an in vitro study. *European Journal of Clinical Microbiology & Infectious Diseases,* 28**,** 1443-1446.

Verrecchia, L. (2007) Monitoring of immobilised phage activity over time. Unpublished Work. University of Strathclyde.

Virgina Semiconductor, I. (2009) Virginia Semiconductor Inc. silicon wafer information sheet.

Wada, M., Lkhagvadorj, E., Bian, L., Wang, C., Chiba, Y., Nagata, S., Shimizu, T., Yamashiro, Y., Asahara, T. & Nomoto, K. (2010) Quantitative reverse transcription-PCR assay for the rapid detection of methicillin-resistant *Staphylococcus aureus*. *Journal of Applied Microbiology,* 108**,** 779-788.

Wan, J. H., Johnson, M. L., Guntupalli, R., Petrenko, V. A. & Chin, B. A. (2007) Detection of *Bacillus anthracis* spores in liquid using phage-based magnetoelastic micro-resonators. *Sensors and Actuators B-Chemical,* 127**,** 559-566.

Wang, J., Rivas, G., Cai, X., Palecek, E., Nielsen, P., Shiraishi, H., Dontha, N., Luo, D., Parrado, C., Chicharro, M., Farias, P. A. M., Valera, F. S., Grant, D. H., Ozsoz, M. & Flair, M. N. (1997) DNA electrochemical biosensors for environmental monitoring. A review. *Analytica Chimica Acta,* 347**,** 1-8.

Wegener, J., Sieber, M. & Galla, H. J. (1996) Impedance analysis of epithelial and endothelial cell monolayers cultured on gold surfaces. *Journal of Biochemical and Biophysical Methods,* 32**,** 151-170.

Wong, Y. Y., Ng, S. P., Ng, M. H., Si, S. H., Yao, S. Z. & Fung, Y. S. (2002) Immunosensor for the differentiation and detection of *Salmonella* species based on a quartz crystal microbalance. *Biosensors & Bioelectronics,* 17**,** 676-684.

World Health Organisation (2008) Cholera Annual Report 2007. *Weekly Epidemiological Record, 83 (31), 269-284.* Geneva.

Yakovleva, J., Davidsson, R., Lobanova, A., Bengtsson, M., Eremin, S., Laurell, T. & Emneus, J. (2002) Microfluidic enzyme immunoassay using silicon microchip with immobilized antibodies and chemiluminescence detection. *Analytical Chemistry,* 74**,** 2994-3004.

Yamamoto, Y. (2002) PCR in diagnosis of infection: detection of bacteria in cerebrospinal fluids. *Clinical and Diagnostic Laboratory Immunology,* 9**,** 508-514.

Yang, L., Yanbin, L. & Gisela, E. F. (2004a) Interdigitated array microelectrode-based electrochemical impedance immunosensor for detection of *Escherichia coli* O157:H7. *Analytical Chemistry,* 76**,** 1107-1113.

Yang, L., Li, Y., Griffis, C. L. & Johnson, M. G. (2004b) Interdigitated microelectrode (IME) impedance sensor for the detection of viable *Salmonella typhimurium*. *Biosensors and Bioelectronics,* 19**,** 1139-1147.

Yang, L., Ruan, C. & Li, Y. (2003) Detection of viable *Salmonella typhimurium* by impedance measurement of electrode capacitance and medium resistance. *Biosensors and Bioelectronics,* 19**,** 495-502.

Yang, L. J. (2008) Electrical impedance spectroscopy for detection of bacterial cells in suspensions using interdigitated microelectrodes. *Talanta,* 74**,** 1621-1629.

Yang, L.-M. C., Tam, P. Y., Murray, B. J., Mcintire, T. M., Overstreet, C. M., Weiss, G. A. & Penner, R. M. (2006) Virus electrodes for universal biodetection. *Analytical Chemistry,* 78**,** 3265-3270.

Yang, S. & Rothman, R. E. (2004) PCR-based diagnostics for infectious diseases: uses, limitations, and future applications in acute-care settings. *The Lancet Infectious Diseases,* 4.

Yemini, M., Levi, Y., Yagil, E. & Rishpon, J. (2007) Specific electrochemical phage sensing for *Bacillus cereus* and *Mycobacterium smegmatis. Bioelectrochemistry,* 70**,** 180-184.

Yuan, B. L., Pham, M. & Nguyen, T. H. (2008) Deposition kinetics of bacteriophage MS2 on a silica surface coated with natural organic matter in a radial stagnation point flow cell. *Environmental Science & Technology,* 42**,** 7628-7633.

Zerda, K. S., Gerba, C. P., Hou, K. C. & Goyal, S. M. (1985) Adsorption of viruses to charge-modified silica. *Applied and Environmental Microbiology,* 49**,** 91-95.

Zheng, S., Liu, M., Kasdan, H. L. & Tai, Y. C. (2006) Platinum black electroplated impedance particle sensor. *2006 1st IEEE International Conference on Nano/Micro Engineered and Molecular Systems, Vols 1-3.* New York, Ieee.

Zimmermann, U. & Neil, G. A. (1996) *Electromanipulation of Cells,* Boca Raton, Florida, CRC Press, Inc.

Zou, Z. W., Kai, J. H., Rust, M. J., Han, J. & Ahn, C. H. (2007) Functionalized nano interdigitated electrodes arrays on polymer with integrated microfluidics for direct bio-affinity sensing using impedimetric measurement. *Sensors and Actuators a-Physical,* 136**,** 518-526.

Zourob, M., Elwary, S. & Turner, A. (2008) *Principles of bacterial detection: biosensor, recognition receptors and microsystems,* New York, Springer.

Appendix A

Impedance (Z) of a resistor (R) and capacitor (C) in parallel as illustrated in Figure A.1.
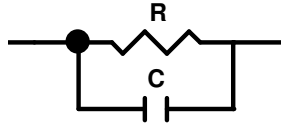
Figure A.1. A resistor (R) and capacitor (C) connected in parallel.

Note that X_C is the capacitive reactance and is defined as follows:

$$X_C = \frac{1}{\omega C}$$

For impedances in parallel, the reciprocal of the total impedance is the sum of the reciprocal of the impedance for each circuit element:

$$\frac{1}{Z} = \frac{1}{R} + \frac{1}{-jX_C}$$

$$\frac{1}{Z} = \frac{R - jX_C}{-jRX_C}$$

$$\Rightarrow Z = \frac{-jRX_C}{R - jX_C} = \frac{-jRX_C}{R - jX_C} \times \frac{R + jX_C}{R + jX_C}$$

Since $(a+b)(a-b) = a^2 - b^2$

then $(R + jX_C)(R - jX_C) = R^2 - j^2 X_C^2 = R^2 + X_C^2$

Therefore, inserting the above into the espresion for Z the following is obtained:

$$Z = \frac{-jR^2 X_C - j^2 R X_C^2}{R^2 + X_C^2} = \frac{RX_C^2 - jR^2 X_C}{R^2 + X_C^2}$$

Splitting into real and imaginary components: $Z = \frac{RX_C^2}{R^2 + X_C^2} - j\frac{R^2 X_C}{R^2 + X_C^2}$

Appendix B

The HABA Assay

HABA (4'-hydroxyazobenzene-2-carboxylic acid) dye binds to avidin, producing a yellow-orange solution which absorbs at 500 nm. When biotin is added to a HABA/avidin solution it will displace HABA due to its higher affinity for avidin. This will lead to a decrease in absorbance at 500 nm that is proportional to the amount of HABA displaced. The change in absorbance can be used to determine how much biotin is present using the following protocol.

Method

The HABA assay was used to estimate the level of biotin incorporated onto phages. The protocol was as follows. A HABA/avidin solution was prepared by adding 10 mg of avidin and 600 µl of 10 mM HABA to 19.4 ml PBS. The absorbance of this solution was then recorded at 500 nm in a 1 ml cuvette, containing 900 µl of the HABA/avidin solution, using a spectrophotometer (Biomate 5, Thermo Spectronic, USA). This absorbance value is denoted as $A_{500}H\backslash A$. The biotinylated phage suspension (100 µl) was then added to the cuvette and absorbance at 500 nm was repeated for the reaction mixture ($A_{500}H\backslash A\backslash B$). From the two absorbance readings it is then possible to estimate the concentration of biotin per ml of reaction mixture (mmol/ml) using Equation B.1, as adapted from the supplier's instructions [Pierce Biotechnology Inc., 2006].

$$C_R = \frac{(0.9 \times A_{500}H \backslash A) - A_{500}H \backslash A \backslash B}{34000} \qquad \textit{Equation B.1}$$

Since the original biotinylated phage sample was diluted 10-fold in the reaction mixture, the concentration of biotin for the original sample (mmol/ml) can be calculated by multiplying by a factor of 10:

$$C_O = C_R \times 10 \qquad \textit{Equation B.2}$$

The number of biotin molecules per ml in the original sample can be calculated from the number of moles of biotin calculated in Equation B.2 using the following formula where N is the number of entities (for example, molecules) and L is Avogadro's constant:

$$N = moles \times L = \frac{C_O}{1000} \times L$$

Equation B.3

The ratio of biotin molecules to phages can then be simply calculated by dividing the result of Equation B.3 by the phage concentration (PFU/ml).

Results

The results of the HABA assay for a phage suspension of 10.52 Log_{10} PFU/ml biotinylated with 1 mg/ml biotin are shown in Table B.1. From these results a biotin/phage ratio of 1.17×10^3 was determined following the calculations outlined previously. Also displayed in Table B.1 are absorbance values for a biotinylated phage solution which was not passed through the de-salting column. Results are discussed in Chapter 5, Section 5.1.4.2.

Table B.1. Results of the HABA test for biotin incorporation. Results are reported in terms of absorbance level at 500 nm and were obtained for biotinylated phage suspensions before and after being passed though a de-salting column to remove excess biotin.

	Absorbance at 500 nm	
	Before de-salting column	**After de-salting column**
HABA/Avidin	1.238	1.238
HABA/Avidin/B-phage	0.176	1.114